

INFORMATION TO USERS

This manuscript has been reproduced from the microfilm master. UMI films the text directly from the original or copy submitted. Thus, some thesis and dissertation copies are in typewriter face, while others may be from any type of computer printer.

The quality of this reproduction is dependent upon the quality of the copy submitted. Broken or indistinct print, colored or poor quality illustrations and photographs, print bleedthrough, substandard margins, and improper alignment can adversely affect reproduction.

In the unlikely event that the author did not send UMI a complete manuscript and there are missing pages, these will be noted. Also, if unauthorized copyright material had to be removed, a note will indicate the deletion.

Oversize materials (e.g., maps, drawings, charts) are reproduced by sectioning the original, beginning at the upper left-hand corner and continuing from left to right in equal sections with small overlaps. Each original is also photographed in one exposure and is included in reduced form at the back of the book.

Photographs included in the original manuscript have been reproduced xerographically in this copy. Higher quality 6" x 9" black and white photographic prints are available for any photographs or illustrations appearing in this copy for an additional charge. Contact UMI directly to order.

UMI

A Bell & Howell Information Company
300 North Zeeb Road, Ann Arbor MI 48106-1346 USA
313/761-4700 800/521-0600

University of Alberta

**An Evaluation of Ground Penetrating Radar for Investigation of Palsa
Evolution, Macmillan Pass, Northwest Territories**

by

Celesa Lyra Horvath



A thesis submitted to the Faculty of Graduate Studies and Research in partial fulfillment of
the requirements for the degree of Master of Science

Department of Earth and Atmospheric Sciences

Edmonton, Alberta

Spring 1998



National Library
of Canada

Acquisitions and
Bibliographic Services

395 Wellington Street
Ottawa ON K1A 0N4
Canada

Bibliothèque nationale
du Canada

Acquisitions et
services bibliographiques

395, rue Wellington
Ottawa ON K1A 0N4
Canada

Your file *Votre référence*

Our file *Notre référence*

The author has granted a non-exclusive licence allowing the National Library of Canada to reproduce, loan, distribute or sell copies of this thesis in microform, paper or electronic formats.

The author retains ownership of the copyright in this thesis. Neither the thesis nor substantial extracts from it may be printed or otherwise reproduced without the author's permission.

L'auteur a accordé une licence non exclusive permettant à la Bibliothèque nationale du Canada de reproduire, prêter, distribuer ou vendre des copies de cette thèse sous la forme de microfiche/film, de reproduction sur papier ou sur format électronique.

L'auteur conserve la propriété du droit d'auteur qui protège cette thèse. Ni la thèse ni des extraits substantiels de celle-ci ne doivent être imprimés ou autrement reproduits sans son autorisation.

0-612-28946-X

Canada

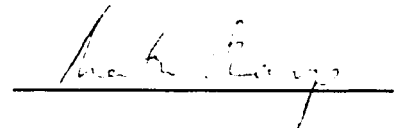
University of Alberta

Faculty of Graduate Studies and Research

The undersigned certify that they have read, and recommend to the Faculty of Graduate Studies and Research for acceptance, a thesis entitled "An Evaluation of Ground Penetrating Radar for Investigation of Palsa Evolution, Macmillan Pass, Northwest Territories" submitted by Celesa Lyra Horvath in partial fulfillment of the requirements for the degree of Master of Science.



G.P. Kershaw
Supervisor



M.J. Sharp
Committee Member



D.C. Sego
Committee Member

16 April 1998

Dedicated, with love and gratitude, to my mother, Susan Horvath

ABSTRACT

The utility of ground penetrating radar (GPR) for investigation of perennially frozen peatlands is examined. Palsa evolution is inferred from GPR and conventional data from two sites near Macmillan Pass, Northwest Territories. Data processing techniques adapted from seismic applications are tested.

GPR consistently imaged sub-peat topography in palsas and fens, and detailed fen stratigraphy, but generally did not clearly image palsa core stratigraphy. Radar-imaged domed strata and frost penetration into underlying mineral sediment are correlated with palsa genesis by ice segregation, an inference supported by coring. Stratigraphic discontinuities are correlated with a known palsa collapse scar; GPR may therefore support reconstructions of peatland history by imaging stratigraphic signatures of pre-existing permafrost landforms. Thaw degradation at depth was imaged by GPR and corroborated by coring and historical evidence. Seismic data processing improved vertical resolution and lateral continuity of fen reflections, but was less effective in improving resolution of radar data from palsas.

ACKNOWLEDGEMENTS

The following agencies and companies provided financial, logistical, or other assistance which made this work possible: Natural Sciences and Engineering Research Council (grants to C.L. Horvath and Dr. G.P. Kershaw); Canadian Circumpolar Institute; Geological Survey of Canada; Jacques Whitford Environment Limited; the University of Alberta Faculty of Graduate Studies and Research; and the Canadian Federation of University Women.

This research was undertaken under the supervision of Dr. Peter Kershaw of the Department of Earth and Atmospheric Science (previously Department of Geography), University of Alberta. Equipment, field station facilities, and logistical support were provided by Dr. Kershaw. In particular, I am grateful for his patience and support during the preparation of this thesis, as well as for useful discussions and feedback regarding the ideas put forth herein.

Thanks are due also to the other members of my supervisory committee, Dr. Dave Sego and Dr. Martin Sharp. Dr. Sego's input to my thesis proposal and subsequent feedback helped to refine some of my ideas pertaining to the radar. Dr. Sharp's critical review of earlier drafts of this thesis, and many insightful discussions during periglacial course work, helped to focus the research on pertinent issues.

The ground penetrating radar surveys and fen coring were undertaken together with Inez Kettles (Geological Survey of Canada) and Stephen D. Robinson (McGill University). I appreciate their helpful guidance and discussions regarding the results of those surveys both during and after the field season. (The steak, fresh food, and enjoyable conversation they brought with them to the field was also appreciated.)

Assistance in the field was capably provided by Mike Getty, John Pedersen, and James Vaughan (Department of Geography, University of Calgary), Heather Klappstein (Department of Geography, University of Alberta), and Volker Schlott (Universität Marburg). The field season was immeasurably more enjoyable as a result of their company, as well as that of Anne Meyer (Universität Marburg). Special thanks to Heather for listening, sharing the incredible drive, and tolerating my choice of music ("There she goes, ...").

Additional support and encouragement in the field were provided by Ken John and Lois Hill; George and Brody Calef and Norman and Barb Barichello of Oldsquaw Lodge (use of the trailer at Mile 222, the occasional lift to my field sites, and excellent hospitality); and Dr. Chris Burn (Department of Geography, Carleton University).

Mr. Les Davis of Sensors & Software Inc., Mississauga, Ontario, helpfully provided clarification of several problems related to the ground penetrating radar system. Dr. Don Lawton (Department of Geology and Geophysics, University of Calgary) generously provided access to seismic data processing facilities, as well as helpful advice regarding geophysics. Darryl Parry (Department of Geology and Geophysics, University of Calgary) took time away from his own research to instruct me in the use of the seismic data processing software.

I express special thanks to the late Kent Holden, who gave freely of his time in assisting me with the enhancement and interpretation of the digital aerial photography, and who was a good friend to both Colm and me. Randy Pakan and Colm Ó Cofaigh scanned the photographic images.

Thanks to all those who made life interesting and enjoyable during my time on campus and in Edmonton. At the risk of missing someone, I am particularly grateful for the friendship and good times shared at the Power Plant, folk fest, and elsewhere with Rod Smith, Sandra Mackay-Smith, John England, Martin Sharp, James Hooper, Vince Miller, Mark Skidmore, John Woodward, Jeff Bond, Björn Tenbrüggen, Anne Meyer, and Shul Gordon.

I am thankful for the support of my colleagues and friends at Jacques Whitford, and also for the special friendship of David Baldwin, Julie Mouzar, Kim Voro, John Shimeld, Peter Morash, Steve Robinson (in fact, the words *can* apply at grad school - see page 22!), Tomás and Joan Ó Cofaigh, and the “lads.”

Very special thanks to my mother, Susan Horvath, who has been generous with her love, support, and encouragement, and has given me the strength to make these accomplishments possible. I also thank my brothers and sisters, and their families, for their love and support.

Finally, with much love, I thank Colm Ó Cofaigh. I have been very fortunate to have his love, support, and patience throughout this period. Colm has contributed to this thesis in so many ways, from editing portions of the text and assisting in preparing the plates, to making our home a haven from the pressures of work and thesis, and most importantly, providing constant encouragement to keep the light at the end of the tunnel well lit.

TABLE OF CONTENTS

1.0	Introduction	1
1.1	Rationale for the Research	1
1.2	Potential Applications of GPR to Perennially Frozen Peatlands	1
1.3	Objectives	6
1.4	Description of the Study Area	8
1.4.1	Regional description	8
1.4.2	Site descriptions	11
1.5	Organization of the Thesis	13
1.6	Literature Cited	16
2.0	A Review of Ground Penetrating Radar Applications for Investigation of Perennially Frozen Peatlands	22
2.1	Introduction	22
2.2	Ground Penetrating Radar Applications	23
2.2.1	Peat Thickness and Volume	23
2.2.2	Peat Properties	26
2.2.3	Ground Ice Distribution and Characteristics in Peat	30
2.2.4	Evolution Inferences from Peat Stratigraphy and Structure	37
2.2.5	Characteristics of Mineral Substrate	38
2.3	Summary and Conclusions	41
2.4	Literature Cited	44
3.0	Radar Stratigraphy and Seismic Data Processing Techniques Applied to Two Palsa Fen Sites, Macmillan Pass, Northwest Territories	53
3.1	Introduction	53
3.2	Study Area	53
3.3	Ground Penetrating Radar	56
3.4	Field Methods	61

3.5	Data Processing	61
3.6	Display and Interpretation of Radar Data	66
3.7	Results and Interpretation	70
3.7.1	Peat Thickness, Peat - Mineral Sediment Interface	70
3.7.2	Internal Peat Stratigraphy - Fens	77
3.7.3	Internal Peat Stratigraphy - Palsas	83
3.7.4	Frozen - Unfrozen Interfaces	89
3.8	Conclusions	97
3.9	Literature Cited	99
4.0	Trends in Palsa Evolution At Two Sites	104
4.1	Introduction	104
4.2	Study Area	104
4.3	Methods	107
4.4	Results	111
4.4.1	Analysis and Interpretation of Aerial Photographs	111
4.4.2	Surficial Characteristics	113
4.4.3	Subsurface Characteristics	114
4.5	Interpretation	119
4.6	Discussion	129
4.7	Conclusions	132
4.8	Literature Cited	134
5.0	Summary and Conclusions	137
5.1	Literature Cited	141
Appendix A	Principles of Ground Penetrating Radar	142
A.1	Principles	143
A.2	Radio wave behaviour and material electrical properties	143
A.2.1	Dielectric constant	143

A.2.2	Signal attenuation	148
A.2.3	Signal reflection	149
A.2.4	Resolution	149
A.3	Velocity and Depth Calculations	150
A.4	Data Collection	155
A.5	Basic Data Processing	156
A.6	Display and Interpretation of Radar Data	157
A.7	Literature Cited	161
Appendix B	Observations of Peat Characteristics From Coring	163
B.1	Porsild's Field	164
B.2	Dale Creek	168
Appendix C	Area Calculations of Palsas At Porsild's Field and Dale Creek for 1949, 1972, and 1981	171
C.1	Porsild's Field	172
C.2	Dale Creek	185
Appendix D	Thaw Depth Measurements	193
Appendix E	Letters of Copyright Permission	207

LIST OF TABLES

Table 4-1.	Porsild's Field: Summary of Temporal Variation in Areal	
	Extent of Palsas	112
Table 4-2.	Dale Creek: Summary of Temporal Variation in Areal	
	Extent of Palsas	112

LIST OF FIGURES

Figure 1-1.	Model of the formation of a dome-shaped palsa	3
Figure 1-2.	Stratigraphic cross-section of a dome-shaped palsa mound	4
Figure 1-3.	Stratigraphic cross-section of a peat plateau with collapsing edge	5
Figure 1-4.	Study area location map	9
Figure 1-5.	Location of Porsild's Field and Dale Creek peatland study sites	10
Figure 2-1.	Refracted radar event from shallow thaw layer	33
Figure 2-2.	Contrast in character of radar reflections across transition between unfrozen and frozen subsurface conditions	35
Figure 2-3.	Radar image artifacts produced by irregular near-vertical interface between unfrozen and frozen peat	36
Figure 2-4.	Stratigraphic cross-section of a dome-shaped palsa mound	39
Figure 2-5.	Stratigraphic cross-section of a peat plateau with collapsing edge	40
Figure 3-1.	Study area location map	54
Figure 3-2.	Location of Porsild's Field and Dale Creek peatland study sites	55
Figure 3-3.	Geometry of GPR signal path through simplified subsurface	59
Figure 3-4.	Survey configuration to generate continuous subsurface radar reflection profile through simplified subsurface	60
Figure 3-5.	Example of spectral analysis of ground penetrating radar data	63
Figure 3-6.	Image artifacts produced by point and dipping subsurface reflectors	67
Figure 3-7a.	Comparison of time variable gain control <i>versus</i> constant gain for identification of peat - mineral sediment interface on radar profiles	71
Figure 3-7b.	Comparison of time variable gain control <i>versus</i> constant gain for identification of peat - mineral sediment interface on radar profiles	72
Figure 3-8.	Inferred peat - mineral sediment interface at Porsild's Field	73
Figure 3-9.	Variation in inferred peat - mineral sediment interface in unfrozen peat at Porsild's Field	75
Figure 3-10.	Signal attenuation below the base of permafrost at Porsild's Field	76

Figure 3-11.	Radar imaging of peat - mineral sediment interface across frozen - unfrozen transition at Dale Creek	78
Figure 3-12.	Fen profile prior to deconvolution	79
Figure 3-13.	Zero-phase spiking deconvolution of fen profile	80
Figure 3-14.	Spiking deconvolution of fen profile	81
Figure 3-15.	Predictive deconvolution of fen profile	82
Figure 3-16.	Coherency filter applied to fen profile	84
Figure 3-17.	Coherency filter and deconvolution applied to fen profile	85
Figure 3-18a.	Radar profile showing inferred stratigraphic signature of known collapse scar, Porsild's Field	86
Figure 3-18b.	Application of coherency filter to radar profile showing inferred stratigraphic signature of known collapse scar	87
Figure 3-19.	Refracted radar event from shallow thaw layer	88
Figure 3-20.	Noise multiples introduced into radar data by processing	90
Figure 3-21.	Stratigraphic cross-section of a dome-shaped palsa mound	91
Figure 3-22.	Migration of radar profile, Dale Creek	92
Figure 3-23a.	Radar profile showing sub-vertical frozen - unfrozen interface and associated complex reflection patterns	94
Figure 3-23b.	Migration of radar profile to enhance imaging of sub-vertical frozen - unfrozen interface	95
Figure 3-24.	Radar imaging of inferred flat-lying unfrozen peat strata below frozen wedge of palsa core	96
Figure 4-1.	Study area location map	105
Figure 4-2.	Location of Porsild's Field and Dale Creek peatland study sites	106
Figure 4-3.	Radar profile of palsa # 1 (GPR Transect # 1) at Porsild's Field	120
Figure 4-4.	Radar profile of palsas # 4 and # 5 (GPR Transect # 3) at Porsild's Field	122
Figure 4-5.	Radar imaging of peat - mineral sediment interface at Dale Creek	124
Figure 4-6.	Radar imaging of palsa cores at Dale Creek	125

Figure 4-7.	Radar profile of palsas # 1 and # 2 (GPR Transect # 2) at Porsild's Field	126
Figure 4-8a.	Radar profile showing inferred stratigraphic signature of known collapse scar, Porsild's Field	127
Figure 4-8b.	Application of coherency filter to radar profile showing inferred stratigraphic signature of known collapse scar	128

LIST OF PLATES

Plate 1-1.	Porsild's Field study site	12
Plate 1-2.	Dale Creek study site	14
Plate 3-1.	Porsild's Field study site	57
Plate 3-2.	Dale Creek study site	58
Plate 4-1.	Porsild's Field study site	108
Plate 4-2.	Dale Creek study site	109
Plate 4-3.	Palsa at Dale Creek site, showing asymmetrical profile	115
Plate 4-4.	Palsa at Dale Creek site, showing ground squirrel burrowing	116
Plate 4-5.	Palsa at Dale Creek site, showing exposed peat	117

1.0 INTRODUCTION

1.1 Rationale for the Research

Ground penetrating radar (GPR) is rapidly gaining recognition in a variety of earth science and related disciplines as a time-effective tool for collecting subsurface stratigraphic and structural information. GPR involves the transmission of high frequency (typically ranging from 10 MHz to 1000 MHz) electromagnetic pulses into the ground and the detection of signal energy reflected back to the surface from interfaces where there is a contrast in electrical properties.

Both the number of studies using GPR and the diversity of applications have grown dramatically in recent years, as the technology becomes more widely available. The utility of GPR for mapping peat deposits was recognized in the mid- to late 1970s, closely following the development of this technology (*cf.* Morey and French, 1977; Bogorodskii and Trepov, 1979; Finkel'shteyn, *et al.*, 1979). Since then, GPR-based peatland studies have primarily focused on continuous depth and stratigraphic profiling of peat deposits (Bjelm, 1980; Ulriksen, 1980; Remote Applications Inc., 1982; Baraniak, 1983; Worsfold, *et al.*, 1986; Meyer, 1989; Nobes, *et al.*, 1989; Pelletier, *et al.*, 1991; Hänninen, 1992a, b), although data regarding various peat properties have also been derived from GPR surveys (*e.g.*, Lowe, 1985; Warner, *et al.*, 1990; Morey and French, 1977).

GPR has also been used extensively for detection and mapping of permafrost (Scott, *et al.*, 1974; Annan, *et al.*, 1975; Annan and Davis, 1976; Seguin, *et al.*, 1989; Judge, *et al.*, 1991; Zhonggong, *et al.*, 1993), measurement of the active layer (Pilon, *et al.*, 1985; Doolittle, *et al.*, 1990), and delineation of massive ground ice (Dallimore and Davis, 1987; LaFleche, *et al.*, 1988; Moorman and Judge, 1989; Barry and Pollard, 1992; Robinson, *et al.*, 1992; Robinson, *et al.*, 1993) and pingo core ice (Kovacs and Morey, 1985).

It thus seems logical to extend the application of GPR to investigations of perennially frozen peatlands; however, few such studies have been undertaken to date (Doolittle, *et al.*, 1992; Pilon, *et al.*, 1992; Kettles and Robinson, 1996), and there has been little attempt to enhance the raw GPR data through processing techniques. Thus, an evaluation of the suitability of GPR techniques for investigations of peatlands, in particular those associated with perennially frozen ground, provides a timely and relevant contribution.

A review of the periglacial geomorphological literature highlights several theories regarding permafrost development and degradation in peatlands with respect to which GPR may prove a useful tool in future investigations. These potential applications are briefly described below in the context of the pertinent literature.

1.2 Potential Applications of GPR to Perennially Frozen Peatlands

The Lappish and Finnish term *palsa* was originally used to describe frozen-cored peaty hummocks occurring in bogs (Seppälä, 1972, 1988). Classic dome-shaped palsas typically

range from 0.5 m to over 7 m in height, 10 m to 30 m in width, and 15 m to 150 m in length (Seppälä, 1988). The term has also been applied to a range of perennially frozen landforms of varying morphology (*i.e.*, sinuous, complex, and plateau forms), consisting of peat and/or mineral sediment, and occurring within both the discontinuous and continuous permafrost zones. The present-day terminology is based largely on external morphology and suffers from a persistent lack of understanding of the relevant genetic processes.

Stratigraphic Evidence for Genesis

Seppälä (1988) described a model for development of a classic dome-shaped palsa which comprises the formation by ice segregation of a frozen core in peat which progressively penetrates deeper over time until it anchors in mineral sediment as a mature palsa (Figure 1-1). During this process, peat and mineral sediment layers are domed due to upward volume expansion upon freezing. The topographic expression of a palsa is attributable to this doming, in conjunction with buoyancy of the relatively lower density frozen peat (Zoltai, 1972).

Washburn (1983) argued that palsas may also develop as “similar-appearing degradation forms due to disintegration of an extensive peaty deposit” (*i.e.*, a peat plateau), a position supported by a number of workers (*e.g.*, Lagarec (1980, 1982) and Allard, *et al.* (1987) in Québec, P'yavchenko (1969) and Novikov and Usova (1979) in the Soviet Union). Peat plateaus are generally flat, perennially frozen peatlands elevated 1 m to 1.5 m above the surface of the surrounding fen or bog. They may range in extent from a few square metres to several square kilometres (Zoltai, 1972; Zoltai and Tarnocai, 1975; Seppälä, 1988). Permafrost in peat plateaus comprises segregated and pore ice, and may extend into underlying mineral soil (NRCC, 1988). Peat plateaus can be characterized by collapsing edges and thermokarst depressions (Zoltai, 1972).

Washburn (1983) acknowledged that these aggradational and degradational forms may be difficult to distinguish. Somr and King (1990) described a polygonal peat plateau comprised of individual contemporaneous, *aggradational* mounds, defined by polygonal desiccation, dilation, and/or thermal contraction cracks, but which may have a degraded appearance due to seasonal fluvial erosion through the polygonal trough network. Thus, it is clear that, based on analysis of the external form alone, the evolution of an individual or group of palsa(s) or palsa-scale frost mound(s) may be subject to a variety of interpretations.

However, Schunke (1981) (in Washburn, 1983) and Hinkel (1988) suggested genesis of palsa-scale frost mounds may be inferred from stratigraphic evidence. They suggested that the domed stratigraphy produced in an individual palsa mound by the classic ice segregation model of genesis (Figure 1-2) could be distinguishable from the truncated flat-lying stratigraphy that may be expected in individual mounds eroded from a previously more extensive flat-lying peat plateau (Figure 1-3). In this regard, GPR could potentially provide internal stratigraphic information from palsa-scale frost mounds, which may assist in determining their genesis.

Figure 1-1. Model of the formation of a dome-shaped palsa.

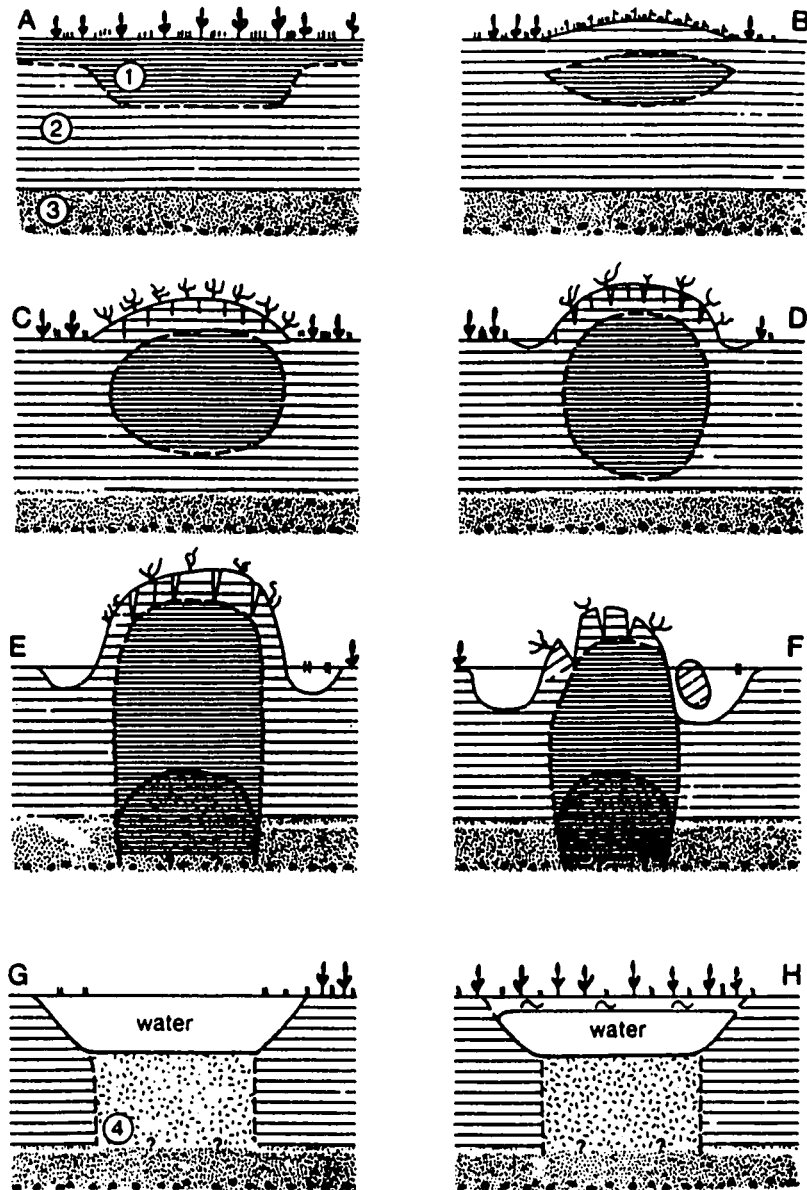
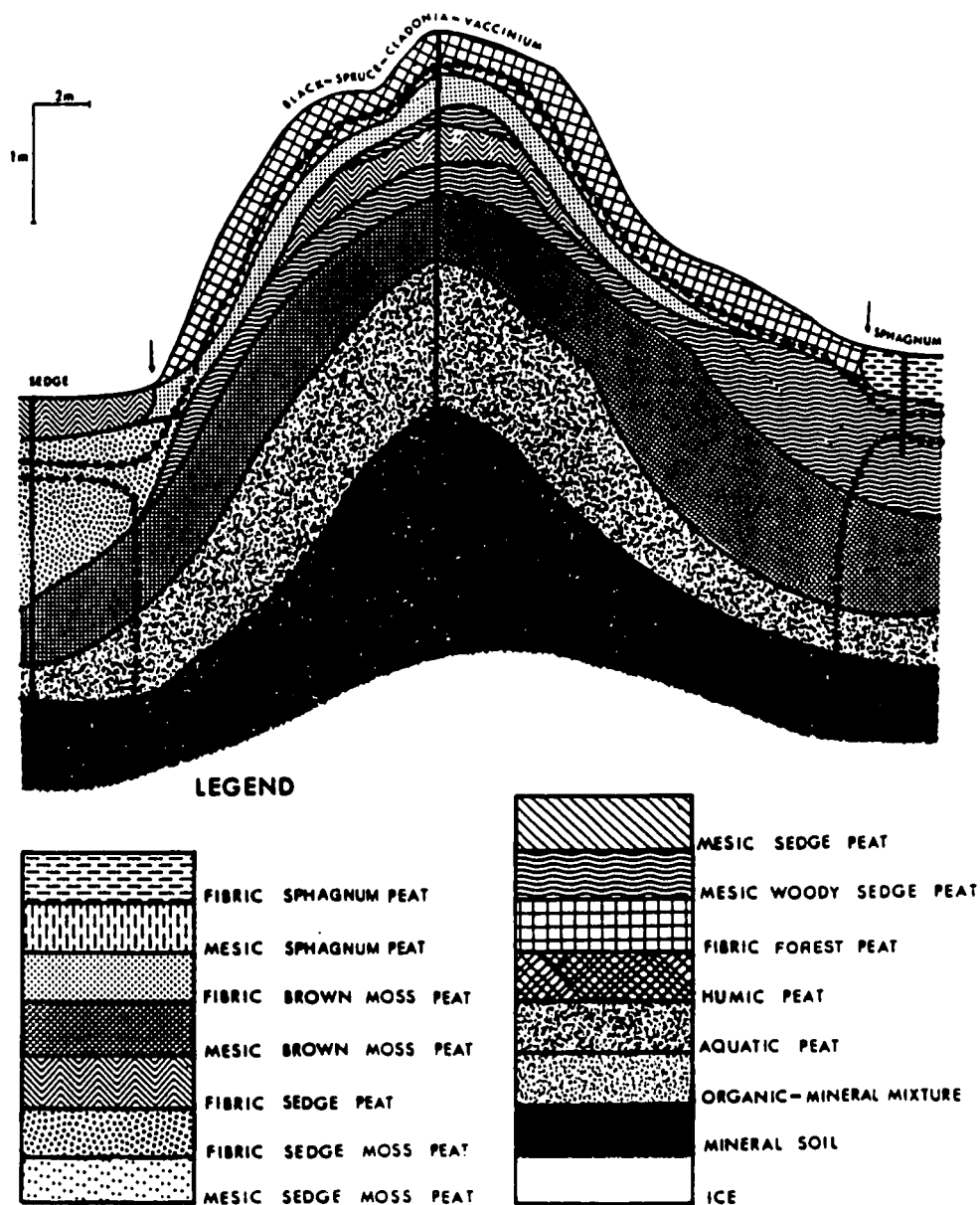


Figure shows successive stages (A to H) in Seppälä's general model of the formation of the frozen core (1) of a palsa in a mire (2) with a till substratum (3). A: The beginning of the thaw season. B: End of the first thaw season. C: Embryo palsa. D: Young palsa. E: Mature palsa. F: Old collapsing palsa surrounded by a large water body. G: Fully thawed palsa giving a circular pond on the mire: the thawed peat is decomposed (4). H: New peat formation starts in the pond.

Source: Palsas and related forms (Seppälä, 1988). In M.J. Clark, editor, *Advances in Periglacial Geomorphology*. Copyright (1988, John Wiley & Sons, Ltd.). Reprinted by permission of John Wiley & Sons, Ltd.

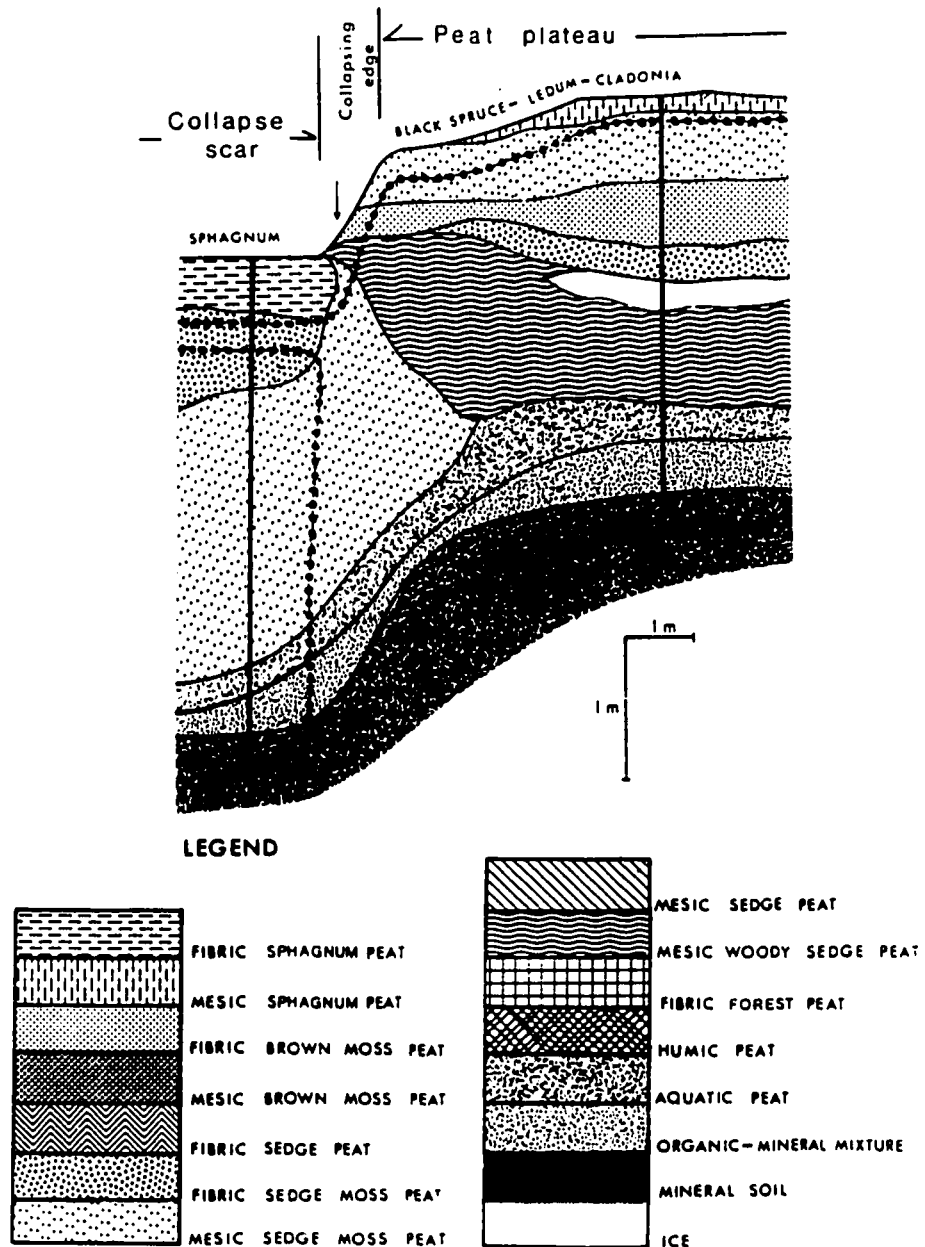
Figure 1-2. Stratigraphic cross-section of a dome-shaped palsa mound.



Note doming of individual peat strata conformable with external morphology. Palsa located at 67°06'N, 134°17'W.

Source: Perennially frozen peatlands in the western Arctic and subarctic of Canada (Zoltai and Tarnocai, 1975). *Canadian Journal of Earth Sciences* 12, 28-43. Copyright (1975, NRC Research Press). Reprinted by permission of National Research Council Research Press.

Figure 1-3. Stratigraphic cross-section of a peat plateau with collapsing edge.



Note truncated, flat-lying strata in elevated portion of peat plateau. Peat plateau located at 66°49'N, 135°21'W.

Source: Perennially frozen peatlands in the western Arctic and subarctic of Canada (Zoltai and Tarnocai, 1975). *Canadian Journal of Earth Sciences* 12, 28-43. Copyright (1975, NRC Research Press). Reprinted by permission of National Research Council Research Press.

Collapse Scars

When a palsa or peat plateau degrades, thawing of the frozen core leads to the eventual collapse of the peat to or below the level of the fen (Figure 1-1). It is reasonable to expect that the underlying peat stratigraphy will be disrupted relative to adjacent areas of peat that were not affected by permafrost. If a distinct stratigraphic signature associated with a collapsed palsa or peat plateau can be interpreted from the GPR results, the data could be used to delineate areas within a peatland where permafrost previously occurred. This may contribute to the determination of palsa mound genesis, where their development may, solely on the basis of external morphology, be alternatively attributed to degradation of a pre-existing more extensive peat plateau (Zoltai and Tarnocai, 1975; Lagarec, 1982) or to individual mound development by the classic ice segregation model (Seppälä, 1988).

Frost Bulb Delineation

Nelson, *et al.* (1992) suggested that palsas may be initiated and maintained by buoyancy, whereby the relatively low density of a layer of perennially frozen peat will cause it to 'float' within the wetland, thus giving it topographic expression. Incipient buoyant palsa forms were described by Zoltai (1972) and Allard, *et al.* (1987), and modelled by Outcalt and Nelson (1984). In contrast, Kershaw and Gill (1979) observed basal thaw in palsas and suggested it was symptomatic of overall degradation of the features. Irrespective of genetic mechanism, the size and shape of the frozen core of a palsa can reasonably be expected to change over the course of palsa development. For example, buoyant palsa forms may represent a phase in permafrost aggradation prior to 'anchoring' of the permafrost to the mineral substrate, as described above (Seppälä, 1988; Zoltai, 1972).

GPR could prove a useful tool in future investigations of the formative processes of palsas, if it can effectively map the interface between frozen and unfrozen peat at depth. In this way, spatial and temporal variations in the size and shape of the frozen core of a palsa or related feature could be monitored.

1.3 Objectives

The objectives of this thesis are:

- Objective 1:** to evaluate the suitability of GPR for investigation of perennially frozen peatlands (including stratigraphy and identification of frozen - unfrozen and peat - mineral sediment interfaces) and evaluation of genetic processes;
- Objective 2:** to evaluate available techniques for processing GPR data containing noise, weak signals, and diffraction patterns which may obscure the stratigraphy and limit the usefulness of the raw data; and
- Objective 3:** to apply GPR, supplemented with conventional techniques, to characterize and compare trends in palsa evolution at two palsa fens in northern Canada.

These objectives, and the techniques employed to achieve them, are further discussed below.

Objective 1: To evaluate the suitability of GPR for investigation of perennially frozen peatlands (including stratigraphy and identification of frozen - unfrozen and peat - mineral sediment interfaces) and evaluation of genetic processes.

Despite the recent rapid growth in the popularity of GPR for field studies in a wide range of disciplines, the technique has not been subjected to a rigorous methodological review, particularly with respect to its suitability for permafrost research in organic soils. Thorn (1988:5) noted that “a ‘sophisticated’ technique applied inappropriately is neither sophisticated nor powerful.” It is important, therefore, not only to evaluate GPR with respect to its usefulness for the intended application, but also to develop expertise with the use of the technique to avoid inappropriate application or interpretation. Given the lack of treatment in the literature, an evaluation of GPR techniques for investigating peatlands, particularly those which are perennially frozen, would be a timely and relevant contribution.

To meet this objective, an assessment of potential applications of GPR in perennially frozen peatlands was undertaken on the basis of a review of:

- available literature pertaining to GPR applications in peatlands;
- relevant theoretical geophysical principles; and
- analysis of data compiled from field trials.

Chapter 2 contains a review of pertinent literature, while an overview of GPR principles is provided in Appendix A. Methods of data compilation, processing, analysis, and interpretation are examined in greater detail in Chapter 3.

Objective 2: To evaluate available techniques for processing GPR data containing noise, weak signals, and diffraction patterns which may obscure the stratigraphy and limit the usefulness of the raw data.

GPR is analogous to seismic exploration techniques, as in each of these techniques the signal wave propagates and attenuates through earth media at velocities controlled by the material properties, and is reflected at local electric and elastic discontinuities, respectively (Fisher, *et al.*, 1992a; Majjala, 1992). The similarities between propagation of electromagnetic (EM) and acoustic (seismic) waves in earth materials suggests that data processing techniques developed for analysis of seismic data, such as deconvolution and migration, can successfully be applied to GPR data; however, few such studies have been undertaken (Hogan, 1988; LaFleche, *et al.*, 1991; Majjala, 1992; Fisher, *et al.*, 1992a, b; Fisher, *et al.*, 1994).

In addition to the basic data processing tools incorporated within currently available GPR systems, this study tested a variety of advanced data processing techniques developed for seismic data, to evaluate their effectiveness in enhancing image quality and improving ease of GPR data interpretation. The results of this analysis, which was based on GPR data compiled from two peatland sites specifically for this thesis, are presented in Chapter 3.

Objective 3: To apply GPR, supplemented with conventional techniques, to characterize and compare trends in palsa evolution at two palsa fens in northern Canada.

To achieve a more reliable and meaningful evaluation of the suitability of GPR for this application, a study of GPR effectiveness in theory must be complemented with an assessment of its efficacy in practice. Thus, two case studies from palsa fen sites are presented, in which analysis and interpretation of the GPR data have been supplemented with conventional field study techniques. The latter include: analysis of aerial photographs; field measurements of surface morphology; coring of frozen and unfrozen peat; and review of available literature and historical records.

The data were examined to identify contemporary, as well as spatial and temporal variations in, stratigraphic and morphologic characteristics of the palsas and peatlands which may reflect genetic and/or degradational processes. Specific problems considered in this regard include the following.

- Does the historic and contemporary surface and subsurface morphology of the palsas corroborate Kershaw and Gill's (1979) observations of permafrost degradation at the sites?
- Do the palsas at the two sites have a consistent and comparable trend towards degradation over the period of record (50 years)?
- Are the contemporary palsa morphology and characteristics of the peatland/fen compatible with aggradation of the features as individual mounds vs. degradation from a more extensive peat plateau?

1.4 Description of the Study Area

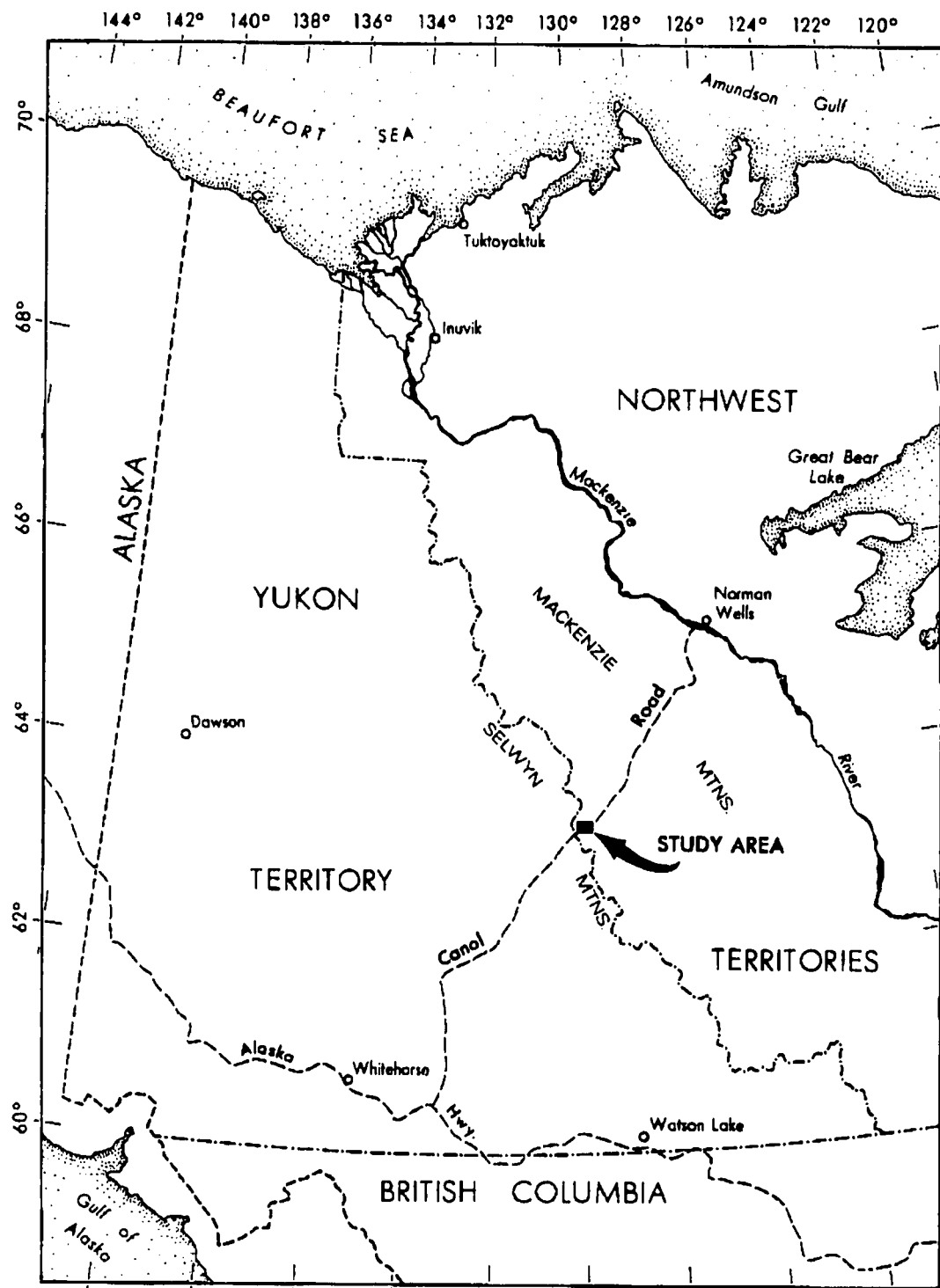
Field studies in support of this thesis were carried out at two palsa fens located in the Macmillan Pass area of the Selwyn Mountains, Northwest Territories (Figures 1-4 and 1-5).

1.4.1 Regional description

The study area is characterized by rugged alpine terrain within the zone of widespread discontinuous permafrost (NRCC, 1988). The distribution of permafrost appears to be limited to high elevations, palsa fens and peat plateaus at lower elevations, and few isolated sites with locally favourable conditions. The area is underlain by folded and faulted Proterozoic and Paleozoic metamorphosed sedimentary and intrusive granitic rocks (Gill, 1975). Wetlands occur in low-lying basins, and although common, are not extensive in area. Organic deposits reaching over 5 m thickness occur in the wetlands (Skaret, 1995).

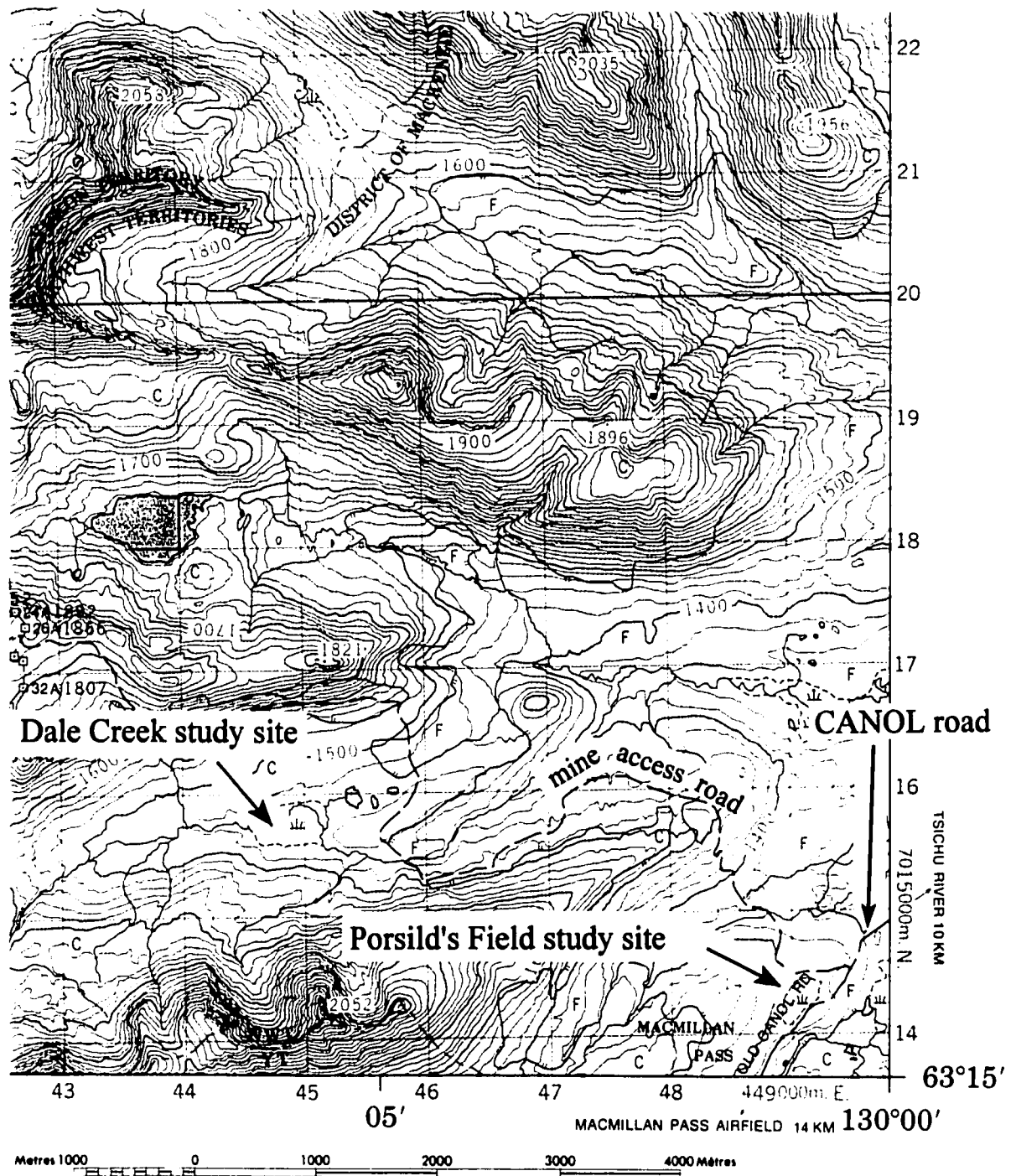
The study area lies above the timberline, although isolated krummholz stands of fir and spruce occur in sheltered locations at low elevations. Vegetation is characteristic of arctic/alpine tundra, and ranges from predominantly lichen communities at high elevations, and on slopes and exposed areas, to mixed lichen-grass, lichen-shrub, and shrub-moss communities at

Figure 1-4. Study area location map.



Source: G. Lester, Department of Earth and Atmospheric Sciences (formerly Department of Geography), University of Alberta.

Figure 1-5. Location of Porsild's Field and Dale Creek peatland study sites.



Map scale 1:50,000. Contour interval 20 metres.

Source: Keele Peak, Sheet 105-O/8, Surveys and Mapping Branch, Department of Energy, Mines and Resources, Ottawa, 1982.

various elevations, to extensive shrub-dominated communities at lower elevations (Kershaw and Kershaw, 1983).

The study area is located within an alpine continental climatic regime (Kershaw, 1983). Climatic data for the study area are limited, however, as there have been no long-term, continuously reporting meteorological stations established in the vicinity. Climatic data collected by AMAX Northwest Mining Company Ltd. between October, 1974, and August, 1982, from the Tsichu River station were summarized by Kershaw and Kershaw (1983). This recording station was located approximately 10 km to 15 km east of the study sites, at an elevation of approximately 1280 m, and was situated within the broad, relatively flat-bottomed valley of the Tsichu River. During the recording period, the mean annual air temperature was -7.7°C , and mean annual total precipitation was 490 mm (water equivalent). Snow was recorded in all months. Mean daily temperatures were above freezing from May to September, and maximum precipitation occurs between July and October. No data for wind speed or direction were compiled. More recent microclimate data indicate that the mean annual air temperature from a 1250 m elevation site several kilometres east of the Tsichu River station was only 0.7°C cooler than the mean annual air temperature at the Dale Creek site (-6.7°C), approximately 15 km to the west, for the one-year record analysed (August, 1990, to July, 1991) (Kershaw and Skaret, 1993).

1.4.2 Site descriptions

The study sites were selected on the basis of their accessibility (particularly with respect to the GPR equipment), available aerial photographic and historical records, proximity to one another, and treatment in the literature.

Porsild's Field

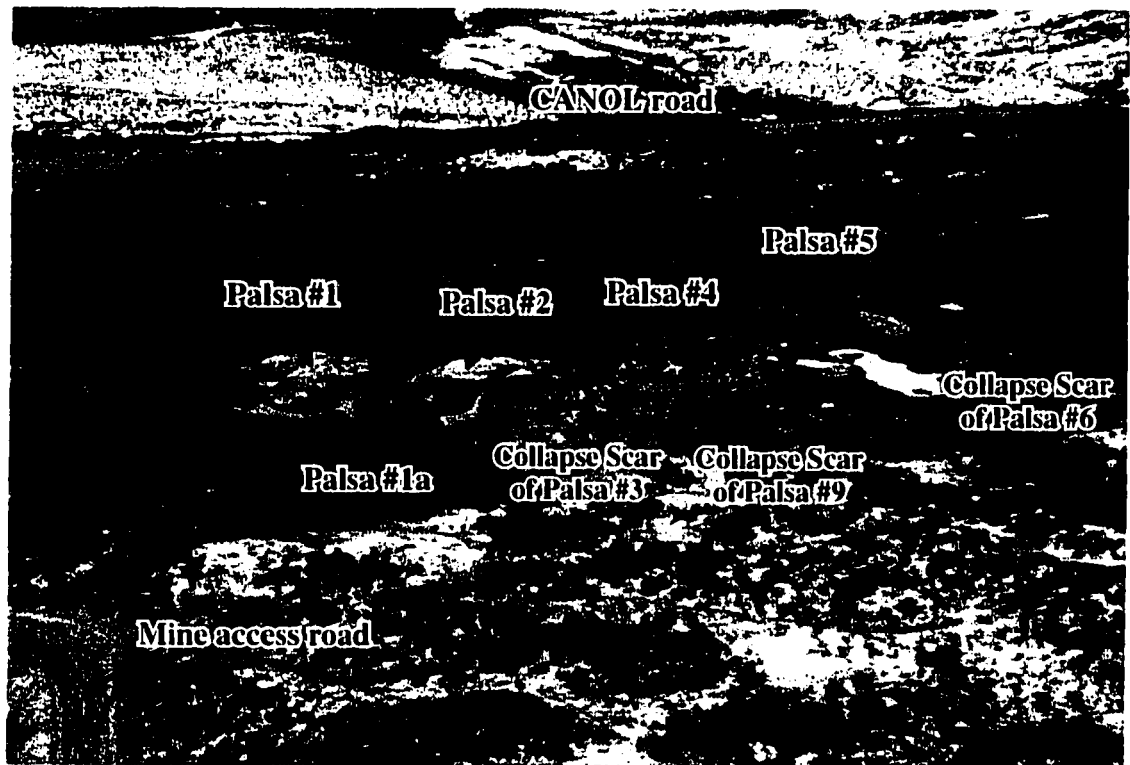
The Porsild's Field study site, so named for its earliest description by Porsild (1945, 1951), is located in Macmillan Pass, adjacent to the CANOL road, at an elevation of approximately 1390 m asl ($63^{\circ}15'15''\text{N}$, $130^{\circ}01'05''\text{W}$). The pass is oriented approximately ENE-WSW, parallel to the direction of prevailing winds, and thus functions as an effective wind gap (Gill, 1975; Kershaw and Kershaw, 1983).

At this site, there were six separate palsa mounds (Plate 1-1) in 1994, although it is clear from available records that the mounds were more numerous in the past (Kershaw and Gill, 1979). The palsas ranged in height from 0.8 m to 2.5 m above the fen, with long axes ranging from *ca.* 10.5 m to *ca.* 39 m.

The CANOL road is located immediately south of the fen. On the northern, western, and eastern edges of the fen, the land surface slopes gently upward, away from the fen. The access road to the Dale Creek study site is located near the eastern edge of the fen; however, it does not impinge on the fen.

Shrub-dominated communities bordered the fen, while *Carex aquatilis* and *Eriophorum* spp. and mosses were predominant in the fen, and lichen-moss (*Cladina* spp./*Cetraria*

Plate 1-1. Porsild's Field study site.



Aerial view of five extant palsas at Porsild's Field, as well as collapse scars of pre-existing palsas known from historic records. (Palsa #7, not shown, is located to the west (right) of palsa #5.) The CANOL road passes east to west adjacent to the fen. The access road to the MacTung mine property is visible at the lower left. South is at the top of the photograph. Photo taken July 22, 1994.

Photo credit: Stephen D. Robinson, McGill University.

spp./*Polytrichum* spp.) dominated the palsa surfaces. A few low (*ca.* 40 cm) shrubs (*Betula glandulosa*) occur on palsa #5. Bare peat occurred on deflated palsa surfaces and edges. Slumping and ground squirrel burrowing also exposed peat on palsa margins.

Dale Creek

The Dale Creek study site is located in a neighbouring valley 4 km to the northwest of the Porsild's Field study site (63° 16' 15" N, 130° 06' 00" W), at an elevation of approximately 1470 m asl. This valley is also oriented approximately ENE-WSW, parallel to the direction of prevailing winds (Gill, 1975; Kershaw and Kershaw, 1983).

At this site, five simple dome-shaped palsas and one complex palsa, consisting of several smaller mounds joined by lower saddle areas, were present (Plate 1-2). For this study, data were collected from the simple palsa forms only, as deep and/or broad areas of open water curtailed GPR access to the complex feature. The five palsas which were studied ranged in height from 1.35 m to 3.0 m above the surface of the fen, and in diameter from *ca.* 16.5 m to *ca.* 47.5 m.

Immediately to the south of the fen, the land surface slopes gently upward at less than 10° over bedrock, diamict, and colluvium. To the north and west, the ground surface is flat and slightly above the level of the fen. The fen drains eastward into Dale Creek.

Vegetation on the five palsas that were studied was similar to the Porsild's Field site, although bare peat was usually restricted to the edges of the palsas, where the peat was cracked, slump blocks were present, and ground squirrel burrowing was extensive, particularly on the higher palsas and on their east and southeast sides.

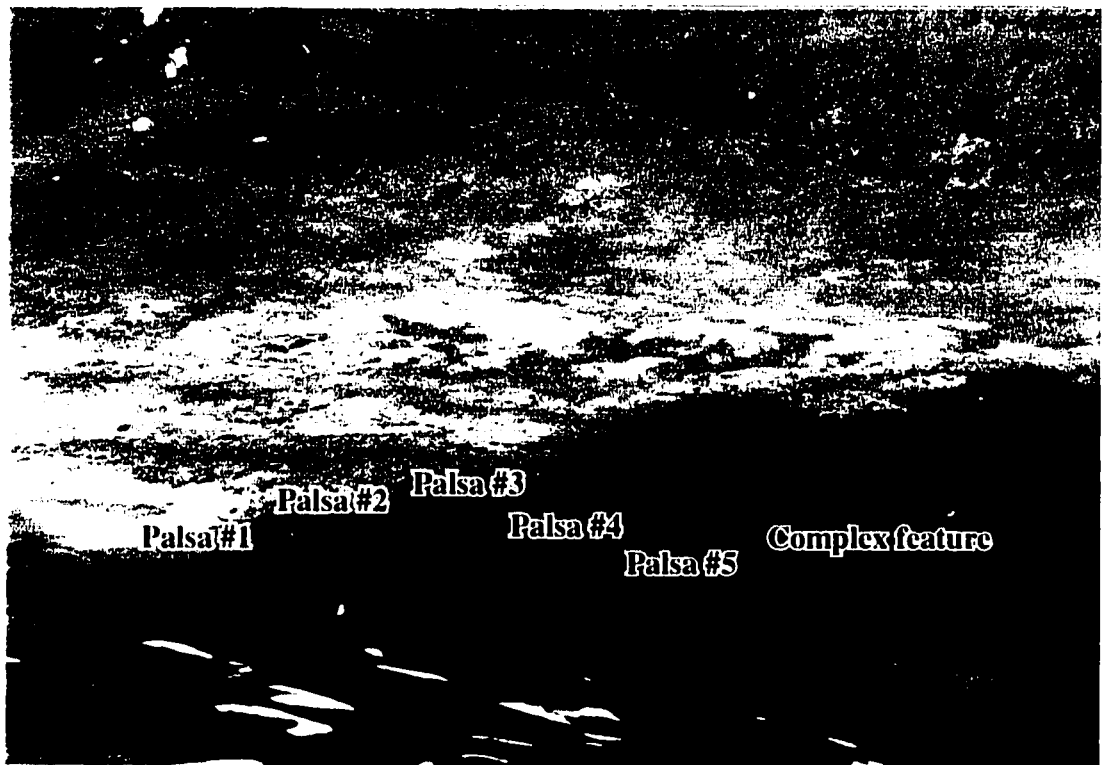
1.5 Organization of the Thesis

This chapter comprises an introductory chapter to the thesis, and describes the rationale, objectives, and methodology of the study. A description of the study area is also provided.

Chapter 2 (Manuscript 1) comprises an assessment of GPR techniques for peatland investigations, particularly with respect to perennially frozen peatlands; a review of literature pertaining to similar GPR applications and to relevant geophysical principles forms the basis for this evaluation. Chapter 3 (Manuscript 2) presents raw and processed GPR data, analyses, and interpretation for the two palsa fen sites, and includes an evaluation of the effectiveness of available processing techniques. Chapter 4 (Manuscript 3) includes an evaluation of observable trends in palsa development at the two sites, based on analysis and interpretation of data from GPR and conventional techniques, and an evaluation of the contribution of GPR to investigation of palsa evolution. Chapter 5 comprises a general Summary and Conclusions chapter.

Appendix A provides a theoretical review of the principles of GPR for the benefit of those readers unfamiliar with the technique. Appendix B documents observations of peat characteristics in cores taken from each site. Appendix C summarizes area calculations for

Plate 1-2. Dale Creek study site.



Aerial view showing five simple dome-shaped palsas and one complex feature consisting of several smaller mounds joined by lower saddle areas, at Dale Creek study site. North is at the top of the photograph. Photo taken July 6, 1994.

the palsas derived from time-sequence aerial photographs. Appendix D provides thaw depth measurements taken along the GPR transects at the time of the radar surveys. Appendix E provides letters of copyright permission.

1.6 Literature Cited

- Allard, M., Seguin, M.K. and Lévesque, R. 1987. Palsas and mineral permafrost mounds in northern Québec. In Gardiner, V., editor, *International Geomorphology 1986 Part II*, John Wiley & Sons Ltd., Chichester, England, 285-309.
- Annan, A.P. and Davis, J.L. 1976. Impulse radar sounding in permafrost. *Radio Science* 11 (4), 383-394.
- Annan, A.P., Davis, J.L. and Scott, W.J. 1975. Impulse radar profiling in permafrost. In *Report of Activities, Part C. Geological Survey of Canada Paper 75-1C*, 343-351.
- Baraniak, D.W. 1983. Exploration for surface peat deposits using ground penetrating radar. In Fuchsman, C.H. and Spigarelli, S.A., editors, *Proceedings, International Symposium on Peat Utilization*, Bemidji, Minnesota: Bemidji State University, 105-121.
- Barry, P.J. and Pollard, W.H. 1992. Ground penetrating radar investigations of ground ice on the Fosheim Peninsula, Ellesmere Island, Northwest Territories. In *Proceedings of the Third National Student Conference on Northern Studies*, Ottawa, Ontario: Musk-ox Special Publication 39, 59-66.
- Bjelm, L. 1980. Geological interpretation with subsurface interface radar in peatlands. In *Proceedings, 6th International Peat Congress*, Duluth, Minnesota: International Peat Society, 7-8.
- Bogorodskii, V.V. and Trepov, G.V. 1979. Radar measurements of the thickness of peat and sapropel beds. *Soviet Physics, Technical Physics* 24 (3), 388-390.
- Dallimore, S.R. and Davis, J.L. 1987. Ground probing radar investigations of massive ground ice and near surface geology in continuous permafrost. In *Current Research, Part A. Geological Survey of Canada Paper 87-1A*, 913-918.
- Doolittle, J.A., Hardisky, M.A. and Black, S. 1992. A ground-penetrating radar study of Goodream palsas, Newfoundland, Canada. *Arctic and Alpine Research* 24 (2), 173-178.
- Doolittle, J.A., Hardisky, M.A. and Gross, M.F. 1990. A ground-penetrating radar study of active layer thicknesses in areas of mist sedge and wet sedge tundra near Bethel, Alaska, U.S.A. *Arctic and Alpine Research* 22 (2) 175-182.
- Finkel'shteyn, M.I., Kutev, V.A., Vlasov, O.P., Strekalkin, Ye.A. and Bogatyrev, Ye.F. 1979. Radar subsurface probing of peaty soil. *Doklady Akademii Nauk SSSR, Earth Sciences Sections* 247 (1), 24-26.

- Fisher, E., McMechan, G.A., and Annan, A.P. 1992a. Acquisition and processing of wide-aperture ground-penetrating radar data. *Geophysics* 57, 495-504.
- Fisher, E., McMechan, G.A., Annan, A.P. and Cosway, S.W. 1992b. Examples of reverse-time migration of single-channel, ground penetrating radar profiles. *Geophysics* 57, 577-586.
- Fisher, S.C., Stewart, R.R. and Jol, H.M. 1994. Processing ground penetrating radar data. In *GPR '94, Proceedings of the Fifth International Conference on Ground Penetrating Radar*, Kitchener, Ontario: Waterloo Centre for Groundwater Research and Canadian Geotechnical Society, 2, 661-675.
- Gill, D. 1975. *Cirque Lake I.B.P. Study Area*. Environmental Services Group, AMAX Northwest Mining Co. Ltd., Vancouver, B.C. (139p.).
- Hänninen, P. 1992a. *Application of ground penetrating radar and radio wave moisture probe techniques to peatland investigations*. Geological Survey of Finland, Bulletin 361 (71p.).
- Hänninen, P. 1992b. Application of ground penetrating radar techniques to peatland investigations. In Hänninen, P. and Autio, S., editors, *Fourth International Conference on Ground Penetrating Radar*, Rovaniemi, Finland: Geological Survey of Finland, Special Paper 16, 217-221.
- Hinkel, K.M. 1988. Frost mounds formed by degradation at Slope Mountain, Alaska, USA. *Arctic and Alpine Research* 20, 76-85.
- Hogan, G. 1988. Migration of ground penetrating radar data: a technique for locating subsurface targets. In Fitterman, D., Bell, R., Corbett, J., Davenport, C., Hulse, S., and Bierley, C., editors, *Proceedings of the Symposium on the Application of Geophysics to Engineering and Environmental Problems*, Society of Engineering and Mineral Exploration Geophysicists: United States Geological Survey, 809-822.
- Judge, A.S., Tucker, C.M., Pilon, J.A. and Moorman, B.J. 1991. Remote sensing of permafrost by ground-penetrating radar at two airports in Arctic Canada. *Arctic* 44, Supp. 1, 40-48.
- Kershaw, G.P. 1983. *Long-term ecological consequences in tundra environments of the CANOL Crude Oil Pipeline Project, N.W.T., 1942-1945*. Ph.D. Thesis, Department of Geography, University of Alberta, Edmonton, Alberta.
- Kershaw, G.P. and Gill, D. 1979. Growth and decay of palsas and peat plateaus in the Macmillan Pass - Tsichu River area, Northwest Territories, Canada. *Canadian Journal of Earth Sciences* 16 (7), 1362-1374.

- Kershaw, G.P. and Kershaw, L.J. 1983. *Geomorphology and vegetation of the MacTung study area, Yukon/N.W.T.* AMAX Northwest Mining Co. Ltd., Vancouver, B.C. (106p.).
- Kershaw, G.P. and Skaret, K.D. 1993. Microclimatic characteristics of palsas along an altitudinal gradient, Mackenzie Mountains, NWT, Canada. In *Permafrost, Sixth International Conference, Proceedings*, South China University of Technology Press, 1, 338-343.
- Kettles, I.M. and Robinson, S.D. 1996. A ground-penetrating radar study of peat landforms in the discontinuous permafrost zone near Fort Simpson, Northwest Territories, Canada. In Trettin, C., M. Jurgenson, D. Grigal, M. Gale and J. Jeglum, editors, *Northern Forested Wetlands: Ecology and Management*, CRC, Lewis Publishers, Boca Raton, Florida, 147-160.
- Kovacs, A. and Morey, R.M. 1985. Impulse radar sounding of frozen ground. In Brown, J., Metz, M.C., and Hoekstra, P., editors, *Workshop on Permafrost Geophysics*, Golden, Colorado: United States Army Cold Regions Research and Engineering Laboratory, Special Report 85-5, 28-40.
- LaFleche, P.T., Judge, A.S., Moorman, B.J., Cassidy, B. and Bedard, R. 1988. Ground probing radar investigations of gravel roadbed failures, Rae Access road, N.W.T. In *Current Research, Part D. Geological Survey of Canada Paper 88-1D*, 129-135.
- LaFleche, P.T., Todoeschuck, J.P., Jensen, O.G. and Judge, A.S. 1991. Analysis of ground-probing radar data: predictive deconvolution. *Canadian Geotechnical Journal* 28, 134-139.
- Lagarec, D. 1980. *Étude géomorphologie de paises et autres buttes cryogènes en Hudsonie (Nouveau-Québec)*. Ph.D. thesis, Université Laval.
- Lagarec, D. 1982. Cryogenetic mounds as indicators of permafrost conditions, northern Québec. In *Proceedings of the Fourth Canadian Permafrost Conference*. National Research Council of Canada, Ottawa, 43-48.
- Lowe, D.J. 1985. Application of impulse radar to continuous profiling of tephra-bearing lake sediments and peats: an initial evaluation. *New Zealand Journal of Geology and Geophysics* 28, 667-674.
- Maijala, P. 1992. Application of some seismic data processing methods to ground penetrating radar data. In Hänninen, P. and Autio, S., editors, *Fourth International Conference on Ground Penetrating Radar*, Rovaniemi, Finland: Geological Survey of Finland, Special Paper 16, 103-110.

- Meyer, J.H. 1989. Investigation of Holocene organic sediments - a geophysical approach. *International Peat Journal* 3, 45-57.
- Moorman, B.J. and Judge, A.S. 1989. Delineating massive ice with ground penetrating radar. In *Program with Abstracts, Geological Association of Canada* 14, A76.
- Morey, R.M. and French, R.B. 1977. Mapping peat cover and shallow, discontinuous permafrost using impulse radar. *Geophysics* 42 (7), 1526.
- Nelson, F.E., Hinkel, K.M. and Outcalt, S.I. 1992. Palsa-scale frost mounds. In Dixon, J.C. and A.D. Abrahams, editors, *Periglacial Geomorphology, Proceedings of the 22nd Annual Binghampton Symposium in Geomorphology*, John Wiley & Sons, Chichester, 305-325.
- Nobes, D.C., Theimer, B.D. and Warner, B.G. 1989. Grant 310, Subsurface radar profiling of two peatlands in southern Ontario. In *Geoscience Research Grant Program; summary of research 1988-1989, Ontario Geological Survey, Miscellaneous Paper*, 53-58.
- Novikov, S.M. and Usova, L.I. 1979. Nature and classification of palsa bogs. *Soviet Hydrology, Selected Papers* 18, 109-113.
- NRCC (National Research Council of Canada). 1988. *Glossary of permafrost and related terms*. Permafrost Subcommittee, Associate Committee on Geotechnical Research, National Research Council of Canada, Ottawa, Technical Memorandum No. 142.
- Outcalt, S.I. and Nelson, F. 1984. Computer simulation of buoyancy and snow-cover effects in palsa dynamics. *Arctic and Alpine Research* 16 (2), 259-263.
- Pelletier, R.E., Davis, J.L. and Rossiter, J.R. 1991. Peat analyses in the Hudson Bay Lowlands using ground penetrating radar. In Putkonen, J., editor, *Remote Sensing: Global Monitoring for Earth Management; International Geoscience and Remote Sensing Symposium, Proceedings*, Volume IV, Espoo, Finland: Helsinki University of Technology, 2141-2144.
- Pilon, J.A., Allard, M. and Séguin, M.K. 1992. Ground probing radar in the investigation of permafrost and subsurface characteristics of surficial deposits in Kangiqsualujjuaq, northern Québec. In Pilon, J.A., editor, *Ground penetrating radar*, Ottawa, Ontario: Geological Survey of Canada, Paper 90-94, 41-48.
- Pilon, J.A., Annan, A.P. and Davis, J.L. 1985. Monitoring permafrost ground conditions with ground probing radar. In Brown, J., Metz, M.C., and Hoekstra, P., editors, *Workshop on Permafrost Geophysics*, Golden, Colorado: United States Army Cold Regions Research and Engineering Laboratory, Special Report 85-5, 71-73.

- Porsild, A.E. 1945. *The alpine flora of the east slope of Mackenzie Mountains, Northwest Territories*. Canada Department of Mines and Resources, Mines and Geology Branch. National Museum of Canada, Bulletin No. 101 (Biological Series No. 30) (35p.).
- Porsild, A.E. 1951. *Botany of southeastern Yukon adjacent to the Canol Road*. Canada Department of Resources and Development, National Parks Branch. National Museum of Canada, Bulletin No. 121 (Biological Series No. 41) (400p.).
- P'yavchenko, N.I. 1969. *Swampy forests and bogs of Siberia (Zabolochnennyye lesa i bolota Sibiri)*. U.S. Army Foreign Science and Technology Centre technical translation, FSTC-HT-23-310-70 (215p.).
- Remote Applications Inc. 1982. *The use of impulse radar techniques for depth profiling of peat deposits*. National Research Council of Canada, Division of Energy Research and Development, Ottawa, Ontario.
- Robinson, S.D., Moorman, B.J., Judge, A.S. and Dallimore, S.R. 1993. The characterization of massive ground ice at Yaya Lake, Northwest Territories using radar stratigraphy techniques. In *Current Research, Part B. Geological Survey of Canada Paper 93-1B*, 23-32.
- Robinson, S.D., Moorman, B.J., Judge, A.S., Dallimore, S.R. and Shimeld, J.W. 1992. The application of radar stratigraphic techniques to the investigation of massive ground ice at Yaya Lake, Northwest Territories. In *Proceedings of the Third National Student Conference on Northern Studies*, Ottawa, Ontario: Musk-ox Special Publication 39, 39-49.
- Schunke, E. 1981. Zur kryogenen Bodendynamik der arktischen Tundren Nordamerikas und Nordeuropas. *Polarforschung* 51, 161-174.
- Scott, W.J., Campbell, K.J. and Orange, A.S. 1974. EM pulse survey method in permafrost. In Collett, L.C. and Brown, R.J.E., editors, *Proceedings of a Symposium on Permafrost Geophysics*, Ottawa, Ontario: National Research Council of Canada, Associate Committee on Geotechnical Research, Technical Memorandum 113, 92-96.
- Seguin, M.K., Allard, M., Pilon, J., Lévesque, R. and Fortier, R. 1989. Geophysical detection and characterization of ground ice in northern Québec. In *Program with Abstracts, Geological Association of Canada* 14, A76.
- Seppälä, M. 1972. The term 'palsa'. *Zeitschrift für Geomorphologie* 16, 463.
- Seppälä, M. 1988. Palsas and related forms. In M.J. Clark, editor, *Advances in Periglacial Geomorphology*. John Wiley & Sons, Chichester, 247-278.

- Skaret, K.D. 1995. Stratigraphic, microclimatic and thawing attributes associated with palsas located in the alpine tundra environment of the Macmillan Pass - Tsichu River region, N.W.T., Canada. M.Sc. Thesis, Department of Geography, University of Alberta, Edmonton, Alberta.
- Somr, C.H. and King, R.H. 1990. Origin of polygonal peat plateaus under conditions of continuous permafrost, Truelove Lowland, Devon Island, N.W.T. In *Permafrost-Canada: Proceedings of the Fifth Canadian Permafrost Conference*. Université Laval, Centre d'études nordiques. Collection Nordicana No. 54, 11-16.
- Thorn, C.E. 1988. *An introduction to theoretical geomorphology*. Unwin Hyman, Boston (247p.).
- Ulriksen, C.P.F. 1980. Investigation of peat thickness with radar. In *Proceedings, 6th International Peat Congress*, Duluth, Minnesota: International Peat Society, 126-129.
- Warner, B.G., Nobes, D.C. and Theimer, B.D. 1990. An application of ground penetrating radar to peat stratigraphy of Ellice Swamp, southwestern Ontario. *Canadian Journal of Earth Sciences* 27, 932-938.
- Washburn, A.L. 1983. What is a palsa? In *Abhandlungen der Akademie der Wissenschaften in Göttingen, Mathematisch-Physikalische Klasse* 35, 34-47.
- Worsfold, R.D., Parashar, S.K. and Perrott, T. 1986. Depth profiling of peat deposits with impulse radar. *Canadian Geotechnical Journal* 23, 142-154.
- Zhonggong, Z., Yizhi, H. and Zhiying, X. 1993. Use of ground penetrating radar for the detection of permafrost and delineation of its distribution under the asphalted road of Qinghai-Xizang highway. In *Permafrost, Sixth International Conference, Proceedings*, Volume I, Beijing, China: South China University of Technology Press, 758-763.
- Zoltai, S.C. 1972. Palsas and peat plateaus in central Manitoba and Saskatchewan. *Canadian Journal of Forest Research* 2, 291-302.
- Zoltai, S.C. and Tarnocai, C. 1975. Perennially frozen peatlands in the western arctic and subarctic of Canada. *Canadian Journal of Earth Sciences* 12, 28-43.

2.0 A REVIEW OF GROUND PENETRATING RADAR APPLICATIONS FOR INVESTIGATION OF PERENNIALY FROZEN PEATLANDS

2.1 Introduction

Ground penetrating radar (GPR) provides two- and three-dimensional subsurface stratigraphic and structural information from a variety of earth media in a manner analogous to seismic techniques. GPR involves the transmission of high frequency (typically ranging from 10 MHz to 1000 MHz) electromagnetic pulses into the ground and the detection of signal energy reflected back to the surface from interfaces where there is a contrast in electrical properties. This contrast may be caused by a change in moisture content, density, composition (*i.e.*, organic *vs.* mineral sediment), or temperature (Annan, 1992; Theimer, *et al.*, 1994:182). A continuous profile of subsurface interfaces with electrical contrast is produced by plotting the two-way travel time of the reflected energy against antennae position at successive points along a survey transect. Inferences may then be made regarding what each interface represents, based on the nature of the reflected energy, and on point verification by coring. A detailed treatment of GPR principles is beyond the scope of this report; the reader is referred to Davis and Annan (1989), Arcone (1984), and Annan (1992). An overview of GPR principles is provided in Appendix A.

Commonly available GPR systems are portable, and consist of an operating console and portable computer, battery power source, and transmitting and receiving antennae, connected by fibre optic cables. Interchangeable antennae of various frequencies allow flexibility in survey design according to subsurface material and target characteristics; greater subsurface resolution is provided by higher frequency antennae, at the expense of reduced signal penetration depth (Annan and Davis, 1976; Davis and Annan, 1989; Robinson, *et al.*, 1992). Data are recorded digitally, allowing processing techniques such as topographic correction, noise reduction filters, and signal gain for compensation of signal attenuation to be applied. Moreover, data are acquired in real time, allowing the surveyor to review the data in the field and make adjustments to the survey configuration as necessary to optimize the results.

These features have contributed to the recent, rapid growth in GPR applications in a wide range of disciplines. The technique has been used for applications as diverse as: detection of buried pipes, drums, and barrels (Scaife, *et al.*, 1990); fracture mapping (Benson and Yuhr, 1990) and mine hazard detection (Foss and Leckenby, 1987); delineation of groundwater contamination plumes (Clasen, 1989); archaeological investigations (Toshioka, *et al.*, 1990); and pavement evaluation (Laug, *et al.*, 1992). Its use in geomorphological studies has included: mapping of sediment stratigraphy and thickness; freshwater bathymetry (Annan and Davis, 1977); sinkhole mapping (Clasen, 1989); and soil variability (Collins and Doolittle, 1987).

The utility of GPR for mapping peat deposits was recognized in the mid- to late 1970s, closely following the development of this technology (*cf.* Morey and French, 1977; Bogorodskii and Trepov, 1979; Finkel'shteyn, *et al.*, 1979). Since then, GPR-based peatland studies have focused on continuous depth and stratigraphic profiling of peat deposits (Bjelm,

1980; Ulriksen, 1980; Remote Applications Inc., 1982; Baraniak, 1983; Worsfold, *et al.*, 1986; Meyer, 1989; Nobes, *et al.*, 1989; Pelletier, *et al.*, 1991; Hänninen, 1992a, b), although data regarding moisture content, bulk density, mineral sediment characteristics, acrotelm-catotelm boundary¹, position of buried wood and stumps, and depth of seasonal freezing have also been derived from GPR surveys (*e.g.*, Lowe, 1985; Warner, *et al.*, 1990; Morey and French, 1977).

GPR has also been used extensively for detection and mapping of permafrost (Scott, *et al.*, 1974; Annan, *et al.*, 1975; Annan and Davis, 1976; Seguin, *et al.*, 1989; Judge, *et al.*, 1991; Zhonggong, *et al.*, 1993), measurement of the active layer (Pilon, *et al.*, 1985; Doolittle, *et al.*, 1990), and delineation of massive ground ice (Dallimore and Davis, 1987; LaFleche, *et al.*, 1988; Moorman and Judge, 1989; Barry and Pollard, 1992; Robinson, *et al.*, 1992; Robinson, *et al.*, 1993) and pingo core ice (Kovacs and Morey, 1985).

It thus seems logical to extend the application of GPR to investigations of perennially frozen peatlands; however, few such studies have been undertaken to date (Doolittle, *et al.*, 1992; Pilon, *et al.*, 1992; Kettles and Robinson, 1996). The purpose of this paper is to review the potential uses of GPR in this environment, based on a review of current literature and GPR principles, outlining advantages and limitations of the technique, and identifying areas where further research may be warranted. Many of the applications for which GPR is commonly used in unfrozen peatlands and permafrost in other soil types are directly relevant to investigations in perennially frozen peatlands, and are also considered here.

2.2 Ground Penetrating Radar Applications

2.2.1 Peat Thickness and Volume

Accurate determination of peat deposit thickness and volume is required for management of extraction or exploitation of peat for energy (Worsfold, *et al.*, 1986; Tolonen, *et al.*, 1984; Hänninen, 1992a; Baraniak, 1983) or other uses, as well as for post-production site rehabilitation (Welsby, 1988; Baraniak, 1983), infrastructure engineering (Saarenketo, *et al.*, 1992; Tolonen, *et al.*, 1984), modelling of mire growth (Hänninen, 1992a), modelling of greenhouse gas fluxes (Gorham, 1991; Pelletier, *et al.*, 1991; Davis and Pelletier, 1991), and studies of hydrology and landform development.

With regard to periglacial geomorphological studies, delineation of the peat - mineral sediment interface may be helpful in evaluating the role of mineral sediment in palsa development. Fine-grained mineral sediments subject to freezing are susceptible to ice

¹

The acrotelm is the surface layer of a peatland which is characterized by high hydraulic conductivity, variable water content, fluctuating water table, periodic air entry, presence of peat-forming aerobic microorganisms, and a live matrix of growing plant material. The catotelm is the lower layer or core of peat in a peatland, which is not subject to water content variability over time, has low hydraulic conductivity, is not subject to air entry, and lacks peat-forming aerobic microorganisms (Ingram, 1978).

segregation and frost heaving, particularly where high water contents occur. Forsgren (1968), Salmi (1968), and Zoltai (1972) suggested that the height typically attained by palsas (up to 7 m or more) was attributable to the penetration of permafrost into the underlying mineral sediment and consequent frost heaving.

Traditionally, peat deposit thickness and volume estimates have been derived based on average depth values determined by manual sampling at a few points in a given or representative deposit, in conjunction with areal measurements calculated from remotely sensed images (Remote Applications Inc., 1982; Worsfold, *et al.*, 1986). However, the disadvantages of this approach are several: manual coring is time-consuming and costly (Bjelm, 1980), particularly where peatlands are extensive and not easily accessible (Worsfold, *et al.*, 1986); the accuracy of depth and volume estimates depend on the number of sampled deposits and the intensity of point sampling within each deposit (Worsfold, *et al.*, 1986); and variations in sub-peat topography are poorly represented (Bjelm, 1980; Chernetsov, *et al.*, 1988; also *cf.* Baraniak, 1983). Nevertheless, coring and analysis of the retrieved peat core remain essential to determine peat type, macrofossils, and physical and chemical properties.

Fortuitously, the interface between peat and underlying mineral sediment is usually readily detected by GPR, due to the differences in electrical properties between these media. GPR reflections are strongest where the contrast in dielectric permittivity across an interface is large. Davis, *et al.* (1977) and others have shown that the dielectric permittivity is predominantly controlled by water content; variations in water content as low as one to three percent by weight are theoretically detectable by GPR (Hänninen, 1992a:27; Theimer, *et al.*, 1994:200). Theimer, *et al.* (1994) recorded water content in unfrozen fen peat between 80 % to 95 %, compared to approximately 30 % measured in underlying mineral sediments. The peat - mineral sediment interface typically represents the largest subsurface change in water content in peatlands, and therefore yields the strongest amplitude subsurface reflection event on GPR profiles (Theimer, *et al.*, 1994:199).

However, radar detection of the base of peat may be limited where: (1) high conductivity of pore water in the basal peat (due to diffusion from underlying sediments with high conductivity) causes excessive signal attenuation (Theimer, *et al.*, 1994); (2) the contrast in moisture content at the base of peat is absent due to the presence of underlying sapropel², gyttja³, or clays with high moisture content (Chernetsov, *et al.*, 1988; Hänninen, 1992b); and/or (3) the presence of frost reduces the dielectric contrast at this interface.

Where frozen, the dielectric contrast at the peat - mineral sediment interface is reduced; while the dielectric permittivity of unfrozen peat ranges from 60 to 80 (Hänninen, 1992a) and that of geological materials from 5 to a maximum of 40 for clays (Hänninen, 1992a), typical

2

Aquatic detritus composed predominantly of organic detritus and/or clay minerals.

3

Predominantly coprogenic aquatic mud.

permittivity values for various types of perennially frozen earth materials range from 2 to 4 (Annan, *et al.*, 1975). Thus, the peat - mineral sediment interface may be difficult to distinguish under frozen conditions (Kettles and Robinson, 1996); this problem may be exacerbated by signal scattering in ice-rich peat. Nevertheless, Kettles and Robinson (1996) were able to continuously image the peat - mineral sediment interface below a peat plateau near Fort Simpson (Mackenzie Valley), Northwest Territories, with 100 MHz antennae.

Unfrozen peat depths up to 10 m have successfully been measured using GPR (Morey and French, 1977; Meyer, 1989; Tiuri, *et al.*, 1983; Welsby, 1988; Theimer, *et al.*, 1994); Welsby (1988) suggests that 10 m peat thickness is probably an upper limit for radar wave penetration (for antennae with frequency = 80 MHz) given signal attenuation in organics. This is consistent with results reported by Theimer (1990) and Theimer, *et al.* (1994), who calculated that penetration depths of at least 10 m (by 100 MHz to 200 MHz antennae) should be attainable where bulk electrical conductivity is less than 25 mS m⁻¹, and depths of 3 m to 4 m where bulk electrical conductivity is between 25 mS m⁻¹ and 50 mS m⁻¹, based on typical peatland electrical properties, subsurface conditions, and radar system parameters. Bulk electrical conductivity in peatlands typically falls below 40 mS m⁻¹ and often below 15 mS m⁻¹ (Theimer, *et al.*, 1994). However, exceptionally high bulk electrical conductivity values in peat have been documented, for example, by Sims, *et al.* (1987) in the Hudson's Bay Lowlands (450 mS m⁻¹; Theimer, *et al.*, 1994) and by Theimer, *et al.* (1994) at Mer Bleue, Ontario (380 mS m⁻¹), where peat deposits are underlain by glaciolacustrine clays.

Most researchers have found that depth measurements obtained from (unmigrated) GPR data are comparable to those obtained by manual coring. Correlation coefficients of $r=0.99$ and $r=0.94$ between depth values obtained from manual coring and inferred from GPR were reported by Ulriksen (1980) and Tolonen, *et al.* (1984:6) (both using 120 MHz antennae), and by Hänninen (1992b:219), respectively. Accuracy has also been expressed as deviation between manually determined and radar-inferred depths, ranging from ± 2.5 cm to 10 cm (Doolittle, 1987), ± 50 mm (Welsby, 1988:104), ± 0.1 m (Chernetsov, *et al.*, 1988:20), to ± 150 mm (Worsfold, *et al.*, 1986: 149), and as percentage of total peat depth, given by Tolonen, *et al.* (1984:1) as 7.5 % at 90 % confidence level, and by Saarenketo, *et al.* (1992:304) as 10 %.

Observed deviations between manual coring and radar-inferred depths have been attributed to bottom roughness and spatial discrepancies between the radar "footprint" and coring point, non-vertical coring, rounding off, lateral and vertical radar signal velocity variations, and patchy distribution of frost (Worsfold, *et al.*, 1986; Bjelm, 1980; Chernetsov, *et al.*, 1988; Doolittle, 1987). With respect to the latter point, frozen conditions cause radar signal propagation velocity to increase; at higher velocities, radar reflections from interfaces at depth appear shallower due to the decreased travel time of the signal energy.

With respect to volume estimates, Worsfold, *et al.* (1986:150) reported agreement between manually derived and radar-inferred volume estimates usually within 5 %, with increased accuracy obtained when signal propagation velocity was calculated for each peat deposit (*versus* an average or composite velocity derived from several representative deposits).

However, the continuity of GPR data minimizes over/underestimates of peat depth and volume that could result where point measurements are taken in areas of anomalous peat thickness (Bjelm, 1980; Baraniak, 1983; Chernetsov, *et al.*, 1988). To calculate the volume of peat, the cross-sectional area of peat is calculated for parallel transects across the peatland. The total volume of peat is then the sum of the peat volumes between each transect, calculated as the product of the average cross-sectional area of adjacent transects, and the distance separating the transects.

A grid of GPR transects across a peat deposit have been used to generate contour maps of the peat - mineral sediment interface, synthetic cross-sections, and three dimensional maps, all of which are valuable tools for applied topics such as resource extraction planning, road and drainageway placement, and development of reclamation plans for mined areas (Baraniak, 1983; Chernetsov, *et al.*, 1988; Welsby, 1988; Hänninen, 1992a; Saarenketo, *et al.*, 1992), or for research subjects such as peat accumulation rates.

It has been shown that depth and volume data provided by GPR are comparable in accuracy to those obtained by manual coring. The advantages of GPR over conventional methods for delineating the peat - mineral sediment interface therefore lie primarily in its ability to provide laterally continuous subsurface data rapidly and with minimal effort. GPR does not, however, obviate the need for coring to confirm depth to the base of peat, particularly in areas where discontinuous frost conditions may occur.

2.2.2 Peat Properties

Data regarding lateral and vertical variations in peat properties, such as peat type (plant species composition), moisture content, density, and degree of humification/decomposition are important to evaluate energy value (Bjelm, 1980), potential gas flux (Gorham, 1991; Pelletier, *et al.*, 1991; Davis and Pelletier, 1991), and mire growth history (Lowe, 1985). Furthermore, the position of the water table, acrotelm-catotelm boundary, peat-sapropel boundary, and presence of boulders, stumps, logs, or other obstructions within the peat or at the peat - mineral sediment interface are important considerations for peat extraction planning (Ulriksen, 1980; Worsfold, *et al.*, 1986; Doolittle, 1987; Chernetsov, *et al.*, 1988; Warner, *et al.*, 1990; Hänninen, 1990, 1992a, b). In addition, information regarding lateral continuity, structure, and composition of peat strata may contribute to the evaluation and interpretation of mire growth history (Hänninen, 1992a) and related landform development. For example, such data may reveal variations in dominance of peat-forming plant species, signalling changes during peat accumulation between wet and dry conditions associated with the aggradation and degradation of permafrost in palsas and peat plateaus (Zoltai and Tarnocai, 1975).

However, the use of GPR to obtain this type of detailed information has met with limited success. To date its reliability in this regard appears largely dependent on the extent and accuracy of point sampling and analyses of peat properties available to support GPR interpretations.

GPR responds to changes in the dielectric permittivity of the media through which the radar signal passes, which, as noted earlier, is controlled mainly by water content. A change in dielectric permittivity, however, may reflect a change in any one or more of several parameters of interest, not restricted to moisture content, and including peat type, degree of humification, density, or temperature/phase. Thus, variations in all of these properties must be verified in peat samples for radar reflections to be attributed reliably to a change in a specific peat property. Even so, it may not be possible to consistently correlate radar reflections with a change in any single peat property, as discussed below.

Furthermore, gradual changes in dielectric permittivity are not detectable by GPR. Generally, to be detectable, a permittivity contrast must occur over a distance approximately equivalent to one quarter of the signal wavelength, in turn a function of antenna frequency and dielectric permittivity of the medium (Tiuri, *et al.*, 1983; Theimer, *et al.*, 1994). For typical values of dielectric permittivity in shallow, unfrozen, saturated peatlands, resolution may range from *ca.* 4 cm to 6 cm (at 200 MHz) to *ca.* 17 cm to 20 cm (at 50 MHz) (Theimer, *et al.*, 1994).

Moisture Content

It has been shown by Davis, *et al.* (1977) (also Topp, *et al.*, 1980, and Ulriksen, 1980) that the dielectric permittivity is strongly dependent on the soil water content and only weakly dependent on other soil properties such as soil type, density, and temperature. Tiuri, *et al.* (1983:136) reported a coefficient of determination (r^2) of 0.89 between water content by volume and dielectric permittivity for 60 peat samples from six different mires.

It follows that GPR is able to detect changes in moisture content within the peat where these are of sufficient magnitude and/or abruptness; Hänninen (1992a) reported radar interfaces to depths of less than 4 m that were attributable to changes in moisture content of approximately one percent. However, Theimer, *et al.* (1994) suggest that moisture content variations of less than two percent (over 15 cm depth intervals) are at the lower limit of detectability, and random, minor changes in water content generated incoherent discontinuous reflections from the internal section of peatlands. Water loss during peat sample recovery continues to be problematic; to reliably correlate GPR reflections with such small changes in moisture content, peat sampling techniques which offer accurate determination of *in situ* water content must be used (Theimer, *et al.*, 1994).

Notwithstanding the above, the water table in peatlands typically generates a strong reflection (Ulriksen, 1980), although this may be obscured by surface events (*i.e.*, radar events produced by signal energy travelling through the air and along the ground surface, referred to as the air and ground waves, and noise multiples) where the water table occurs close to the surface (Jol and Smith, 1991). Nobes, *et al.* (1989), Warner, *et al.* (1990), and Theimer, *et al.* (1994) describe a laterally continuous reflection attributed to a 3 % to 5 % change in moisture content in the near-surface unsaturated zone, which they suggest represents the transition from the surface aerobic zone (acrotelm) to the anaerobic zone (catotelm; Ingram, 1978).

To add to the complexity of GPR interpretation, moisture content in peat is related to degree of humification, peat type, and density (Hänninen, 1992a, b), and changes in these parameters

are often associated with changes in moisture content, as illustrated by many of the following examples.

Humification/Decomposition

Bjelm (1980) found that changes in the degree of humification were more easily identified from radar profiles than changes in peat type (*i.e.*, *Carex*- versus *Sphagnum*-dominated peat), due to the change in water content associated with degree of humification. However, he noted that peat with different degrees of humification could be represented by the same reflection across the GPR profile. Tolonen, *et al.* (1984) found that radar reflections were correlative with a minimum change in degree of decomposition of 2 von Post units⁴ in 78 % of cases ($n = 23$).

Warner, *et al.* (1990) and Theimer (1990) note that humification is greatest in the acrotelm, which they were able to tentatively identify on radar profiles primarily due to the moisture content change across the acrotelm-catotelm boundary. Chernetsov, *et al.* (1988) described a laterally continuous interlayer which was attributed to a change in moisture content of 5 % and an associated change in the degree of decomposition of 15 %. These cases illustrate the difficulty associated with attributing GPR reflections to a change in any *single* peat property.

Peat Type

Where peat-forming plant species are characteristic of a specific feature in a peatland, for example, *Sphagnum*-dominated hummocks and ridges versus *Carex*-dominated pools, identification of subsurface boundaries between peat types may assist in evaluating the evolution of the peatland (Hänninen, 1992a). Pelletier, *et al.* (1991) correlated radar reflections with denser peat layers observed in peat samples from pits and cores. They suggested these denser peat layers may be evidence of changes in the dominance of peat-forming plant species due to locally variable conditions. However, they did not provide macrofossil information or other supporting paleoecological data.

Carex- and *Sphagnum*-dominated peats differ in their water retention characteristics, as well as in particle size and bulk density characteristics (Hänninen, 1992a), and consequently may be discernible on GPR profiles. Hänninen (1992a:27) was able to correlate certain radar reflections with the transition from *Carex* to *Sphagnum* peat, associated with a change in humification and moisture content. *Carex* peat is more typically characterized by gradual moisture variations, and thus generates few internal reflections. In contrast, *Sphagnum* peat is typically characterized by sudden, pronounced moisture and humification variations which are manifested as numerous reflection interfaces within the peat (Hänninen, 1992a); however,

4

The von Post classification scheme grades humification on a scale from 1 (none) to 10 (complete decomposition). The degree of humification considers the extent of decomposition, structure of plant material (*i.e.*, 'identifiable' to 'not discernable'), content of amorphous material (*i.e.*, 'none' to 'high'), nature of material extruded on squeezing in the hand (*e.g.*, amount and colour of water, amount of paste), and the nature of the residue (von Post (1922) in Hobbs (1986)).

Hänninen also observed layers of *Sphagnum* peat with little internal heterogeneity and therefore few internal radar reflections.

Tolonen, *et al.* (1984) found that radar reflections were correlative with an observed change in peat-forming plant species (of one or two peat constituents) in only 58 % of cases ($n = 43$). Changes in peat type described by Warner, *et al.* (1990) from coring data are not clearly manifested on GPR profiles, except as they coincide with the acrotelm-catotelm boundary described earlier.

Density

Tiuri, *et al.* (1983:136) found a strong inverse relationship between bulk density of peat and dielectric constant, with a coefficient of determination (r^2) of 0.93 ($n = 48$); density variations should therefore be detectable by GPR, particularly as these are closely related to moisture content variations.

Warner, *et al.* (1990) identified two main zones of relatively high bulk density in an Ontario bog; these were the gytja and clay at the base of peat, and the base of the acrotelm. Both of these zones produced strong reflections on radar profiles. Pelletier, *et al.* (1991) were able to correlate GPR reflections with denser peat strata observed in coring; however, they did not measure associated moisture content variations. In longitudinal and transverse GPR profiles of road embankments built over peat, Saarenketo, *et al.* (1992) identified a compaction interface, also observed in weight penetration tests, resulting from peat compression by embankment loading.

However, Worsfold, *et al.* (1986:149) found that some “marked” changes in bulk density could be correlated with radar reflections, but that some “equally large” variations in this parameter did not generate reflections. Furthermore, some interfaces identified by radar did not appear to correlate with any measured peat properties (bulk density, conductivity, degree of humification, percent moisture content, parent material). Similarly, Bjelm (1980) noted that some radar reflections were not identified by drilling, and conversely, that some stratigraphic interfaces identified by drilling did not correlate with radar reflections.

These examples serve to emphasize the need for point verification of GPR interpretations. Clearly, GPR cannot provide any direct information regarding internal variations in peat properties, and therefore cannot eliminate the need for peat sample collection and detailed analysis where this type of information is desired (*cf.* Worsfold, *et al.*, 1986). Such applications would additionally require a greater understanding of the theoretical interrelationships between various peat properties, not restricted to site-specific data. Moreover, peat stratigraphy varies between deposits and laterally and vertically within the same deposit (Hänninen, 1992a). Where detailed point observations of peat properties are made, the continuous profiling offered by GPR represents a valuable tool for interpolating identified strata between sample points and for assessing internal homogeneity or heterogeneity of a given peat deposit (*e.g.*, Hänninen, 1992a; Tiuri, *et al.*, 1983; Worsfold, *et al.*, 1986; Tolonen, *et al.*, 1984; Pelletier, *et al.*, 1991).

Buried Objects

Buried logs and stumps in peat deposits may be of interest to researchers for paleoecological reconstructions (*e.g.*, Lowe, 1985), but are more frequently perceived, along with boulders at the peat - mineral sediment interface, as potential obstacles to peat extraction. Forsgren (1968), Åhman (1976), and Worsley, *et al.* (1995) documented boulders at the base of peat heaved up from the underlying mineral soil in palsas; additional observations of this phenomenon could further our understanding of the nature of frost action within palsas underlain or cored by mineral sediment. Due to their random distribution, buried objects in peat are not effectively located by conventional coring methods.

Point objects typically generate hyperbolic diffraction events which are easily identifiable on the radar profile. Buried wood has been inferred on radar profiles from peatlands by Bjelm (1980), Lowe (1985), Worsfold, *et al.* (1986), Welsby (1988), Chernetsov, *et al.* (1988), Meyer (1989), and Hänninen (1992b). In some, but not all cases, the presence of buried wood has been confirmed by drilling and/or observation of wood in drained and extracted peat. Chernetsov, *et al.* (1988) were able to trace a laterally continuous stump horizon at 1 m to 2 m depth in peat reaching more than 6 m in thickness; the presence of the stumps was confirmed by drilling.

Where peat is underlain by till, colluvium, regolith, or other coarse-grained sediment, point diffractions at the peat - mineral sediment interface may reasonably be expected. Doolittle (1987) has described complex radar reflections from boulders at the soil-bedrock interface. Boulders at the base of peat were inferred by Worsfold, *et al.* (1986) but not confirmed by drilling. In contrast, no diffraction patterns were evident from a boulder pavement at the peat - mineral sediment interface in GPR data collected by Pilon, *et al.* (1992). Signal diffraction was also not encountered in extremely bouldery deposits surveyed by Smith (D. Smith, pers. comm., 1995), suggesting that deposits of this nature may mimic a continuous stratigraphic layer when surveyed by radar.

2.2.3 Ground Ice Distribution and Characteristics in Peat

There is a strong dielectric contrast between freshwater ($\epsilon = 80 - 81$) and freshwater ice ($\epsilon = 3 - 4$) (Worsfold, *et al.*, 1986; Hänninen, 1992a:11); a similarly strong contrast exists between wet, unfrozen peat ($\epsilon = 60 - 80$; Hänninen, 1992a:11) and frozen soils ($\epsilon = 2 - 4$; Annan, *et al.*, 1975). Theoretically then, the location and orientation of interfaces between frozen and unfrozen peat can be mapped by GPR.

Seasonal Frost

There is a strong dielectric contrast at the base of the seasonal frost layer, generating a strong radar reflection, the resolution of which depends on the depth of frost and radar system parameters; Worsfold, *et al.* (1986) were unable to resolve the seasonally frozen peat layer, measured at 100 mm to 150 mm depth, on radar profiles collected using 80 MHz to 400 MHz ground-based antennae and 80 MHz to 120 MHz airborne antennae. Theimer (1990) was also unable to distinguish the base of frost (measured *ca.* 40 cm depth) from the radar events representing signal travel through the air and along the ground surface. Deeper seasonal frost

may be more easily distinguishable on GPR profiles; Morey and French (1977) were able to clearly identify the base of seasonal frost measured at approximately 1 m depth using VHF radar of unspecified frequency. Higher frequency (*i.e.*, 1000 MHz) antennae, which provide greater resolution at shallower depths, may be more useful in delineating the base of seasonal frost, but nevertheless, may not be able to overcome signal interference by direct air and ground wave events and signal 'ringing.'

Signal 'ringing' occurs when the signal energy 'bounces' between the strong dielectric contrasts at the base of frost and the ground surface; each successive reflection of energy is recorded by the receiving antenna, generating multiple reflections parallel to the ground surface. These multiples commonly obscure other near-surface reflections and hinder image interpretation. Warner, *et al.* (1990) and Theimer (1990) had limited success in removing these multiples through data processing. Worsfold, *et al.* (1986: 153) suggested that the frozen surface layer should allow greater signal penetration (particularly from an airborne platform) since the dielectric contrast at the air-ground interface would be much less. However, this effect may be obviated by signal 'ringing' in the near-surface.

Hänninen (1992a, b) also noted that wet layers within the snowpack and between the snow and peat may attenuate the signal and cause signal 'ringing.' Furthermore, the controlling effect on dielectric permittivity of unfrozen water content (Davis, *et al.*, 1977; Topp, *et al.*, 1980), manifested by the large documented range in dielectric permittivity of wet, unfrozen peat ($\epsilon = 60 - 80$), suggests that slight internal variations in moisture, density, and/or humification which may be detectable when the peat is unfrozen may not be detectable when frozen, given the smaller dielectric range ($\epsilon = 2 - 4$; Annan, *et al.*, 1975). Furthermore, the resolution of GPR in frozen peat is reduced due to signal scatter and absorption by ice and liquid water (Doolittle, *et al.*, 1992; Arcone, 1984), and by increased signal velocity. Thus, while accessibility to and stability of the peatland surface may be better during the winter (Warner, *et al.*, 1990), surveying when seasonal ground frost is absent is recommended when data on internal peat variability are desired (Hänninen, 1992a, b, 1990).

Frost Bulbs

Using a sequence of GPR profiles, Saarenketo, *et al.* (1992) were able to identify frost bulbs in peat under road embankments, on the basis of temporal changes in reflection characteristics and spatial variations in signal attenuation. Progressive thaw of a frost bulb below the road embankment was inferred by a phenomenon referred to as velocity pullup (Coffeen, 1984; *e.g.*, Kettles and Robinson, 1996), whereby signal energy reflected from interfaces at a given depth below a frost bulb are recorded sooner by the receiving antenna, and imaged shallower, due to the higher velocity of signal propagation through frozen material; when the frost bulb had thawed, subsurface interfaces were imaged deeper, at their real relative positions.

Frost bulbs were also inferred where thaw caused laterally continuous reflections to appear displaced downwards relative to adjacent frozen ground, due both to the pullup phenomenon and volume reduction during phase change from ice to water. In addition, signal attenuation was greater in areas of inferred thaw, presumably due to conduction by pore water. Areas of inferred thaw corresponded to observed surface subsidence.

Permafrost

To date, GPR application to investigations of perennially frozen peatlands has been limited (Doolittle, *et al.*, 1992; Pilon, *et al.*, 1992; Kettles and Robinson, 1996). In contrast, the application of GPR to permafrost and massive ground ice in other environments is well documented.

Active Layer

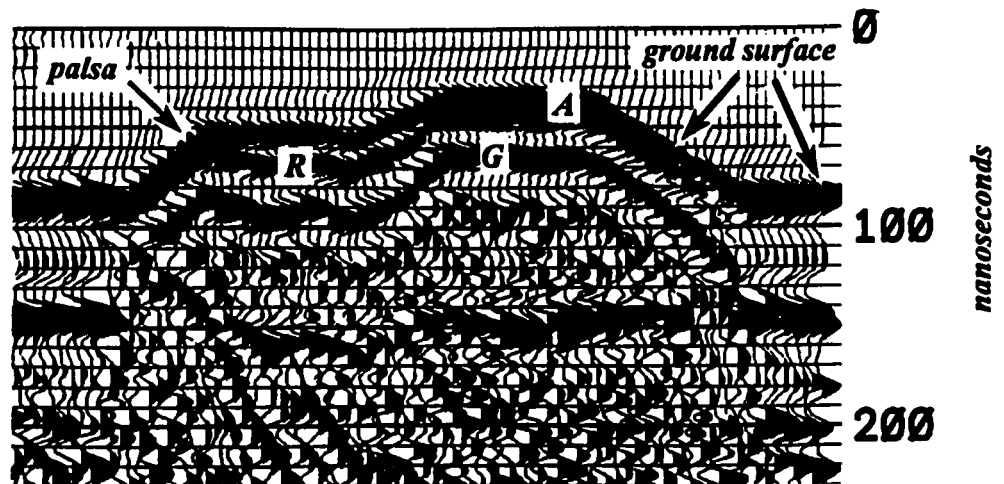
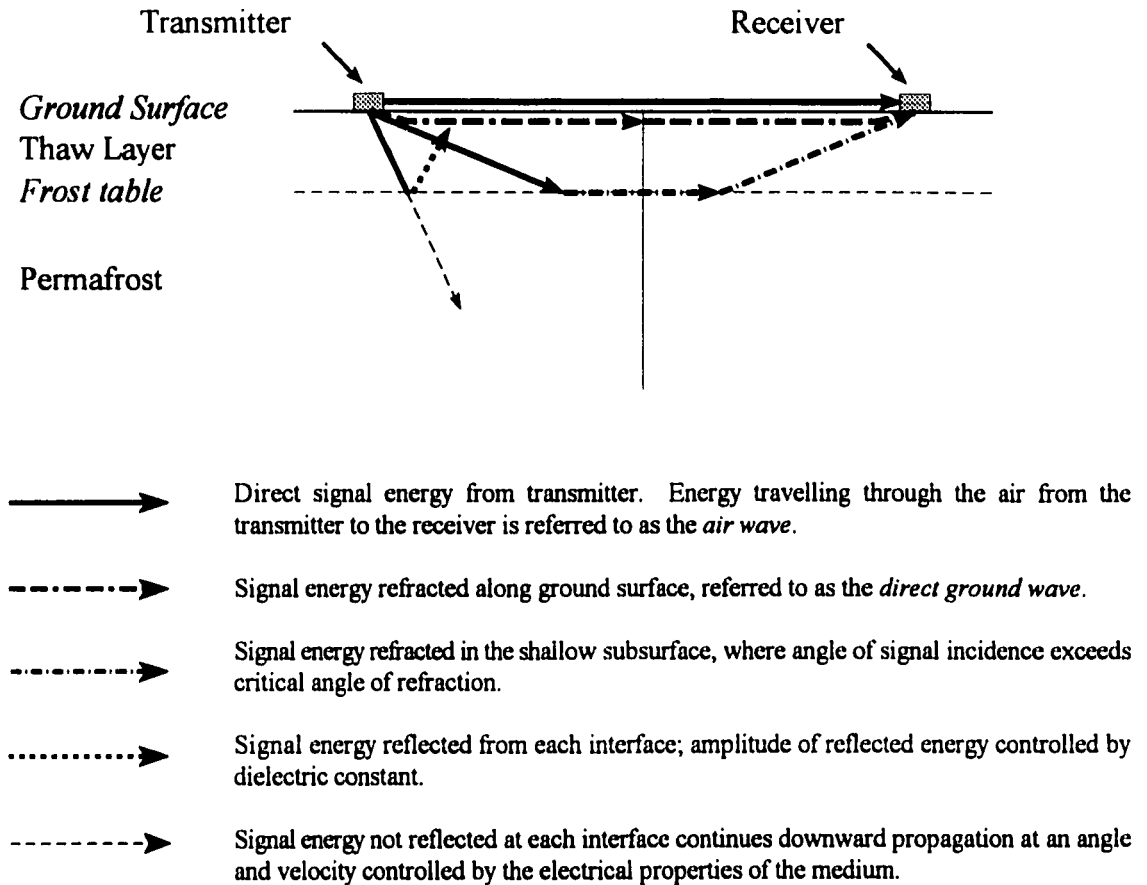
The depth of annual thaw on palsas and peat plateaus is typically less than 70 cm (Seppälä, 1988; Brown, 1968). Thus, although the permafrost table represents a strong dielectric contrast, the resulting radar reflection may not be distinguishable from other near-surface returns, such as the direct air and ground waves, particularly when relatively low frequency antennae are used. However, Doolittle, *et al.* (1992), using 500 MHz antennae, were able to clearly distinguish a laterally continuous reflection which they correlated with the base of the active layer, at an average 44 cm depth; this is consistent with the improved resolution in the near-surface offered by higher frequency antennae. Signal penetration, however, was correspondingly reduced. These results are comparable to those reported from non-peatland investigations; using 500 MHz antennae, Doolittle, *et al.* (1990) were able to map active layer depths as shallow as 38 cm in moist sedge tundra.

Signal propagation velocity through the active layer in peat was calculated by Doolittle, *et al.* (1992) to be 0.057 m ns^{-1} , faster than typical signal velocities through unfrozen, wet fen (0.03 m ns^{-1} to 0.04 m ns^{-1}), but slower than typical velocities for frozen peat (0.08 m ns^{-1} to 0.12 m ns^{-1}) (Robinson, 1993); the dielectric constant was determined to be 27.2, also intermediate between typical permittivity values for (wet) unfrozen peat and frozen soils (see above). (These values are comparable to values determined for the active layer in moist sedge tundra; Doolittle, *et al.*, 1990.)

The slow signal propagation velocity through the thaw layer must be considered when inferring depths of subsurface interfaces in permafrost landforms; the presence of a thawed layer at the surface will result in interfaces appearing deeper (*i.e.*, longer travel time) on the radar profile than they actually are. Average signal propagation velocities derived from Common Mid Point (CMP) surveys (see Appendix A) represent an integrated velocity over the entire vertical profile and to some extent account for the presence of a low velocity surface layer. Complication of the subsurface velocity structure (by a low velocity surface layer) may be avoided by winter surveying; however, difficulties with seasonal frost and reduced dielectric contrast may then be encountered, as described above.

Where the thaw layer is shallow, radar signal energy may be refracted along the top of the permafrost, travelling at a higher velocity than signal energy refracted along the ground surface; refracted energy from the top of permafrost may therefore reach the receiving antenna prior to the ground wave (*cf.* Coffeen, 1986) (S.D. Robinson, pers. comm., 1995) (Figure 2-1). This phenomenon, in conjunction with other near-surface events, complicates interpretation of shallow subsurface data.

Figure 2-1. Refracted radar event from shallow thaw layer.



Radar signal energy refracted along the frost table below a shallow thaw layer, as it may appear on the radar profile, as *R*, between *A*, the air wave, and *G*, the direct ground wave. Depth to frost in this zone averaged 48 cm at the time of the GPR survey.

Lateral Frozen - Unfrozen Interfaces

The horizontal transition from unfrozen to frozen peat may be manifested on the GPR image in several ways. Radar returns from frozen peat were described by Hayley (1989) as “more intense” than returns from unfrozen peat. Saarenketo, *et al.* (1992) also documented greater attenuation of the signal in unfrozen peat. Pilon, *et al.* (1992) delimited talik areas within a peat plateau near Kangiqsualujuaq, Québec, on the basis of increased signal attenuation.

Signal scatter from pore ice and segregated ice lenses results in typically more chaotic, laterally discontinuous reflections in frozen peat, particularly ice-rich peat, compared to the typically laterally continuous reflections observed in unfrozen peat (Kettles and Robinson, 1996) (Figure 2-2). Excessive signal scatter and attenuation may also occur in partially frozen, warm or degrading permafrost (*e.g.*, the ‘frozen fringe’; NRCC, 1988), due to the presence of unfrozen water within the frozen material. Presence of ground ice may therefore be inferred on the basis of the character of radar reflections.

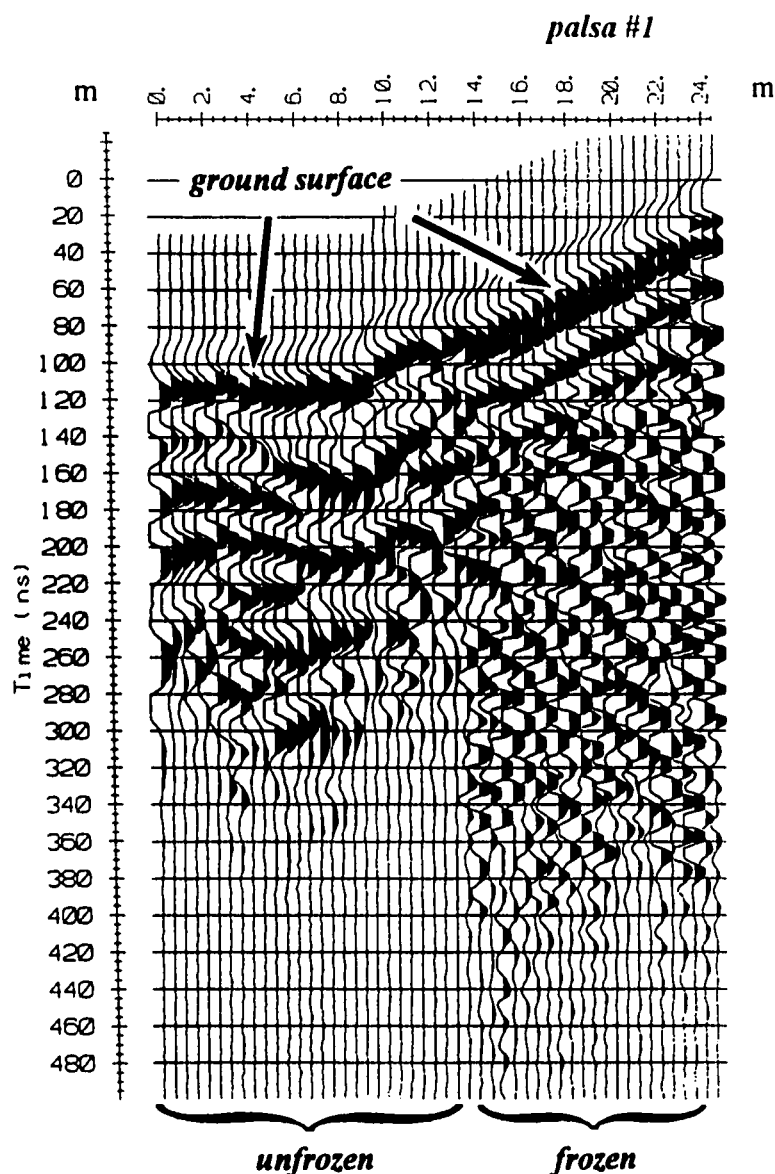
Reflections generally appear shallower and compressed relative to one another in frozen peat due to greater radar signal velocity (Doolittle, *et al.*, 1992). Signal penetration, however, is increased, as attenuation due to conductivity is reduced relative to unfrozen, wet peat.

Irregular near-vertical interfaces between frozen and unfrozen peat may generate false images of reflections dipping symmetrically away from the interface (although the relative strength of these reflections on either side of the interface may vary) (Doolittle, *et al.*, 1992; Kettles and Robinson, 1996). The false images are produced when radar signal energy spreading geometrically from the transmitting antenna strikes irregularities on the vertical interface and is reflected back to the receiving antenna; as the radar is unable to discern directional information, the received energy is imaged as a reflection situated below the antennae array. As the antennae approach the interface, the signal path length between the antennae and the interface is shortened, and the apparent reflector at depth is imaged progressively shallower (Figure 2-3). This phenomenon is similar to the hyperbolic diffraction pattern produced by point reflectors.

Depth of Permafrost

Enhanced signal penetration afforded by increased signal propagation velocity and low attenuation in frozen material may allow inferences regarding the depth to which permafrost has developed under palsas and peat plateaus. Signal attenuation (manifested by lack of radar returns) at depth may be indicative of unfrozen conditions. Conversely, chaotic, discontinuous, high-frequency radar returns suggest frozen conditions at depth, up to or greater than the depth of signal penetration (Kettles and Robinson, 1996). Thus, Pilon, *et al.* (1992) were able to define the base of permafrost under a peat plateau at Kangiqsualujuaq, Québec.

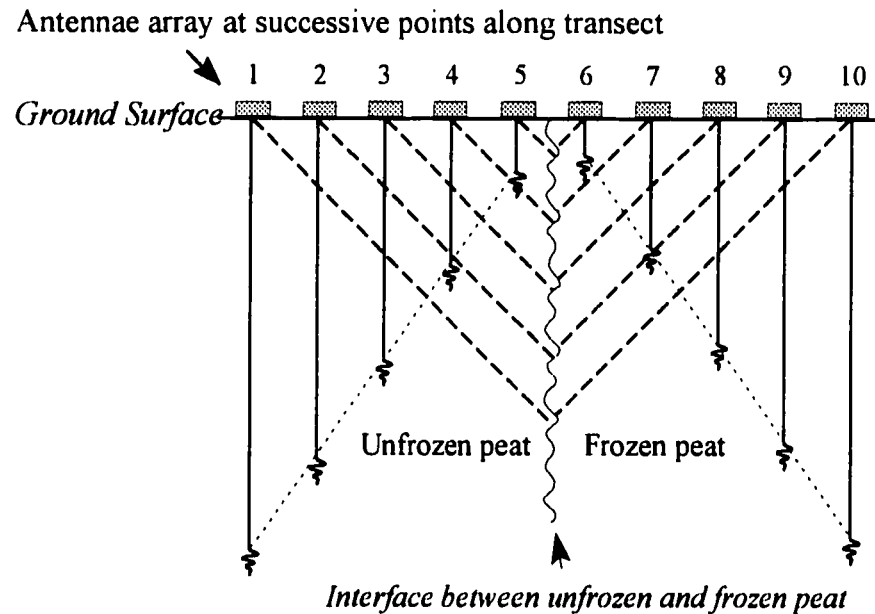
Figure 2-2. Contrast in character of radar reflections across transition between unfrozen and frozen subsurface conditions.



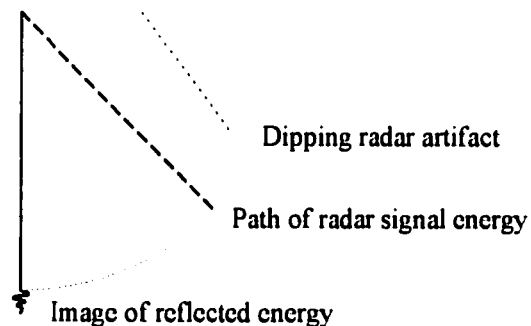
Radar profile across the transition from fen to the core of a palsa illustrates the contrast in the characteristics of radar reflections from unfrozen and frozen subsurface materials: signal scatter from pore ice and segregated ice lenses results in typically more chaotic, laterally discontinuous reflections in frozen peat and/or mineral sediment (between 13 m and 24 m on the horizontal scale), compared to the typically laterally continuous reflections observed in unfrozen peat (between 0 m to 12 m on the horizontal scale).

Plot produced from pulseEKKO IV radar operating software. Processing steps include topographic correction, automatic (time variable) gain control, trace-to-trace averaging, and down-trace averaging.

Figure 2-3. Radar image artifacts produced by irregular near-vertical interface between unfrozen and frozen peat.



where:



Dipping radar artifact as shown may be generated when radar signal energy spreading geometrically from the transmitting antenna strikes irregularities on the vertical interface and is reflected back to the receiving antenna; as the radar is unable to discern directional information, the received energy is imaged as a reflection situated vertically below the antennae array. As the antennae pair approaches the interface, the signal path length between the antennae and the interface is shortened, and the apparent interface at depth is imaged progressively shallower.

2.2.4 Evolution Inferences from Peat Stratigraphy and Structure

The ability of GPR to image small variations in peat properties and in vertical and lateral stratigraphy and stratigraphic continuity in peatlands may assist in the study of peatland evolution. Specific examples are provided below.

Depositional Environment

Changes in the depositional environment within the basin may be inferred where gyttja and sapropel can be distinguished at the base of peat. Hänninen (1992a, b, 1990) was able to correlate radar reflections with interfaces between peat and sapropel rich in organic detritus, peat and clay-rich sapropel, and between organic-rich and clay-rich sapropel, although the weak contrast in moisture content between peat and organic-rich sapropel makes these contacts more difficult to distinguish on the radar profiles. Kettles and Robinson (1996) correlate a transparent zone lacking internal stratigraphy to well decomposed, structureless peat observed in cores.

Warner, *et al.* (1990) and Nobes, *et al.* (1989) correlated complex basal reflections in peat with the presence of a thin, discontinuous gyttja and peaty gyttja layer overlying the mineral substrate, as observed in cores. The presence of a basal gyttja or aquatic peat layer suggests initial deposition in a body of open standing water (National Wetlands Working Group, 1988).

Tephrostratigraphy

GPR may be useful for tephrostratigraphy where distinct ash layers are preserved within a peat deposit; however, Lowe (1985) met with limited success in this regard, due to the diffuseness and depth variability of tephra layers (which occurred between 1 m to > 3 m depth), and excessive signal noise from coarse, woody fragments in the peat. Theimer (1990) suggests that data processing may improve the coherency and resolution of reflections from diffuse ash layers, although this technique has yet to be tested.

Palsas and Peat Plateaus

Reconstruction of peatland history and paleoclimate on the basis of perennially frozen peat landforms is typically restricted due to the limited stratigraphic evidence remaining following the collapse of palsas or peat plateaus (Lundqvist, 1969:211-212). However, continuous radar profiling may reveal small vertical and/or lateral disruptions in otherwise continuous fen stratigraphy, not observable in peat cores, that may be indicative of collapsed permafrost-cored peat landforms. This application has not yet been described in the literature.

If GPR were successful in delineating spatial variations in peat type, such data could be helpful in reconstructing the history of permafrost aggradation and degradation within a peatland, where these changes are associated with alternate succession between hydrophilous and xerophilous peat-forming plant species. Where radar reflections are correlative with changes in plant species composition observed in samples, GPR can be used to infer plant community succession (Pelletier, *et al.*, 1991) and development history of ridge-pool (string-pool) topography (Seppälä and Koutaniemi, 1985; Hänninen, 1992a); however, as discussed

in Section 2.2.2 above, peat analyses in conjunction with GPR studies to date have largely failed to provide reliable data to support such applications.

GPR may also prove useful in determining genesis of palsa-scale frost mounds on the basis of internal stratigraphic structure. The characteristically domed stratigraphy of palsas formed as individual mounds by ice segregation may be contrasted with horizontal stratigraphy that may result where palsa-scale frost mounds are erosional remnants of a pre-existing, more extensive plateau formed by ice segregation or another process (*cf.* Hinkel, 1988; Nelson, *et al.*, 1992). Compare Figures 2-4 and 2-5. This application remains to be tested, however.

Unfortunately, scattering of radar signal energy by pore ice and ice lenses, scattering and absorption in near-surface partially thawed layers (Doolittle, *et al.*, 1992; Arcone, 1984), and increased signal propagation velocity through frozen material impair resolution of internal peat stratigraphy and structure, particularly where peat is ice-rich. Useful information, however, may be obtained where local conditions are favourable. Strong (high-amplitude), closely spaced, sub-parallel reflections may be produced by alternating strata of frozen peat, icy peat, and ice lenses (Pilon, *et al.*, 1992; Doolittle, *et al.*, 1992). A strong, laterally continuous reflection was determined by Pilon, *et al.* (1992) to represent a massive ice lens in ice-rich silts below a peat plateau.

However, the evaluation or interpretation of stratigraphic continuity between frozen and unfrozen peat is hindered by the strong contrast in radar signal velocities in these materials. As noted earlier, reflections at a given depth appear shallower and compressed relative to one another in frozen materials. Thus, strata that are laterally continuous from unfrozen to frozen peat may not appear continuous on a GPR profile, further complicating stratigraphic interpretations. The literature currently lacks a thorough examination of radar signal velocity characteristics in varying subsurface conditions and materials. This limits the usefulness of radar data for interpreting subsurface conditions in transitional areas.

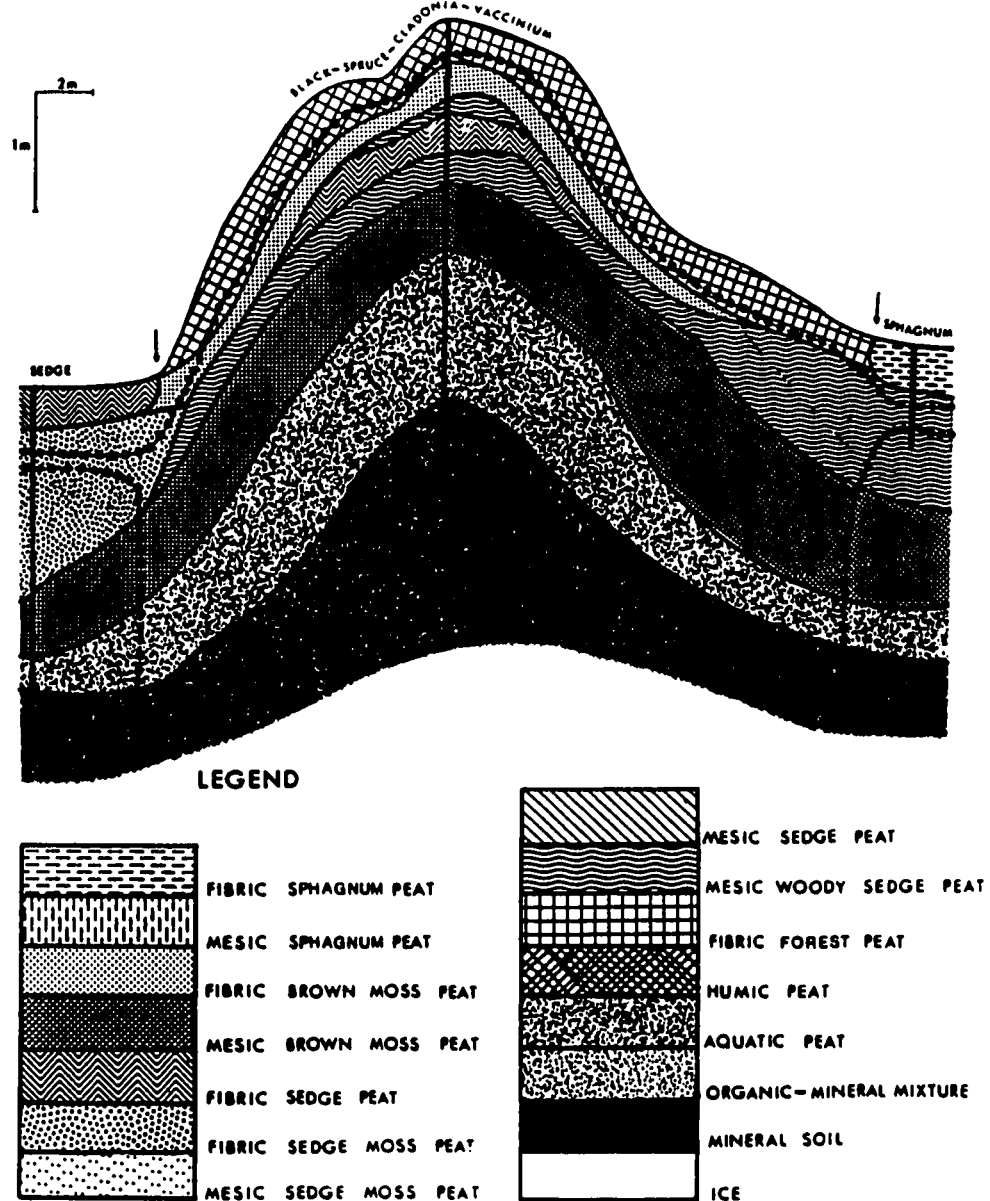
2.2.5 Characteristics of Mineral Substrate

Limited information regarding the nature of sub-peat mineral sediments may be inferred from GPR surveys of peatlands; the success of this interpretation is often predicated on a knowledge of local geologic conditions. This information may be useful in geological and geomorphological mapping, and for evaluating mire growth history and the role of mineral sediment in palsa development.

Sediment Type

Signal attenuation below the base of peat is usually a good indicator of sediment type; in particular, clays tend to attenuate radar energy rapidly, and few reflections are received from this sediment type (Hänninen, 1992a:27). In contrast, some stratification in sub-peat materials may be evident in coarser-grained sediments such as sand (Hänninen, 1992a) and colluvium (Lowe, 1985). Chernetsov, *et al.* (1988) described multiple re-reflections of signal energy from sandy sediments below peat. Bjelm (1980) and Hänninen (1992a) correlated sub-peat

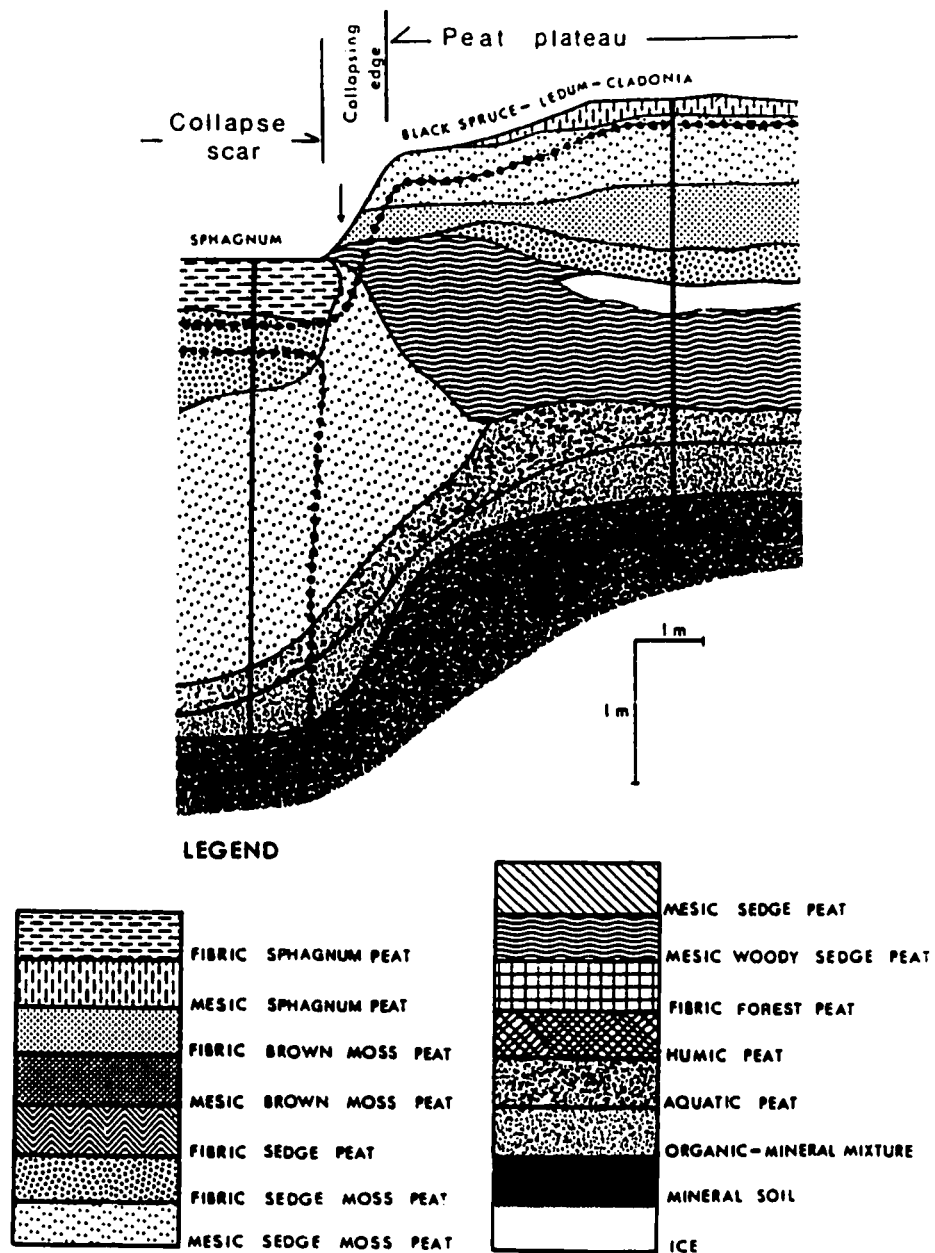
Figure 2-4. Stratigraphic cross-section of a dome-shaped palsa mound.



Note doming of individual peat strata conformable with external morphology. Palsa located at 67°06'N, 134°17'W.

Source: Perennially frozen peatlands in the western Arctic and subarctic of Canada (Zoltai and Tarnocai, 1975). *Canadian Journal of Earth Sciences* 12, 28-43. Copyright (1975, NRC Research Press). Reprinted by permission of National Research Council Research Press.

Figure 2-5. Stratigraphic cross-section of a peat plateau with collapsing edge.



Note truncated, flat-lying strata in elevated portion of peat plateau. Peat plateau located at 66°49'N, 135°21'W.

Source: Perennially frozen peatlands in the western Arctic and subarctic of Canada (Zoltai and Tarnocai, 1975). *Canadian Journal of Earth Sciences* 12, 28-43. Copyright (1975, NRC Research Press). Reprinted by permission of National Research Council Research Press.

reflections with interfaces within mineral sediments, including clay - till and sand - till contacts, and with the till - bedrock interface.

Welsby (1988) suggested that sub-peat topography was a reasonable indicator of sediment type below Irish peatlands; he found that irregular sub-peat topography was characteristic of weathered glacial drift, in contrast to level topography characteristic of unweathered lacustrine silts, clays, and marls.

Boulders

Point reflectors such as boulders typically produce hyperbolic diffraction events that are easily recognizable on GPR profiles. However, as noted in Section 2.2.2 above, hyperbolic returns from boulders have not consistently been documented on GPR profiles.

Bedrock

Bedrock is typically not detected in GPR surveys over peatlands (Bjelm, 1980). However, Doolittle (1987) provides a general indication of typical radar responses from various types of bedrock: bedding planes of sedimentary rocks generate distinct reflections that are relatively easy to interpret, whereas igneous and metamorphic rocks have irregular surfaces that produce complex radar images.

Permafrost

As noted earlier, the presence of permafrost and massive ground ice in mineral sediments underlying peats may be inferred from the GPR profile based on the nature of reflections and signal attenuation.

2.3 Summary and Conclusions

The principal advantages of GPR in peatland investigations lie in rapid, accurate, and continuous imaging of sub-peat topography, evaluation of vertical and lateral homo/heterogeneity and stratigraphic continuity, and delineation of frozen-unfrozen interfaces at depth. In perennially frozen peatlands, GPR can: provide continuous active layer profiling (with high frequency antennae); estimate the depth of permafrost (with low frequency antennae); and identify taliks and unfrozen areas within, adjacent to, and/or below permafrost. For these applications, the continuous imaging of GPR offers more comprehensive spatial data than could be collected by field studies based solely on manual point measurements. In addition, continuous imaging minimizes the risk associated with data acquisition where anomalous subsurface conditions occur.

Investigations focused on evaluating specific peat properties (*e.g.*, energy value, carbon content) may find GPR a valuable tool for interpolating and extrapolating detailed stratigraphic information derived from point measurements, if further work in this area leads to more reliable correlations of radar events with subsurface changes in peat properties.

Signal velocity variations across vertical and lateral transitions in peat properties, particularly ground thermal regime, but also density, moisture content, peat type, and degree of

decomposition, remain poorly defined, and may limit interpretation of (absolute) depth, stratigraphy, and structure, particularly in transitional areas between unfrozen peat and perennially frozen landforms such as palsas and peat plateaus. Consequently, the need for accurate manual measurements of active layer depth, peat thickness, and other *in situ* properties remains.

Ultimately, the extent of manual testing may be reduced by use of GPR, depending on stratigraphic complexity and desired level of detail. However, in the near term, until radar response to changes in peat properties is better understood, future studies should consider increased coring density both at intervals along GPR transects and also as clusters at each coring location. The latter approach may allow information regarding peat properties derived from coring to better approximate the 'footprint' of the radar signal.

As the application of GPR to perennially frozen peatlands is at its inception, further research is warranted to test its viability in this environment. Optimum system configuration is dependent on the dielectric constant of the target media, as well as the target depth and orientation (see Section A.4 in Appendix A). Where the radar transect is to intersect materials with strong electrical contrast, such as the frozen - unfrozen interface (*i.e.*, palsa margin), variable station spacing and antenna separation should be tested to compare data quality from either side of the interface, and to determine appropriate parameters for profiling the transition zone, if this is of interest. The use of multiple system configurations, particularly the use of variable antennae frequency to obtain high resolution near-surface information in conjunction with profiles from depth, should be encouraged, to extend the range of useable information from a given site. Consistency in data processing and presentation in the literature is also desirable to improve comparability of data.

Additional GPR surveys on perennially frozen peatlands need to be conducted to extend the existing database from this environment; currently the number of case studies is too few to prove or refute the utility of GPR in this application. In particular, comparative surveys could be undertaken on palsa-scale frost mounds to test the detectability of definitive structural and stratigraphic variations that may improve our understanding of the formative processes. In particular, the potential for GPR to identify small-scale stratigraphic variations not otherwise observable by conventional methods must be evaluated. For example, where palsas and peat plateaus are known to have degraded and collapsed, GPR could be used to test for distinctive stratigraphic signatures as expressed by lateral and/or vertical stratigraphic discontinuities. If these are shown to occur, GPR may contribute to the determination of genesis of features, particularly those for which historical data are unavailable. However, this activity should ideally be preceded or accompanied by advancement of our theoretical understanding of permafrost landform development in peatlands.

Data processing techniques adapted from seismic methods may enhance coherency and lateral continuity of reflections in frozen media, although little work has been performed to date in this regard (LaFleche, *et al.*, 1991). (GPR data processing in other media has received greater attention; *e.g.*, Hara, *et al.*, 1988; Hogan, 1988; MacArthur, 1988; Olhoeft, 1988; Inkster, *et al.*, 1989; Turner, 1989; Fisher, *et al.*, 1992a, b; Maijala, 1992; Shikun, 1993;

Deshan, 1993; Fisher, *et al.*, 1994.) The use of data processing techniques adapted from seismic methods or developed specifically for GPR data for enhancement where data quality is currently marginal, as in frozen peat, should be further investigated. In particular, noise reduction filters, variable signal amplification, coherency filters, and dip corrections may highlight contrasts within frozen media, allowing improved resolution of internal structure and stratigraphy, and detection of the peat - mineral sediment interface.

Pursuit of these trends would further test the utility of GPR in this environment, to the advantage of research concerning peat as an energy resource, permafrost and related landform evolution, and the effect of global warming on permafrost degradation and consequent increased production of greenhouse gases from peatlands.

2.4 Literature Cited

- Åhman, R. 1976. The structure and morphology of minerogenic palsas in northern Norway. *Biuletyn Peryglacjalny* 26, 25-31.
- Annan, A.P. 1992. *Ground penetrating radar workshop notes*. Sensors & Software Inc., Mississauga, Ontario.
- Annan, A.P. and Davis, J.L. 1976. Impulse radar sounding in permafrost. *Radio Science* 11 (4), 383-394.
- Annan, A.P. and Davis, J.L. 1977. Impulse radar applied to ice thickness measurements and freshwater bathymetry. In *Report of Activities, Part B. Geological Survey of Canada Paper 77-1B*, 117-124.
- Annan, A.P., Davis, J.L. and Scott, W.J. 1975. Impulse radar profiling in permafrost. In *Report of Activities, Part C. Geological Survey of Canada Paper 75-1C*, 343-351.
- Arcone, S.A. 1984. *Pulse transmission through frozen silt*. U.S. Cold Regions Research and Engineering Laboratory, Report 84-17 (8p.)
- Baraniak, D.W. 1983. Exploration for surface peat deposits using ground penetrating radar. In Fuchsman, C.H. and Spigarelli, S.A., editors, *Proceedings, International Symposium on Peat Utilization*, Bemidji, Minnesota: Bemidji State University, 105-121.
- Barry, P.J. and Pollard, W.H. 1992. Ground probing radar investigations of ground ice on the Fosheim Peninsula, Ellesmere Island, Northwest Territories. In *Proceedings of the Third National Student Conference on Northern Studies*, Ottawa, Ontario: Musk-ox Special Publication 39, 59-66.
- Benson, R.C. and Yuhr, L.M. 1990. Evaluation of fractures in silts and clay using ground penetrating radar. In Lucius, J.E., Olhoeft, G.R., and Duke, S.K., editors, *Third International Conference on Ground Penetrating Radar*, Denver, Colorado: United States Geological Survey, Open File Report, 11.
- Bjelm, L. 1980. Geological interpretation with subsurface interface radar in peatlands. In *Proceedings, 6th International Peat Congress*, Duluth, Minnesota: International Peat Society, 7-8.
- Bogorodskii, V.V. and Trepov, G.V. 1979. Radar measurements of the thickness of peat and sapropel beds. *Soviet Physics, Technical Physics* 24 (3), 388-390.

- Brown, R.J.E. 1968. Occurrence of permafrost in Canadian peatlands. In *Proceedings of the Third International Peat Congress*, Québec: Energy, Mines and Resources and National Research Council, 174-181.
- Chernetsov, E.A., Beletsky, N.A., and Baev, M.Yu. 1988. Radar profiling of peat and gyttja deposits. In *Proceedings, 8th International Peat Congress*, Leningrad: International Peat Society, 15-21.
- Clasen, M.J. 1989. *Application of alternative surface geophysical techniques to hydrogeologic surveys*. Unpublished Master's thesis, University of South Florida.
- Coffeen, J.A. 1986. *Seismic Exploration Fundamentals: seismic techniques for finding oil, second edition*, Tulsa: PennWell Publishing Company (347p.).
- Collins, M.E. and Doolittle, J.A. 1987. Using ground penetrating radar to study soil microvariability. *Soil Science Society of America Journal* 51 (2), 491-493.
- Dallimore, S.R. and Davis, J.L. 1987. Ground probing radar investigations of massive ground ice and near surface geology in continuous permafrost. In *Current Research, Part A. Geological Survey of Canada Paper* 87-1A, 913-918.
- Davis, J.L. and Annan, A.P. 1989. Ground-penetrating radar for high-resolution mapping of soil and rock stratigraphy. *Geophysical Prospecting* 37, 531-551.
- Davis, J.L. and Pelletier, R.E. 1991. Ground penetrating radar utility for peat analyses in the Hudson Bay Lowlands. In *EOS, Transactions*, American Geophysical Union 72(17), 79.
- Davis, J.L., Topp, G.C. and Annan, A.P. 1977. Measuring soil water content in situ using time-domain reflectometry techniques. In *Report of Activities, Part B. Geological Survey of Canada Paper* 77-1B, 33-36.
- Deshan, Y. 1993. Point stacking and trace stacking of GPR map. *Earth Sciences - Journal of China University of Geosciences* 18(3), 311-314 (english abstract only).
- Doolittle, J.A. 1987. Using ground-penetrating radar to increase the quality and efficiency of soil surveys. In Reynolds, W.U. and Petersen, G.W., editors, *Soil Survey Techniques*, Soil Science Society of America, Special Publication No. 20, 11-32.
- Doolittle, J.A., Hardisky, M.A. and Black, S. 1992. A ground-penetrating radar study of Goodream palsas, Newfoundland, Canada. *Arctic and Alpine Research* 24 (2), 173-178.

- Doolittle, J.A., Hardisky, M.A. and Gross, M.F. 1990. A ground-penetrating radar study of active layer thicknesses in areas of moist sedge and wet sedge tundra near Bethel, Alaska, U.S.A. *Arctic and Alpine Research* 22 (2), 175-182.
- Finkel'shteyn, M.I., Kutev, V.A., Vlasov, O.P., Strekalkin, Ye.A. and Bogatyrev, Ye.F. 1979. Radar subsurface probing of peaty soil. *Doklady Akademii Nauk SSSR, Earth Sciences Sections* 247 (1), 24-26.
- Fisher, E., McMechan, G.A., and Annan, A.P. 1992a. Acquisition and processing of wide-aperture ground-penetrating radar data. *Geophysics* 57, 495-504.
- Fisher, E., McMechan, G.A., Annan, A.P. and Cosway, S.W. 1992b. Examples of reverse-time migration of single-channel, ground penetrating radar profiles. *Geophysics* 57, 577-586.
- Fisher, S.C., Stewart, R.R. and Jol, H.M. 1994. Processing ground penetrating radar data. In *GPR '94, Proceedings of the Fifth International Conference on Ground Penetrating Radar*, Kitchener, Ontario: Waterloo Centre for Groundwater Research and Canadian Geotechnical Society, 2, 661-675.
- Forsgren, B. 1968. Studies of palsas in Finland, Norway and Sweden, 1964-1966. *Biuletyn Peryglacjalny* 17, 117-123.
- Foss, M.M. and Leckenby, R.J. 1987. *Coal mine hazard detection using in-seam ground penetrating radar transillumination*. United States Bureau of Mines, Report of Investigations, 9062 (27p.).
- Gorham, E. 1991. Northern peatlands role in the carbon cycle and probable responses to climate warming. *Ecological Applications* 1, 182-195.
- Hänninen, P. 1990. New electric methods for peatland resources. In Kauranne, L.K. and L.-K. Königsson, editors, *Economic Quaternary Geology in the Nordic Countries*. *Striae* 29, 47-50.
- Hänninen, P. 1992a. *Application of ground penetrating radar and radio wave moisture probe techniques to peatland investigations*. Geological Survey of Finland, Bulletin 361 (71p.).
- Hänninen, P. 1992b. Application of ground penetrating radar techniques to peatland investigations. In Hänninen, P. and Autio, S., editors, *Fourth International Conference on Ground Penetrating Radar*, Rovaniemi, Finland: Geological Survey of Finland, Special Paper 16, 217-221.

- Hara, T., Sakayama, T., Suzuki, T., and Arai, I. 1988. Synthetic aperture processing applied to georadar records. In *Second International Symposium on Geotechnical Applications of Ground Penetrating Radar (Abstracts)*, 38.
- Hayley, D.W. 1989. Maintenance of a railway grade over permafrost in Canada. *The Northern Engineer* 21(3), 4-10.
- Hinkel, K.M. 1988. Frost mounds formed by degradation at Slope Mountain, Alaska, USA. *Arctic and Alpine Research* 20, 76-85.
- Hobbs, N.B. 1986. Mire morphology and the properties and behaviour of some British and foreign peats. *Quarterly Journal of Engineering Geology, London* 19, 7-80.
- Hogan, G. 1988. Migration of ground penetrating radar data: a technique for locating subsurface targets. In Fitterman, D., Bell, R., Corbett, J., Davenport, C., Hulse, S., and Bierley, C., editors, *Proceedings of the Symposium on the Application of Geophysics to Engineering and Environmental Problems*, Society of Engineering and Mineral Exploration Geophysicists: United States Geological Survey, 809-822.
- Ingram, H.A.P. 1978. Soil layers in mires: function and terminology. *Journal of Soil Science* 29, 224-227.
- Inkster, D.R., Rossiter, J.R., Goodman, R., Galbraith, M. and Davis, J.L. 1989. Ground penetrating radar for subsurface environmental applications. In *Proceedings of the Thematic Conference on Remote Sensing for Exploration Geology (Seventh)*. 127-140.
- Jol, H.M. and Smith, D.G. 1991. Ground penetrating radar of northern lacustrine deltas. *Canadian Journal of Earth Sciences* 28, 1939-1947.
- Judge, A.S., Tucker, C.M., Pilon, J.A. and Moorman, B.J. 1991. Remote sensing of permafrost by ground-penetrating radar at two airports in Arctic Canada. *Arctic* 44, Supp. 1, 40-48.
- Kettles, I.M. and Robinson, S.D. 1996. A ground-penetrating radar study of peat landforms in the discontinuous permafrost zone near Fort Simpson, Northwest Territories, Canada. In Trettin, C., M. Jurgenson, D. Grigal, M. Gale and J. Jeglum, editors, *Northern Forested Wetlands: Ecology and Management*, CRC, Lewis Publishers, Boca Raton, Florida, 147-160.
- Kovacs, A. and Morey, R.M. 1985. Impulse radar sounding of frozen ground. In Brown, J., Metz, M.C., and Hoekstra, P., editors, *Workshop on Permafrost Geophysics*, Golden, Colorado: United States Army Cold Regions Research and Engineering Laboratory, Special Report 85-5, 28-40.

- LaFleche, P.T., Judge, A.S., Moorman, B.J., Cassidy, B. and Bedard, R. 1988. Ground probing radar investigations of gravel roadbed failures, Rae Access road, N.W.T. In *Current Research, Part D. Geological Survey of Canada Paper 88-1D*, 129-135.
- LaFleche, P.T., Todoeschuck, J.P., Jensen, O.G. and Judge, A.S. 1991. Analysis of ground-probing radar data: predictive deconvolution. *Canadian Geotechnical Journal* 28, 134-139.
- Laug, C., Scullion, T. and Chan, P. 1992. Using ground penetrating radar technology for pavement evaluation in Texas, USA. In Hänninen, P. and Autio, S., editors, *Fourth International Conference on Ground Penetrating Radar*, Rovaniemi, Finland: Geological Survey of Finland, Special Paper 16, 277-283.
- Lowe, D.J. 1985. Application of impulse radar to continuous profiling of tephra-bearing lake sediments and peats: an initial evaluation. *New Zealand Journal of Geology and Geophysics* 28, 667-674.
- Lundqvist, J. 1969. Earth and ice mounds: a terminological discussion. In Péwé, T.L., editor, *The Periglacial Environment, past and present*: McGill - Queen's University Press, Montreal, 203-215.
- MacArthur, J. 1988. Real time Kirchhoff migration on ground penetrating radar data. In *Second International Symposium on Geotechnical Applications of Ground Penetrating Radar*, 40-41.
- Maijala, P. 1992. Application of some seismic data processing methods to ground penetrating radar data. In Hänninen, P. and Autio, S., editors, *Fourth International Conference on Ground Penetrating Radar*, Rovaniemi, Finland: Geological Survey of Finland, Special Paper 16, 103-110.
- Meyer, J.H. 1989. Investigation of Holocene organic sediments - a geophysical approach. *International Peat Journal* 3, 45-57.
- Moorman, B.J. and Judge, A.S. 1989. Delineating massive ice with ground penetrating radar. In *Program with Abstracts, Geological Association of Canada* 14, A76.
- Morey, R.M. and French, R.B. 1977. Mapping peat cover and shallow, discontinuous permafrost using impulse radar. *Geophysics* 42 (7), 1526.
- National Wetlands Working Group (Canada Committee on Ecological Land Classification). 1988. *Wetlands of Canada. Ecological Land Classification Series No. 24*. Sustainable Development Branch, Environment Canada, Ottawa and Polyscience Publications Inc., Montreal (452p.).

- Nelson, F.E., Hinkel, K.M. and Outcalt, S.I. 1992. Palsa-scale frost mounds. In Dixon, J.C. and Abrahams, A.D., editors, *Periglacial Geomorphology, Proceedings of the 22nd Annual Binghampton Symposium in Geomorphology*: John Wiley & Sons, Chichester, 305-325.
- Nobes, D.C., Theimer, B.D. and Warner, B.G. 1989. Grant 310, Subsurface radar profiling of two peatlands in southern Ontario. In *Geoscience Research Grant Program; summary of research 1988-1989*, Ontario Geological Survey, Miscellaneous Paper, 53-58.
- NRCC (National Research Council of Canada). 1988. *Glossary of permafrost and related terms*. Permafrost Subcommittee, Associate Committee on Geotechnical Research, National Research Council of Canada, Ottawa, Technical Memorandum No. 142.
- Olhoeft, G. 1988. Applications and limitations of computer-processed ground-penetrating radar data. In *Second International Symposium on Geotechnical Applications of Ground Penetrating Radar (Abstracts)*, 37.
- Pelletier, R.E., Davis, J.L. and Rossiter, J.R. 1991. Peat analyses in the Hudson Bay Lowlands using ground penetrating radar. In Putkonen, J., editor, *Remote Sensing: Global Monitoring for Earth Management; International Geoscience and Remote Sensing Symposium, Proceedings*, Volume IV, Espoo, Finland: Helsinki University of Technology, 2141-2144.
- Pilon, J.A., Allard, M. and Séguin, M.K. 1992. Ground probing radar in the investigation of permafrost and subsurface characteristics of surficial deposits in Kangiqsualujuaq, northern Québec. In Pilon, J.A., editor, *Ground penetrating radar*, Ottawa, Ontario: Geological Survey of Canada, Paper 90-94, 41-48.
- Pilon, J.A., Annan, A.P. and Davis, J.L. 1985. Monitoring permafrost ground conditions with ground probing radar. In Brown, J., Metz, M.C., and Hoekstra, P., editors, *Workshop on Permafrost Geophysics*, Golden, Colorado: United States Army Cold Regions Research and Engineering Laboratory, Special Report 85-5, 71-73.
- Remote Applications Inc. 1982. *The use of impulse radar techniques for depth profiling of peat deposits*. National Research Council of Canada, Division of Energy Research and Development, Ottawa, Ontario (94p. plus appendices).
- Robinson, S.D. 1993. *Geophysical and geomorphological investigations of massive ground ice, Fosheim Peninsula, Ellesmere Island, Northwest Territories*. Unpublished M.Sc. Thesis, Department of Geography, Queen's University, Kingston, Ontario (171p.).
- Robinson, S.D., Moorman, B.J., Judge, A.S. and Dallimore, S.R. 1993. The characterization of massive ground ice at Yaya Lake, Northwest Territories using radar stratigraphy

techniques. In *Current Research, Part B. Geological Survey of Canada Paper 93-1B*, 23-32.

- Robinson, S.D., Moorman, B.J., Judge, A.S., Dallimore, S.R. and Shimeld, J.W. 1992. The application of radar stratigraphic techniques to the investigation of massive ground ice at Yaya Lake, Northwest Territories. In *Proceedings of the Third National Student Conference on Northern Studies*, Ottawa, Ontario: Musk-Ox Special Publication 39, 39-49.
- Saarenketo, T., Hietala, K. and Salmi, T. 1992. GPR applications in geotechnical investigations of peat for road survey purposes. In Hänninen, P. and Autio, S., editors, *Fourth International Conference on Ground Penetrating Radar*, Rovaniemi, Finland: Geological Survey of Finland, Special Paper 16, 293-305.
- Salmi, M. 1968. Development of palsas in Finnish Lapland. In *Proc. Third Int. Peat Congress*, Quebec, Canada, 182-189.
- Scaife, J.E., Giamou, P. and Annan, A.P. 1990. Case history; GPR evaluation for detection of buried pipes and barrels at the Columbia test site, Waterloo, Ontario, Canada. In Lucius, J.E., Olhoeft, G.R., and Duke, S.K., editors, *Third International Conference on Ground Penetrating Radar*, Denver, Colorado: United States Geological Survey, Open File Report, 60.
- Scott, W.J., Campbell, K.J. and Orange, A.S. 1974. EM pulse survey method in permafrost. In Collett, L.C. and Brown, R.J.E., editors, *Proceedings of a Symposium on Permafrost Geophysics*, Ottawa, Ontario: National Research Council of Canada, Associate Committee on Geotechnical Research, Technical Memorandum 113, 92-96.
- Seguin, M.K., Allard, M., Pilon, J., Lévesque, R. and Fortier, R. 1989. Geophysical detection and characterization of ground ice in northern Québec. In *Program with Abstracts, Geological Association of Canada* 14, A76.
- Seppälä, M. 1988. Palsas and related forms. In Clark, M.J., editor, *Advances in Periglacial Geomorphology*: John Wiley & Sons, Chichester, 247-278.
- Seppälä, M. and Koutaniemi, L. 1985. Formation of a string and pool topography as expressed by morphology, stratigraphy and current processes on a mire in Kuusamo, Finland. *Boreas* 14, 287-309.
- Shikun, D. 1993. Application of Kirchhoff integral migration method to processing GPR image. *Earth Science - Journal of China University of Geosciences* 18(3), 303-309 (english abstract only).

- Sims, R.A., Wickware, G.M. and Cowell, D.W. 1987. Wetlands of the southern Hudson Bay coast in Ontario. In Rubec, C.D.A. and Overend, R.P., editors, *Proceedings, Symposium '87, Wetlands/Peatlands*, Edmonton, Alberta, 435-442.
- Theimer, B.D. 1990. *Principles of bog characterization using ground penetrating radar*. M.Sc. thesis, University of Waterloo, Waterloo, Ontario (232p.).
- Theimer, B.D., Nobes, D.C. and Warner, B.G. 1994. A study of the geoelectrical properties of peatlands and their influence on ground-penetrating radar surveying. *Geophysical Prospecting* 42, 179-209.
- Tiuri, M., Toikka, M., Marttila, I. and Tolonen, K. 1983. The use of radio wave probe and subsurface interface radar in peat resource inventory. In Robertson, R.A., editor, *Remote Sensing in Peat and Terrain Resource Surveys, Proceedings of Symposium of IPS Commission I*, Aberdeen, Scotland: International Peat Society, 1331-143.
- Tolonen, K., Rummukainen, A., Toikka, M. and Marttila, I. 1984. Comparison between conventional peat geological and improved electronic methods in examining economically important peatland properties. In *Proceedings, Seventh International Peat Congress*, Dublin: Irish National Peat Committee, vol. 2, 1-10.
- Topp, G.C., Davis, J.L. and Annan, A.P. 1980. Electromagnetic determination of soil water content: measurements in coaxial transmission lines. *Water Resources Research*, 16(3), 574-582.
- Toshioka, T., Osada, M. and Sakayama, T. 1990. Application of ground penetrating radar to archaeological investigation. In Lucius, J.E., Olhoeft, G.R., and Duke, S.K., editors, *Third International Conference on Ground Penetrating Radar*, Denver, Colorado: United States Geological Survey, Open File Report, 67.
- Turner, G. 1989. Data processing techniques for the location of one dimensional objects using ground probing radar. *Exploration Geophysics* 20, 379-382.
- Ulriksen, C.P.F. 1980. Investigation of peat thickness with radar. In *Proceedings, 6th International Peat Congress*, Duluth, Minnesota: International Peat Society, 126-129.
- von Post, L. 1922. Sveriges Geologiska Undersöknings torvinventering och nogra av dess hittills vunna resultat (SGU peat inventory and some preliminary results). *Svenska Mosskulturforeningens Tidskrift, Jönköping, Sweden* 36, 1-37.
- Warner, B.G., Nobes, D.C. and Theimer, B.D. 1990. An application of ground penetrating radar to peat stratigraphy of Ellice Swamp, southwestern Ontario. *Canadian Journal of Earth Sciences* 27, 932-938.

- Welsby, J. 1988. The utilisation of geo-radar in monitoring cutover peatlands. In *Proceedings, 8th International Peat Congress*, Leningrad: International Peat Society, 99-107.
- Worsfold, R.D., Parashar, S.K. and Perrott, T. 1986. Depth profiling of peat deposits with impulse radar. *Canadian Geotechnical Journal* 23, 142-154.
- Worsley, P., Gurney, S.D., and Collins, P.E.F. 1995. Late Holocene 'mineral palsas' and associated vegetation patterns: a case study from Lac Hendry, Northern Québec, Canada and significance for European Pleistocene thermokarst. *Quaternary Science Reviews* 14, 179-192.
- Zhonggong, Z., Yizhi, H. and Zhiying, X. 1993. Use of ground penetrating radar for the detection of permafrost and delineation of its distribution under the asphalted road of Qinghai-Xizang highway. In *Permafrost, Sixth International Conference, Proceedings*, Volume I, Beijing, China: South China University of Technology Press, 758-763.
- Zoltai, S.C. 1972. Palsas and peat plateaus in central Manitoba and Saskatchewan. *Canadian Journal of Forest Research* 2, 291-302.
- Zoltai, S. C. and Tarnocai, C. 1975. Perennially frozen peatlands in the western arctic and subarctic of Canada. *Canadian Journal of Earth Sciences* 12, 28-43.

3.0 RADAR STRATIGRAPHY AND SEISMIC DATA PROCESSING TECHNIQUES APPLIED TO TWO PALSA FEN SITES, MACMILLAN PASS, NORTHWEST TERRITORIES

3.1 Introduction

Ground penetrating radar (GPR) provides a continuous, high resolution profile of subsurface variations in electrical properties, which, through theoretical analysis, interpretation, and correlation with known site conditions, can be used to infer subsurface changes in material properties, such as moisture content, density, composition, and temperature (Annan, 1992). As a result, GPR has become widely accepted in a variety of earth science and related fields as a time-effective, non-invasive method for collecting spatially extensive and continuous subsurface stratigraphic and structural information.

Since its development in the 1970s, GPR has been used for mapping of peat deposits, and extensively for permafrost applications, such as detection and mapping of permafrost, measurement of active layer thickness, and delineation of massive ground ice and pingo core ice (see Chapter 1 for pertinent references). However, application of GPR to investigations of perennially frozen peatlands has been limited (Doolittle, *et al.*, 1992; Pilon, *et al.*, 1992; Kettles and Robinson, 1996).

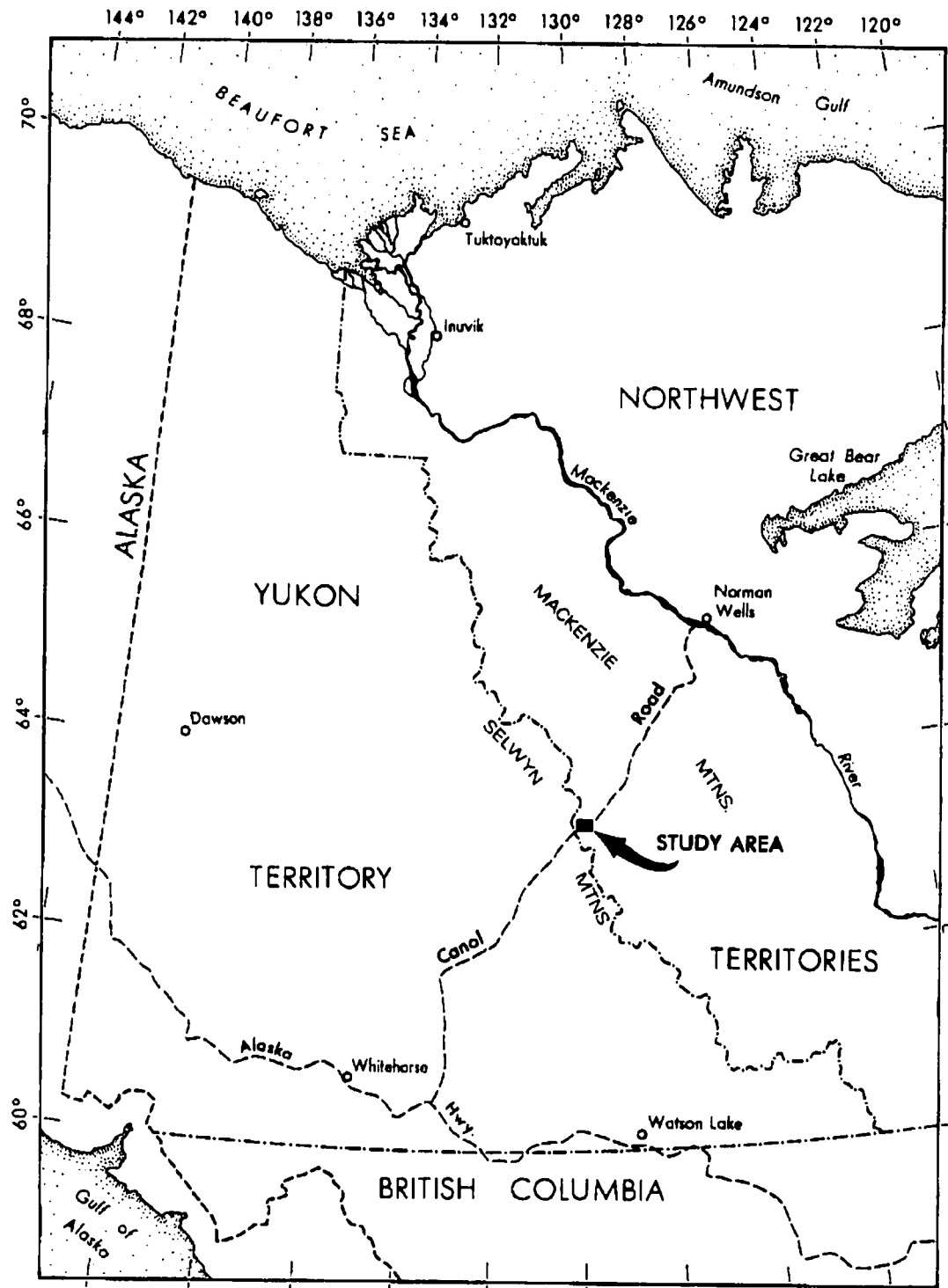
Traditionally, studies of peat stratigraphy and permafrost characteristics in peatlands have been based on coring and sample analyses at a limited number of locations. This approach can be time consuming and labour intensive. Furthermore, peat thickness, the nature and distribution of permafrost, and properties of peat and underlying sediment can have a high degree of lateral and vertical variability which can be overlooked by conventional methods.

The purpose of this study was to evaluate the suitability of GPR for imaging the stratigraphy and subsurface structure of frozen and unfrozen peat and underlying sediments, and for characterizing permafrost bodies in peatlands. In addition, the potential for data enhancement using processing techniques adapted from seismic methods was investigated.

3.2 Study Area

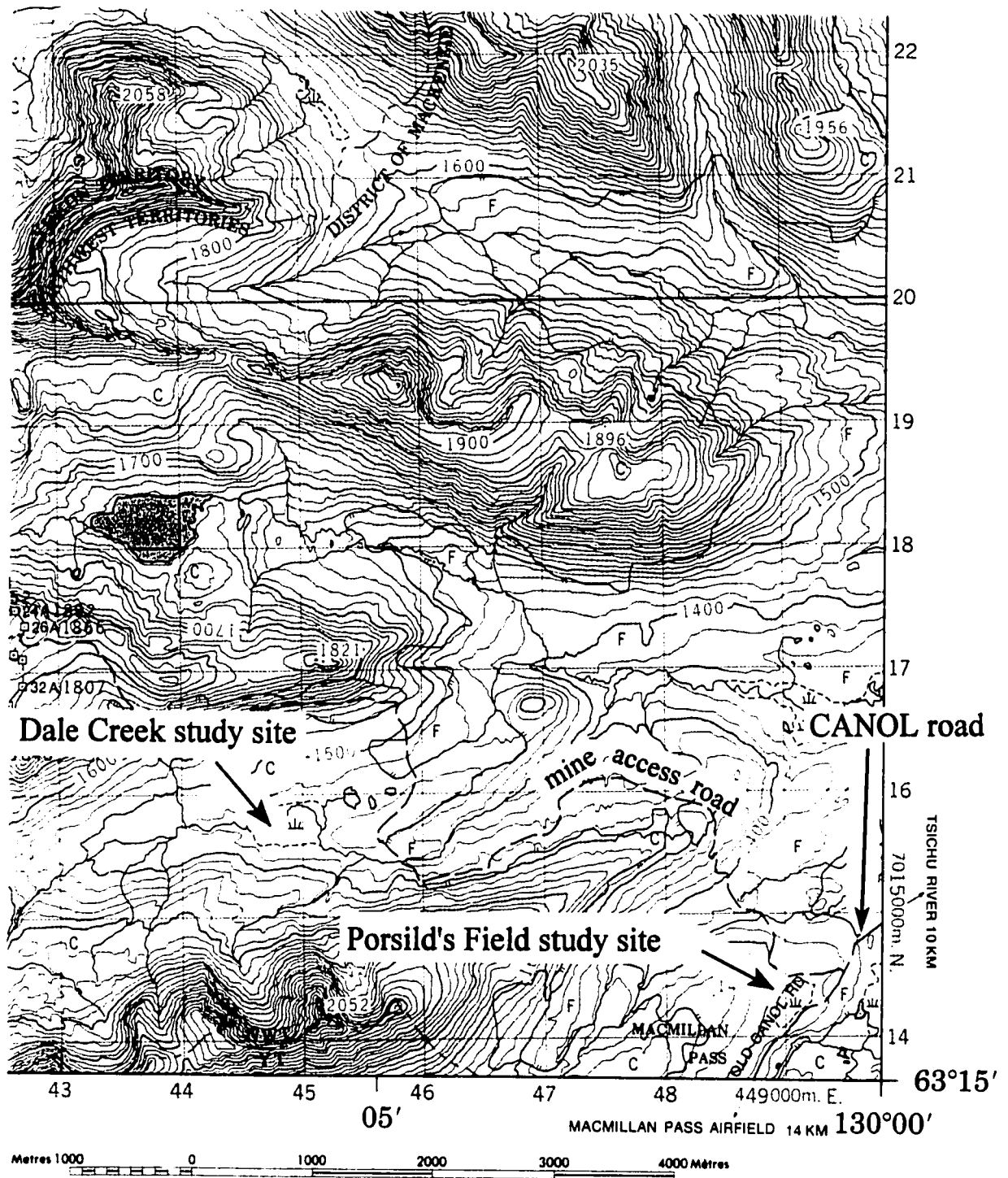
GPR data for this study were collected from two peatland sites located in the Macmillan Pass area of the Selwyn Mountains, Northwest Territories (Figures 3-1 and 3-2); the sites were selected on the basis of their accessibility (particularly with respect to the GPR equipment), available aerial photographic and historical records, proximity to one another, and treatment in the literature. The study area is characterized by rugged alpine terrain within the zone of widespread discontinuous permafrost (NRCC, 1988). The distribution of permafrost appears to be limited to high elevations, in peatlands (*i.e.*, palsas and peat plateaus) at lower elevations, and few isolated sites with locally favourable conditions. The area is underlain by folded and faulted Proterozoic and Paleozoic metamorphosed sedimentary and intrusive granitic rocks (Gill, 1975). Wetlands occur in low-lying basins, and although common, are not extensive in area. Organic deposits reaching over 5 m thickness occur in the wetlands.

Figure 3-1. Study area location map.



Source: G. Lester, Department of Earth and Atmospheric Sciences (formerly Department of Geography), University of Alberta.

Figure 3-2. Location of Porsild's Field and Dale Creek peatland study sites.



Map scale 1:50,000. Contour interval 20 metres.

Source: Keele Peak, Sheet 105-O/8, Surveys and Mapping Branch, Department of Energy, Mines and Resources, Ottawa, 1982.

The Porsild's Field site, so named (Kershaw and Gill, 1979) for its description by Porsild (1945, 1951), is located in Macmillan Pass, adjacent to the CANOL road, at an elevation of approximately 1390 m asl ($63^{\circ}15'15''\text{N}$, $130^{\circ}01'05''\text{W}$). At this site, there were six separate palsa mounds in 1994 (Plate 3-1), although it is clear from available records that the mounds were more numerous in the past (Kershaw and Gill, 1979). The palsas ranged in height from 0.8 m to 2.5 m above the fen, with long axes ranging from *ca.* 10.5 m to *ca.* 39 m.

The Dale Creek study site ($63^{\circ}16'15''\text{N}$, $130^{\circ}06'00''\text{W}$) is located in a neighbouring valley to the north of the Porsild's Field study site, at an elevation of approximately 1470 m asl. At this site, five simple dome-shaped palsas and one complex palsa, consisting of several smaller mounds joined by lower saddle areas, were present (Plate 3-2). For this study, data were collected from the simple palsa forms only, as deep and/or broad areas of open water curtailed GPR access to the complex feature. The five palsas which were studied ranged in height from 1.35 m to 3.0 m above the surface of the fen, and in diameter from *ca.* 16.5 m to *ca.* 47.5 m.

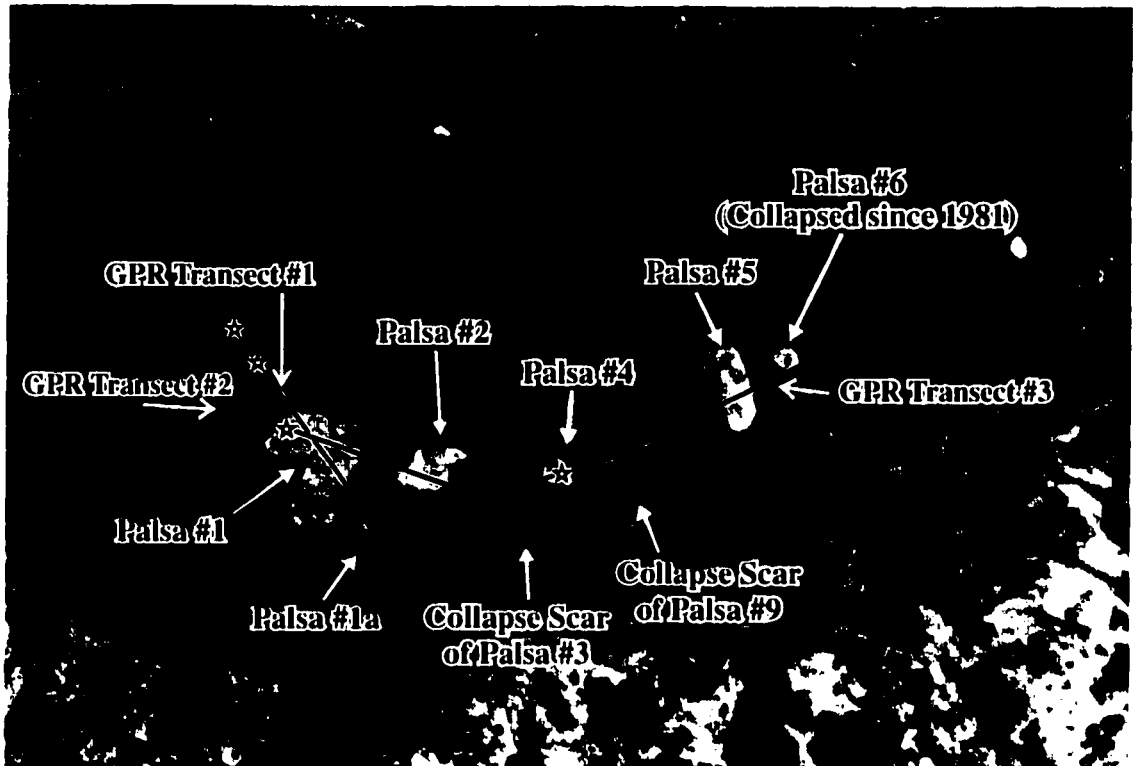
At both sites, shrub-dominated communities bordered the fens, while *Carex aquatilis* and *Eriophorum* spp. and mosses were predominant in the fen, and lichen-moss (*Cladina* spp./*Cetraria* spp./*Polytrichum* spp.) dominated palsa surfaces (G.P. Kershaw, pers. comm., 1994). Bare peat occurred on deflated palsa surfaces and edges where the peat was cracked and/or slumped, and ground squirrel burrowing was extensive.

3.3 Ground Penetrating Radar

GPR involves the transmission of high frequency (typically ranging from 10 MHz to 1000 MHz) electromagnetic (EM) pulses into the ground and the detection of signal energy reflected back to the surface from interfaces where there is a contrast in electrical properties (Figure 3-3); this contrast may be caused by a change in moisture content, density, composition, or temperature (Annan, 1992). The velocity of the radar signal propagation, the attenuation of the radar signal, and the amplitude of the signal energy reflected from each subsurface interface are controlled by the electrical properties of the materials through which the radar signal passes (Davis and Annan, 1989).

Data are recorded as the two-way travel time (*i.e.*, from the transmitting antenna down to the reflecting interface and up to the receiving antenna), in nanoseconds, of the reflected energy *versus* position, in metres, at evenly spaced points along a survey transect, generating a continuous profile of subsurface interfaces with electrical contrast (Figure 3-4). Inferences are then made regarding what each interface represents, based on the nature of the reflected energy (*i.e.*, amplitude, frequency, lateral continuity across the profile, orientation of reflections, signal attenuation); this interpretation is typically supported by point verification using borehole or coring data. The depth to each interface is estimated using the recorded two-way travel time and the signal propagation velocity through the subsurface, the latter derived from a Common Mid Point (CMP) velocity sounding conducted in the field (*cf.* Annan, *et al.*, 1975; Annan and Davis, 1976; Morey and Kovacs, 1985). A more detailed treatment of GPR principles is provided by Davis and Annan (1989) (also *cf.* Arcone, 1984; Annan, 1992). An overview of GPR principles is provided in Appendix A.

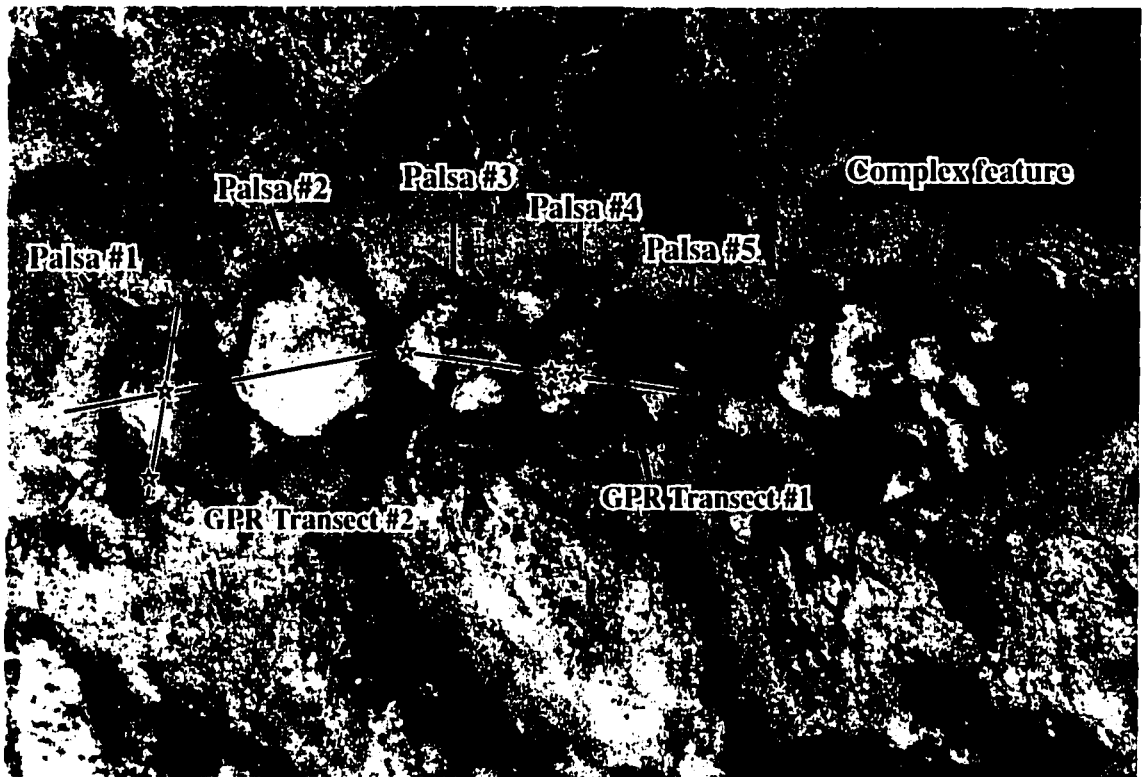
Plate 3-1. Porsild's Field study site.



Aerial view of extant palsas in Porsild's Field, as well as collapse scars of pre-existing palsas known from historic records. GPR Transect #1 crosses palsa #1 from southeast to northwest. GPR Transect #2 crosses palsas #1 and #2 from east to west. GPR Transect #3 crosses palsas #4 and #5 from east to west, and intersects the edge of the collapse scar of pre-existing palsas #9 and #6. (Palsa #7 and the collapse scar of palsa #8, located in the upper right of the photo, were not surveyed.) Coring locations are indicated by stars. South is at the top of the photograph.

Photo credit: Aerial photograph W1727, 143525, August 7, 1981.

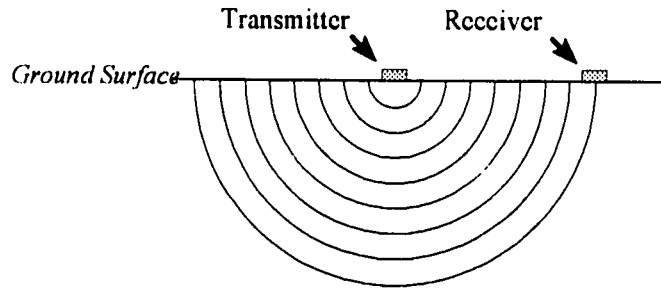
Plate 3-2. Dale Creek study site.



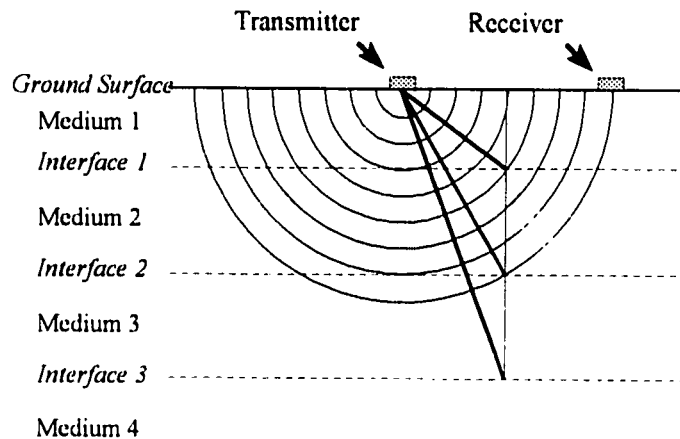
Aerial view showing five simple dome-shaped elliptical palsas and one complex feature consisting of several smaller mounds joined by lower saddle areas, at Dale Creek study site. GPR Transect #1 crosses palsas #5 to #1, from east to west. GPR Transect #2 crosses palsa #1 from north to south. Coring locations are indicated by stars. North is at the top of the photograph.

Photo credit: Air photograph W1731, 144908, August 30, 1981

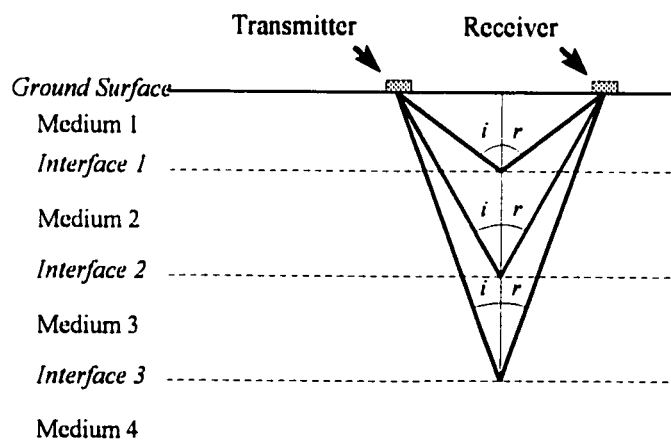
Figure 3-3. Geometry of GPR signal path through simplified subsurface.



- a)** Radar energy travelling outwards from transmitter.

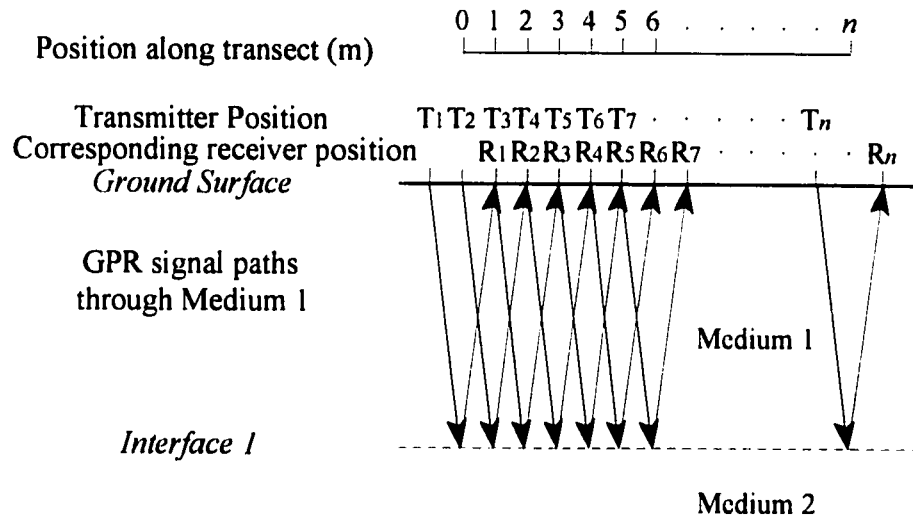


- b)** Straight ray paths show routes of individual points on the radar wave front.

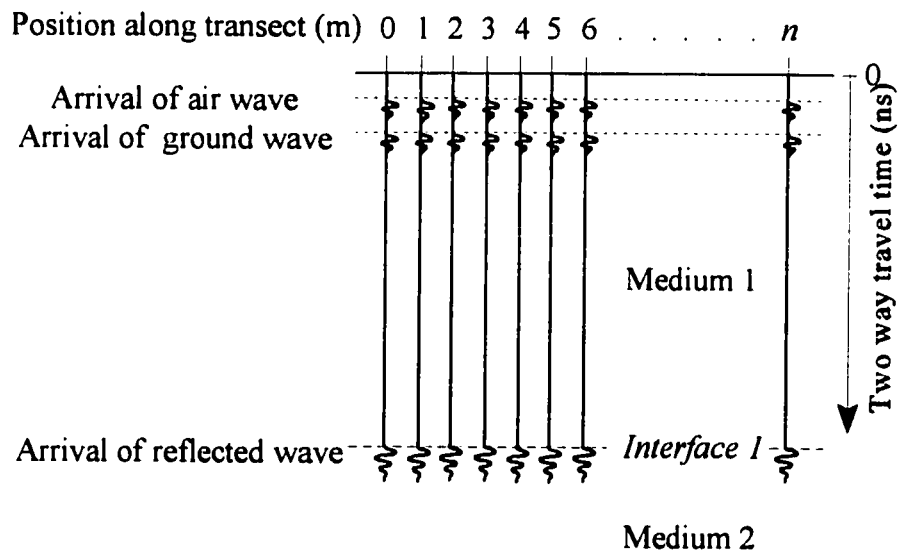


- c)** Radar energy is reflected (r) at an angle equal to the angle of incidence (i) from interfaces with a contrast in electrical properties.

Figure 3-4. Survey configuration to generate continuous subsurface radar reflection profile through simplified subsurface.



- a) Evenly spaced, successive transmitter (T_i) and receiver (R_i) positions in constant step-size survey configuration, to generate continuous profile of data from points on subsurface interface.



- b) Resulting GPR profile from configuration shown in (a). Each trace is plotted at midpoint between transmitter and receiver locations. Note signal from direct air wave, ground wave and reflected wave (see Section 3.6).

Modified from Jol and Smith (1991).

3.4 Field Methods

The GPR data presented in this chapter were collected as single-channel, constant-offset radar reflection profiles using a pulseEKKO IV GPR system with a 400V transmitter and 50 MHz antennae, developed and manufactured by Sensors & Software Inc., of Mississauga, Ontario, Canada. In a single-channel survey, data for each point or station along the survey transect are collected as a single trace using one transmitter and one receiver only. A constant antenna offset ¹ of 2 m and a constant 0.5 m station separation (or step size) ² were used in this study (see Section A.4 in Appendix A for a discussion of survey configuration).

To improve the signal-to-noise ratio, a stacked pulsed radar signal of 128 source excitations was transmitted for each trace (*cf.* Fisher, *et al.*, 1992a, 1992b; Kalantzis, 1994). (This field stacking is distinct from the stacking, *i.e.*, combining of individual traces, that is a common step in seismic data processing (*cf.* Coffeen, 1986:134-138).) For each trace, the signal sine wave was sampled at 1000 points at a sampling interval of 800 ps, for a total time window (*i.e.*, duration of time in which reflected energy is recorded, and thus, the length of each trace) of 800 ns. CMP surveys for determination of signal propagation velocity were conducted at each site and over both frozen and unfrozen terrain; the velocity data obtained by this method are integrated values over the depth of penetration of the profile.

Coring was undertaken in the fens using a Macaulay corer (Jowsey, 1966) and on the palsas using a permafrost corer (Zoltai, 1978). Visible changes in ice content and character, peat characteristics, and occurrence of sediment were noted (Appendix B). Topographic measurements were taken along the transects using an Abney level to allow topographic corrections to be applied to the GPR profiles. Thaw depths along the transects at the time of the surveys were measured using a YSI Tele-thermometer probe with a 0.5°C resolution (Appendix D). Surface conditions of the palsas were noted, such as general vegetation cover, occurrence of bare peat, and presence of cracks, slump blocks, and other disturbances.

3.5 Data Processing

Data were recorded digitally, allowing a variety of processing techniques to be applied. Dead or erroneous traces resulting from system malfunction or operator error during surveying were deleted from the data files during processing. Signal saturation corrections determined by the system manufacturer were applied to the data from the Porsild's Field site, to compensate for receiver saturation or 'overload' and DC offset on the early part of each signal trace due to large amplitude inputs from near-surface energy arrivals (*i.e.*, air wave, ground wave, and near-surface reflections) (Fisher, *et al.*, 1994). Signal saturation

¹

Distance between antennae. In Figure 3-4, antenna offset is distance between T_n and R_n .

²

Distance between radar sampling points (*i.e.*, traces). In Figure 3-4, station separation is distance between T_1 and T_2 , T_2 and T_3 , T_3 and T_4 , and so on.

corrections could not be applied to the Dale Creek data due to an unidentified problem in the data files. Elevation corrections were applied to the data using a topographic correction function included in the radar operating software.

GPR is analogous to seismic exploration techniques, as in each of these techniques the signal wave propagates and attenuates through earth media at velocities controlled by the material properties, and is reflected at local electric and elastic discontinuities, respectively (Fisher, *et al.*, 1992a; Majjala, 1992). The similarities between propagation of EM and acoustic (seismic) waves in earth materials suggest that data processing techniques developed for analysis of seismic data, such as deconvolution and migration, can successfully be applied to GPR data (Hogan, 1988; LaFleche, *et al.*, 1991; Majjala, 1992; Fisher, *et al.*, 1992a, b; Fisher, *et al.*, 1994). The main difference between radar and seismic data is one of scale, where GPR data are recorded in nanoseconds and MHz, and seismic in milliseconds and Hz.

The GPR data collected in this study were converted to SEG-Y seismic format using the pulseEKKO IV software. Data processing was performed at the Department of Geology and Geophysics at the University of Calgary, on a SUN Sparcstation UNIX workstation using the ProMAX 2-D seismic data processing package developed by Advance Geophysical Corporation (version 5.1). Processing steps performed included gain recovery, spectral analysis, spectral shaping, bandpass filtering, velocity analysis, deconvolution, normal moveout correction, time-depth conversion, migration, and coherency filtering (F-X deconvolution); each of these processes are explained briefly below.

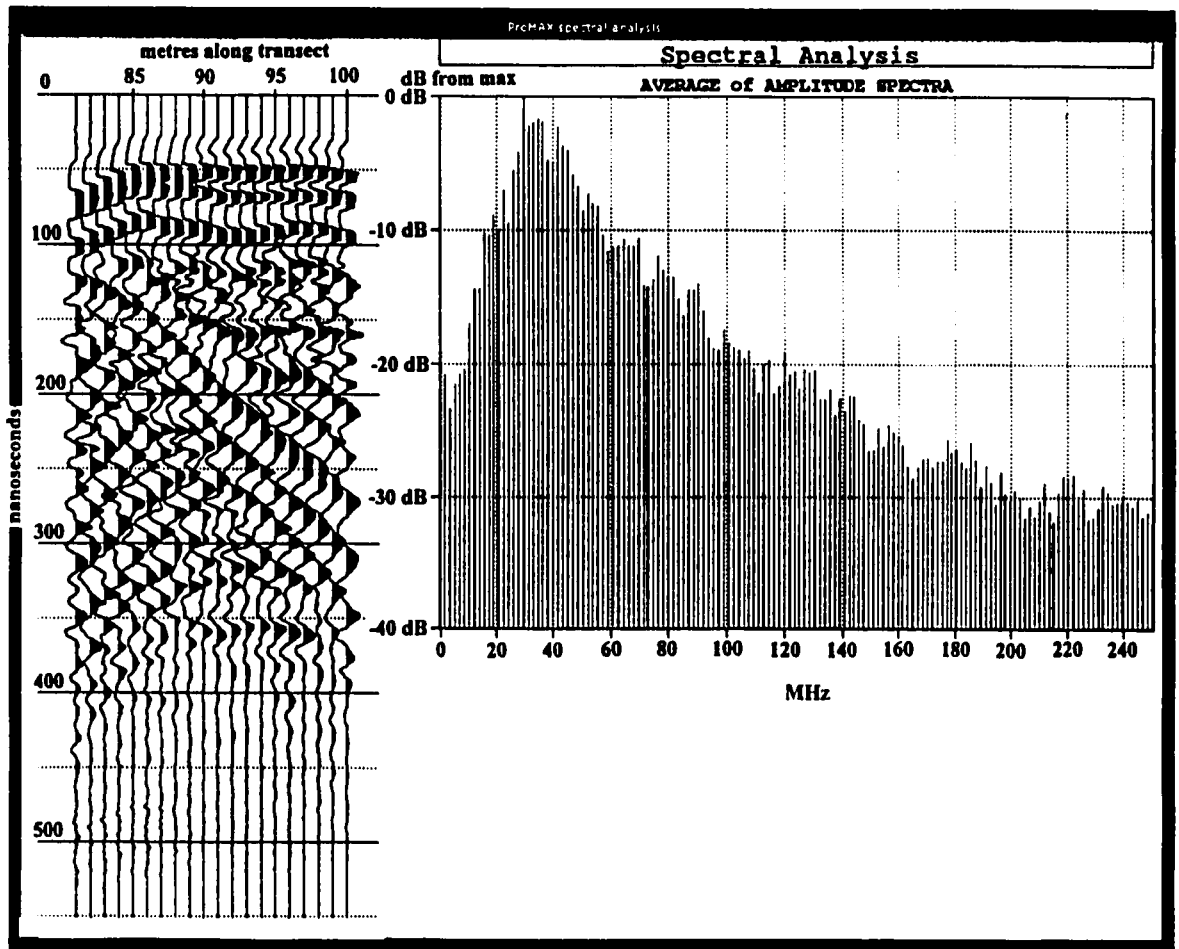
Gain Recovery

Signal attenuation in the subsurface causes reflections from deeper interfaces to be of lower amplitude relative to shallower interfaces with similar electrical contrast. Similarly, reflections from weak interfaces at depth are difficult to resolve on radar profiles displayed with true relative amplitude. A time variable gain function applied to the data will boost signal amplitude with increasing travel time; this enhances stratigraphic detail throughout the profile. However, in profiles displayed with a time variable gain function, true relative amplitude information is lost. Thus, strong reflections produced by interfaces with strong electrical contrast, such as the peat - mineral sediment interface, may be indistinguishable from weaker interfaces, such as internal peat stratification. A constant gain function will boost signal amplitude by the same increment throughout the profile, thus preserving true relative amplitude of radar reflections.

Spectral Analysis

Spectral analysis is a tool, rather than a process applied to enhance the data, which allows the user to determine the dominant or peak frequency bandwidth of the radar signal. This step facilitates the selection of parameters for bandpass filtering to improve the signal-to-noise ratio of the data. In spectral analysis, the average amplitude of samples within a user-specified time window (in this case, the length of the trace encompassing the stratigraphic information, usually 550 ns to 600 ns) is calculated for each frequency between a user-specified range (in this case, 0 MHz to 250 MHz), for each input trace or group of traces, and is plotted relative to the maximum amplitude for each frequency (Figure 3-5). The resulting

Figure 3-5. Example of spectral analysis of ground penetrating radar data.



Spectral analysis of a group of 20 traces from a time window of 0 ns to 550 ns (left) shows the frequency range of the radar signal energy (upper right). Radar signal data are contained in the range where the average amplitude is close to the maximum for a given frequency; in this case, signal data are contained between 10 MHz and 110 MHz. The noise-to-signal ratio increases with deviation of the average amplitude from the maximum amplitude. No signal information is contained in frequencies where the average amplitude is more than 30 dB from the maximum amplitude.

Plot produced from ProMAX v.5.1, after data conversion to SEG-Y seismic format using the pulseEKKO IV operating software.

power spectra can be used to identify the frequency range within which the actual signal information is contained, as the range where the average amplitude is close to the maximum for a given frequency.

Bandpass Filtering

Bandpass filtering improves the signal-to-noise ratio of the data, by restricting the frequency bandwidth to include only those frequencies which contain actual signal information, and to exclude those frequencies which contain predominantly noise. GPR systems are designed to achieve bandwidths approximately equal to the centre frequency (Davis and Annan, 1989); thus, for a system with centre frequency of 50 MHz, as used in this study, the majority of signal information should be contained between approximately 25 MHz and 75 MHz. This bandwidth was used as a guide in selecting bandpass filter parameters. Based on the results of the spectral analyses, low-cut and high-cut frequencies were determined for each transect, below and above which all frequencies were excluded. Low-pass and high-pass frequencies were also specified, between which 100 % of all frequency information was included. A linear taper was used to control the inclusion of frequency information between the cut frequency and the pass frequency. Thus, for this study, a typical bandpass filter would be 15-20-75-100, representing the low-cut (0 %), low-pass (100 %), high-pass (100 %), and high-cut (0 %) frequencies (MHz), respectively.

Spectral Shaping

Spectral shaping allows the user to strengthen signal information contained in frequencies outside the peak frequency bandwidth, by boosting specified frequencies by a specified amount. Thus, spectral shaping functions in a similar manner to bandpass filtering, by forcing unwanted frequencies to 0 %, keeping 100 % of the desired peak frequency bandwidth, and boosting frequencies peripheral to the peak frequency bandwidth by a specified proportion in the output signal. For this study, only the data from the Dale Creek sites were spectrally shaped, as in trials this process did not appear to improve the data from Porsild's Field. Spectral shaping parameters used were 15-0, 25-100, 50-100, 70-75, 105-0, where the first element in each pair represents the frequency in MHz, and the second element the shaping parameter in percent.

Velocity Analysis

ProMAX offers automatic velocity analysis capabilities based on the CMP surveys conducted in the field. Velocity can be instantly calculated for both linear (direct air and ground wave) arrivals and hyperbolic arrivals (subsurface interfaces), where these are distinct on the CMP profile.

Deconvolution

The radar transmitter produces a compact signal wavelet, which becomes stretched and 'convoluted' as it travels through earth materials and interacts with system instruments; the stretched wavelet (which may include undesirable reverberations, multiples, or ghosting) recorded by the receiving antenna may interfere with or overlap successive reflections, reducing vertical resolution of the data. Deconvolution improves vertical resolution by compressing the recorded wavelet into a better approximation of the original compact wavelet

(Coffeen, 1986; LaFleche, *et al.*, 1991; Maijala, 1992). The process uses autocorrelation to identify the basic wavelet of the data, then applies inverse filters to remove the effects of convolution (ProMAX v.5.1 on-line guide; Coffeen, 1986).

Normal Moveout Correction

The constant antenna offset used in this study causes distortion of subsurface reflections, due to the geometry of the signal path; shallow interfaces appear deeper (*i.e.*, longer travel time) than they actually are, because the signal path length includes a larger horizontal component. Deeper reflections are less distorted, as the signal path approximates a zero-offset path with a negligible horizontal component. This phenomenon is referred to as normal moveout (NMO) in seismic terminology. NMO correction calculates the amount of moveout at each sample point, based on user-specified velocity and antenna separation, and stretches the waveform to more accurately represent the true subsurface position of individual reflections. However, at very shallow depths, and for data with wide offsets or very slow velocities, the stretching may cause excessive distortion of the data; to avoid this distortion and artifacts generated by this distortion when other processing functions are applied to the data, the upper part of each trace, including the air and ground waves, is muted (*cf.* Fisher, *et al.*, 1992a).

Time - Depth Conversion

The original radar data are recorded as two-way travel time *versus* position along the survey transect. ProMAX allows the user to input time- and space-variant velocity data to convert the profile data to depth *versus* position. However, the CMP surveys conducted for this study provided velocity data which are integrated over the depth of penetration of the profile. Thus, a detailed velocity structure which represents vertical and lateral velocity variations caused by anomalous subsurface conditions (*e.g.*, acrotelm, thaw layer, frozen lenses or wedges) was not available to support this processing step. Even with core data providing descriptions of subsurface conditions, signal velocity variations across vertical and lateral transitions in peat properties, particularly ground thermal regime, but also density, moisture content, peat type, and degree of decomposition, remain poorly defined, and any proposed velocity structure would be simple and/or speculative.

Time - depth conversion was applied unsuccessfully to several of the radar profiles, producing considerable distortion of reflections in the vicinity of known transition from frozen to unfrozen peat. (This processing step may be more successful for areas of homogenous subsurface characteristics.) Depth calculations to support interpretation of the radar stratigraphy were therefore derived from the integrated velocity data in conjunction with depths measured by coring (see also Section 3.6 below, and Section A.3 in Appendix A).

Migration

Migration is a procedure to reduce the artifacts and false dips caused by the beam width of the radar system. Most of the energy from the radar transmitter is designed to travel approximately vertically; however, some of the energy will radiate spherically outwards from the transmitter and may be reflected from any point or interface whose surface is oriented perpendicular to the incident energy. The radar may therefore 'see' and record energy from object(s) located along the survey transect ahead of or behind the antennae array; however,

the radar is unable to discern directional information, and such reflections are imaged as an interface vertically below the antennae array. Thus, as the antennae array moves past such objects, a hyperbolic diffraction pattern is characteristically produced on the radar profile (Figure 3-6a). Similarly, dipping interfaces are typically imaged with shallower, broader slopes (Figure 3-6b). Migration collapses diffractions and correctly positions dipping events by refocusing the energy up-dip to its point of origin (*cf.* Fisher, *et al.*, 1992b; Majjala, 1992; Kalantzis, 1994; Fisher, *et al.*, 1994) (Coffeen, 1986).

Time migration methods do not handle strong lateral velocity variations well (J. Bancroft, pers. comm., 1995; ProMAX v.5.1 on-line guide). Furthermore, depth migration methods demand a well-defined velocity structure and time-to-depth conversion, which as noted above, remain speculative for this application (J. Bancroft, pers. comm., 1995). Therefore, transitions between frozen and unfrozen peat, where velocities changed by as much as 2.5 times, could not be reliably migrated. Sections of the profiles where velocity was assumed to be laterally and vertically constant were migrated using a Memory Stolt F-K (frequency-wavenumber) time migration process. This migration method offers computational efficiency compared to other time migration methods, but may not properly image steeply dipping interfaces when velocity varies significantly with depth (ProMAX v.5.1 on-line guide).

Coherency Filtering

An F-X (frequency-space) deconvolution function was applied to the data to reduce random noise and to improve coherency (*i.e.*, lateral continuity) of reflections. This process converts the data from the time domain to the frequency domain, then uses a user-specified operator length (*e.g.*, 100 ns time window length and overlap) and space window (*e.g.*, 15 traces, 5 samples) to predict the signal one trace ahead; the difference between the predicted and actual signal is assumed to be noise and is removed. The data are then reconverted to the time domain.

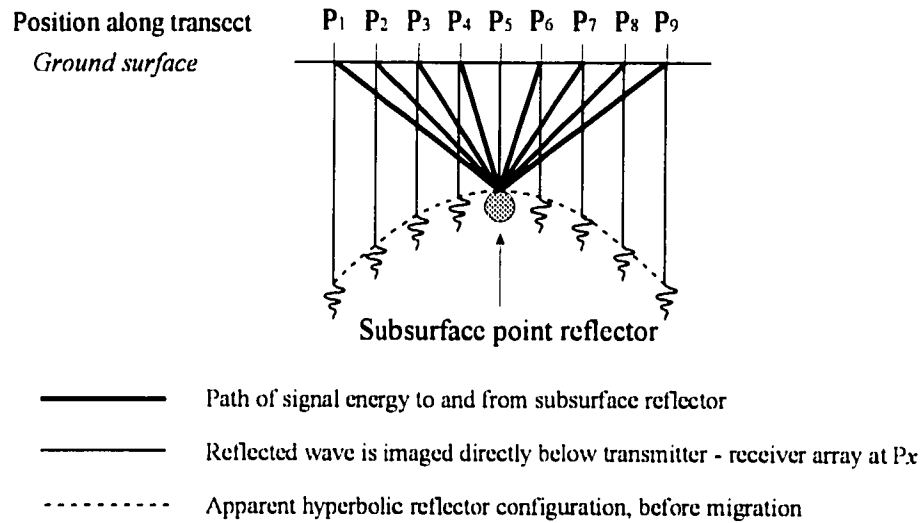
3.6 Display and Interpretation of Radar Data

Time versus Depth Scales

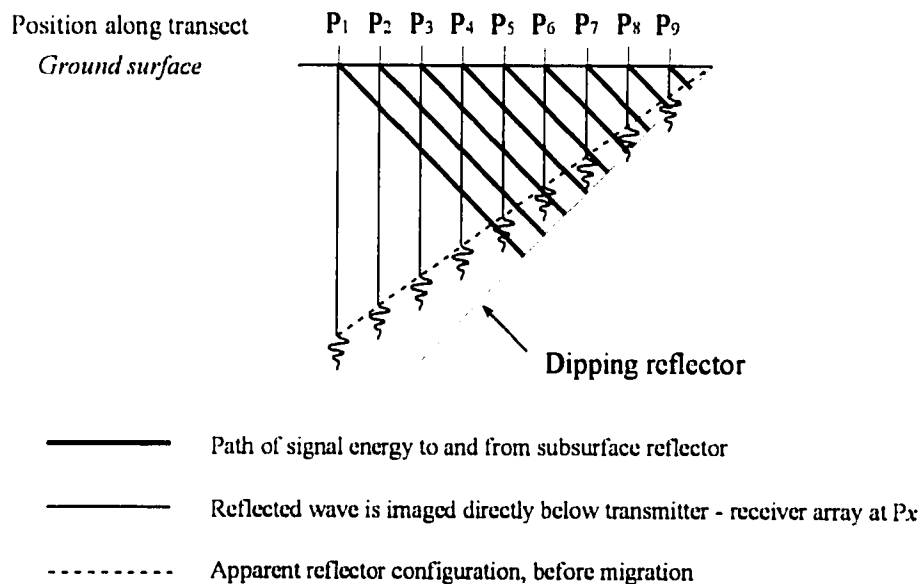
The radar profiles presented in the following sections are plotted with time (in nanoseconds) on the vertical scale. The conversion of data from the time domain to depth is prone to error (Coffeen, 1984). Vertical and lateral velocity variations caused by subsurface anomalies, and the horizontal component of the signal path in the subsurface (particularly at shallow depths) compromise the accuracy of depth conversion. Furthermore, velocity determined from normal moveout curvature, as in a CMP survey, is not very accurate, and the accuracy of this technique decreases with depth (Coffeen, 1984).

The subsurface conditions encountered and survey configuration used in this study present several limitations to conversion of time data to depth: the presence of a surface layer of relatively low moisture content (upper thaw layer on palsas, acrotelm in fens) over deeper, saturated material presents a strong velocity contrast; the presence of frozen conditions, the boundary of which is known in places to be non-vertical (*i.e.*, wedge-like), presents a strong and irregular velocity contrast; peat characteristics display a large degree of vertical and

Figure 3-6. Image artifacts produced by point and dipping subsurface reflectors.



- a)** Hyperbolic diffraction pattern produced as antenna array 'sees' point reflector at successive positions, P_x, along the survey transect. Reflected energy is imaged vertically below mid-point of antenna array.



- b)** Dipping reflectors are imaged with broader, shallower slopes.

Modified from Coffeen (1986).

lateral variability, and thus, velocity; and antenna separation introduces a large horizontal component to the signal path, especially in the shallow subsurface. In addition, coring intercepted few major subsurface interfaces which could be correlated to reflections on the radar profile; thus, depth values calculated from converted data often could not be verified against real depth data.

Depth scales which account for the near-surface horizontal component of the signal path can be generated by the radar software (although not the seismic software), using velocity determined from CMP surveys. These depth scales are non-linear (*i.e.*, the vertical scale is more compressed at shallower depths where a larger proportion of the signal travel time is attributable to the horizontal component of the signal path). However, these depth scales would not account for the spatial velocity variations noted above.

Further, non-linear depth scales are of limited utility where topographic correction, which is itself a useful step to improve the illustration of subsurface structure, is applied to the data. Topographic correction introduces a non-uniform datum from which signal travel time is measured (and depth of reflections calculated); a non-linear depth scale would be applicable to only the one elevation with which the zero depth marker coincides.

In consideration of the above points, the radar profiles presented in this thesis are plotted with a time scale only. For the purposes of interpretation, depth of individual interfaces is estimated on the basis of the integrated velocity derived from the CMP survey and the actual two-way signal travel time of the reflection of interest. However, the reader will observe that the uppermost portion of each trace contains no signal information: this “dead” time is added to the trace to accommodate the illustration of relief. Thus, the actual two-way travel time of a reflection cannot be read directly from the vertical time scale, but must be determined by subtracting the “dead” time prior to the first radar event, the direct air wave³. Because the travel time of the direct air wave is known, this radar event serves as a datum from which to measure two-way signal travel time. In all cases in this study, the direct air wave begins at 6.7 ns.

Notwithstanding the above, in subsequent text and figures, for the ease of the reader, reference to specific reflections in the radar profiles is given in nanoseconds, **read directly from the vertical time scale**. Approximate depth, estimated from the actual two-way signal travel time, is given in brackets, where relevant. Unless otherwise noted, depths noted in the text are calculated using signal propagation velocities of $0.038 \text{ m}\cdot\text{ns}^{-1}$ in unfrozen peat, and $0.095 \text{ m}\cdot\text{ns}^{-1}$ and $0.097 \text{ m}\cdot\text{ns}^{-1}$ in frozen peat at the Porsild’s Field and Dale Creek sites, respectively. (Depths of major subsurface interfaces intercepted by coring were comparable to depths calculated from these velocities.)

3

The direct air wave, *A*, is the first radar event on the radar profiles, and is produced by signal energy travelling at the speed of light ($0.3 \text{ m}\cdot\text{ns}^{-1}$) through the air from the transmitter to the receiver.

Certain processing functions (*i.e.*, NMO correction) cause extreme distortion in the shallow portion of the profile. On these profiles, the direct air and ground waves⁴ are muted, and cannot be used as a datum from which to determine two-way signal travel time. Therefore, depth values are not estimated for profiles to which this processing step has been applied. In cases where depth data are desired from these profiles, the depth of individual reflections may be estimated from other non-processed profiles on which the same reflections can be identified with confidence.

Topography

Topographic corrections have been applied to the data to provide a more realistic illustration of subsurface structure. The vertical exaggeration of each profile varies depending on plotting parameters and is indicated on each figure.

Factors in Interpretation

The earliest radar events on the radar profiles (the direct air and ground waves, and noise multiples) typically do not contain much, if any, information on subsurface conditions. Subsequent radar events represent interfaces within the peat and underlying mineral sediment, and are of greater interest to the interpreter. Key factors of which the reader should be aware when interpreting the radar profiles include the following.

- Radar signal velocity in frozen peat is approximately 2.5 times the velocity in unfrozen peat; thus, all subsurface reflections in frozen peat will appear considerably 'shallower' (*i.e.*, shorter two-way travel time) and vertically compressed on the radar profile relative to those in unfrozen peat. A single subsurface interface at a constant actual depth across the profile which crosses laterally from frozen to unfrozen conditions would therefore appear as distinct reflections plotted at different times on the vertical scale (*e.g.*, the peat - mineral sediment interface in Figure 3-7b). This visual distortion must be considered when attempting to trace individual strata across transitional zones, and to relate stratigraphy in the fen with that observed in palsas.
- In transition areas or areas with anomalous subsurface conditions, artificial time structures may be evident on the radar profile in the time domain. For example, a zone of high velocity material will cause subsequent reflections to arrive sooner and appear shallower on the profile (velocity pullup; Coffeen, 1984) (*e.g.*, see Figure 3-24 and related text). Thus, a flat-lying interface overlain in one area by a zone of high velocity (*e.g.*, frost) will appear as a flat reflection with a raised 'bump' below the zone of high velocity.
- Spatial aliasing may cause artificial structures to appear on the radar profile; this occurs when the eye sees an artificial pattern which is complementary or opposite to an actual pattern in the data.

4

The direct ground wave, *G*, is typically the second radar event on the radar profiles, and is produced by refracted signal energy travelling along the air - ground interface.

3.7 Results and Interpretation

Three transects were surveyed at the Porsild's Field site, crossing four palsas (Plate 3-1). Two intersecting transects were surveyed at the Dale Creek site, crossing five palsas (Plate 3-2). (However, the utility of data from Transect #2 is limited, because heavy rain during surveying along this transect caused excessive signal attenuation due to energy loss to the air.)

3.7.1 Peat Thickness, Peat - Mineral Sediment Interface

In unfrozen peat, the peat - mineral sediment interface represents the greatest subsurface change in water content (and therefore dielectric permittivity; *cf.* Davis, *et al.*, 1977) in peatlands, and therefore yields the strongest amplitude subsurface reflection event on GPR profiles (Theimer, *et al.*, 1994:199). Where frozen, the dielectric contrast at the peat - mineral sediment interface is reduced; therefore, this interface may be difficult to distinguish under frozen conditions (Kettles and Robinson, 1996); this may be exacerbated by signal scattering in ice-rich peat.

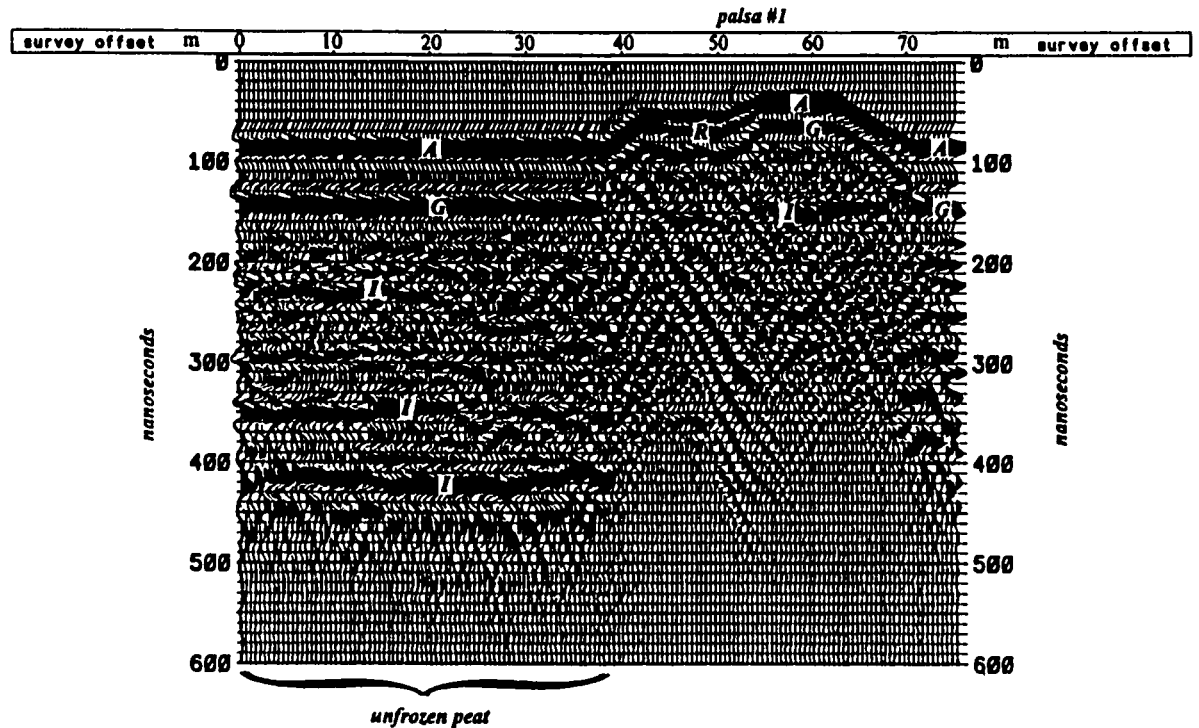
Little or no stratigraphy is visible in the unfrozen peat below the direct ground wave in the unprocessed GPR profiles when displayed without application of gains to compensate for signal attenuation. With application of any time variable gain control (*e.g.*, automatic gain control (AGC) or spreading and exponential gain), more detailed stratigraphic information becomes visible, but relative amplitude information is lost; inferences regarding the strength of any particular reflection relative to others are therefore unreliable (Figure 3-7a). A constant gain function that multiplies all data points by a constant factor retains relative amplitude information while boosting weak, deep reflections. The constant gain function in ProMAX produced the best quality profiles from which the strong reflection at depth inferred to represent the peat - mineral sediment interface could be identified with greater confidence (Figure 3-7b).

Porsild's Field

At the Porsild's Field site, peat thickness in the fen near to palsa #1 exceeded 5 m, the maximum depth to which the available corer could penetrate. A layer of gyttja with some peaty organics was encountered between approximately 455 cm to 500 cm depth in a core taken 7 m from the edge of palsa #1, on Transect #1; this layer is assumed to directly overlie the mineral sediment (basal gyttja or aquatic peat is inferred to reflect initial deposition in a body of open standing water (National Wetlands Working Group, 1988)). Additional coring was conducted near the edge of the fen to retrieve mineral sediment samples; at this location, a similar 12 cm to 16 cm thick layer of gyttja with some coarse organic material (*i.e.*, grass stems) was found to overlie a diamict with silty - clayey matrix and small, angular clasts.

Based on the radar profiles (Transects #1 and #2), peat thickness adjacent to palsas #1 and #2 is estimated to range from 4.9 m to 5.2 m, where clear, high amplitude basal reflections can be identified (Figures 3-7 and 3-8). This agrees with the inferred depth of mineral sediment described above.

Figure 3-7a. Comparison of time variable gain control *versus* constant gain for identification of peat - mineral sediment interface on radar profiles.



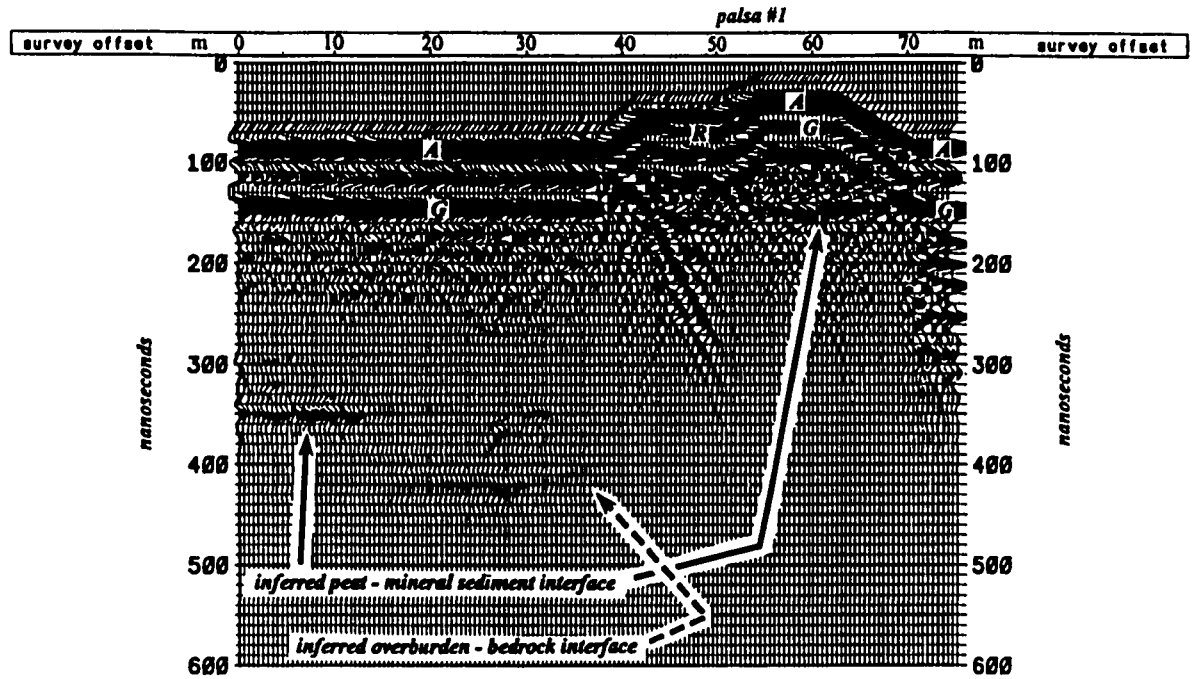
Automatic (time variable) gain control applied. Note detailed stratigraphy in unfrozen fen between 0 and 38 m, to 500 ns (*ca.* 8 m depth); relative amplitude of reflections from subsurface interfaces, *I*, is indistinguishable.

First radar event is direct air wave, *A*, typically followed by direct ground wave, *G*. See Figure 3-19 for discussion of signal refraction, *R*.

Data from Transect #1 at Porsild's Field. Vertical exaggeration *ca.* 2x. Transect crosses unfrozen fen from 0 m to 38 m, frozen palsa #1 from 38 m to 70.5 m, and unfrozen fen from 70.5 m to 75 m.

Plots produced from ProMAX v.5.1, after data conversion to SEG-Y seismic format using the pulseEKKO IV operating software. Other processing steps include signal saturation correction and topographic correction.

Figure 3-7b. Comparison of time variable gain control *versus* constant gain for identification of peat - mineral sediment interface on radar profiles.



Constant gain factor applied. Note strong amplitude reflection between 0 and 13 m at 350 ns (*ca.* 5.2 m depth), inferred to represent the peat - mineral sediment interface. Also note weaker, but still relatively strong reflection between 16 and 38 m at 415 ns (*ca.* 6.4 m depth); this may represent the overburden - bedrock interface.

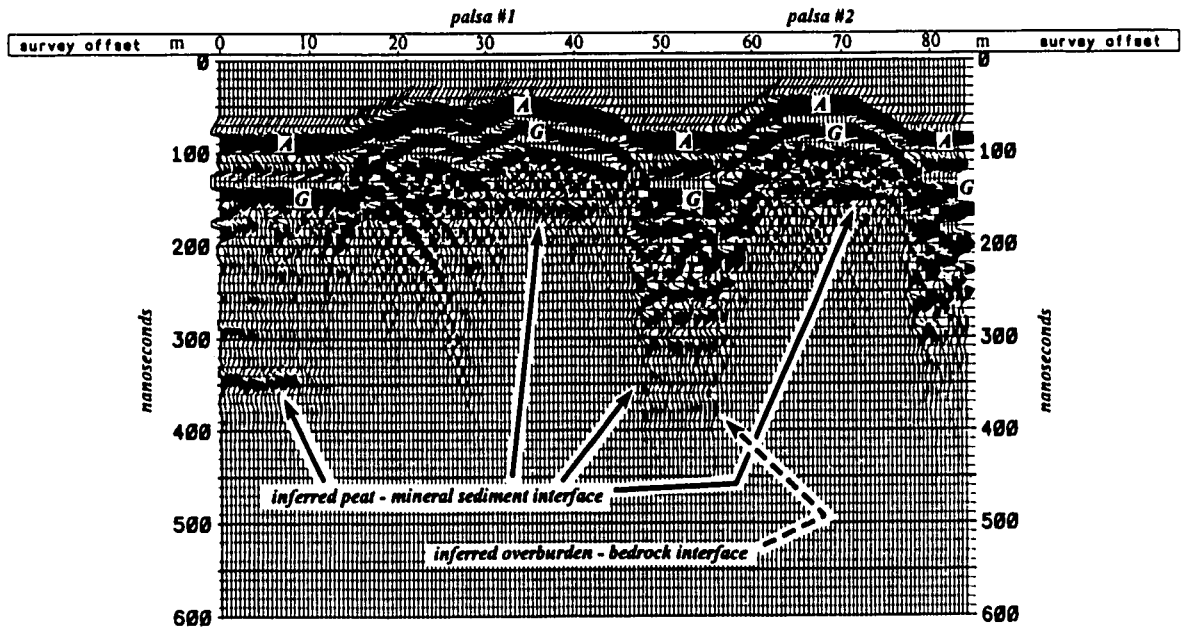
Note strong, laterally continuous reflection at 140 to 160 ns between 46 and 67 m, inferred to represent the peat - mineral sediment interface below the palsa. This reflection lies a maximum of 5.8 m below the surface of palsa #1.

First radar event is direct air wave, *A*, typically followed by direct ground wave, *G*. See Figure 3-19 for discussion of signal refraction, *R*.

Data from Transect #1 at Porsild's Field. Vertical exaggeration *ca.* 2x. Transect crosses unfrozen fen from 0 m to 38 m, frozen palsa #1 from 38 m to 70.5 m, and unfrozen fen from 70.5 m to 75 m.

Plots produced from ProMAX v.5.1, after data conversion to SEG-Y seismic format using the pulseEKKO IV operating software. Other processing steps include signal saturation correction and topographic correction.

Figure 3-8. Inferred peat - mineral sediment interface at Porsild's Field.



Constant gain factor applied. Note strong amplitude reflection between 0 m and 9 m at *ca.* 340 ns (*ca.* 5.0 m depth), inferred to represent the peat - mineral sediment interface in the fen. This is believed to correlate with a weaker reflection at the same time/depth between 47.5 m and 55 m on the transect. A weaker reflection at 370 ns to 380 ns (*ca.* 5.5 m to 5.7 m depth) between 0 m and 9 m and 47.5 m and 55 m, below the inferred base of peat, may represent the overburden - bedrock interface.

Note strong, laterally continuous reflection at 140 ns to 160 ns between 21 m and 44 m, and at 135 ns to 140 ns between 62 m to 74 m, inferred to represent the peat - mineral sediment interface below the palsas. This interface lies a maximum of 5.5 m and 5.0 m below the surface of palsas #1 and #2, respectively.

First radar event is direct air wave, *A*, typically followed by direct ground wave, *G*.

Data from Transect #2 at Porsild's Field. Vertical exaggeration *ca.* 2x. Transect crosses unfrozen fen from 0 m to 14 m, frozen palsa #1 from 14 m to 46.5 m, unfrozen fen from 46.5 m to 59 m, frozen palsa #2 from 59 m to 78.5 m, and unfrozen fen from 78.5 m to 84.5 m.

Plot produced from ProMAX v.5.1, after data conversion to SEG-Y seismic format using the pulseEKKO IV operating software. Other processing steps include signal saturation correction and topographic correction.

Peat thickness in the fen appears to decrease to the west of palsa #2 (Transect #3). Numerous irregular reflections to 300 ns (*ca.* 4.6 m depth) obscure the peat - mineral sediment interface between palsas #2 and #4. However, a clearer, strong reflection below a relatively quiet zone to 260 ns - 270 ns is inferred to represent the peat - mineral sediment interface at approximately 3.9 m to 4.1 m depth between palsas #4 and #5 (Figure 3-9). A strong reflection rising from 330 ns (*ca.* 5.2 m depth) at 103 m to 300 ns (*ca.* 4.6 m depth) at 116.5 m could also represent the peat - mineral sediment interface. This interface could in fact be shallower than it appears on the radar profile, if standing water at the surface between 102 m and 105 m, and water below a floating vegetation mat between 109 m and 120.5 m caused a reduction in the radar signal velocity. A similar depression in the image of the direct ground wave adjacent to palsa #5, between 104 m to 110 m, supports this inference.

A strong, laterally continuous reflection at 140 ns to 160 ns below palsa #1 (Figures 3-7 and 3-8) and at 135 ns to 140 ns below palsa #2 (Figure 3-8) is inferred to represent the peat - mineral sediment interface; this radar interface lies up to 5.8 m below the surface of palsa #1 and 5.0 m below the surface of palsa #2. Mineral sediment was not encountered in coring to 5 m depth on and near the edge of palsa #1 (at 17 m along Transect #1).

Although the dielectric contrast at the peat - mineral sediment interface may be reduced under frozen conditions, the strength of this reflection may indicate a concentration of segregated ice lenses at the peat - mineral sediment interface, as observed in palsas by Cummings and Pollard (1990). Dallimore and Davis (1987) note that strong radar reflections were generated at contacts between sediment and massive ice, despite low contrast in EM signal velocities between these media.

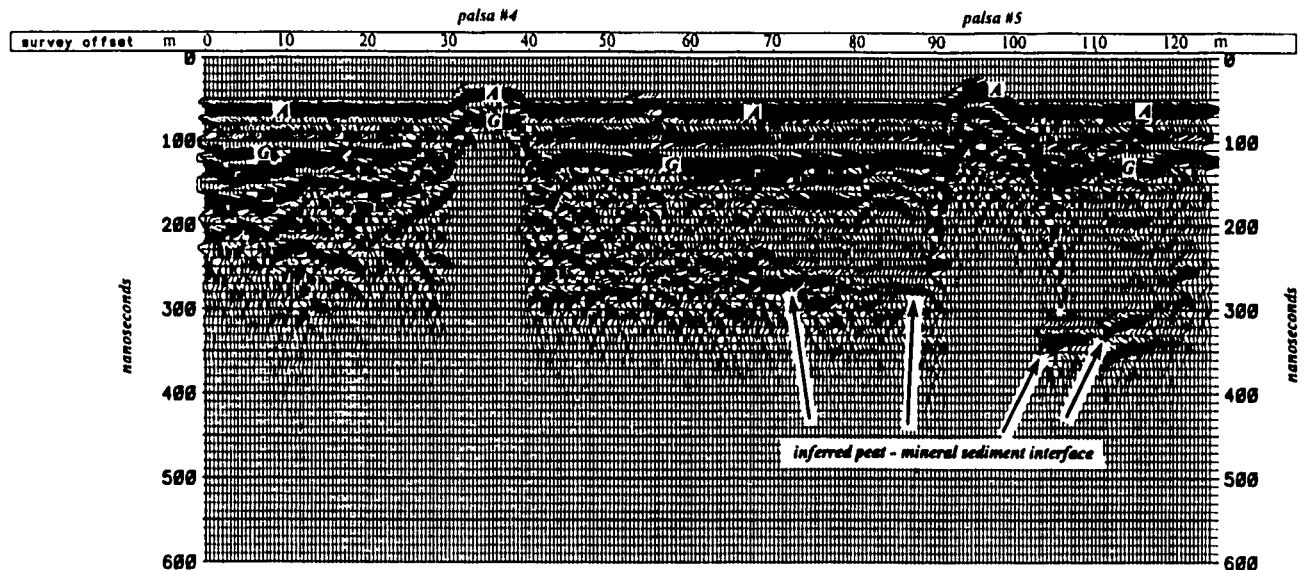
It is also possible that this reflection represents the transition to unfrozen conditions below the frozen palsa core; however, the base of permafrost in similar studies (Pilon, *et al.*, 1992; Kettles and Robinson, 1996) is not typically manifested as a strong reflection but rather as a more or less abrupt attenuation of the radar signal at depth. This can occur if the base of permafrost constitutes a transitional zone with unfrozen water in a frozen fringe, which might not be amenable to detection by GPR (*cf.* Tiuri, *et al.*, 1983; Theimer, *et al.*, 1994).

Such signal attenuation was observed below palsa #4 on Transect #3. Coring on this palsa encountered unfrozen peat below 300 cm, and met refusal in mineral sediment at 320 cm depth; no core was recovered below 300 cm. A reflection at 102 ns to 110 ns on the radar profile (*ca.* 3.1 m to 3.6 m depth) is inferred to represent the base of peat (Figure 3-10). The radar signal was completely attenuated below this reflection, probably due to the unfrozen conditions and/or clay content in the mineral sediment.

Dale Creek

The peat - mineral sediment interface at the Dale Creek site was shallow in comparison; clayey mineral sediment with few small clasts a few mm in diameter was encountered at 110 cm depth on palsa #4 and at 95 cm on palsa #1. Sediment with clasts up to 2 cm diameter was encountered in the unfrozen fen adjacent to the palsas at 125 cm (between palsas #2 and

Figure 3-9. Variation in inferred peat - mineral sediment interface in unfrozen peat at Porsild's Field.



Numerous high amplitude reflections to 300 ns (*ca.* 4.6 m depth) obscure the peat - mineral sediment interface in the fen between palsas #2 and #4 (0 m to 30 m on the radar profile) and west of palsa #4 (40 m to 72 m). A strong, laterally continuous reflection at 260 ns to 270 ns (*ca.* 3.9 m to 4.1 m depth) between 72 m and 90 m may represent the peat - mineral sediment interface. However, no cores were obtained from unfrozen peat on this transect. A core taken from palsa #4 at 35 m on Transect #3 met refusal at 320 cm depth.

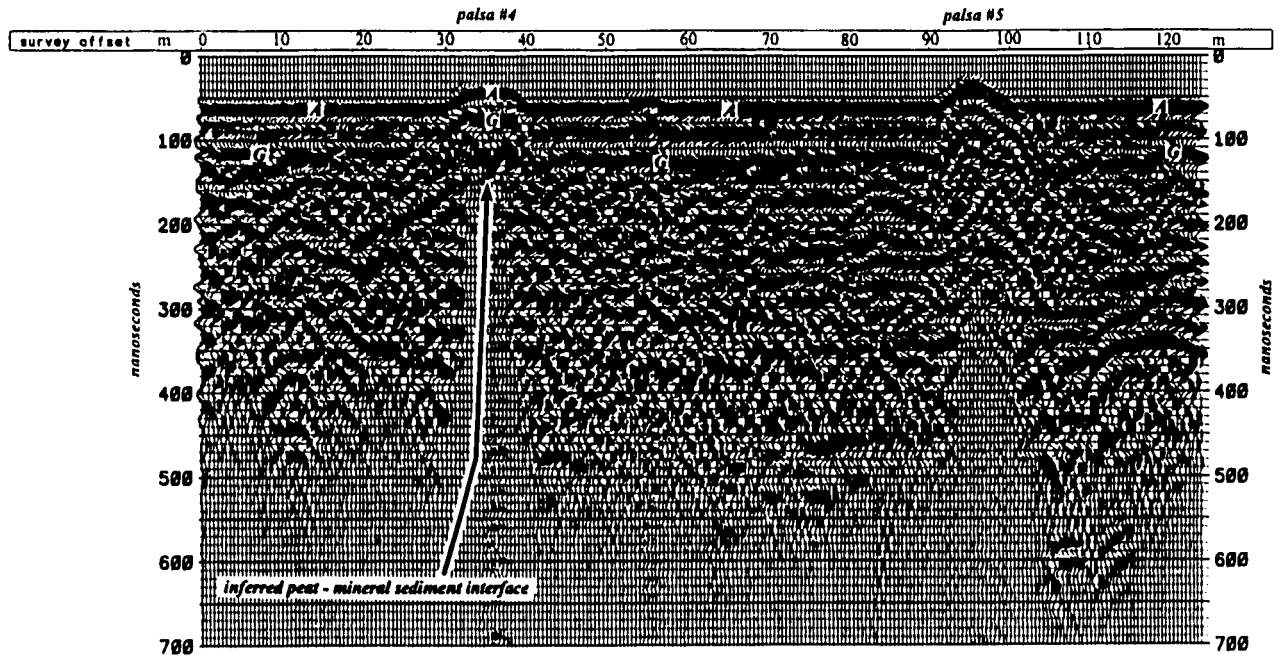
A strong reflection rising from 330 ns (*ca.* 5.2 m depth) at 103 m to 300 ns (*ca.* 4.6 m depth) at 116.5 m may also represent the peat - mineral sediment interface. Standing water at the surface between 102 m and 105 m on the transect, and water below a floating vegetation mat between 109 m to 120.5 m may have reduced the radar signal velocity, causing subsurface interfaces to appear deeper. A depression in the image of the direct ground wave, *G*, adjacent to palsa #5 supports this inference.

First radar event is direct air wave, *A*, typically followed by direct ground wave, *G*.

Data from Transect #3 at Porsild's Field. Vertical exaggeration *ca.* 2x. Transect crosses unfrozen fen from 0 m to 30 m, frozen palsa #4 from 30 m to 40 m, unfrozen fen from 40 m to 92.5 m, frozen palsa #5 from 92.5 m to 102 m, and unfrozen fen from 102 m to 125 m.

Plot produced from ProMAX v.5.1, after data conversion to SEG-Y seismic format using the pulseEKKO IV operating software. Other processing steps include signal saturation correction, topographic correction, and constant gain.

Figure 3-10. Signal attenuation below the base of permafrost at Porsild's Field.



Irregular reflection between 33.5 m (110 ns; *ca.* 3.6 m depth) and 38 m (102 ns; *ca.* 3.1 m depth) is inferred to represent the base of peat below palsa #4. Coring at 35 m along the transect met refusal at 320 cm depth. Attenuation of the signal below this reflection may result from unfrozen conditions and/or clay content in the mineral sediment. Note that this reflection is not visible on the constant gain radar profile (Figure 3-9).

Despite good signal penetration, no distinct reflection inferred to represent the peat - mineral sediment interface below palsa #5 (92.5 m to 102 m) is visible on the profile. The internal stratigraphy of the palsa appears to be domed; this structure may be related to ice segregation and palsa formation.

First radar event is direct air wave, *A*, typically followed by direct ground wave, *G*.

Data from Transect #3 at Porsild's Field. Vertical exaggeration *ca.* 2x. Transect crosses unfrozen fen from 0 m to 30 m, frozen palsa #4 from 30 m to 40 m, unfrozen fen from 40 m to 92.5 m, frozen palsa #5 from 92.5 m to 102 m, and unfrozen fen from 102 m to 125 m.

Plot produced from ProMAX v.5.1, after data conversion to SEG-Y seismic format using the pulseEKKO IV operating software. Other processing steps include signal saturation correction, topographic correction, and automatic (time-variable) gain control.

#3) to 230 cm depth (adjacent to palsa #1). Peat thickness over mineral sediment on palsa #2 at the Dale Creek site measured by Skaret (1995) ranged from 135 cm to 205 cm. A strong reflection approximately parallel with the ground surface, inferred to represent the base of peat, can be traced across the transition from frozen to unfrozen peat (Figure 3-11).

3.7.2 Internal Peat Stratigraphy - Fens

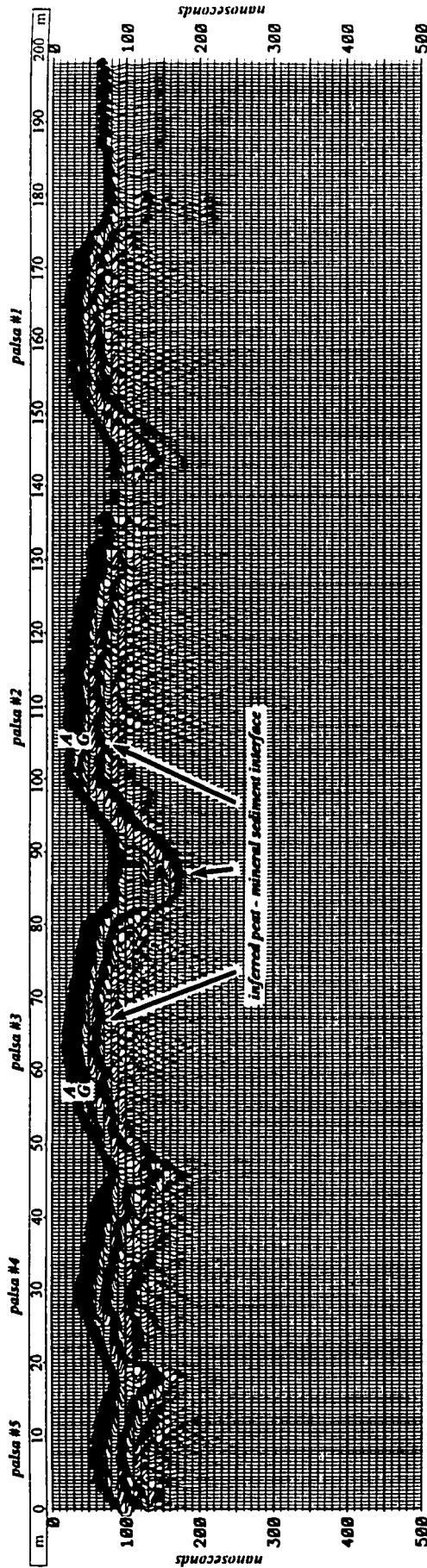
Coring showed peat stratigraphy in the fens at both sites was complex, with numerous layers of sedgy peat, varying in density, water content, and humification, and ranging from 2 cm to greater than 100 cm in thickness. At the Porsild's Field site, a thin, diffuse tephra layer (2 cm to 4 cm thick) occurred between *ca.* 30 cm and 50 cm depth, and a well-decomposed layer of peat, up to *ca.* 25 cm thick, was underlain by a layer of gyttja, which was underlain by mineral sediment.

When displayed with a time variable gain control, the radar profiles reveal detailed stratigraphy in the unfrozen peat at the Porsild's Field site (Figure 3-7a). Wavy, subparallel, laterally continuous reflections can be traced across the profile, and relate to changes in dielectric permittivity; the dielectric permittivity is strongly controlled by water content (Davis, *et al.*, 1977; Topp, *et al.*, 1980), but may also be influenced by density, peat type, temperature, and degree of decomposition. Thus, reliable correlation of a given radar event with a change in any one of these peat properties is problematic. Moreover, the accuracy of moisture content and density measurements from Macaulay cores, as were collected for this study, appears to be inadequate for the purposes of correlation with radar reflections. Sampling compression of the peat, due to the cutting resistance of fibrous matter, can affect the water content, particularly in less decomposed peat (Hobbs, 1986). Further, the Macaulay corer does not seal fully during sample recovery, and there was visible loss of water during core retrieval. As GPR may detect changes in moisture content as low as one percent (Hänninen, 1992), and this degree of accuracy could not be obtained, this study could not and did not attempt to correlate moisture content changes with radar reflections.

This problem is also illustrated by previous studies using GPR in peatlands which have had limited success in reliably correlating a given reflection with a subsurface change in a particular peat property. Bjelm (1980) observed that some interfaces identified by radar were not observed in drilling, and conversely, that some stratigraphic interfaces identified by drilling did not correlate with radar reflections. He also noted that different degrees of decomposition, and thus, different levels of dielectric contrast, could be represented by the same radar event across a profile. Similarly, Worsfold, *et al.* (1986) found that some "marked" changes in bulk density could be correlated with radar reflections, but that some "equally large" variations in bulk density did not generate reflections. Further, they observed that some radar reflections did not appear to correlate with any measured peat properties.

Some observed strata in the peat are thinner than the resolution of the GPR system configuration used in data collection for this study (*ca.* 0.8 m; Robinson, *et al.*, 1992), and may therefore be difficult to distinguish on the radar profiles. Deconvolution of the radar data to improve vertical resolution was attempted (Figures 3-12 to 3-15). Zero-phase spiking

Figure 3-11. Radar imaging of peat - mineral sediment interface across frozen - unfrozen transition at Dale Creek.

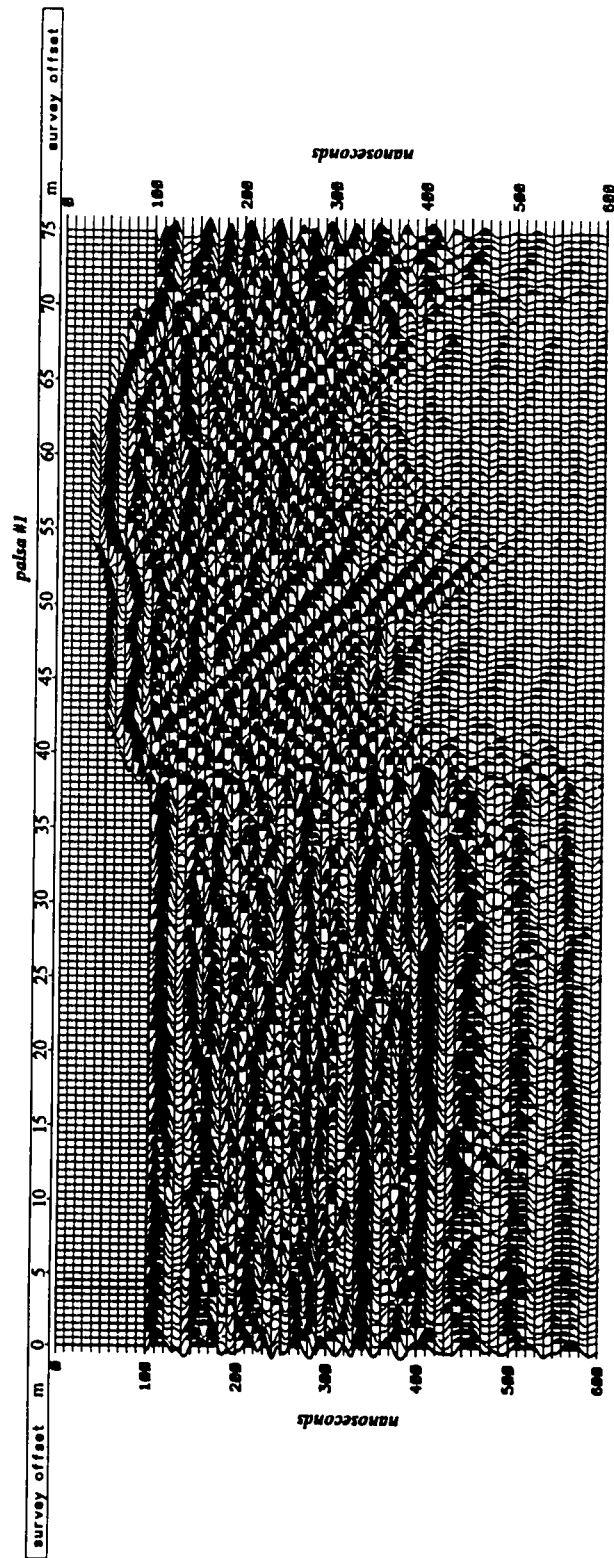


The strong laterally continuous reflection approximately parallel to the ground surface, occurring 15 ns to 35 ns after the direct air and ground wave arrivals (A, G) in the palsas is inferred to represent the peat - mineral sediment interface. This reflection can be traced across the frozen - unfrozen interface, e.g., between 85 m and 100 m along the transect. The reflection *appears* to be shallower on the palsas due to higher signal velocity in frozen peat. However, peat thickness in the fen (125 cm at 83 m) is comparable to that on the palsas (95 cm to 205 cm). Where the palsas are more closely spaced (i.e., palsas #3 and #4) or where the frozen - unfrozen transition is more abrupt (i.e., 80 m to 85 m, as denoted by steeper palsa side), the peat - mineral sediment interface reflection is subcontinuous to discontinuous. Signal attenuation between 132 m and 142 m was caused by energy loss to the air during a heavy rain at the time of the survey.

Data from Transect #1 at Dale Creek. Vertical exaggeration is ca. 2x. Transect crosses five palsas from east to west, separated by unfrozen fen, and unfrozen meadow west of palsa #1 (180 m to 198.5 m).

Plot produced from ProMAX v.5.1, after data conversion to SEG-Y seismic format using the pulseEKKO IV operating software. Other processing steps include topographic correction and a low constant gain factor.

Figure 3-12. Fen profile prior to deconvolution.

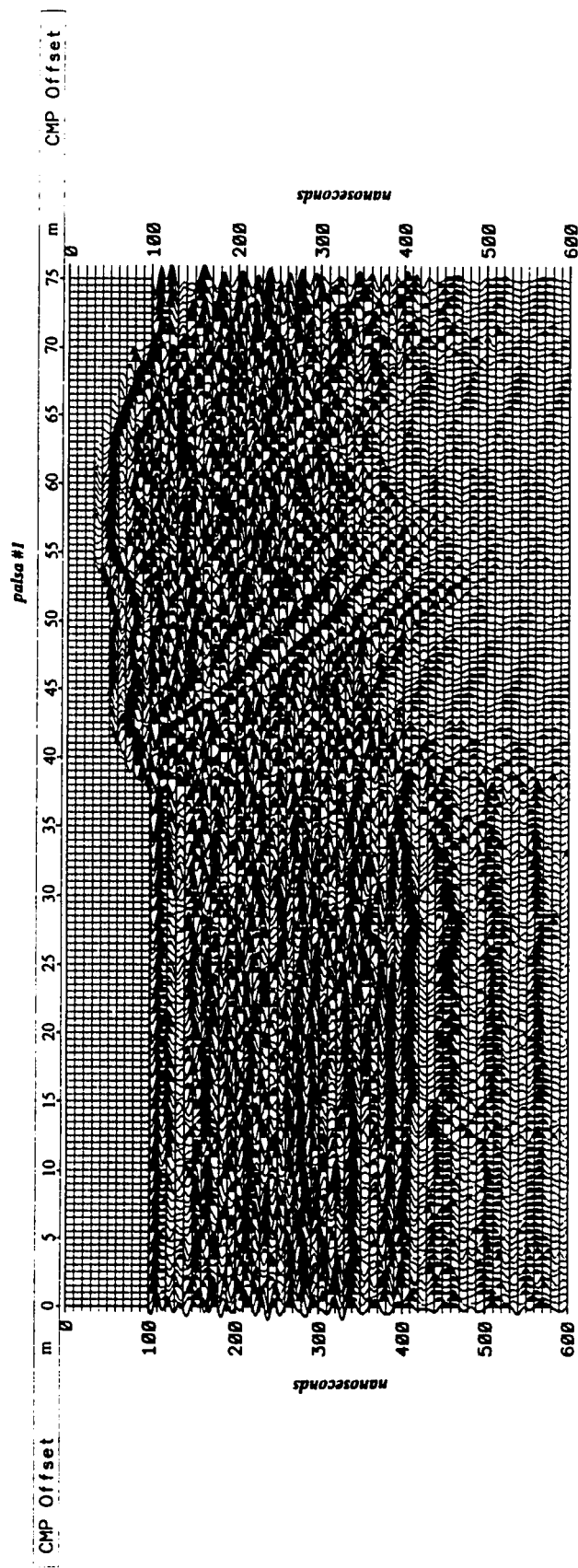


Profile prior to deconvolution. Compare with Figures 3-13 to 3-17.

Data from Transect #1 at Porsild's Field. Vertical exaggeration *ca.* 1.2x. Transect crosses unfrozen fen from 0 m to 38 m, frozen palsa #1 from 38 m to 70.5 m, and unfrozen fen from 70.5 m to 75 m.

Plot produced from ProMAX v.5.1, after data conversion to SEG-Y seismic format using the pulseEKKO IV operating software. Other processing steps include signal saturation correction, automatic (time-variable) gain control, bandpass filter, normal moveout correction, and topographic correction. **N.B.** Some portion of the direct air and ground waves are muted as a byproduct of normal moveout correction, particularly in the fens.

Figure 3-13. Zero-phase spiking deconvolution of fen profile.

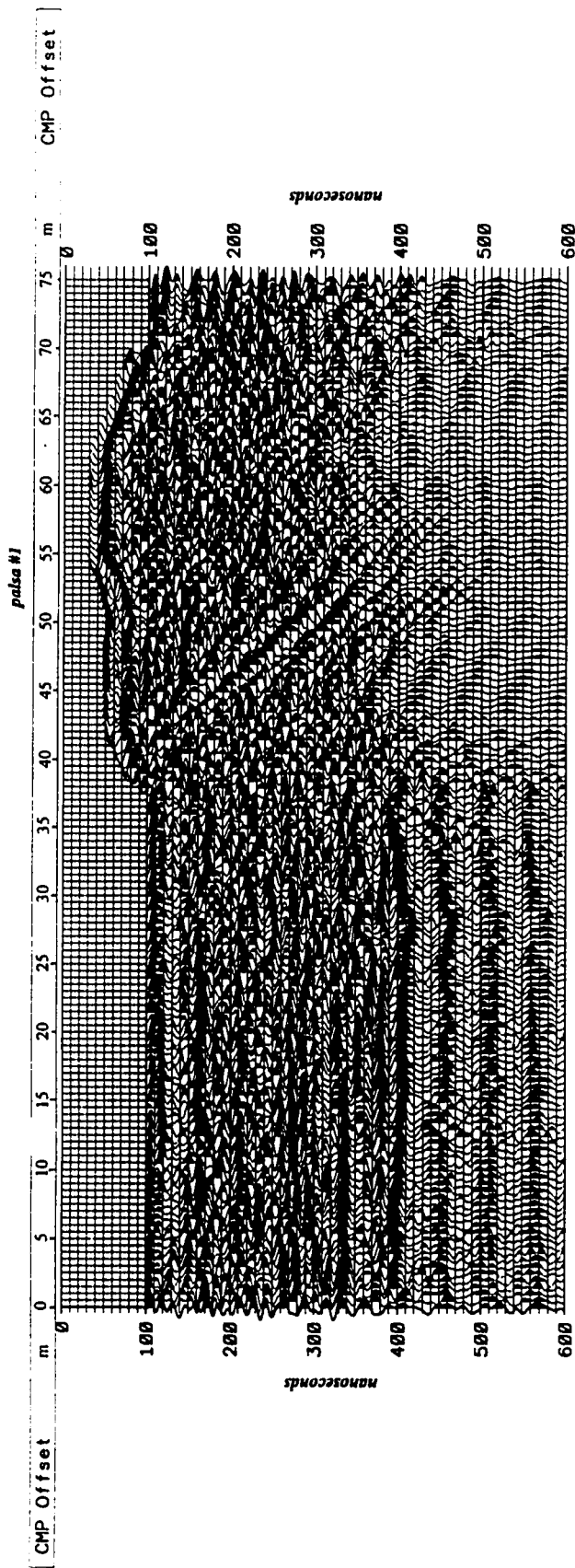


Profile after zero-phase spiking deconvolution; note improved resolution of fen reflections, particularly between 200 ns and 300 ns. Compare with Figures 3-12 and 3-14 to 3-17.

Data from Transect #1 at Porsild's Field. Vertical exaggeration ca. 1.2x. Transect crosses unfrozen fen from 0 m to 38 m, frozen palsa #1 from 38 m to 70.5 m, and unfrozen fen from 70.5 m to 75 m.

Plot produced from ProMAX v.5.1, after data conversion to SEG-Y seismic format using the pulseEKKO IV operating software. Other processing steps include signal saturation correction, automatic (time-variable) gain control, bandpass filter, normal moveout correction, topographic correction, and zero-phase spiking deconvolution. **N.B.** Some portion of the direct air and ground waves are muted as a byproduct of normal moveout correction, particularly in the fens.

Figure 3-14. Spiking deconvolution of fen profile.

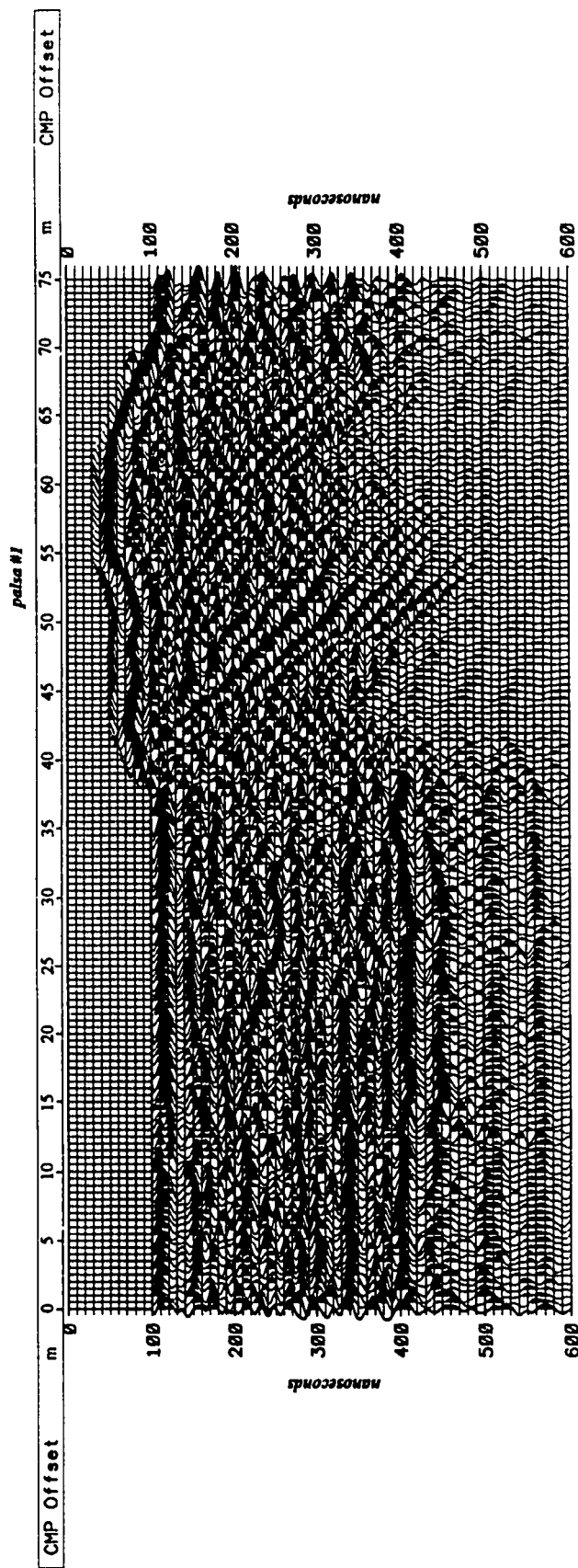


Profile after spiking deconvolution; note improved resolution of fen reflections, particularly between 200 ns and 300 ns. Compare with Figures 3-12, 3-13, and 3-15 to 3-17.

Data from Transect #1 at Porsild's Field. Vertical exaggeration ca. 1.2x. Transect crosses unfrozen fen from 0 m to 38 m, frozen palsa #1 from 38 m to 70.5 m, and unfrozen fen from 70.5 m to 75 m.

Plot produced from ProMAX v 5.1, after data conversion to SEG-Y seismic format using the pulseEKKO IV operating software. Other processing steps include signal saturation correction, automatic (time-variable) gain control, bandpass filter, normal moveout correction, topographic correction, and spiking deconvolution. **N.B.** Some portion of the direct air and ground waves are muted as a byproduct of normal moveout correction, particularly in the fens.

Figure 3-15. Predictive deconvolution of fen profile.



Profile after predictive deconvolution; resolution of fen reflections is not as well enhanced as from zero-phase spiking deconvolution or spiking deconvolution. Compare with Figures 3-12 to 3-14, 3-16, and 3-17.

Data from Transect #1 at Porsild's Field. Vertical exaggeration *ca.* 1.2x. Transect crosses unfrozen fen from 0 m to 38 m, frozen palsa #1 from 38 m to 70.5 m, and unfrozen fen from 70.5 m to 75 m.

Plot produced from ProMAX v.5.1, after data conversion to SEG-Y seismic format using the pulseEKKO IV operating software. Other processing steps include signal saturation correction, automatic (time-variable) gain control, bandpass filter, normal moveout correction, topographic correction, and predictive deconvolution. **N.B.** Some portion of the direct air and ground waves are muted as a byproduct of normal moveout correction, particularly in the fens.

deconvolution was found to best enhance the vertical resolution of the data, when compared with spiking deconvolution; both of these were found to better enhance the data than predictive deconvolution (*cf.* LaFleche, *et al.*, 1991; Maijala, 1992; Fisher, *et al.*, 1994). Deconvolution also improved lateral continuity of reflections.

Lateral continuity was also improved in the fens by application of a coherency filter (Figure 3-16). In areas where peat strata were flat-lying, the coherency filter applied in conjunction with deconvolution further sharpened the appearance of reflections (Figure 3-17). However, where reflections were wavy, these steps did not appear to facilitate interpretation.

GPR Transect #3 at Porsild's Field crossed the edge of a known collapse scar of a pre-existing palsa west of palsa #4 (Plate 3-1) (Kershaw and Gill, 1979). The radar profile shows an apparent decrease in lateral continuity of reflections between 40 m and 65 m, compared to the stratigraphy between 65 m and 90 m (Figure 3-18a). A coherency filter was applied to the data to test for and enhance continuity in reflections across this area of the profile; the observed discontinuity persisted through this processing step (Figure 3-18b). This pattern may be related to the collapse of the pre-existing palsa.

The White River volcanic ash, dated 1250 BP (Lerbekmo, *et al.*, 1975), was observed in cores from the fens; however, this layer is too close to the surface (<55 cm depth) and too diffuse and thin (up to 3 cm thick) to be mapped using the 50 MHz antennae. These results are consistent with those of Lowe (1985), who found that reliable identification of tephra layers in peat using GPR was hampered by the variability in depth and diffuseness of the tephra layers where they occur in peat, as compared to lake sediments.

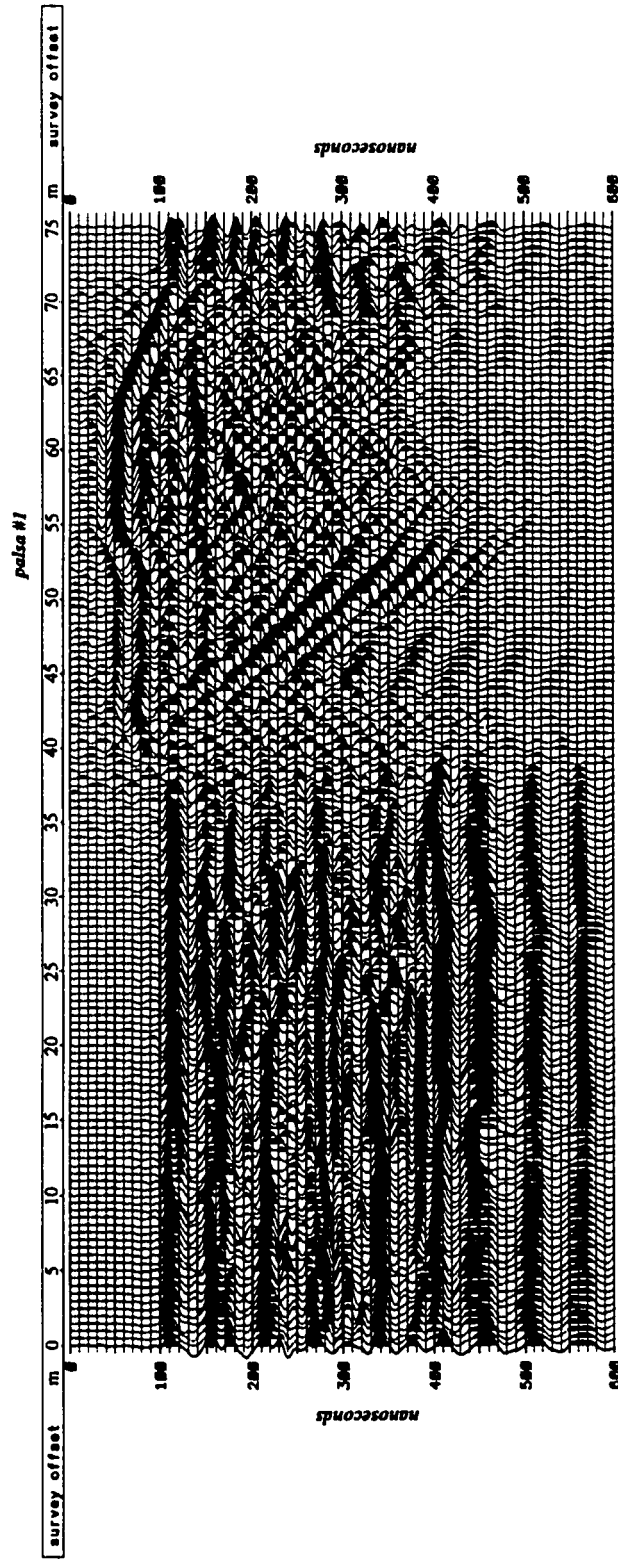
3.7.3 Internal Peat Stratigraphy - Palsas

Stratification observed in cores from the frozen peat was not as distinct as in the fens; the peat consisted of fibrous peat, increasingly icy with depth, with pore ice, ice crystals up to 5 mm in diameter, and ice lenses and veins up to 9 cm thick. Where permafrost extended into the underlying mineral sediment, as at Dale Creek, there was an apparent increase in ice lenses and veins above the peat - mineral sediment interface.

On the 50 MHz radar profiles, the frost table is not typically distinguishable from the direct air and ground waves due to its shallow depth, despite the strong dielectric contrast at this interface. However, where the active layer is thin, radar energy may refract and travel along the frost table at a greater velocity than the direct ground wave travelling through the dry, unfrozen peat at the ground surface, arriving at the receiving antenna prior to the direct ground wave; this arrival can in some cases be differentiated from the air and ground waves on the radar profile (Figure 3-19). Use of higher frequency antennae (*e.g.*, 500 MHz) would facilitate differentiation of the active layer if this was of interest (Doolittle, *et al.*, 1992).

Scattering of radar signal energy by pore ice and ice lenses, scattering and absorption in near-surface thawed and partially thawed layers (Doolittle, *et al.*, 1992; Arcone, 1984), and increased signal propagation velocity through frozen material (Kettles and Robinson, 1996)

Figure 3-16. Coherency filter applied to fen profile.

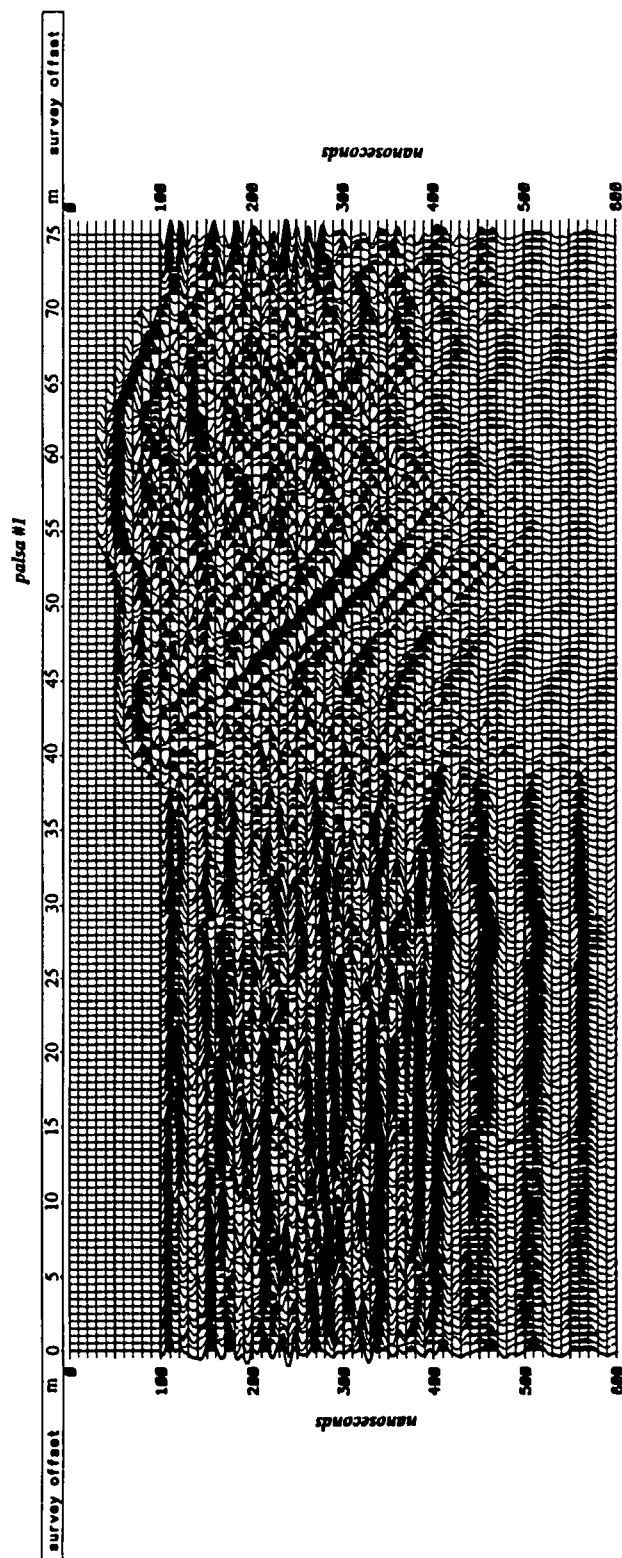


Profile after application of F-X deconvolution as a coherency filter. Note improvement in lateral continuity of fen reflections. Compare with Figures 3-12 to 3-15 and 3-17.

Data from Transect #1 at Porsild's Field. Vertical exaggeration ca. 1.2x. Transect crosses unfrozen fen from 0 m to 38 m, frozen palsa #1 from 38 m to 70.5 m, and unfrozen fen from 70.5 m to 75 m.

Plot produced from ProMAX v.5.1, after data conversion to SEG-Y seismic format using the pulseEKKO IV operating software. Other processing steps include signal saturation correction, automatic (time-variable) gain control, bandpass filter, normal moveout correction, topographic correction, and F-X deconvolution. **N.B.** Some portion of the direct air and ground waves are muted as a byproduct of normal moveout correction, particularly in the fens.

Figure 3-17. Coherency filter and deconvolution applied to fen profile.

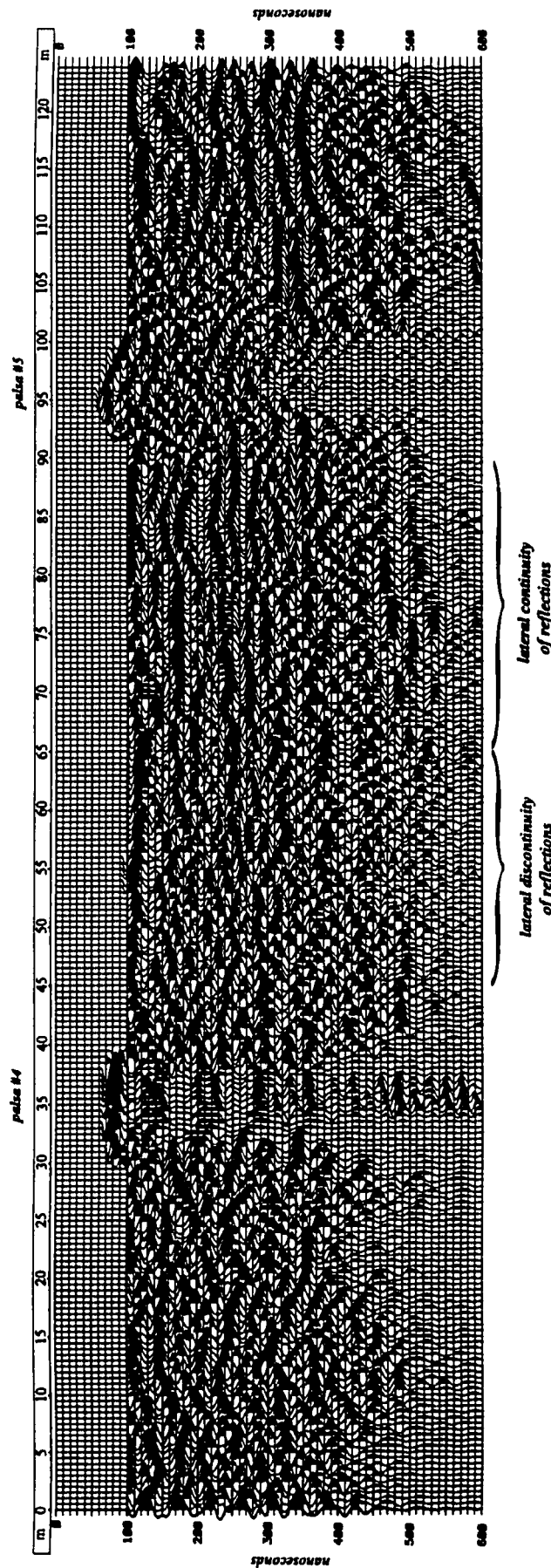


Profile after zero-phase spiking deconvolution, for improved vertical resolution, and F-X deconvolution as a coherency filter for improved lateral continuity of reflections. Note improved resolution particularly between 200 ns and 300 ns. Compare with Figures 3-12 to 3-16.

Data from Transect #1 at Porsild's Field. Vertical exaggeration ca. 1.2x. Transect crosses unfrozen fen from 0 m to 38 m, frozen palsa #1 from 38 m to 70.5 m, and unfrozen fen from 70.5 m to 75 m.

Plot produced from ProMAX v.5.1, after data conversion to SEG-Y seismic format using the pulseEKKO IV operating software. Other processing steps include signal saturation correction, automatic (time-variable) gain control, bandpass filter, normal moveout correction, topographic correction, zero-phase spiking deconvolution, and F-X deconvolution. **N.B.** Some portion of the direct air and ground waves are muted as a byproduct of normal moveout correction, particularly in the fens.

Figure 3-18a. Radar profile showing inferred stratigraphic signature of known collapse scar, Porsild's Field.

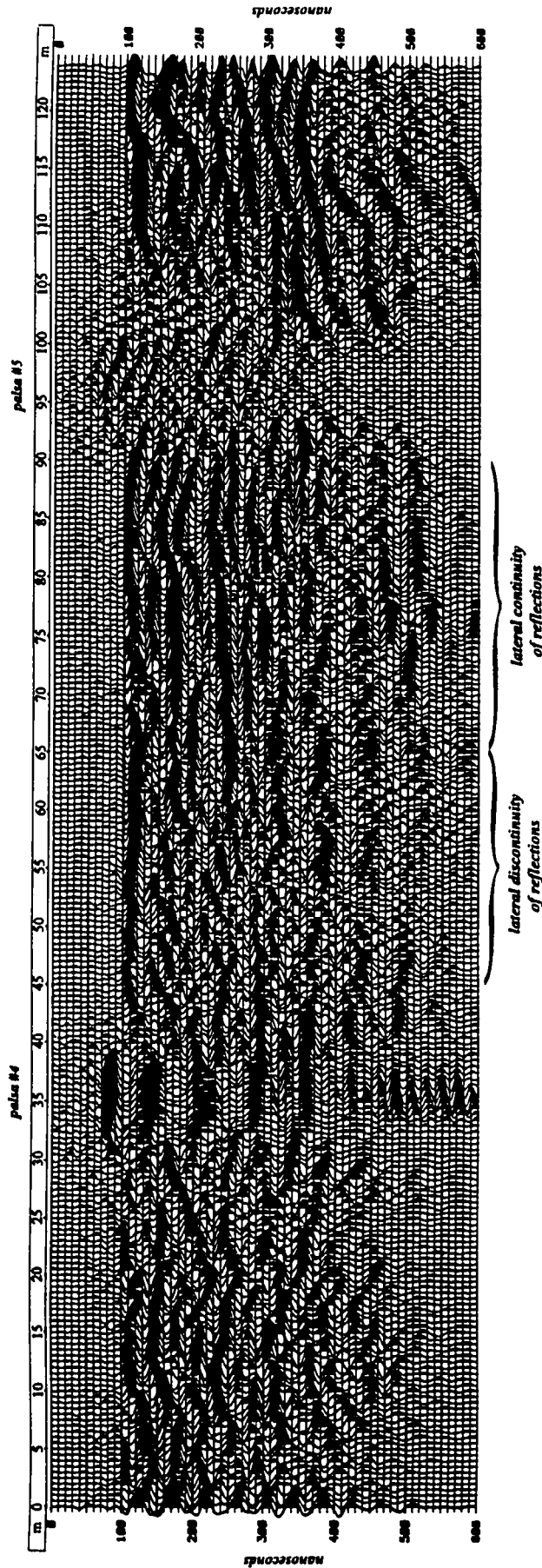


Radar profile prior to application of F-X deconvolution as a coherency filter. Note apparent decrease in lateral continuity of reflections between 45 m and 65 m on the transect, between 130 ns to 300 ns, compared to stratigraphy between 65 m and 90 m; this pattern may be associated with a pre-existing palsa adjacent to this location. The radar transect intersects the edge of the collapse scar at 54.5 m to 58 m, where slightly elevated peat may represent the rim of the collapsed palsa (palsa #9; Kershaw and Gill, 1979).

Data from Transect #3 at Porsild's Field. Vertical exaggeration *ca.* 1.2x. Transect crosses unfrozen fen from 0 m to 30 m, frozen palsa #4 from 30 m to 40 m, unfrozen fen from 40 m to 92.5 m, frozen palsa #5 from 92.5 m to 102 m, and unfrozen fen from 102 m to 125 m.

Plots produced from ProMAX v.5.1, after data conversion to SEG-Y seismic format using the pulseEKKO IV operating software. Other processing steps include signal saturation correction, automatic (time variable) gain control, bandpass filter, normal moveout correction, and topographic correction. **N.B.** Some portion of the direct air and ground waves are muted as a byproduct of normal moveout correction, particularly in the fens.

Figure 3-18b. Application of coherency filter to radar profile showing inferred stratigraphic signature of known collapse scar.

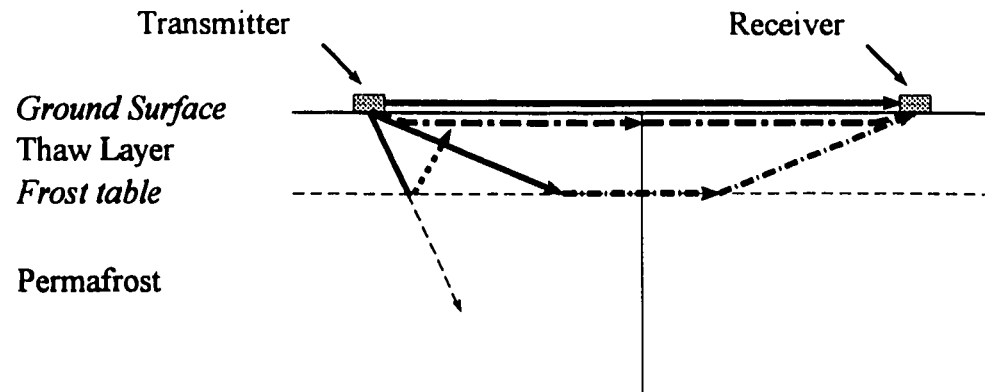


Profile after application of F-X deconvolution as a coherency filter. Note the persistence of the apparent decrease in lateral continuity of reflections between 45 m and 65 m, compared to stratigraphy between 65 m and 90 m, through this processing step. This pattern may represent the stratigraphic signature of the collapsed palsa.

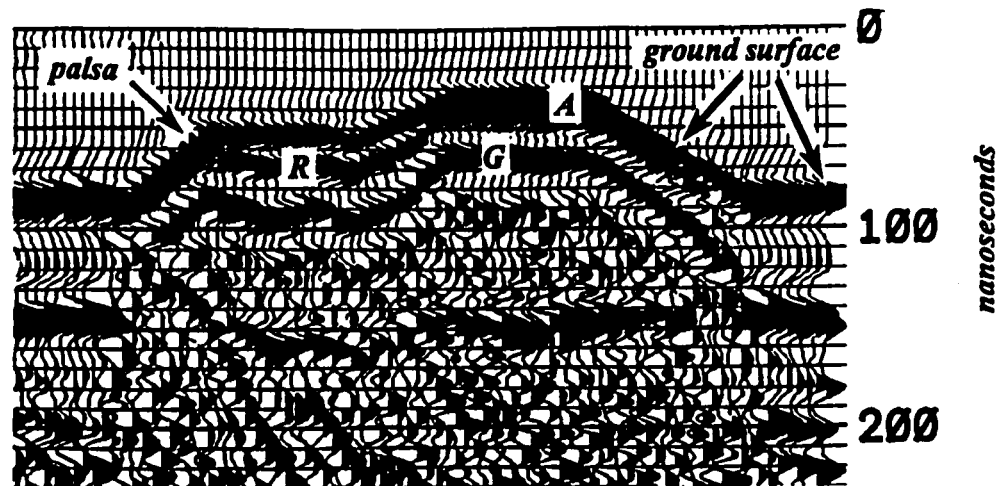
Data from Transect #3 at Porsild's Field. Vertical exaggeration *ca.* 1.2x. Transect crosses unfrozen fen from 0 m to 30 m, frozen palsa #4 from 30 m to 40 m, unfrozen fen from 40 m to 92.5 m, frozen palsa #5 from 92.5 m to 102 m, and unfrozen fen from 102 m to 125 m.

Plots produced from ProMAX v.5.1, after data conversion to SEG-Y seismic format using the pulseEKKO IV operating software. Other processing steps include signal saturation correction, automatic (time variable) gain control, bandpass filter, normal moveout correction, and topographic correction. **N.B.** Some portion of the direct air and ground waves are muted as a byproduct of normal moveout correction, particularly in the fens.

Figure 3-19. Refracted radar event from shallow thaw layer.



- Direct signal energy from transmitter. Energy travelling through the air from the transmitter to the receiver is referred to as the *air wave*.
- - - - -→ Signal energy refracted along ground surface, referred to as the *direct ground wave*.
- · - · - · -→ Signal energy refracted in the shallow subsurface, where angle of signal incidence exceeds critical angle of refraction.
- · · · ·→ Signal energy reflected from each interface; amplitude of reflected energy controlled by dielectric constant.
- - - - -→ Signal energy not reflected at each interface continues downward propagation at an angle and velocity controlled by the electrical properties of the medium.



Radar signal energy refracted along the frost table below a shallow thaw layer, as it may appear on the radar profile, as *R*, between *A*, the air wave, and *G*, the direct ground wave. Depth to frost in this zone averaged 48 cm at the time of the GPR survey.

impair resolution of internal peat stratigraphy and structure, particularly where peat is ice-rich. Deconvolution did not appear to improve the resolution, and in some cases hindered interpretation. Coherency filtering also did not improve resolution or lateral continuity in palsas, except for the inferred peat - mineral sediment interface. In some cases, processing steps such as automatic gain control, bandpass filtering, and NMO correction introduced noise multiples into the profiles, particularly at depth and at frozen - unfrozen interfaces; subsequent processing flows tended to accentuate these multiples and obscure radar stratigraphy (Figure 3-20).

The evaluation or interpretation of stratigraphic continuity between frozen and unfrozen peat requires the calculation of two different depth scales, due to the strong velocity contrast; signal velocity in unfrozen peat is approximately 40 % of velocity in frozen peat. Reflections at a given depth in frozen media appear shallower and compressed relative to one another; for example, a flat-lying interface at 5 m depth would produce a reflection at approximately 268 ns in the fen (two-way travel time, based on fen velocity of $0.038 \text{ m}\cdot\text{ns}^{-1}$), compared to approximately 107 ns in the palsas (based on frozen peat velocity of $0.095 \text{ m}\cdot\text{ns}^{-1}$). Thus, strata that are laterally continuous from unfrozen to frozen peat (Figure 3-21) may not appear continuous on a GPR profile. Nevertheless, a reflection inferred to represent the same interface (*e.g.*, peat - mineral sediment interface) may be visible in both the fens and the palsas (*cf.* Figure 3-7b). However, in some cases, a reflection representing a laterally continuous interface may be continually traced across the frozen - unfrozen interface (*e.g.*, peat - mineral sediment interface on Figure 3-11).

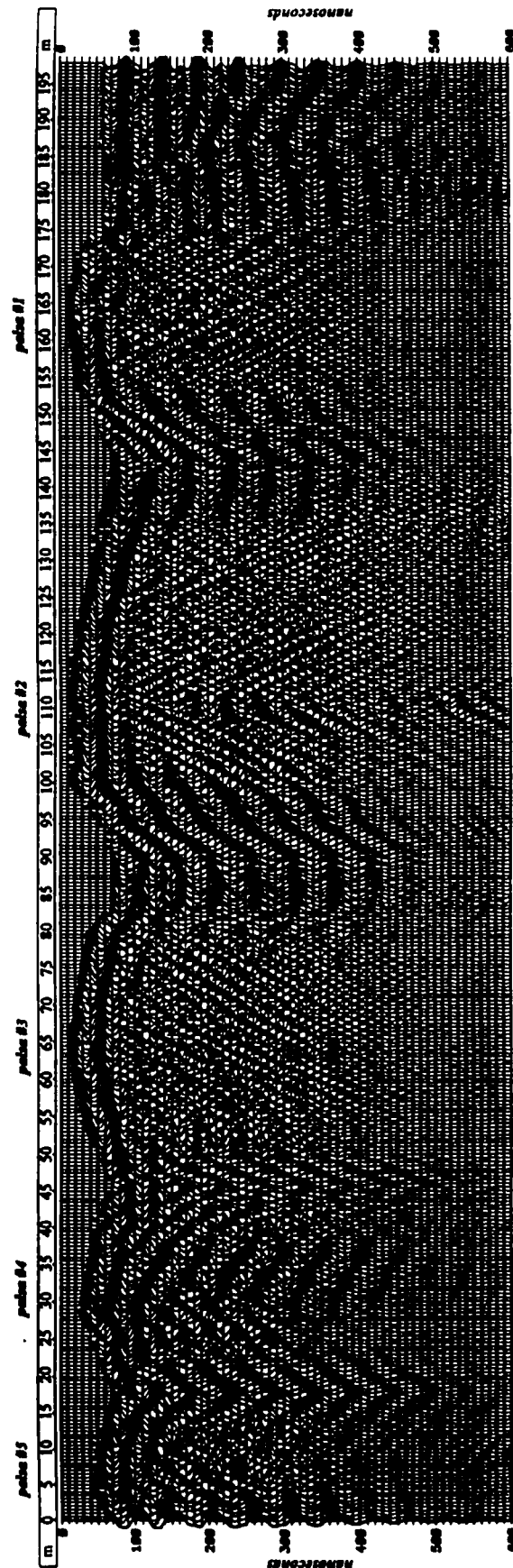
A strong hyperbolic diffraction pattern originating from near the inferred peat - mineral sediment interface is visible at 111 m, below palsa #2 at Dale Creek (Figure 3-20). This radar pattern is characteristic of a point reflector such as a stump or boulder (*cf.* Doolittle, 1987; Worsfold, *et al.*, 1986; Ulriksen, 1980; Welsby, 1988). Åhman (1976) and Worsley, *et al.* (1995) have documented boulders at the base of peat which were heaved up from the underlying mineral sediment in palsas. Boulders and stumps have been observed on other palsas in the study area (G.P. Kershaw, pers. comm., 1995). Migration successfully collapsed the diffraction (Figure 3-22), which had obscured other radar returns. Smaller diffractions and dipping events on this profile (*i.e.*, 124 m, 156 m, 168 m to 172 m) were also collapsed through migration, improving the overall appearance of the profile, although individual laterally continuous reflections remain poorly resolved.

Signal penetration below palsa #5 at Porsild's Field was good, and some apparently domed stratigraphy inferred to be related to ice segregation and palsa formation (Seppälä, 1988) could be seen at depth, possibly extending into mineral sediment (Figure 3-10). This palsa was not cored due to time constraints.

3.7.4 Frozen - Unfrozen Interfaces

In areas of unfrozen peat, the GPR returns are generally characterized by laterally continuous reflections and penetration to depths of 7 m to 8 m, in contrast to returns from frozen peat,

Figure 3-20. Noise multiples introduced into radar data by processing.

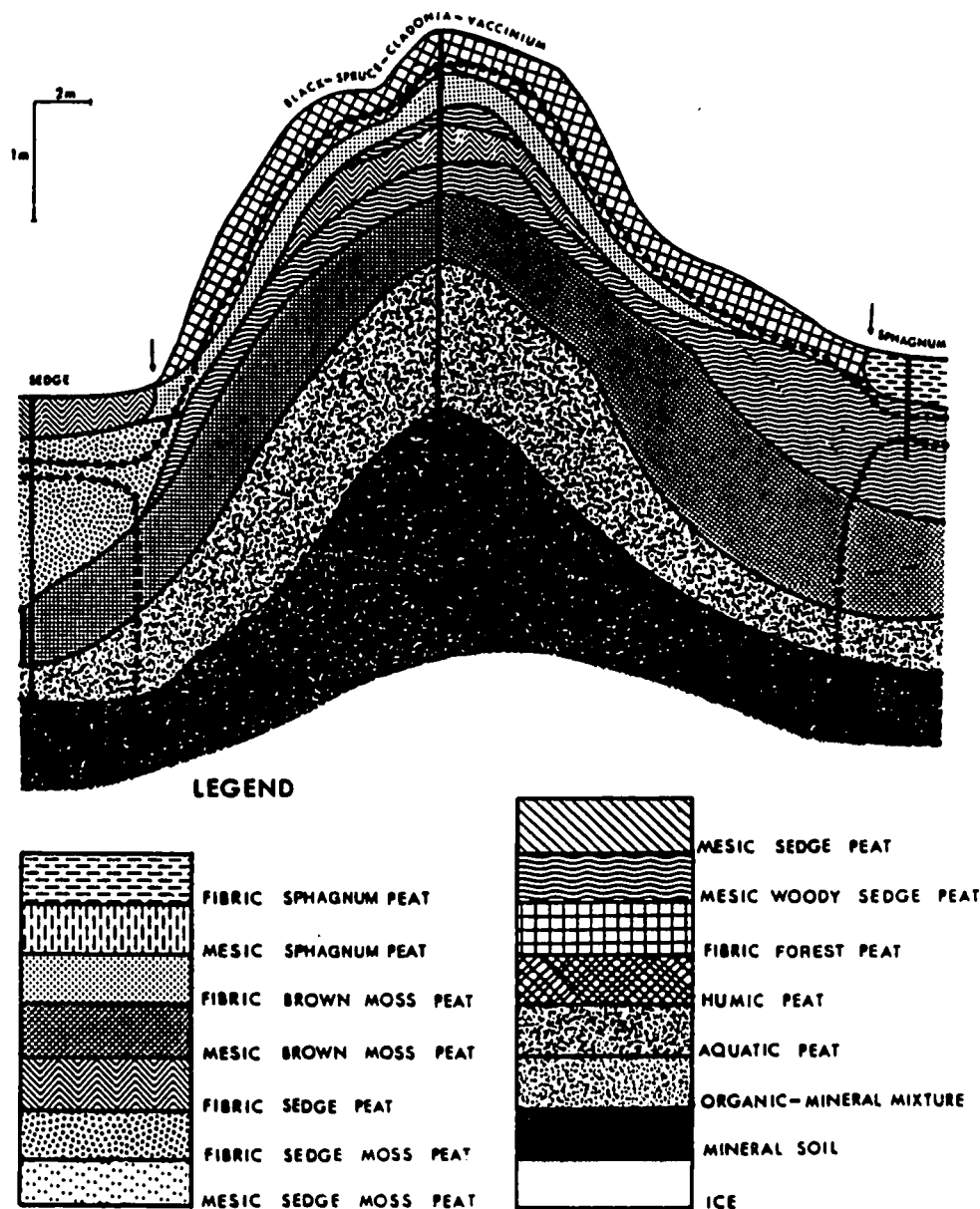


Radar profile illustrating noise multiples introduced and accentuated by some processing steps, particularly in unfrozen peat and below palsas # 4 and #5 (from west), 0 m to 40 m.

Data from Transect #1 at Dale Creek. Vertical exaggeration is ca. 2x. Transect crosses five palsas from east to west, separated by unfrozen fen, and unfrozen meadow west of palsa #1 (180 m to 198.5 m).

Plot produced from ProMAX v.5.1, after data conversion to SEG-Y seismic format using the pulseEKKO IV operating software. Other processing steps include automatic (time variable) gain control, normal moveout correction, bandpass filter, topographic correction and F-X deconvolution. **N.B.** Some portion of the direct air and ground waves are muted as a byproduct of normal moveout correction, particularly in the fens.

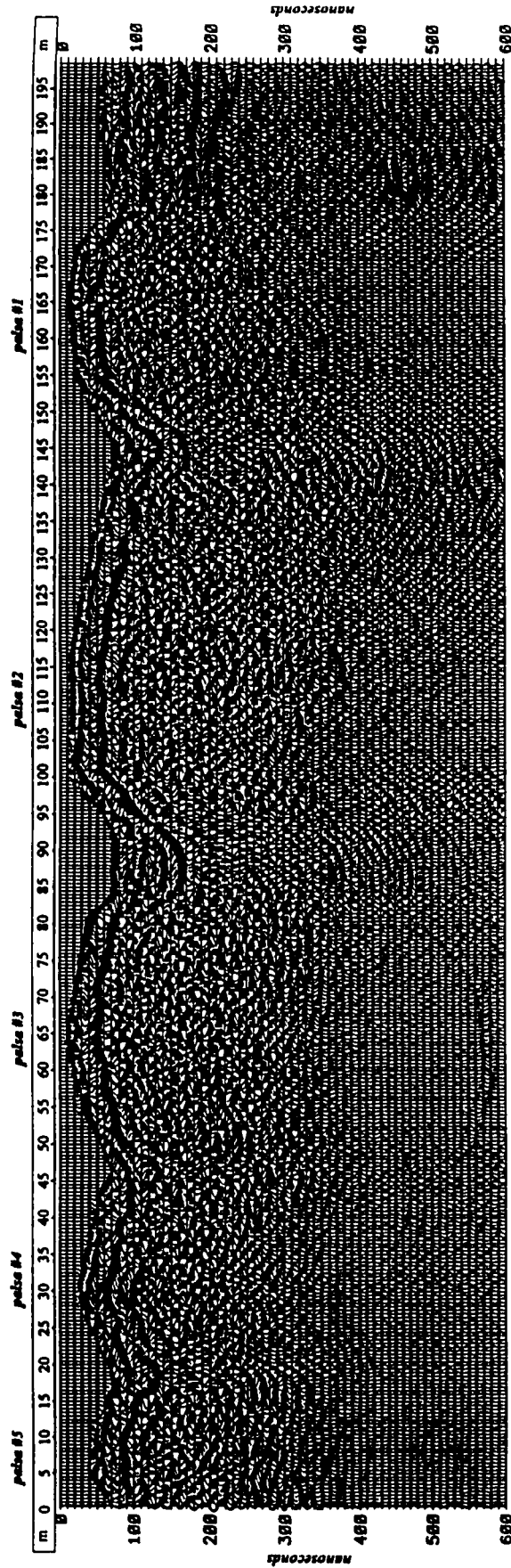
Figure 3-21. Stratigraphic cross-section of a dome-shaped palsa mound.



Note doming of individual peat strata conformable with external morphology. Some strata are continuous across the frozen - unfrozen interface. Palsa located at 67°06'N, 134°17'W.

Source: Perennially frozen peatlands in the western Arctic and subarctic of Canada (Zoltai and Tarnocai, 1975). *Canadian Journal of Earth Sciences* 12, 28-43. Copyright (1975, NRC Research Press). Reprinted by permission of National Research Council Research Press.

Figure 3-22. Migration of radar profile, Dale Creek.



Migration has collapsed point diffraction at 111 m, as well as repositioned dipping reflections, *i.e.*, between 125 m to 130 m, 155 m to 160 m, and 168 m to 172 m. Migration resulted in an overall improvement in the appearance of the profile; however, individual reflections remain poorly resolved within the palsa cores. Compare with Figures 3-11 and 3-20.

Data from Transect #1 at Dale Creek. Vertical exaggeration is *ca.* 2x. Transect crosses five palsas from east to west, separated by unfrozen fen, and unfrozen meadow west of palsa #1 (180 m to 198.5 m).

Plot produced from ProMAX v.5.1, after data conversion to SEG-Y seismic format using the pulseEKKO IV operating software. Other processing steps include automatic (time variable) gain control, bandpass filter, normal moveout correction, F-K migration, topographic correction, and zero-phase spiking deconvolution. **N.B.** Some portion of the direct air and ground waves are muted as a byproduct of normal moveout correction, particularly in the fens.

which are typically chaotic (due to scattering by ice crystals and pinch-out of lenses), with little lateral continuity, and similar penetration depths.

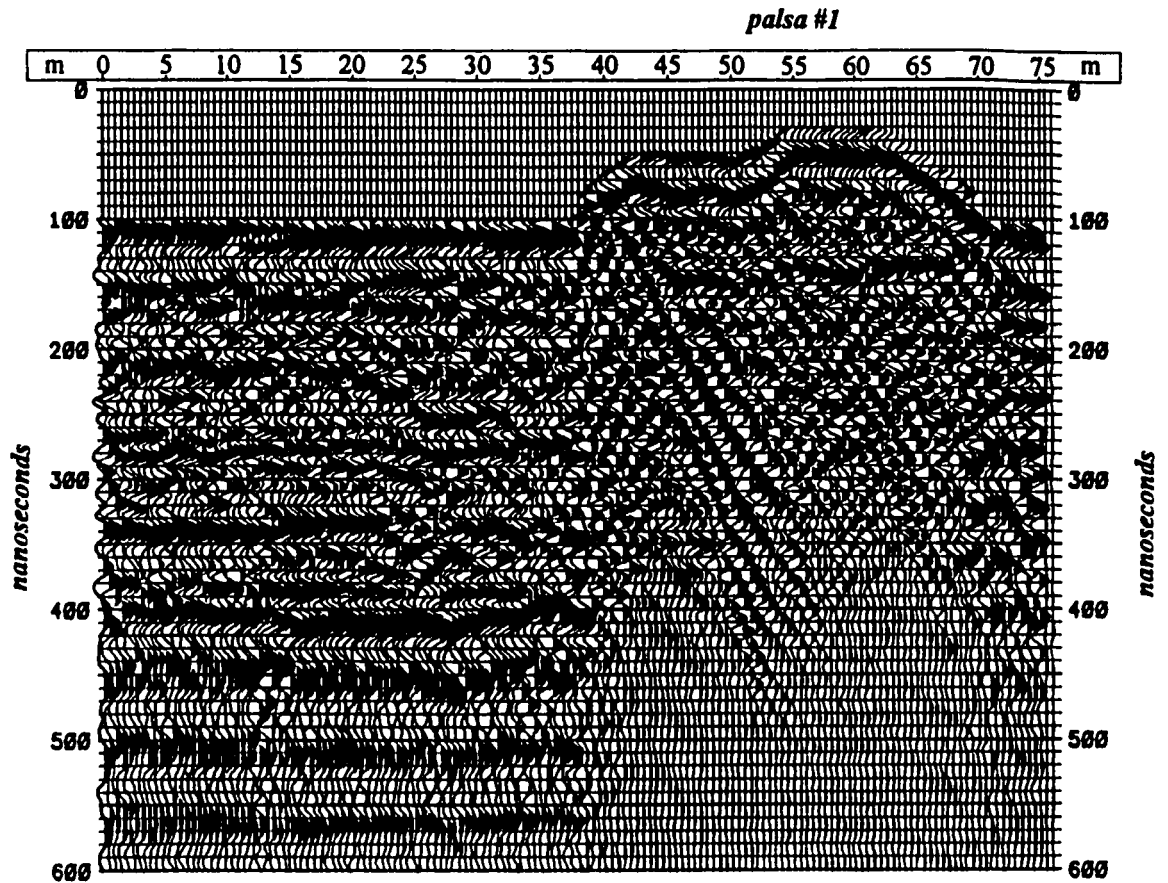
Chaotic radar returns characteristic of frozen, ice-rich ground are visible below the inferred peat - mineral sediment interface in palsas at Dale Creek (palsas #1 to #3 on Transect #1; Figure 3-22). This suggests that the underlying sediment was frozen at least to the depth of signal penetration. As noted earlier, the base of permafrost in palsas and peat plateaus may not be manifested as a strong reflection but as attenuation of the radar signal at depth (*cf.* Kettles and Robinson, 1996; Pilon, *et al.*, 1992).

Kershaw and Gill (1979) described thawed conditions below the permafrost core of palsas #3 and #4 at the Porsild's Field site. Palsa #3 has since completely degraded; coring at palsa #4 encountered 300 cm of frozen peat over approximately 20 cm of unfrozen peat overlying mineral sediment at approximately 320 cm depth. Signal attenuation below palsa #4 (Figure 3-10) probably results from both the unfrozen conditions and clay content in the underlying sediment.

The transition between frozen and unfrozen peat at palsa #1 at Porsild's Field produced a complex and unusual radar pattern. Coring near the edge of the palsa encountered unfrozen material below 490 cm of frozen peat; this frozen - unfrozen interface appears to correlate with a strong dipping reflection on both radar transects intersecting this palsa (Figures 3-7b and 3-8). The dipping radar event extends downwards towards the centre of the palsa, below the inferred base of peat. Apparent multiples of the dipping reflection extend from 150 ns at 40 m to 320 ns at 55 m, with parallel reflections below this extending to 450 ns (Figures 3-7a and 3-23a). This dipping radar event is not considered to be part of a hyperbolic reflection as it does not possess the smooth curve typical of a hyperbolic reflection; also, a series of subapical/subjacent reflections dipping in the opposite direction occur immediately below this event. This radar pattern may be indicative of narrowing of the permafrost core with depth in palsas (*cf.* Zoltai and Tarnocai, 1971:119), and may be a result of thaw degradation. The absence of a similar dipping reflection on the opposite side of the palsa may indicate that the frozen - unfrozen interface at depth is more nearly vertical which may be related to less advanced thaw degradation.

Below the dipping reflection on Transect #1, a number of reflections dipping the opposite direction, away from the palsa, are visible (at 38 m to 45 m, Figure 3-24; compare Figures 3-7a and 3-23a). This radar pattern may be related to a phenomenon referred to as velocity pullup, where laterally continuous reflections appear shallower where they are overlain by frozen material, due to the faster signal propagation velocity through frozen media (Coffeen, 1984; *cf.* Saarenketo, *et al.*, 1992, and Kettles and Robinson, 1996). Looking from left to right on the profile, reflections arrive progressively earlier as the inferred permafrost core thickens. However, this interpretation remains speculative, in the absence of confirmation by coring to this depth. Apparent multiples of the strong dipping reflection complicate interpretation of the radar pattern of this transition zone.

Figure 3-23a. Radar profile showing sub-vertical frozen - unfrozen interface and associated complex reflection patterns.

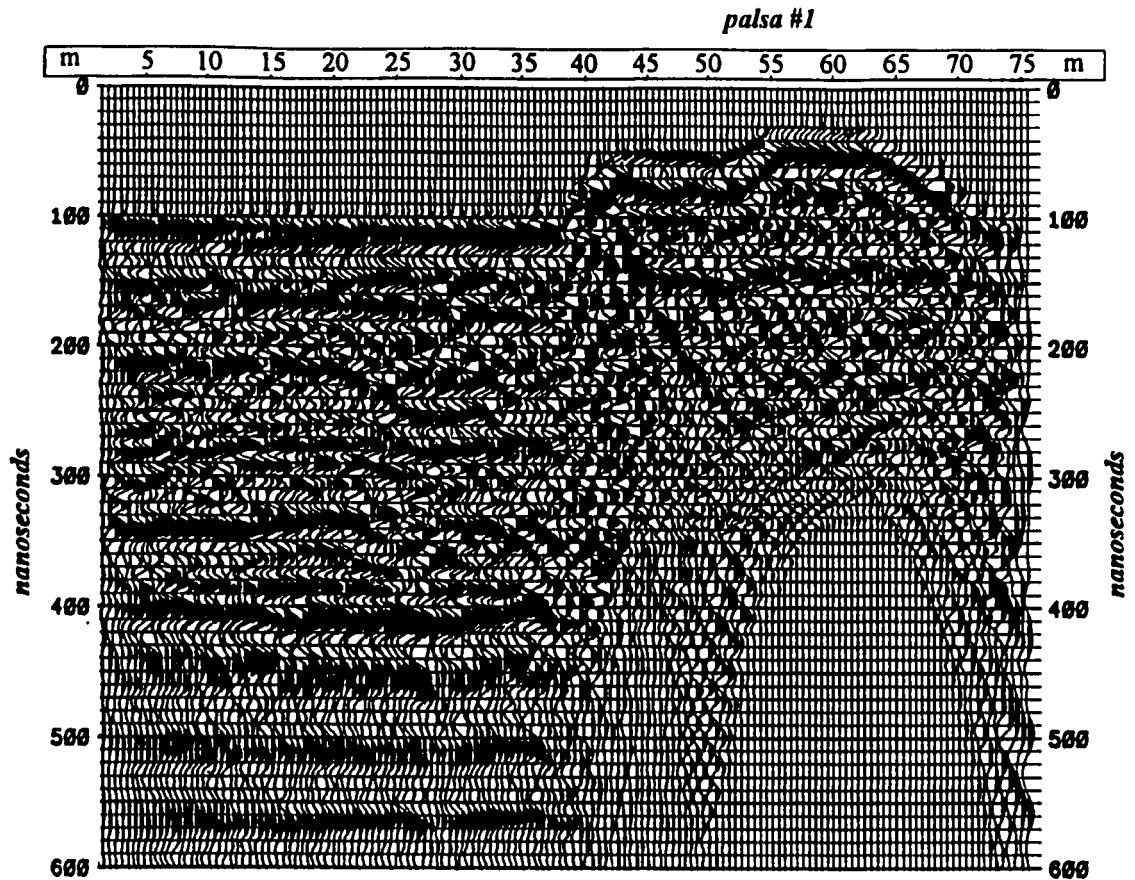


Radar profile prior to application of Memory Stolt F-K time migration to reposition dipping reflections. Note series of strong dipping reflections below the palsa, the topmost extending from 105 ns at 40 m, to 320 ns at 55 m, and parallel reflections below this extending to 450 ns. Also note reflections dipping away from the palsa core at depth between 38 m and 45 m (see Figure 3-24). Compare with Figure 3-23b.

Data from Transect #1 at Porsild's Field. Vertical exaggeration *ca.* 2x. Transect crosses unfrozen fen from 0 m to 38 m, frozen palsa #1 from 38 m to 70.5 m, and unfrozen fen from 70.5 m to 75 m.

Plot produced from ProMAX v.5.1, after data conversion to SEG-Y seismic format using the pulseEKKO IV operating software. Other processing steps include signal saturation correction, automatic (time variable) gain control, normal moveout correction, bandpass filter, F-K migration, and topographic correction. **N.B.** Some portion of the direct air and ground waves are muted as a byproduct of normal moveout correction, particularly in the fens.

Figure 3-23b. Migration of radar profile to enhance imaging of sub-vertical frozen - unfrozen interface.



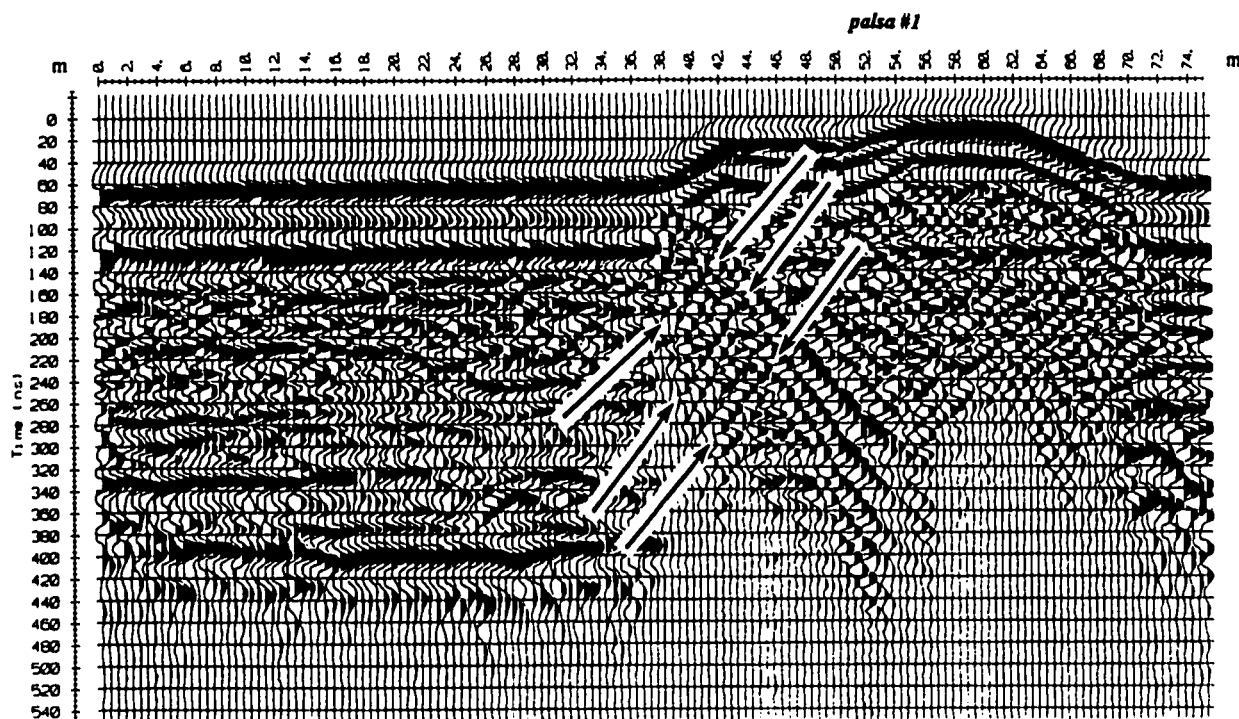
Profile after Memory Stolt F-K time migration. The series of strong dipping reflections below the palsa have been collapsed, and may have been noise multiples. Poorly resolved reflections dipping towards the palsa core remain, however, between 38 m and 45 m, at 100 ns to 150 ns; these may be true reflections generated by the frozen - unfrozen interface, which coring has shown to extend inwards from the palsa margin towards the centre.

The reflections dipping away from the palsa core at depth between 38 m and 45 m (see Figure 3-24) were not collapsed by migration, but remain poorly resolved; these may be flat-lying fen strata imaged progressively shallower, looking from left to right, due to velocity pullup of reflected signal energy below the high velocity frozen palsa core near the surface (see text).

Data from Transect #1 at Porsild's Field. Vertical exaggeration *ca.* 2x. Transect crosses unfrozen fen from 0 m to 38 m, frozen palsa #1 from 38 m to 70.5 m, and unfrozen fen from 70.5 m to 75 m.

Plot produced from ProMAX v.5.1, after data conversion to SEG-Y seismic format using the pulseEKKO IV operating software. Other processing steps include signal saturation correction, automatic (time variable) gain control, normal moveout correction, bandpass filter, F-K migration, and topographic correction. **N.B.** Some portion of the direct air and ground waves are muted as a byproduct of normal moveout correction, particularly in the fens.

Figure 3-24. Radar imaging of inferred flat-lying unfrozen peat strata below frozen wedge of palsa core.



This radar profile best illustrates the reflections dipping away from the palsa core between 38 m and 45 m, below 130 ns, highlighted by the arrows. This reflection pattern may be generated by velocity pullup of fen reflections as signal energy travels through a high velocity layer near the surface, *i.e.*, the marginal wedge of the frozen palsa, causing the flat-lying reflections to appear progressively shallower towards the palsa core.

Data from Transect #1 at Porsild's Field. Vertical exaggeration *ca.* 2x. Transect crosses unfrozen fen from 0 m to 38 m, frozen palsa #1 from 38 m to 70.5 m, and unfrozen fen from 70.5 m to 75 m.

Plot produced from pulseEKKO IV radar operating software. Processing steps include topographic correction, automatic (time variable) gain control, trace-to-trace averaging and down-trace averaging.

Time migration to correctly position dipping radar events could not be reliably applied to the data due to the strong velocity contrast across the frozen - unfrozen interface. Nevertheless, time migration was applied using a simple time- and space-variant velocity structure, assuming the strong dipping reflection represented the frozen - unfrozen interface (Figure 3-23). The multiples of this reflection were collapsed, and poorly resolved dipping reflections remain between 38 m and 45 m at 100 ns to 150 ns, dipping towards the palsa core; these may be true reflections from the frozen - unfrozen interface, which has been shown by coring to be a non-vertical boundary extending from the palsa margin towards the centre. The reflections dipping away from the palsa at depth between 38 m and 45 m, inferred to be unfrozen fen strata, also persist but are poorly resolved.

Depth migration was not applied, as the velocity structure at depth remains poorly defined.

3.8 Conclusions

While GPR can rapidly image subsurface stratigraphy in peatlands and permafrost bodies in peatlands, the degree to which reliable inferences can be made regarding peat properties and permafrost characteristics depends on site-specific conditions and detailed point source verification.

GPR consistently imaged detailed stratigraphy within the peat and, to a lesser degree, underlying mineral sediment in unfrozen fen; however, correlation of individual reflections with specific strata observed in cores was limited. The peat - mineral sediment interface could be consistently and reliably identified in both fen and palsas, due to the strong dielectric contrast at this interface, and was confirmed by coring at some locations. Orientation of strata in both frozen and unfrozen peat and mineral sediment could be inferred from the radar profiles. Excessive signal scatter due to ice obscured internal peat stratigraphy in the palsas; vertical resolution in the palsas was also reduced due to high signal propagation velocities, generating high penetration depth to return time ratios. Vertical resolution and lateral continuity of reflections can be improved by deconvolution and coherency filtering processes through commercially available seismic data processing software, although this did not facilitate correlation with cores for strata other than the few major stratigraphic interfaces intercepted by coring (*e.g.*, the peat - mineral sediment, peat - gyttja, and frozen - unfrozen interfaces). The data compiled for this study were inadequate to test the effectiveness of data processing to improve the resolution of diffuse tephra layers in peat.

Small vertical and/or lateral stratigraphic discontinuities associated with collapsed palsas or peat plateaus that are not detectable with conventional coring methods may be imaged by GPR; this should be further tested at other locations where peatland history is known. If successful, this application would contribute to reconstruction of peatland history on the basis of perennally frozen peat landforms, which is typically restricted due to the limited stratigraphic evidence preserved following the collapse of palsas or peat plateaus (*cf.* Lundqvist, 1969:211-212).

Peat stratigraphy typically cannot be traced between the fens and the palsas due to the strong contrast in signal propagation velocity across the frozen - unfrozen interface. At the Porsild's Field site, interpretation of radar reflections across the fen - palsa transition was complicated by thaw degradation at depth. Thawing at the margins of the permafrost core of palsa #1 at this site is inferred on the basis of signal attenuation, velocity pullup of fen reflections below a 'wedge' of ground ice near the palsa edge, and observation of unfrozen conditions below frozen peat in cores.

Frozen - unfrozen interfaces could otherwise be consistently traced using GPR, based on a change in radar reflection character from chaotic, discontinuous reflections in palsas to laterally continuous, wavy, sub-parallel reflections in the fen.

The relationship between radar events and causative peat properties remains poorly defined. Improved peat sample retrieval methods (*e.g.*, reduced water loss, compaction), in conjunction with more detailed coring and sample analyses, would facilitate reliable correlation of observed strata with radar reflections. Ultimately, the extent of manual testing may be reduced by use of GPR, but only when radar response to changes in peat properties is better understood. The complex inhomogeneity of peatland characteristics and the numerous factors affecting the dielectric permittivity in peatlands suggest that GPR will remain of limited utility in detailed stratigraphic studies. Therefore, the primary advantages of GPR currently include its ability to image structural information, in particular spatial continuity, as well as its ability to detect gross stratigraphic features, such as interfaces between peat and mineral sediment, peat and gyttja, and the acrotelm and catotelm, as well as the interface between frozen and unfrozen peat.

Seismic data processing techniques were successful in improving data resolution in the fens, and to a lesser extent in the palsas. However, the processing can be time-consuming, particularly for inexperienced users. Unless the improved resolution offered by advanced data processing is accompanied by more detailed characterization of peat properties, the time investment demanded by the use of seismic data processing techniques may not be warranted. Notwithstanding this, it is clear that advanced data processing can improve the quality of the data, particularly in unfrozen peat.

As the application of GPR to perennially frozen peatlands is at its inception, further research is warranted to test its viability in this environment. Additional GPR surveys on perennially frozen peatlands need to be conducted to extend the existing database from this environment; currently, the number of case studies is too few to conclusively evaluate the utility of GPR in this application. Similarly, seismic data processing techniques should be tested on other datasets from this environment to test the conclusions reached here.

3.9 Literature Cited

- Åhman, R. 1976. The structure and morphology of minerogenic palsas in northern Norway. *Biuletyn Peryglacjalny* 26, 25-31.
- Annan, A.P. 1992. *Ground penetrating radar, workshop notes*. Sensors & Software Inc., Mississauga, Ontario.
- Annan, A.P. and Davis, J.L. 1976. Impulse radar sounding in permafrost. *Radio Science* 11 (4), 383-394.
- Annan, A.P., Davis, J.L. and Scott, W.J. 1975. Impulse radar profiling in permafrost. In *Report of Activities, Part C. Geological Survey of Canada Paper 75-1C*, 343-351.
- Arcone, S.A. 1984. *Pulse transmission through frozen silt*. U.S. Cold Regions Research and Engineering Laboratory, Report 84-17 (8p.)
- Bjelm, L. 1980. Geological interpretation with subsurface interface radar in peatlands. In *Proceedings, 6th International Peat Congress*, Duluth, Minnesota: International Peat Society, 7-8.
- Coffeen, J.A. 1986. *Seismic Exploration Fundamentals: seismic techniques for finding oil, second edition*, Tulsa: PennWell Publishing Company (347p.).
- Coffeen, J.A. 1984. *Interpreting Seismic Data*, Tulsa: PennWell Publishing Company (260p.).
- Cummings, C.E. and Pollard, W.H. 1990. Cryogenetic categorization of peat and mineralcored palsas in the Schefferville area, Quebec. In *Permafrost-Canada, Proceedings of the Fifth Canadian Permafrost Conference*, Université Laval, Centre d'études nordiques. Collection Nordicana, No. 54, 95-102.
- Dallimore, S.R. and Davis, J.L. 1987. Ground probing radar investigations of massive ground ice and near surface geology in continuous permafrost. In *Current Research, Part A. Geological Survey of Canada Paper 87-1A*, 913-918.
- Davis, J.L. and Annan, A.P. 1989. Ground-penetrating radar for high-resolution mapping of soil and rock stratigraphy. *Geophysical Prospecting* 37, 531-551.
- Davis, J.L., Topp, G.C. and Annan, A.P. 1977. Measuring soil water content in situ using time-domain reflectometry techniques. In *Report of Activities, Part B, Geological Survey of Canada, Paper 77-1B*, 33-36.

- Doolittle, J.A. 1987. Using ground-penetrating radar to increase the quality and efficiency of soil surveys. In Reynolds, W.U. and Petersen, G.W., editors, *Soil Survey Techniques*, Soil Science Society of America, Special Publication No. 20, 11-32.
- Doolittle, J.A., Hardisky, M.A. and Black, S. 1992. A ground-penetrating radar study of Goodream palsas, Newfoundland, Canada. *Arctic and Alpine Research* 24 (2), 173-178.
- Fisher, E., McMechan, G.A. and Annan, A.P. 1992a. Acquisition and processing of wide-aperture ground-penetrating radar data. *Geophysics* 57, 495-504.
- Fisher, E., McMechan, G.A., Annan, A.P. and Cosway, S.W. 1992b. Examples of reverse-time migration of single-channel, ground penetrating radar profiles. *Geophysics* 57, 577-586.
- Fisher, S.C., Stewart, R.R. and Jol, H.M. 1994. Processing ground penetrating radar data. In *GPR '94, Proceedings of the Fifth International Conference on Ground Penetrating Radar*, Kitchener, Ontario: Waterloo Centre for Groundwater Research and Canadian Geotechnical Society, 2, 661-675.
- Gill, D. 1975. Cirque Lake I.B.P. Study Area. Environmental Services Group, AMAX Northwest Mining Co. Ltd., Vancouver, B.C. 139pp.
- Hänninen, P. 1992. *Application of ground penetrating radar and radio wave moisture probe techniques to peatland investigations*. Geological Survey of Finland, Bulletin 361 (71p.)
- Hobbs, N.B. 1986. Mire morphology and the properties and behaviour of some British and foreign peats. *Quarterly Journal of Engineering Geology, London* 19, 7-80.
- Hogan, G. 1988. Migration of ground penetrating radar data: a technique for locating subsurface targets. In Fitterman, D., Bell, R., Corbett, J., Davenport, C., Hulse, S., and Bierley, C., editors, *Proceedings of the Symposium on the Application of Geophysics to Engineering and Environmental Problems*, Society of Engineering and Mineral Exploration Geophysicists: United States Geological Survey, 809-822.
- Jol, H.M. and Smith, D.G. 1991. Ground penetrating radar of northern lacustrine deltas. *Canadian Journal of Earth Sciences* 28, 1939-1947.
- Jowsey, P.C. 1966. An improved peat sampler. *New Phytologist*, 65:245-248.
- Kalantzis, F. 1994. Imaging of reflection seismic and radar wavefields: monitoring of steam heated oil reservoirs and characterization of nuclear waste repositories. Unpublished Ph.D. Thesis, Department of Physics, University of Alberta, Edmonton, Alberta. 297pp.

- Kershaw, G.P. and Gill, D. 1979. Growth and decay of palsas and peat plateaus in the Macmillan Pass - Tsichu River area, Northwest Territories, Canada. *Canadian Journal of Earth Sciences* 16(7), 1362-1374.
- Kettles, I.M. and Robinson, S.D. 1996. A ground-penetrating radar study of peat landforms in the discontinuous permafrost zone near Fort Simpson, Northwest Territories, Canada. In Trettin, C., M. Jurgenson, D. Grigal, M. Gale and J. Jeglum, editors, *Northern Forested Wetlands: Ecology and Management*, CRC, Lewis Publishers, Boca Raton, Florida, 147-160.
- LaFleche, P.T., Todoeschuck, J.P., Jensen, O.G. and Judge, A.S. 1991. Analysis of ground-probing radar data: predictive deconvolution. *Canadian Geotechnical Journal* 28, 134-139.
- Lerbekmo, J.F., Westgate, J.A., Smith, D.G.W., and Denton. 1975. New data on the character and history of the White River volcanic eruption, Alaska. In Suggate, R.P. and M.M. Cresswell, editors, *Quaternary Studies*. Royal Society of New Zealand. 203-209.
- Lowe, D.J. 1985. Application of impulse radar to continuous profiling of tephra-bearing lake sediments and peats: an initial evaluation. *New Zealand Journal of Geology and Geophysics* 28, 667-674.
- Lundqvist, J. 1969. Earth and ice mounds: a terminological discussion. In Péwé, T.L., editor, *The Periglacial Environment, past and present*. McGill - Queen's University Press, Montreal, 203-215.
- Maijala, P. 1992. Application of some seismic data processing methods to ground penetrating radar data. In Hänninen, P. and Autio, S., editors, *Fourth International Conference on Ground Penetrating Radar*, Rovaniemi, Finland: Geological Survey of Finland, Special Paper 16, 103-110.
- Morey, R.M. and Kovacs, A. 1985. Analysis of wide-angle reflection and refraction measurements. In Brown, J., Metz, M.C., and Hoekstra, P., editors, *Workshop on Permafrost Geophysics*, Golden, Colorado: United States Army Cold Regions Research and Engineering Laboratory, Special Report 85-5, 53-60.
- National Wetlands Working Group (Canada Committee on Ecological Land Classification). 1988. *Wetlands of Canada. Ecological Land Classification Series No. 24*. Sustainable Development Branch, Environment Canada, Ottawa and Polyscience Publications Inc., Montreal. (452p.)
- Pilon, J.A., Allard, M. and Séguin, M.K. 1992. Ground probing radar in the investigation of permafrost and subsurface characteristics of surficial deposits in Kangiqsualujuaq,

northern Québec. In Pilon, J.A., editor, *Ground penetrating radar*, Ottawa, Ontario: Geological Survey of Canada, Paper 90-94, 41-48.

Porsild, A.E. 1951. *Botany of southeastern Yukon adjacent to the Canol Road*. Canada Department of Resources and Development, National Parks Branch. National Museum of Canada, Bulletin No. 121 (Biological Series No. 41). 400pp.

Porsild, A.E. 1945. *The alpine flora of the east slope of Mackenzie Mountains, Northwest Territories*. Canada Department of Mines and Resources, Mines and Geology Branch. National Museum of Canada, Bulletin No. 101 (Biological Series No. 30). 35pp.

Robinson, S.D., Moorman, B.J., Judge, A.S., Dallimore, S.R. and Shimeld, J.W. 1992. The application of radar stratigraphic techniques to the investigation of massive ground ice at Yaya Lake, Northwest Territories. In *Proceedings of the Third National Student Conference on Northern Studies*, Ottawa, Ontario: Musk-Ox Special Publication 39, 39-49.

Saarenketo, T., Hietala, K. and Salmi, T. 1992. GPR applications in geotechnical investigations of peat for road survey purposes. In Hänninen, P. and Autio, S., editors, *Fourth International Conference on Ground Penetrating Radar*, Rovaniemi, Finland: Geological Survey of Finland, Special Paper 16, 293-305.

Seppälä, M. 1988. Palsas and related forms. In Clark, M.J., editor, *Advances in Periglacial Geomorphology*: John Wiley & Sons, Chichester, 247-278.

Skaret, K.D. 1995. Stratigraphic, microclimatic and thawing attributes associated with palsas located in the alpine tundra environment of the Macmillan Pass - Tsichu River region, N.W.T., Canada. M.Sc. Thesis, Department of Geography, University of Alberta, Edmonton, Alberta.

Theimer, B.D., Nobes, D.C. and Warner, B.G. 1994. A study of the geoelectrical properties of peatlands and their influence on ground-penetrating radar surveying. *Geophysical Prospecting* 42, 179-209.

Tiuri, M., Toikka, M., Marttila, I. and Tolonen, K. 1983. The use of radio wave probe and subsurface interface radar in peat resource inventory. In Robertson, R.A., editor, *Remote Sensing in Peat and Terrain Resource Surveys, Proceedings of Symposium of IPS Commission I*, Aberdeen, Scotland: International Peat Society, 1331-143.

Topp, G.C., Davis, J.L. and Annan, A.P. 1980. Electromagnetic determination of soil water content: measurements in coaxial transmission lines. *Water Resources Research*, 16(3), 574-582.

- Ulriksen, C.P.F. 1980. Investigation of peat thickness with radar. In *Proceedings, 6th International Peat Congress*, Duluth, Minnesota: International Peat Society, 126-129.
- Welsby, J. 1988. The utilisation of geo-radar in monitoring cutover peatlands. In *Proceedings, 8th International Peat Congress*, Leningrad: International Peat Society, 99-107.
- Worsfold, R.D., Parashar, S.K. and Perrott, T. 1986. Depth profiling of peat deposits with impulse radar. *Canadian Geotechnical Journal* 23, 142-154.
- Worsley, P., Gurney, S.D., and Collins, P.E.F. 1995. Late Holocene 'mineral palsas' and associated vegetation patterns: a case study from Lac Hendry, Northern Québec, Canada and significance for European Pleistocene thermokarst. *Quaternary Science Reviews* 14, 179-192.
- Zoltai, S.C. 1978. A portable sampler for perennially frozen stone-free soils. *Canadian Journal of Soil Science* 58:521-523.
- Zoltai, S.C. and Tarnocai, C. 1971. Properties of a wooded palsa in northern Manitoba. *Arctic and Alpine Research* 3(2), 115-129.

4.0 TRENDS IN PALSA EVOLUTION AT TWO SITES

4.1 Introduction

Kershaw and Gill (1979) documented degradation of palsas over a 34-year period (1944-1978) at Porsild's Field, in the Macmillan Pass area of the Northwest Territories (Figure 4-1), based on interpretation of available aerial and ground photography, and field observations. Coring of palsas at this site indicated the presence of unfrozen peat below the frozen core of some palsas. Permafrost degradation in palsas and peat plateaus was also observed to have occurred over this time period at other locations throughout the Macmillan Pass - Tsichu River area, resulting, in some cases, in complete collapse of features, and in others, reduction in areal extent. No new features were observed to have developed. The observed changes in permafrost features were attributed to a regional climatic warming trend by elimination of other factors, including anthropogenic disturbance and change in vegetation type.

Recently, additional work has been undertaken by the present author at the Porsild's Field site and at a site in the neighbouring valley of Dale Creek (Figure 4-2). This work has involved analysis of time-sequence aerial photography (including more recent coverage than was available in 1979), coring of frozen and unfrozen sediments, field observations and conventional measurements of the features, and application of ground penetrating radar (GPR) as a tool to obtain extensive subsurface stratigraphic information. The objective of this chapter is to interpret trends in development of the palsas at the two sites, particularly over the last 50 years, based on this new evidence.

In particular, this chapter examines the available data to identify contemporary, as well as spatial and temporal variations in, stratigraphic and morphologic characteristics of the palsas and peatlands which may reflect genetic and/or degradational processes. Specific problems considered in this regard include the following.

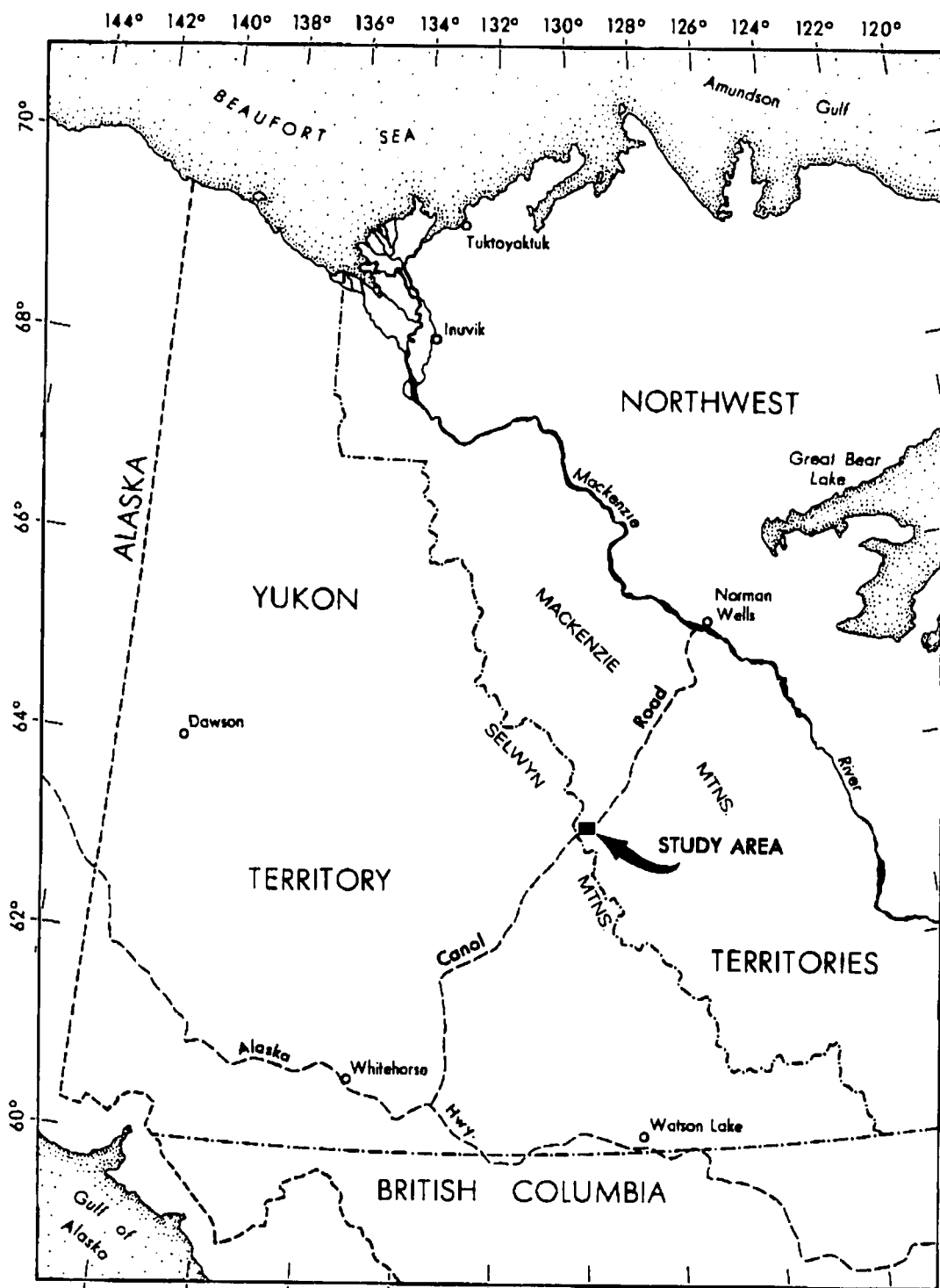
- Do the historic and contemporary surface and subsurface characteristics of the palsas confirm permafrost degradation at the sites, as observed by Kershaw and Gill (1979)?
- Do the palsas at the two sites show a consistent and comparable trend towards degradation over the period of record (50 years)?
- Are the contemporary palsa morphology and characteristics of the peatland/fen compatible with aggradation of the features as individual mounds vs. degradation from a more extensive peat plateau?

Based on case studies of the two palsa fen sites, this chapter also examines the utility of GPR for studies of peatland evolution.

4.2 Study Area

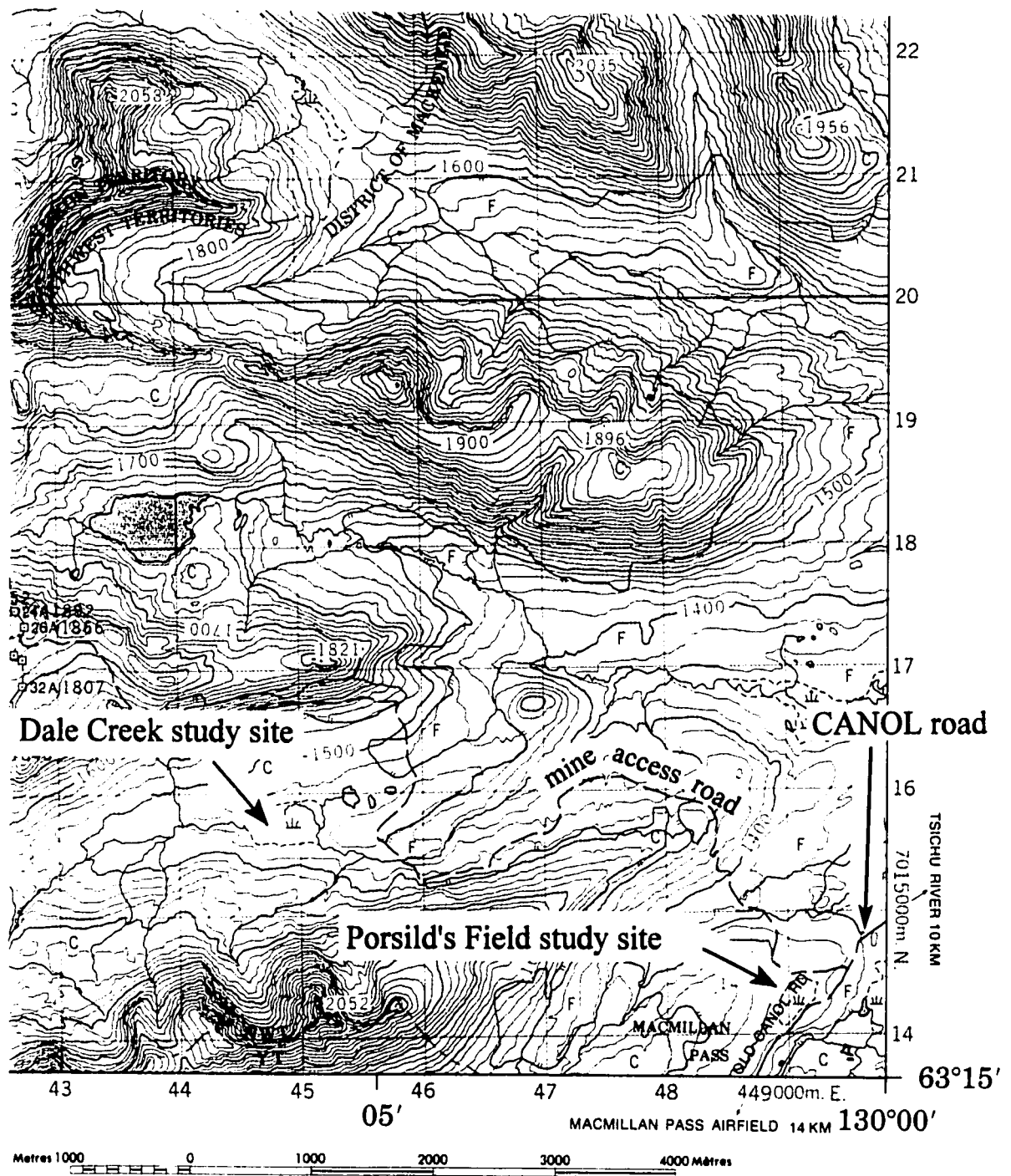
The study area is located in the Selwyn Mountains, near the CANOL road, close to the border between the Yukon and Northwest Territories (Figure 4-1). The area is characterized by

Figure 4-1. Study area location map.



Source: G. Lester, Department of Earth and Atmospheric Sciences (formerly Department of Geography), University of Alberta.

Figure 4-2. Location of Porsild's Field and Dale Creek peatland study sites.



Map scale 1:50,000. Contour interval 20 metres.

Source: Keele Peak, Sheet 105-O/8, Surveys and Mapping Branch, Department of Energy, Mines and Resources, Ottawa, 1982.

rugged, alpine topography, and occurs within the zone of widespread discontinuous permafrost (NRCC, 1988).

The study area is located within an alpine continental climatic regime (Kershaw, 1983). Climatic data are limited for the study area. Data are available for 1974 to 1982 from a station near the Tsichu River, *ca.* 20 km east of Macmillan Pass. Although the period of record is too short to reliably evaluate long-term trends, the data show increases in mean annual air temperature, minimum and maximum temperatures, rainfall, snowfall, and total precipitation (Liang and Kershaw, 1995). These patterns are similar to those observed at other stations with longer records (> 20 years) in the Yukon Plateau, Selwyn Mountains, and Mackenzie Mountains. Increases in mean annual air temperature, and maximum and minimum temperatures were shown to be statistically significant at Tungsten, located approximately 200 km southeast of Macmillan Pass, and at Ross River, located approximately 200 km southwest (Liang and Kershaw, 1995). Notwithstanding these observed long-term trends in air temperature, cold air drainage contributes to locally reduced temperatures at lower elevations in the area, particularly during winter (Kershaw and Skaret, 1993). Mean annual air temperature at Dale Creek in 1990-1991 was -6.69°C (Kershaw and Skaret, 1993).

Data were compiled from two palsa fen sites (Figure 4-2), selected on the basis of accessibility, available aerial photographic and historical records, proximity to one another, and treatment in the literature. The Porsild's Field site, so named (Kershaw and Gill, 1979) for the earliest description of these features by Porsild (1945, 1951), is located in Macmillan Pass, adjacent to the CANOL road, at *ca.* 1390 m asl (63°15'15"N, 130°01'05"W). At this site, six separate palsa mounds were present in 1994 (Plate 4-1), although it is clear from available records that the mounds were more numerous in the past (Kershaw and Gill, 1979).

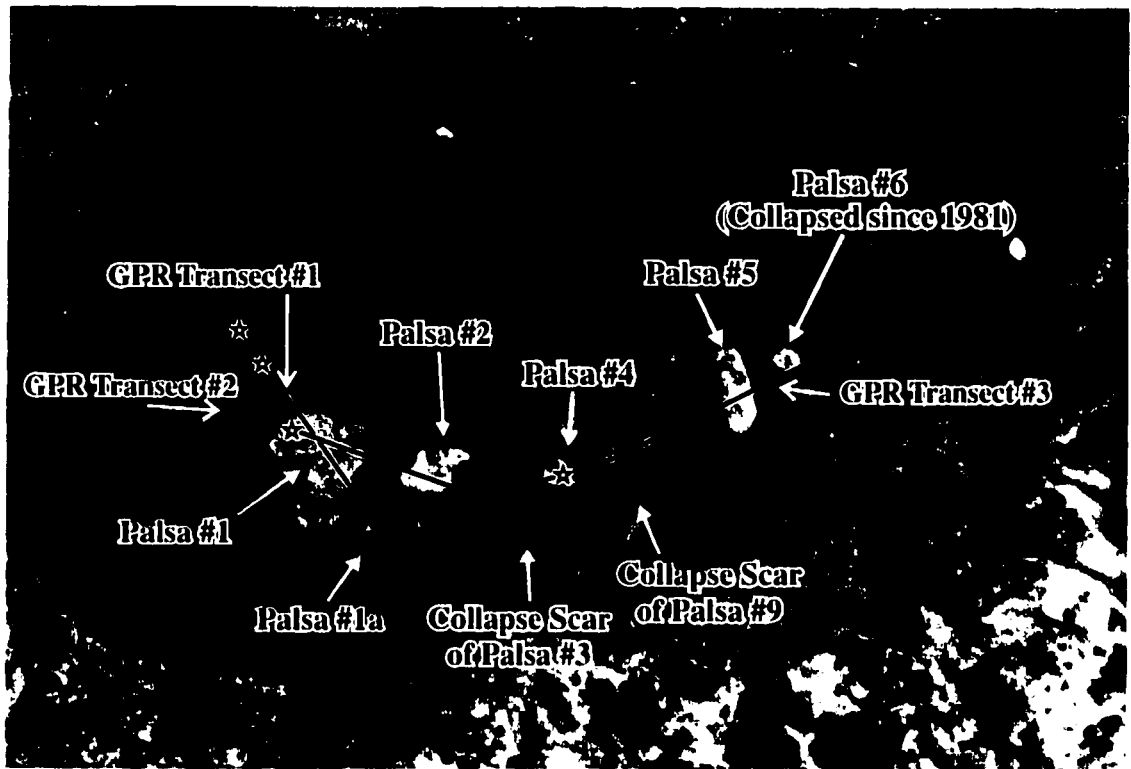
The Dale Creek study site is located in a neighbouring valley 4 km to the northwest of the Porsild's Field study site (63°16'15"N, 130°06'00" W), at *ca.* approximately 1470 m asl. At this site, five classic dome-shaped palsas and one complex feature, consisting of several smaller mounds joined by lower saddle areas, were present (Plate 4-2). For this study, data were collected from the simple palsa forms only, as deep and/or broad areas of open water limited access to the complex feature.

At both sites, shrub-dominated communities bordered the fens, while *Carex aquatilis* and *Eriophorum* spp. and mosses were predominant in the fen, and lichen-moss (*Cladina* spp./*Cetraria* spp./*Polytrichum* spp.) dominated palsa surfaces (G.P. Kershaw, pers. comm., 1994). Bare peat occurred on deflated palsa surfaces and edges where the peat was cracked and/or slumped, and ground squirrel burrowing was extensive.

4.3 Methods

Aerial photographic coverage encompassing both sites is available for the years 1949, 1972, 1974, and 1981. Additional coverage is available for other years; however, these were not examined as they did not provide coverage of both sites in each year. Detailed analysis was performed using the 1949 and 1981 datasets as endpoints, and the 1972 dataset as an

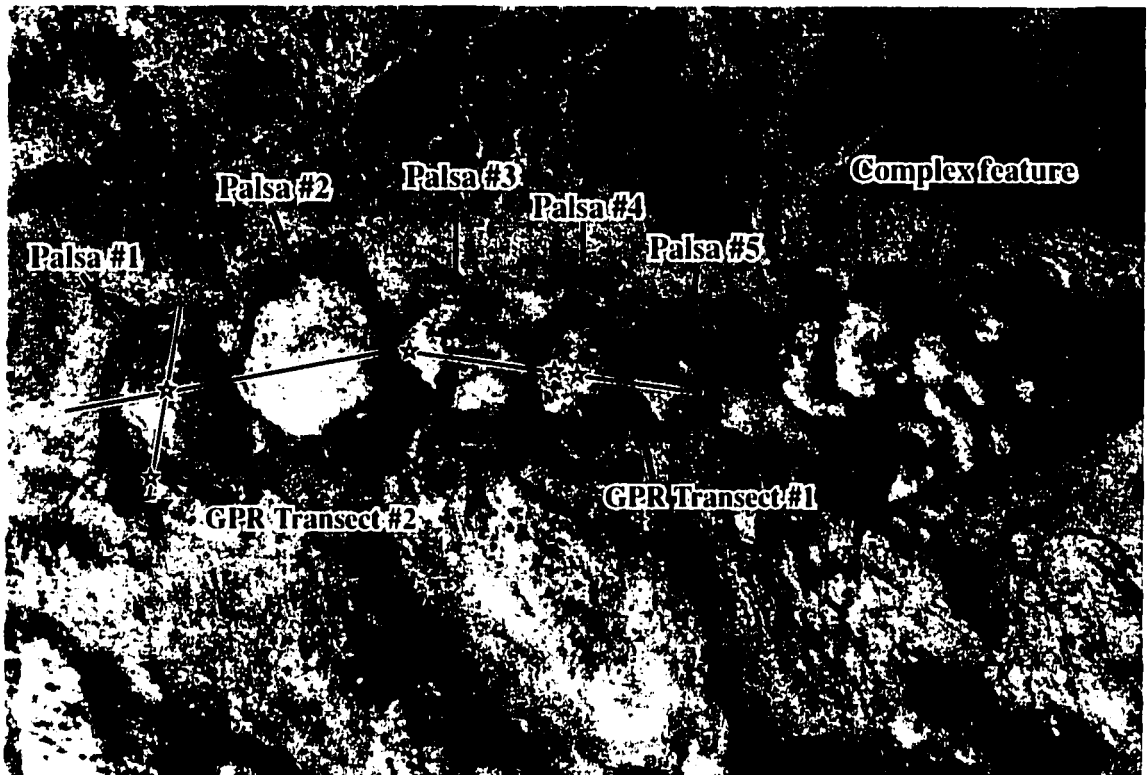
Plate 4-1. Porsild's Field study site.



Aerial view of extant palsas in Porsild's Field, as well as collapse scars of pre-existing palsas known from historic records. GPR Transect #1 crosses palsa #1 from southeast to northwest. GPR Transect #2 crosses palsas #1 and #2 from east to west. GPR Transect #3 crosses palsas #4 and #5 from east to west, and intersects the edge of the collapse scar of pre-existing palsas #9 and #6. (Palsa #7 and the collapse scar of palsa #8, located in the upper right of the photo, were not surveyed.) Coring locations are indicated by stars. South is at the top of the photograph.

Photo credit: Aerial photograph W1727, 143525, August 7, 1981.

Plate 4-2. Dale Creek study site.



Aerial view showing five simple dome-shaped elliptical palsas and one complex feature consisting of several smaller mounds joined by lower saddle areas, at Dale Creek study site. GPR Transect #1 crosses palsas #5 to #1, from east to west. GPR Transect #2 crosses palsa #1 from north to south. Coring locations are indicated by stars. North is at the top of the photograph.

Photo credit: Air photograph W1731, 144908, August 30, 1981

intermediate point of the time series (Appendix C). Photographic enlargements of stereopairs from each of the two sites were made to facilitate mapping of the areal extent of the features. The enlarged images were scanned and enhancements (*i.e.*, contrast, brightening, sharpening) applied, to further assist image interpretation, using tools available in Photoshop software (version 2.5.1) for Windows. The use of digital, enhanced stereopairs compensated for the image quality of the 1949 photography, the resolution of which did not permit areal measurements to be taken directly from the original prints.

Scale of the enlarged photographs was controlled using fixed points on the photos that remained unchanged over time. Using the scale of the photograph and a count of pixels over a measured distance, the area represented by each pixel was determined for each photograph. To calculate area of the palsas, each palsa was manually traced on the digital enhanced photograph, and the pixels within the enclosed trace counted using an automatic software function. Ten traces of each palsa were made for each stereopair, the highest and lowest area value discarded, and the average of the remaining eight values taken as the area of the palsa. Trace data are included in Appendix C.

Ground penetrating radar (GPR) data were collected as single-channel, constant-offset radar reflection profiles using a pulseEKKO IV GPR system with 50 MHz antennae and a 400 V transmitter, manufactured by Sensors & Software Inc., of Mississauga, Ontario. In a single-channel survey, data for each point or station along the survey transect are collected as a single trace using one transmitter and one receiver only. A constant antenna offset of 2 m and a constant 0.5 m station separation were used in this study. Principles of GPR are discussed in Appendix A.

To improve the signal-to-noise ratio, a stacked pulsed radar signal of 128 source excitations was transmitted for each trace (*cf.* Fisher, *et al.*, 1992a, 1992b; Kalantzis, 1994). For each trace, the signal sine wave was sampled at 1000 points at a sampling interval of 800 ps, for a total time window (*i.e.*, duration of time in which reflected energy is recorded, and thus, the length of each trace) of 800 ns. CMP surveys for determination of signal propagation velocity were conducted at each site and over both frozen and unfrozen terrain. Processing of GPR data employed a variety of techniques developed specifically for radar or modified from seismic processing; these are described in Chapter 3.

Coring was undertaken in the fens using a Macaulay peat corer (Jowsey, 1966) and on the palsas using a permafrost corer (Zoltai, 1978). Visible changes in moisture content, ice content and character, peat characteristics, and occurrence of sediment were recorded and are summarized in Appendix B. Bulk density and moisture content were not calculated from the core samples, as neither coring technique offers recovery of undisturbed samples from which these parameters could be reliably determined with a degree of accuracy *sufficient for correlation with radar data*.

Topographic measurements were taken along the transects using an Abney level to allow topographic corrections to be applied to the GPR profiles. Thaw depths at the time of the GPR surveys were measured along the GPR transects using a YSI Tele-thermometer probe

90 cm in length, with a 0.5°C resolution (Appendix D). Surface conditions along the GPR transects were noted, such as general vegetation cover, occurrence of bare peat, and presence of cracks, slump blocks, and other disturbances.

4.4 Results

4.4.1 Analysis and Interpretation of Aerial Photographs

The palsas at Porsild's Field had a greater percentage decline in areal extent (total decline in area of 36.4 %) over the 33 year period (Table 4-1) than did those at Dale Creek (total decline in area of 19.7 %) (Table 4-2) (a statistically significant difference), although the actual decline in areal extent of palsas at Dale Creek (*ca.* 1250 m²) was slightly greater than at Porsild's Field (*ca.* 1210 m²). At both sites, the palsas declined more in areal extent over the 24 year period from 1949 to 1972, than over the 10 year period from 1972 to 1981. Both sites had small apparent increases in areal extent of a few palsas from 1972 to 1981; however, at Dale Creek these increases were less than one percent of the total palsa area, while at Porsild's Field, the increases ranged from 30 % of palsa area to one percent.

At Porsild's Field, the decline in areal extent of palsas between 1949 and 1972 was approximately seven times the decline between 1972 and 1981; these values represent an average annual decline of 1.4 % from 1949 to 1972, and an average annual decline of 0.5 % from 1972 to 1981. (However, actual annual area data are not available for the intervening years; thus, the actual rate of decline in areal extent in any given year is unknown, based on the data presented in this thesis.) Individual palsas experienced a decline in areal extent over the study period ranging from 100 % (total collapse) to 6.1 %.

At Dale Creek, the decline in areal extent of palsas between 1949 and 1972 was approximately 4.6 times the decline between 1972 and 1981; these values represent an average annual decline of 0.7 % from 1949 to 1972, and an average annual decline of 0.4 % from 1972 to 1981. (However, actual annual area data are not available for the intervening years; thus, the actual rate of decline in areal extent in any given year is unknown, based on the data presented in this thesis.) Individual palsas experienced a decline in areal extent over the study period ranging from 32.2 % to 7.8 %. Palsas located several hundred metres distant from the five palsas studied at Dale Creek gradually declined in areal extent between 1949 and 1972, and were completely degraded by 1981.

The enlargement and computer-assisted enhancement of the aerial photographic stereo images allowed more accurate mapping of areal extent of palsas than was possible from the original photographs or from enlarged prints. The analysis showed that palsa # 10 at Porsild's Field was collapsed prior to 1949, and that palsa # 9 collapsed between 1949 and 1972. Also, palsa # 1a was not connected to palsa # 1 in or after 1949 (*cf.* Kershaw and Gill, 1979). However, palsa # 3, which was cored in 1978 by Kershaw and Gill (1979), was not discernible on the 1949 or 1972 aerial photographs, presumably due to its low topographic profile and dark colour of its surface.

Table 4-1. Porsild's Field: Summary of Temporal Variation in Areal Extent of Palsas									
Palsa No.	1949 area (m²)	Change in area 1949-1972		1972 area (m²)	Change in area 1972-1981		1981 area (m²)	Change in area 1949-1981	
		m²	%		m²	%		m²	%
1	953.1	-34.6	3.6	918.5	-23.3	2.5	895.2	-57.9	6.1
1a	160.0	-86.8	54.2	73.2	+21.9	29.9	95.1	-64.9	40.6
2	772.0	-176.5	22.9	595.5	-31.8	5.3	563.7	-208.3	27.0
3	?	n/a	n/a	?	n/a	n/a	?	n/a	n/a
4	236.0	-81.7	34.6	154.3	-7.2	4.7	147.1	-88.9	37.7
5	433.4	-145.7	33.6	287.7	+2.9	1.0	290.6	-142.8	32.9
6	228.1	-163.0	71.5	65.1	+6.5	10.0	71.6	-156.5	68.6
7	154.9	-79.6	51.4	75.3	-20.3	27.0	55.0	-99.9	64.5
8	180.8	-126.7	70.1	54.1	-54.1	100.0	0	-180.8	100.0
9	210.1	-210.1	100.0	0	n/a	n/a	0	-210.1	100.0
10	?	n/a	n/a	?	n/a	n/a	?	n/a	n/a
Total	3328.4	-1104.7	33.2	2223.7	-105.4	4.7	2118.3	-1210.1	36.4
Note that palsas #3 and #10, although recorded in the literature (<i>cf.</i> Kershaw and Gill, 1979), were not distinguishable on the aerial photographs examined for this study.									

Table 4-2. Dale Creek: Summary of Temporal Variation in Areal Extent of Palsas									
Palsa No.	1949 area (m²)	Change in area 1949-1972		1972 area (m²)	Change in area 1972-1981		1981 area (m²)	Change in area 1949-1981	
		m²	%		m²	%		m²	%
1	1393.5	-110.4	7.9	1283.1	+2.0	0.1	1285.1	-108.4	7.8
2	2196.7	-361.2	16.4	1835.5	+4.5	0.2	1840.0	-356.7	16.2
3	1458.9	-404.8	27.7	1054.1	-31.7	3.0	1022.4	-436.5	29.9
4	821.9	-91.2	11.1	730.7	-102.1	14.0	628.6	-193.3	23.5
5	482.6	-94.2	19.5	388.4	-61.7	15.9	326.7	-155.9	32.3
Total	6353.6	-1061.8	16.7	5291.8	-189.0	3.6	5102.8	-1250.8	19.7

There was no apparent change in the colour of the palsa surfaces: areas of palsas at Porsild's Field known from ground surveys in 1994 to be deflated peat corresponded with darker areas on the aerial photographs that were consistently discernible, and generally unchanged in size and shape, over the study period.

There was no apparent change in the character or size of the fen or of drainage patterns at either site over the study period. There also was no apparent change in the vegetation and surficial characteristics of the land adjacent to the palsa fens at either site, with the exception of the construction of a mine access road near the Porsild's Field site prior to 1972 (but which did not impinge on the fen).

Palsa heights were not determined from the aerial photographs; volume changes in the palsa core over time could therefore not be evaluated.

4.4.2 Surficial Characteristics

Porsild's Field

At Porsild's Field, the palsas ranged in height from 0.8 m to 2.5 m at their highest point above the fen. The largest palsas (palsas #1 and #2) were irregular both in shape and in topographic profile (Plate 4-1). Palsas #4 and #5 had approximately symmetrical topographic profiles and circular to ovoid shapes.

Bare peat occurred on deflated palsa tops and at edges, where slumping and/or sliding of blocks exposed fresh peat surfaces. Perimeters of higher palsas (#1 and #2) were characterized by cracking, slumping, and sliding of peat blocks. Cracks occurred on the palsa surfaces, ranging from 10 cm to 36 cm depth and 10 cm to 30 cm width. The cracks were approximately linear, frequently intersecting, and several metres in length, in many cases extending across the palsa from edge to edge. The surfaces of these shallow cracks were typically vegetated, with little exposure of peat.

Palsas # 1a, # 2, and # 4 were surrounded by a "moat" of water, whereas palsa # 1 had standing water on its north, east, and south perimeter. Palsa # 5 had standing water at its west margin. Surface water drained generally eastward through the fen, around the palsas. Overland flow entered the fen from the gentle slopes to the north of the fen.

Several known collapse scars occurred in the fen. These were characterized by circular or ovoid areas of either open water with little or no vegetation (as for palsas # 6 and # 9), or with irregular, slightly elevated surfaces and areas with vigorous growth of emergent vegetation (palsa # 3). Circular or elliptic collapse ramparts or rims around a central depression were not discernible.

Dale Creek

At Dale Creek, the five palsas which were studied ranged in height from 1.35 m to 3.0 m above the surface of the fen. The features were approximately circular in shape, but were asymmetrical in profile; their north and northwest edges typically sloped gently upwards from

the fen surface, whereas their south and east edges were characterized by steep slopes with extensive cracking and slumping of peat blocks (Plate 4-3). Palsas # 1 and # 2 were bordered by flat, relatively dry, slightly elevated meadow-like areas on their northwest sides; frost was not detected under these areas. Except for these areas, and the narrow gaps between adjacent palsas, standing water virtually encircled all of the palsas at Dale Creek. Surface water drained towards the fen from the slopes to the south, and drainage through the fen and valley was eastward.

Ground squirrel burrowing was extensive at the Dale Creek site, particularly on the south and east faces of palsas # 1 and # 2 (Plate 4-4), and there appeared to have been some excavation of the burrows by bears. There was little bare peat on the palsa tops, although there were patches of bare peat on palsa edges where the peat blocks had slumped or slid down the surface slope (Plate 4-5). Deep cracks (≥ 50 cm depth) occurred between slumping and sliding peat blocks at the palsa edges. Minor shallow cracking was evident on the palsa surfaces; ranging from less than 10 cm to 40 cm depth, the surfaces of these cracks were typically vegetated with little exposure of peat.

4.4.3 Subsurface Characteristics

Thaw Layer

At Porsild's Field, average thaw depth on the palsa surfaces ranged from approximately 35 cm to 47.5 cm. At Dale Creek, average thaw depth ranged from approximately 39.5 cm to 45.5 cm. Comparison of thaw depth measurements from within and adjacent to surface cracks in peat indicate that thaw depths immediately below cracks were consistently greater (between 6 cm to 23.5 cm) than those measured nearby the cracks. Thaw depth data are presented in Appendix D.

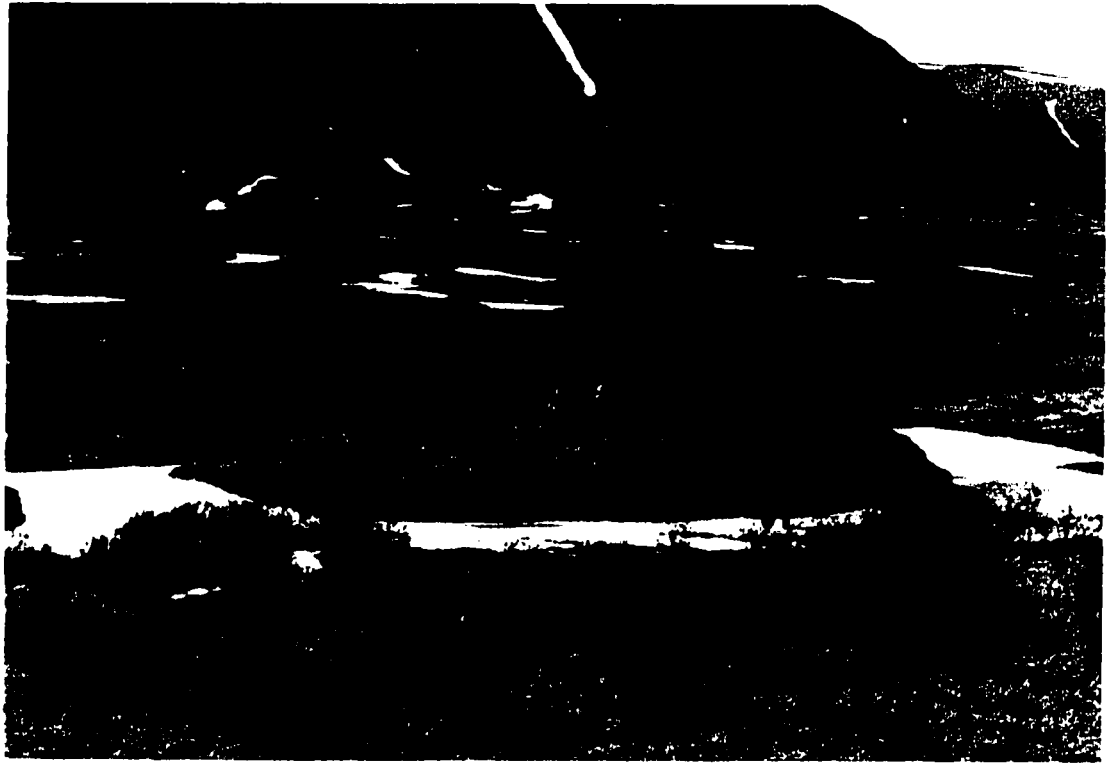
Coring

Two palsa cores and five fen cores were taken at Porsild's Field, while three palsa cores and one fen core were taken at Dale Creek. Locations of coring at Porsild's Field and Dale Creek are shown in Plates 4-1 and 4-2, respectively. Observations of peat characteristics to support radar interpretation are summarized in Appendix B.

Porsild's Field

A tephra layer 2 cm to 4 cm in thickness (the White River ash, dated 1250 BP by Lerbekmo, *et al.* (1975) (Kershaw and Gill, 1979) was encountered at approximately 30 cm depth in two fen cores taken 7 m from the edge of palsa # 1, and at 50 cm depth in a core taken near the edge of the fen. Peat above the tephra layer was fibrous. Below the tephra, peat was increasingly decomposed with depth, showing irregular variation in density and moisture content with depth. Peat thickness near palsa # 1 was in excess of 5 m; gyttja occurred below 450 cm depth. Near the edge of the fen, gyttja was encountered at *ca.* 280 cm depth, overlying mineral sediment at *ca.* 290 cm depth. The mineral sediment consisted of

Plate 4-3. Palsa at Dale Creek, showing asymmetrical profile.



Palsa # 2 at Dale Creek, looking northeast. Note asymmetrical profile, with steep, slumping edge on southeast side and gentle slope on northwest side.

Plate 4-4. Palsa at Dale Creek, showing ground squirrel burrowing.



Palsa # 2 at Dale Creek, looking west. Note exposure of peat by ground squirrel burrowing on steep palsa sides. Cracks demarcate slumping blocks of peat.

Photo credit: Stephen D. Robinson, McGill University.

Plate 4-5. Palsa at Dale Creek site, showing exposed peat.



Palsas # 2 (left) and # 3 at Dale Creek, looking northwest. Note exposure of peat by slumping, sliding of vegetation mat, and groundsquirrel burrowing on steep palsa sides.

Photo credit: Stephen D. Robinson, McGill University.

fine-grained diamict with granules and small pebbles. The tephra layer and gyttja were the only distinct strata that could be identified in all fen cores.

In the core from palsa # 1, a 10 cm thick tephra layer was encountered between 30 cm and 40 cm depth. No tephra was observed in the core from palsa # 4. Ice content varied with depth, ranging from minor disseminated pore ice, to crystals several millimetres in diameter, to variably oriented lenses 1 cm to 9 cm in thickness. Unfrozen peat was encountered below 490 cm depth under palsa # 1. No core was recovered below 300 cm at palsa # 4, except some grit from 320 cm depth. The corer could not penetrate below this depth. No distinct peat strata were correlative between palsa cores.

Dale Creek

Macaulay coring in the fen adjacent to palsa # 1 was attempted, but abandoned at 150 cm depth due to repeated collapse of the hole. Peat to this depth ranged from moderately to well-decomposed. No core was recoverable from other points in the fen where coring was attempted. Mineral sediment, with clasts up to 2 cm in diameter, was encountered by probing at 125 cm depth between palsas # 2 and # 3, and at 230 cm depth in the fen 4 m from the edge of palsa # 1.

Tephra was observed only in one core from palsa # 4, near the surface. (The patchiness of tephra observed at both sites may be attributable to erosion either prior to or following palsa formation, or poor differentiation in cores due to mixing or lack of colour variation.) Ice content in peat varied with depth, consisting of pore ice and crystals up to 7 mm diameter, and variably oriented lenses up to 8 mm thick. Ice content and ice lens frequency was greatest in the 20 cm of peat above the peat - mineral sediment interface. A 40 cm thick layer of gyttja was observed to overlie mineral sediment in the core from palsa # 1. However, no gyttja was observed in the two cores from palsa # 4. Fine-grained mineral sediment with small clasts up to a few millimetres in diameter was encountered at 80 cm to 95 cm depth. Pore ice occurred throughout the mineral sediment. No distinct peat strata were correlative between cores.

Ground Penetrating Radar Results

Three intersecting transects were surveyed at the Porsild's Field site, crossing four palsas (Plate 4-1). Two intersecting transects were surveyed at the Dale Creek site, crossing five palsas (Plate 4-2). The raw and processed GPR data have been analyzed and interpreted in Chapter 3; the reader is referred to that section for additional detail. The following discussion will focus on key features of the data pertinent to the evaluation of palsa evolution. In summary, the GPR effectively imaged sub-peat topography, fen stratigraphy, and to a lesser extent, frozen - unfrozen interfaces. The GPR typically did not effectively image internal peat stratigraphy in the palsas.

Topographic corrections have been applied to the data to facilitate image interpretation. Depth scales are not provided on the diagrams due to the nature of the radar data; a detailed discussion in this regard is provided in Section 3.6 and in Appendix A. For the ease of the

reader, reference to specific reflections in the radar profiles is given in nanoseconds, **read directly from the vertical time scale**. Approximate depth, estimated from the actual two-way signal travel time, is given in brackets, where relevant. Unless otherwise noted, depths are calculated using CMP-derived signal propagation velocities of 0.038 m ns^{-1} in unfrozen peat, and 0.095 m ns^{-1} and 0.097 m ns^{-1} in frozen peat at the Porsild's Field and Dale Creek sites, respectively.

4.5 Interpretation

The coring and radar data were examined to identify subsurface features and characteristics that may elucidate genetic processes that have been or are active in the fens and palsas. Key features and their (inferred) genetic relevance are described in this section, with reference to the data, to support the subsequent discussion of palsa development and degradation at the two sites (Section 4.6).

Basin Characteristics

At Porsild's Field, the GPR imaged a moderate amplitude reflection approximately 1.2 m below the inferred peat - mineral sediment interface in the fen, which may represent the overburden - bedrock interface (Figure 4-3). The radar-imaged peat - mineral sediment interface in the fen varies in depth (*ca.* 3.9 m to 5.2 m) across the GPR transects at Porsild's Field, but appears to be approximately flat-lying.

There were no distinct sub-peat reflections at Dale Creek that could be inferred to represent the overburden - bedrock interface. The peat - mineral sediment interface in palsas is domed. The GPR did image a hyperbolic diffraction pattern generated by a point reflector at the peat - mineral sediment interface; this may have been caused by a boulder in, or at the surface of, the underlying diamict (Figure 3-20).

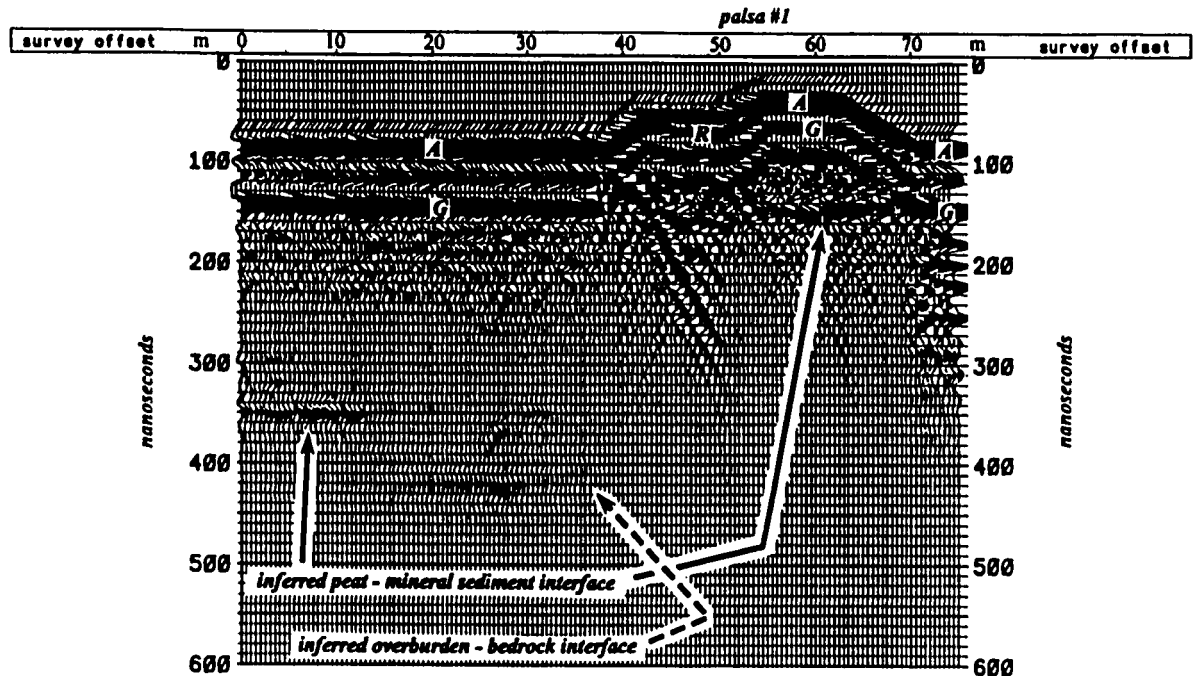
Coring and radar profiles at both sites suggest the peatlands are underlain by fine-grained diamict with small clasts, overlying bedrock. The diamict may be of glacial, colluvial, and/or solifluction origin, based on the prevalence of landforms of such origin in the vicinity of the peatlands.

The presence of a basal gyttja or aquatic peat layer, as observed in fen cores at the Porsild's Field site, is suggestive of initial deposition in a body of open standing water (National Wetlands Working Group, 1988). Insufficient basal samples from the Dale Creek fen, and inconsistent observation of basal gyttja in the palsa cores preclude confirmation of a similar early depositional environment in that basin.

Fen Stratigraphy

The radar profiles show detailed stratigraphy in the unfrozen peat at the Porsild's Field site. Wavy, subparallel, laterally continuous reflections can be traced across the profile. However, reliable correlation of a given radar event with a change in any given peat property, such as moisture content, density, peat type, and degree of decomposition, is problematic. This is due primarily to the inaccuracy of the available peat sampling techniques for the purposes of

Figure 4-3. Radar profile of palsa # 1 (GPR Transect # 1) at Porsild's Field.



Note strong amplitude reflection between 0 and 13 m at 350 ns (*ca.* 5.2 m depth), inferred to represent the peat - mineral sediment interface. Also note weaker, but still relatively strong reflection between 16 and 38 m at 415 ns (*ca.* 6.4 m depth); this may represent the overburden - bedrock interface.

Also note dipping reflection below the left (southeast) edge of the palsa; this is inferred to represent the frozen - unfrozen interface which was intersected by coring.

First radar event is direct air wave, *A*, typically followed by direct ground wave, *G*. See Figure 3-19 for discussion of signal refraction, *R*.

Data from Transect #1 at Porsild's Field. Vertical exaggeration *ca.* 2x. Transect crosses unfrozen fen from 0 m to 38 m, frozen palsa #1 from 38 m to 70.5 m, and unfrozen fen from 70.5 m to 75 m.

Plots produced from ProMAX v.5.1, after data conversion to SEG-Y seismic format using the pulseEKKO IV operating software. Other processing steps include signal saturation correction and topographic correction.

stratigraphic correlation with radar data, as well as the extreme spatial variability of these peat characteristics (see discussion in Section 3.7.2).

Palsa Stratigraphy and Structure

The 50 MHz GPR failed to effectively image the internal peat stratigraphy of palsas # 1, # 2, and # 4 at Porsild's Field. Despite this lack of structural imaging, the chaotic, laterally discontinuous nature of radar returns from the palsas is consistent with signal scatter and reflection in ice-rich sediment (Kettles and Robinson, 1996). However, internal reflections below palsa # 5 suggest that the peat, and possibly also mineral strata within the palsa core (based on the depth of signal penetration > 10 m, where peat thickness in the fen is inferred to be *ca.* 4.1 m to 5.2 m), are in fact domed (Figure 4-4). This structure may be related to palsa formation by ice segregation as described by Seppälä (1988).

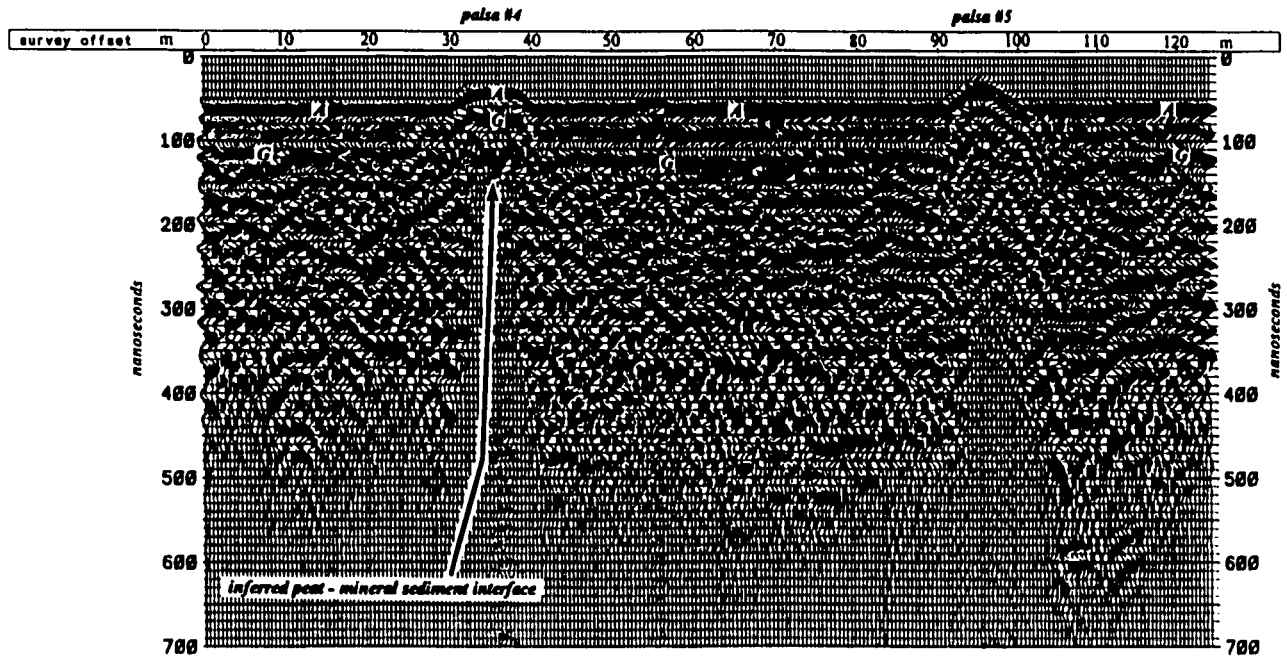
In contrast, the palsas at Dale Creek comprise a relatively thin peat layer (95 to 205 cm in cores) over mineral sediment, based on coring (Appendix B and Skaret (1995)) and GPR data. The peat layer on palsas at Dale Creek was too thin for internal stratigraphy to be effectively imaged by the 50 MHz antennae used in this study: the high amplitude of the direct air and ground waves saturate the receiver, masking other returns from shallow interfaces. Individual reflections from within the mineral sediment were poorly resolved, even after processing; radar returns were chaotic and laterally discontinuous. Coring revealed a concentration of pore ice and ice lenses in the peat immediately above the peat - mineral interface. This structure, and external, domed palsa morphology, are consistent with an ice segregation model of palsa development.

Permafrost Development in Mineral Sediment

Interpretation of GPR and coring data suggest that the thickness of unfrozen peat adjacent to palsas # 1 and # 2 at Porsild's Field is approximately 4.9 m to 5.2 m (see Section 3.7.1). (The GPR data are interpreted to show a relatively flat-lying peat - mineral sediment interface across the fen, decreasing in depth to approximately 4 m adjacent to palsas # 4 and # 5.) The inferred peat - mineral sediment interface lies a maximum of 5.8 m below the surface of palsa # 1 (which, along the radar transects, reaches a maximum height of 2.5 m above the fen) and 5.0 m below the surface of palsa # 2 (which, along the radar transect, reaches a maximum height of 1.95 m above the fen). Thus, below the highest portion of palsa # 1, the inferred peat - mineral sediment interface lies *ca.* 3.0 m to 3.3 m below the level of the fen surface, compared to adjacent to the palsa, where the peat - mineral sediment interface lies *ca.* 5.0 m below the fen surface.

This suggests that the topographic expression of the palsa above the fen surface is largely attributable to frost heave in the underlying mineral sediment (if it is reasonable to assume that the thickness of peat prior to palsa formation was similar between the location of the extant palsas and the adjacent fen, and that the peat - mineral sediment interface was initially approximately flat-lying). Although the GPR data suggest that the mineral sediment beneath palsas # 1 and # 2 is domed due to frost development, this structure is not visibly apparent on the radar profiles. Frost development in mineral sediment would account for the elevation

Figure 4-4. Radar profile of palsas # 4 and # 5 (GPR Transect # 3) at Porsild's Field.



Despite good signal penetration, no distinct reflection inferred to represent the peat - mineral sediment interface below palsa # 5 (92.5 m to 102 m) is visible on the profile. The internal stratigraphy of the palsa appears to be domed, as would be expected with ice segregation.

First radar event is direct air wave, *A*, typically followed by direct ground wave, *G*.

Data from Transect #3 at Porsild's Field. Vertical exaggeration *ca.* 2x. Transect crosses unfrozen fen from 0 m to 30 m, frozen palsa #4 from 30 m to 40 m, unfrozen fen from 40 m to 92.5 m, frozen palsa #5 from 92.5 m to 102 m, and unfrozen fen from 102 m to 125 m.

Plot produced from ProMAX v.5.1, after data conversion to SEG-Y seismic format using the pulseEKKO IV operating software. Other processing steps include signal saturation correction, topographic correction, and automatic (time-variable) gain control.

of the peat - mineral sediment below the palsas and is consistent with ice segregation during palsa development.

At Dale Creek, results from coring and GPR indicate doming of the mineral sediment below the peat cover (Figure 4-5), such that the majority of palsa height must be attributable to permafrost development (with associated heave and ice segregation) within the mineral sediment core. Only 95 cm of the 290 cm height of palsa # 1 at this site consisted of icy peat, while peat thickness near the edge of palsa # 4 was only 120 cm (this palsa reached a height of 220 cm above the level of the fen). (Skaret (1995) measured peat depths between 135 cm and 205 cm on palsa # 2, which in 1994 reached 280 cm height above the level of the fen.)

Chaotic radar returns typical of frozen, ice-rich ground are visible below the inferred peat - mineral sediment interface in palsas at Dale Creek, suggesting the underlying mineral sediment is frozen at least to the depth of signal penetration (>16 m) (Figure 4-6).

Permafrost Configuration in Peat

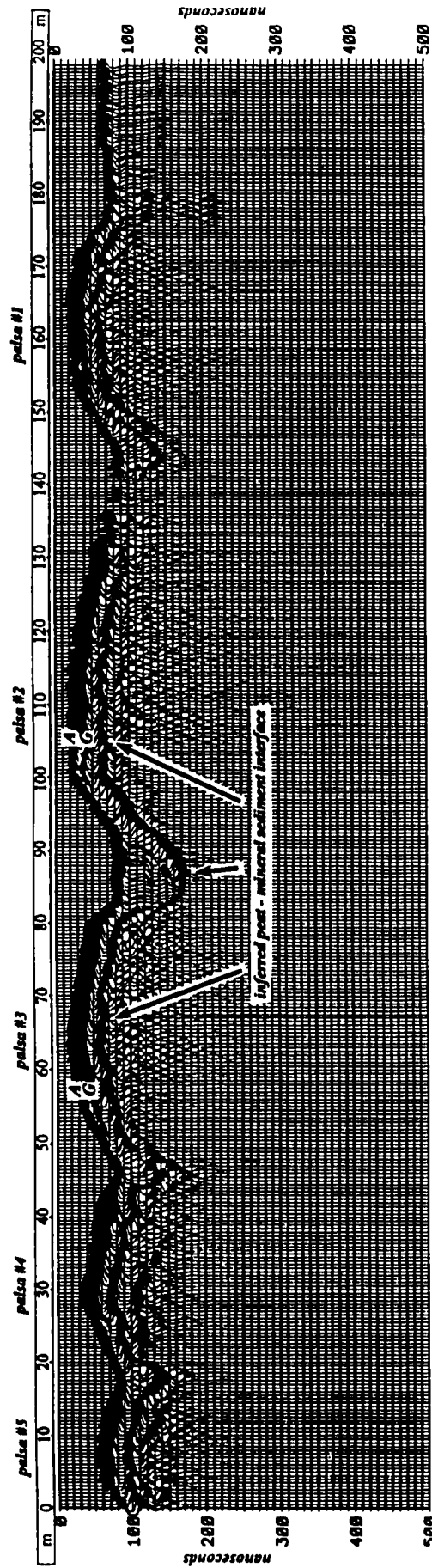
GPR and coring revealed unfrozen peat at depth below the margin of palsa # 1 at Porsild's Field. Coring near the edge of the palsa encountered unfrozen material below 490 cm of frozen peat; this frozen - unfrozen interface appears to correlate with a strong dipping reflection on both radar transects intersecting this palsa (Figures 4-3 and 4-7). (This dipping radar event is not considered to be part of a hyperbolic reflection as it does not possess the smooth curve typical of a hyperbolic reflection; also, a series of subapical/subjacent reflections dipping in the opposite direction occur immediately below this event.) The non-vertical frozen - unfrozen interface shown by coring and radar imagery may be indicative of narrowing of the permafrost core at depth due to thaw degradation, where the permafrost core has become 'detached' from the underlying mineral sediment (*cf.* Zoltai and Tarnocai, 1971:119). The absence of a similar dipping reflection on the opposite side of the palsa may be related to less advanced thaw degradation. Kershaw and Gill (1979) note that palsa # 1a was connected to palsa # 1 in 1944: the northwest edge of palsa # 1 would therefore have been more recently exposed to heat transfer from the fen, and the frozen - unfrozen interface at depth may be more nearly vertical. (Examination of aerial photography indicated that palsa # 1a was not connected to palsa # 1 in 1949 or later years.)

The narrowing of the permafrost core at depth is also manifested in the surficial morphology of the palsa; the portion of palsa # 1 which is inferred to be underlain by unfrozen peat at depth is up to 90 cm lower than the surface of that portion whose permafrost core is inferred to extend into mineral sediment (Figure 4-3). This is consistent with observations made by Zoltai and Tarnocai (1971: 119) of topography variations on a palsa with a permafrost core which extends into mineral sediment only under part of the palsa.

Collapse Scars

GPR Transect # 3 at Porsild's Field crossed the edge of a known collapse scar of a pre-existing palsa (palsa # 9) west of palsa # 4 (Plate 4-1) (*cf.* Kershaw and Gill, 1979). The radar profile shows an apparent decrease in lateral continuity of reflections between 40 m and 65 m, compared to the stratigraphy between 65 m and 90 m (Figure 4-8a). A coherency filter

Figure 4-5. Radar imaging of peat - mineral sediment interface at Dale Creek.

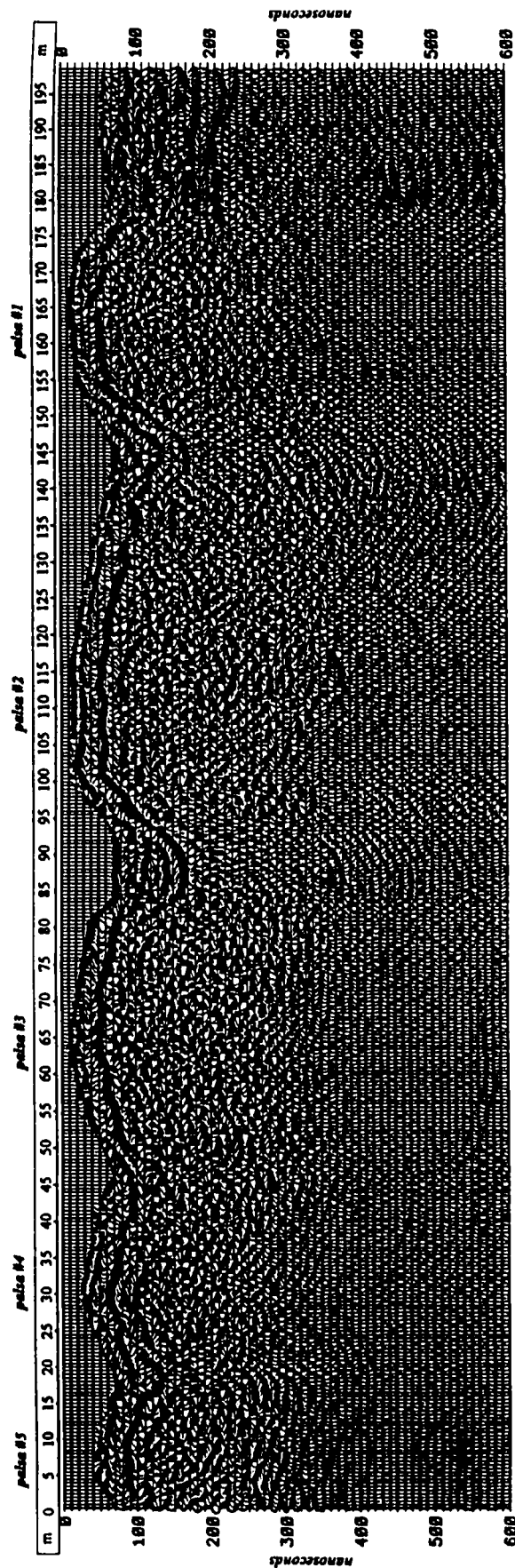


The strong laterally continuous reflection approximately parallel to the ground surface, occurring 15 ns to 35 ns after the direct air and ground wave arrivals (A, G) in the palsas is inferred to represent the peat - mineral sediment interface. This reflection can be traced across the frozen - unfrozen interface, e.g., between 85 m and 100 m along the transect. The reflection *appears* to be shallower on the palsas due to higher signal velocity in frozen peat. However, peat thickness in the fen (125 cm at 83 m) is comparable to that on the palsas (95 cm to 205 cm). Where the palsas are more closely spaced (*i.e.*, palsas # 3 and # 4) or where the frozen - unfrozen transition is more abrupt (*i.e.*, 80 to 85 m, as denoted by steeper palsa side), the peat - mineral sediment interface reflection is subcontinuous to discontinuous. The doming of the interface suggests that the majority of palsa height is attributable to permafrost development within the mineral sediment core.

Data from Transect #1 at Dale Creek. Vertical exaggeration is ca. 2x. Transect crosses five palsas from east to west, separated by unfrozen fen, and unfrozen meadow west of palsa #1 (180 m to 198.5 m). Signal attenuation between 132 m and 142 m was caused by energy loss to the air during a heavy rain at the time of the survey.

Plot produced from ProMAX v.5.1, after data conversion to SEG-Y seismic format using the pulseEKKO IV operating software. Other processing steps include topographic correction and a low constant gain factor.

Figure 4-6. Radar imaging of palsa cores at Dale Creek.

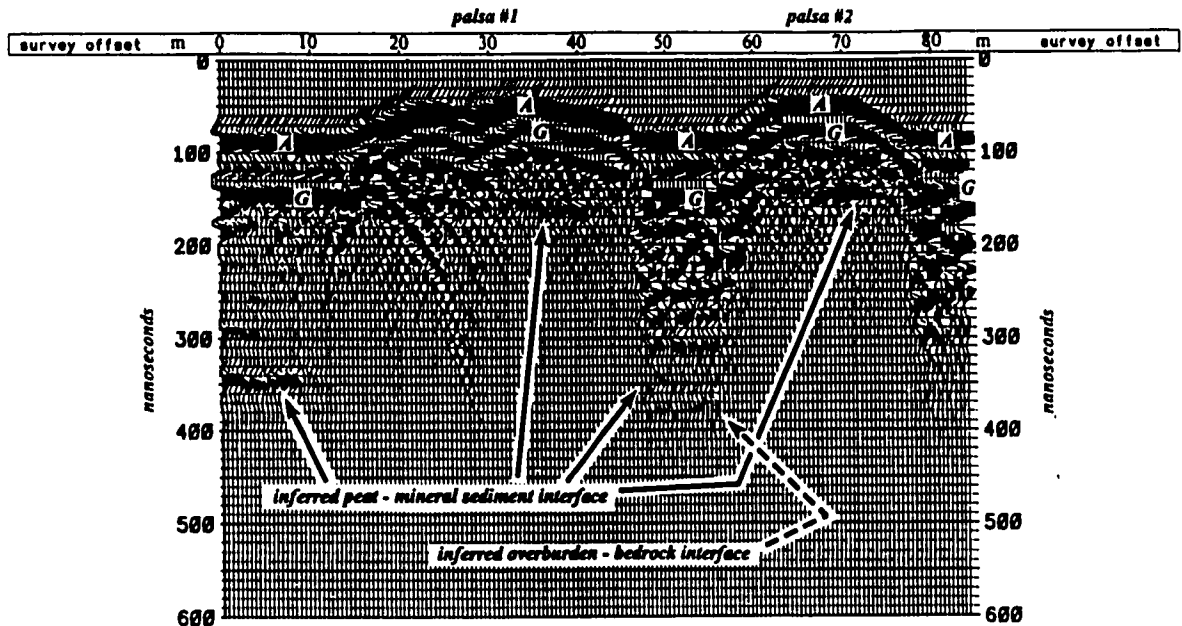


Individual reflections remain poorly resolved within the palsa cores, even after processing. The radar returns from the palsa cores below the inferred peat - mineral sediment interface are chaotic and laterally discontinuous, typical of frozen, ice-rich ground. In contrast, note the laterally continuous, subparallel reflections in the unfrozen meadow area west of palsa # 1 (180 m to 198.5 m).

Data from Transect #1 at Dale Creek. Vertical exaggeration is ca. 2x. Transect crosses five palsas from east to west, separated by unfrozen fen, and unfrozen meadow west of palsa #1 (180 m to 198.5 m).

Plot produced from ProMAX v.5.1, after data conversion to SEG-Y seismic format using the pulseEKKO IV operating software. Other processing steps include automatic (time variable) gain control, bandpass filter, normal moveout correction, F-K migration, topographic correction, and zero-phase spiking deconvolution. **N.B.** Some portion of the direct air and ground waves are muted as a byproduct of normal moveout correction, particularly in the fens.

Figure 4-7. Radar profile of palsas # 1 and # 2 (GPR Transect # 2) at Porsild's Field.



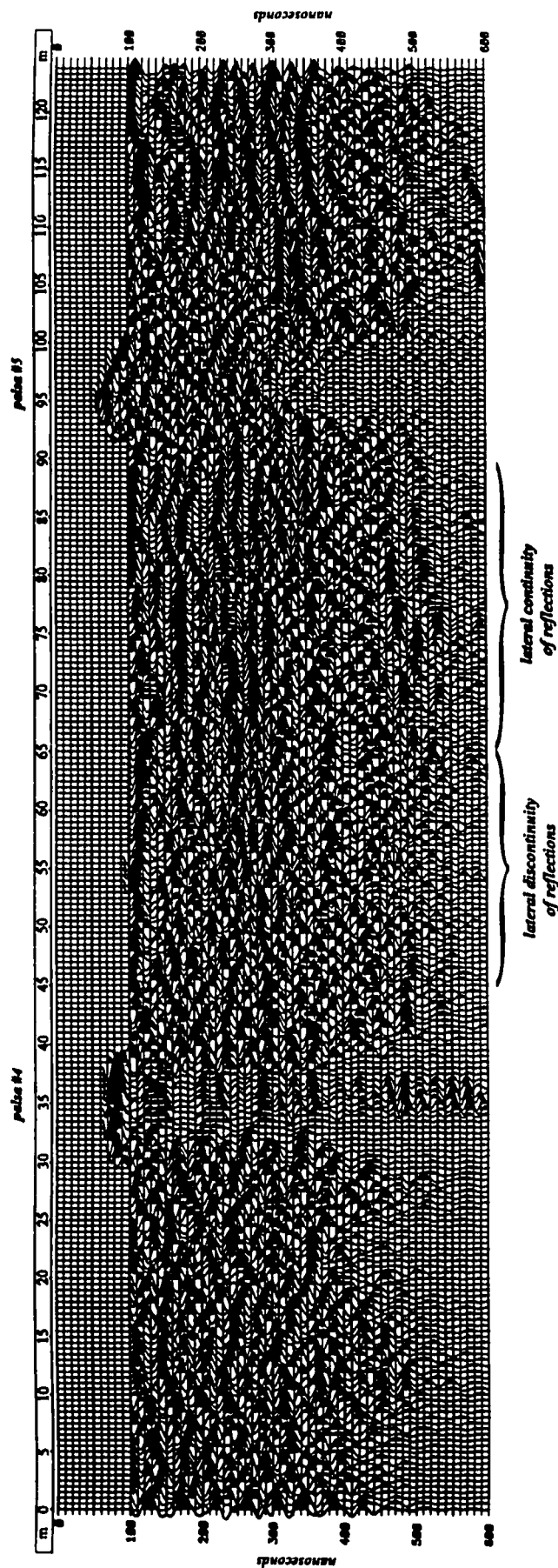
Note dipping reflection below the left (east) edge of palsa # 1; this is inferred to represent the frozen - unfrozen interface which was intersected by coring. A similar dipping reflection is lacking below the west edge of palsa # 1 and below palsa # 2.

First radar event is direct air wave, *A*, typically followed by direct ground wave, *G*.

Data from Transect #2 at Porsild's Field. Vertical exaggeration *ca.* 2x. Transect crosses unfrozen fen from 0 m to 14 m, frozen palsa #1 from 14 m to 46.5 m, unfrozen fen from 46.5 m to 59 m, frozen palsa #2 from 59 m to 78.5 m, and unfrozen fen from 78.5 m to 84.5 m.

Plot produced from ProMAX v.5.1, after data conversion to SEG-Y seismic format using the pulseEKKO IV operating software. Other processing steps include signal saturation correction and topographic correction.

Figure 4-8a. Radar profile showing inferred stratigraphic signature of known collapse scar, Porsild's Field.

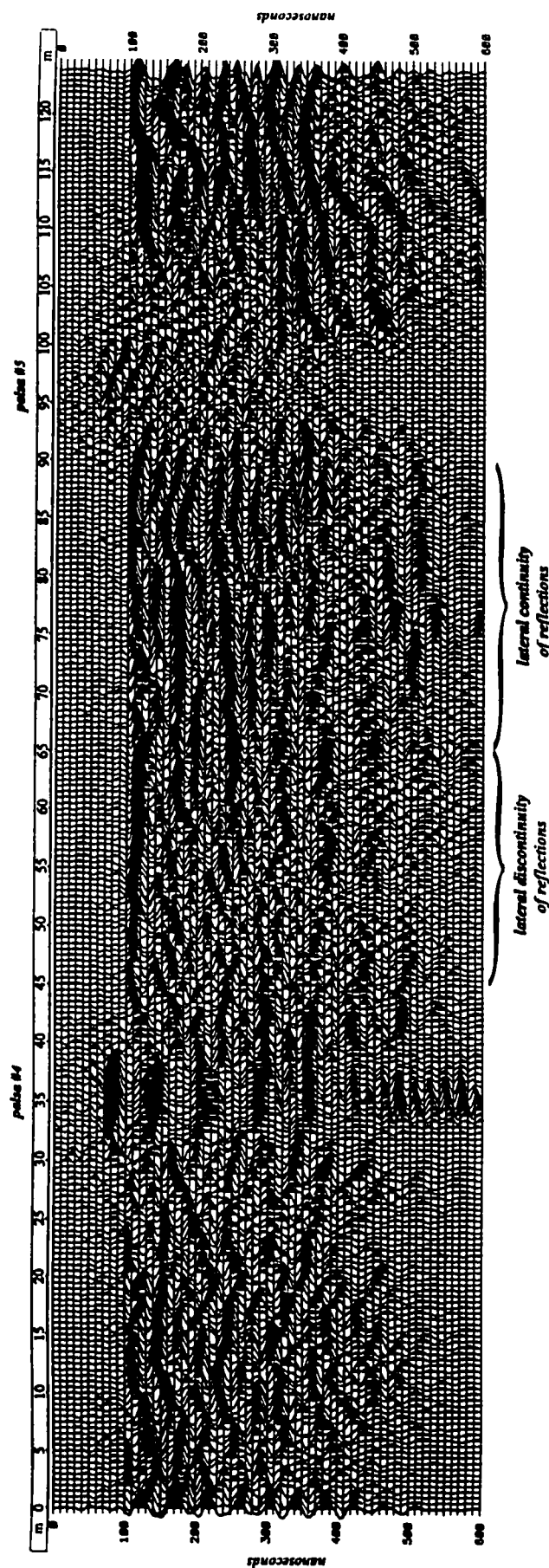


Radar profile prior to application of F-X deconvolution as a coherency filter. Note apparent decrease in lateral continuity of reflections between 45 m and 65 m on the transect, between 130 ns to 300 ns, compared to stratigraphy between 65 m and 90 m; this pattern may be associated with a pre-existing palsa adjacent to this location. The radar transect intersects the edge of the collapse scar at 54.5 m to 58 m, where slightly elevated peat may represent the rim of the collapsed palsa (palsa #9; Kershaw and Gill, 1979).

Data from Transect #3 at Porsild's Field. Vertical exaggeration *ca.* 1.2x. Transect crosses unfrozen fen from 0 m to 30 m, frozen palsa #4 from 30 m to 40 m, unfrozen fen from 40 m to 92.5 m, frozen palsa #5 from 92.5 m to 102 m, and unfrozen fen from 102 m to 125 m.

Plots produced from ProMAX v.5.1, after data conversion to SEG-Y seismic format using the pulseEKKO IV operating software. Other processing steps include signal saturation correction, automatic (time variable) gain control, bandpass filter, normal moveout correction, and topographic correction. **N.B.** Some portion of the direct air and ground waves are muted as a byproduct of normal moveout correction, particularly in the fens.

Figure 4-8b. Application of coherency filter to radar profile showing inferred stratigraphic signature of known collapse scar.



Profile after application of F-X deconvolution as a coherency filter. Note the persistence of the apparent decrease in lateral continuity of reflections between 45 m and 65 m, compared to stratigraphy between 65 m and 90 m, through this processing step. This pattern may represent the stratigraphic signature of the collapsed palsa.

Data from Transect #3 at Porsild's Field. Vertical exaggeration ca. 1.2x. Transect crosses unfrozen fen from 0 m to 30 m, frozen palsa #4 from 30 m to 40 m, unfrozen fen from 40 m to 92.5 m, frozen palsa #5 from 92.5 m to 102 m, and unfrozen fen from 102 m to 125 m.

Plots produced from ProMAX v.5.1, after data conversion to SEG-Y seismic format using the pulseEKKO IV operating software. Other processing steps include signal saturation correction, automatic (time variable) gain control, bandpass filter, normal moveout correction, and topographic correction. **N.B.** Some portion of the direct air and ground waves are muted as a byproduct of normal moveout correction, particularly in the fens.

was applied to the data to test for and enhance continuity in reflections across this area of the profile; the observed discontinuity persisted through this processing step (Figure 4-8b).

The persistence through processing of the GPR-imaged discontinuity in peat strata suggests that this radar pattern may be related to the collapse of palsa # 9, which occurred at some time between 1949 and 1972. However, a similar discontinuity in strata was not observed adjacent to the collapse scar of palsa # 6 (immediately west of palsa # 5, between approximately 110 m to 120 m on GPR Transect # 3), which collapsed some time after 1981. (The radar transect also passed the collapse scar of palsa # 3, east of palsa # 4; however, this was at a greater separation distance. No stratigraphic discontinuity is apparent from radar imaging at this location.)

The inconsistency in collapse scar radar patterns may be a function of proximity to the collapse scar, where the stratigraphic disruption associated with palsa development and collapse occurs only over a limited distance from the palsa edge. The different appearance of the collapse scars (*i.e.*, open, standing water with floating vegetation mat *versus* predominantly infilled with peat and/or growing vegetation, and contrasting radar patterns) could also be related to the volume of peat remaining in the core of the palsa prior to collapse. Erosion of peat from the palsa surface would decrease the amount of peat in the core, which may, upon collapse, result in a collapse scar comprising peat at depth with greater volume of standing water at the surface (*e.g.*, palsa # 6).

No other stratigraphic discontinuities were observed extending from the margins of extant palsas to suggest that the current domed mound morphology of the palsas is a product of erosion or collapse from a pre-existing plateau feature. (Areal decline has occurred at palsa margins, and is apparent in aerial photography and in some cases in radar profiles.)

4.6 Discussion

Palsa Development

The presence of pore ice and ice lenses in peat-cored palsas and in peat above mineral sediment and at the peat - mineral sediment interface in mineral-cored palsas is consistent with ice segregation processes described in the literature. The contribution to palsa doming of mineral sediment observed in both the peat- and mineral-cored palsas is consistent with palsa development by ice segregation as described by Seppälä (1982, 1988).

Porsild's Field

GPR largely failed to provide clear and detailed stratigraphic imaging of peat-cored palsas. Palsa genesis could be inferred from radar imaging of the structure of the palsa core in only one case (palsa # 5) at Porsild's Field, where stratigraphic doming in peat and possibly mineral sediment was visible on the radar profile. However, in all palsas the chaotic nature of radar returns from sediment rich in pore ice and ice lenses may be diagnostic of segregated ice.

Radar imaging did not reveal stratigraphic discontinuities extending from the margins of extant palsas that could suggest that the palsa mounds were produced by erosion from a previously more extensive plateau (although the areal decline of the extant palsas indicate they have degraded from previously more extensive mounds). Nor does the contemporary surface pattern of the fen indicate a pre-existing plateau adjacent to the existing palsas, which pattern may be comparable to the collapse scars of known, pre-existing mounds.

The smaller palsas and visible collapse scars are circular to ovoid in shape. The larger, irregularly shaped palsas (# 1 and # 2) comprise several contiguous segments, each of which is semi-circular to ovoid in shape, and of differing height, suggesting the overall palsa form may be a result of coalescence of several smaller, aggradational mounds.

Dale Creek

At Dale Creek, there is also no evidence to suggest that the mineral-cored palsas (palsas #1 to #5) were eroded from a previously existing plateau, of the type described by Allard, *et al.* (1987), rather than having formed as individual mounds, as described by Worsley, *et al.* (1995). The thin peat forms a continuous cover over the mineral sediment, and there is no evidence of truncation by erosion (as may be expected in a feature eroded from a plateau with flat-lying internal stratigraphy).

The asymmetric profile of the palsas (Plate 4-3) does not appear to be consistent with a plateau origin. This profile may reflect contemporaneous aggradational and degradational processes acting on the palsa. The steep sides and slumping blocks may be a function of maturity and age of that portion of the palsa. Alternatively, snow deposition and accumulation on the high, steep-sided, leeward side of the palsa may reduce winter heat loss, causing thaw degradation and slumping of peat. Over time, these processes could result in migration of the palsa in the windward direction, if wind maintains a thin snow cover on the windward edge of the palsa (encouraging permafrost aggradation), and deposits snow on the leeward, degrading side of the palsa.

The active layer of palsas at Dale Creek does not extend into the mineral sediment; this may contribute to permafrost preservation, as peat blocks do not migrate down-slope over a thin, thawed mineral layer as described by Worsley, *et al.* (1995) in degrading mineral palsas.

Palsa Degradation

Both the historic and contemporary surface and subsurface characteristics of the palsas at Porsild's Field confirm palsa degradation at this site at least since 1949. Aerial photograph interpretation indicates reduction in palsa area and palsa collapse, visible surface features indicate recent and ongoing palsa collapse, and subsurface data indicate unfrozen conditions at depth.

At Dale Creek, aerial photograph interpretation confirms reduction in overall palsa area since 1949, but conclusive subsurface or surficial evidence for degradation at this site is lacking (slumping of palsa edges is ongoing, but is not alone a conclusive indication of overall palsa

degradation; permafrost may be stable or aggrading in other areas of the feature). However, palsas nearby (*ca.* 275 m northwest) to those at Dale Creek have collapsed since 1949.

As noted in Section 4.4.1 above, decline in areal extent of palsas at both sites was greater between 1949 and 1972 than between 1972 and 1981. Maximum, mean, and minimum annual air temperatures at Norman Wells were lower over the period from 1949 to 1975 than in subsequent years (Liang and Kershaw, 1995). However, Liang and Kershaw (1995) noted that snowfall and temperature at Ross River and Norman Wells appeared to be inversely related. Palsa degradation between 1949 and 1972 may, therefore, be attributable to decreased winter heat loss due to greater snowfall. (Thaw season rainfall may also have contributed to increased thaw penetration on palsas; however, rainfall data spanning the period from 1949 to 1972 are available only from Norman Wells, which did not have an increase in rainfall over this period.) However, the observed degradation of permafrost at both sites may be in response to climatic changes that may have occurred prior to the period of study, and indeed prior to the period of climate record for the region (early 1940s at Norman Wells). It is likely that the palsas, having formed during an earlier cold period, are now in disequilibrium with climatic trends of this century (*i.e.*, warming up to and after the 1920s recorded in the North American quadrant of the Arctic (Lachenbruch, *et al.*, 1988)) and recent decades (Liang and Kershaw, 1995).

Regional climate warming trends do not explain the greater percentage decline in areal extent of palsas at Porsild's Field compared to those at Dale Creek, over the study period. Also, the collapsed palsas at Porsild's Field were of low elevation and characterized by gently sloping margins, and were thus atypical of the 'mature' or 'old' stage in Seppälä's (1988) model of cyclic palsa development. Other factors are therefore considered to be acting on the palsas to contribute to the apparent differential rate of degradation between the two sites.

Permafrost degradation at depth, as suggested by subsurface conditions at palsas # 1 and # 4 at Porsild's Field, may be related to subsurface heat transfer from saturated fen peat to the palsa core, where warming mean annual, minimum, and maximum air temperatures observed by Liang and Kershaw (1995) contribute to local fen temperature increases. (The low thermal conductivity of dry peat and low thermal diffusivity of the frozen core in palsas would dampen effects of a surface warming signal. Penetration of a climate warming into the fen would be modulated by evaporative and conductive cooling and latent heat capacity of water, but would nevertheless be greater than through the palsa surface.) This process may represent a more effective transfer of heat to the palsa core than through the palsa surface, where dry surface peat continues to insulate the palsa core from summer heat gain.

This process may be less important in mineral-cored palsas, where the column of saturated peat in the adjacent fen is shallow, and groundwater circulation more restricted. The mineral-cored palsas at Dale Creek had a lower percentage decrease in areal extent over the study period than those at Porsild's Field, which are predominantly cored by icy peat up to 5.0 m thick, and are surrounded by saturated peat of similar depth.

The contribution of fen heat transfer to permafrost degradation in peat-cored palsas has received little attention in the literature (*cf.* Hayley, 1988; Kettles and Robinson, 1996). Harris and Schmidt (1994) suggest that growth and decay of peat plateaus with permafrost core extending into mineral soil is independent of climatic change, and that degradation of these features results from “drowning” of the plateau by peat accumulation in the adjacent fen. However, this hypothesis disregards the influence of heat transfer from saturated fen peat to the palsa core.

Latent heat effects may slow considerably the rate of permafrost degradation at depth, particularly in ice-rich materials (Smith, 1993). The configuration of the frozen - unfrozen interface may therefore display relative temporal stability. The consistency in overall palsa morphology (despite the recorded decline in areal extent), and in observed thawed conditions at depth, suggest some degree of thermal stability at depth. Latent heat effects may also contribute to variations in rate of thaw between peat and mineral cored palsas, as the higher ice content typical of fine-grained mineral sediment in palsas (Seppälä, 1988; Zoltai and Tarnocai, 1971) would require greater energy to thaw.

Unfrozen conditions at depth could indicate either aggradation of permafrost in a growth phase of a palsa (*cf.* Zoltai and Tarnocai, 1971:119) or degradation, and therefore cannot be taken in isolation as conclusive evidence of palsa evolution. However, given the observed consistent decline in palsa area at both sites over the period of study, unfrozen conditions observed below palsa cores at Porsild’s Field are inferred to reflect degradational rather than aggradational processes, with detachment of the permafrost core from basal mineral sediment. Geothermal heat may be contributing to basal thaw, in response to climatic warming at the surface and/or decreased heat loss within the palsa core due to increased snow depth.

The extent to which volume loss contributed to palsa degradation is unknown, as there are insufficient historical palsa height data.

Although aerial photographic analysis revealed ongoing decline in the areal extent of palsas at both sites, the palsas displayed little change in overall shape and configuration. The available data do not exclude the possibility that some palsas may have experienced some permafrost aggradation that was offset by concurrent degradation in other parts of the palsa.

4.7 Conclusions

Based on the data presented above, the following conclusions can be made regarding the evolution of the palsas at the two sites, and the contribution of GPR to such investigations.

Conventional and GPR-derived data from both sites confirm palsa genesis by ice segregation. In this regard, the GPR substantiated evidence gathered using conventional techniques, but did not produce new kinds of information or go beyond facilitating compilation of data regarding peat thickness, stratigraphy, and permafrost distribution. Additional coring and more numerous transects providing three-dimensional subsurface information would enhance the value of GPR in this environment.

The palsas at both sites decreased in areal extent over the study period, consistent with Kershaw and Gill's (1979) observations of permafrost degradation. However, the rate of decline in areal extent is constant neither between the sites nor over time, suggesting that one or more other factors are moderating the effects of regional climate change and/or cyclic palsa evolution.

Such factors may include, but are not necessarily limited to, microclimatic influences (*i.e.*, wind, cold air drainage, snow deposition), for which few historical data are available, and variation in heat transfer processes and efficiency between peat-cored and mineral-cored palsas, which has received little attention in the literature, but which warrants further investigation. Surface cracking, deflation, and slumping of peat blocks from palsa sides were observed at both sites, and did not vary considerably between them, and are therefore not considered to be significant contributors to observed differences in rates of decline in areal extent.

Apparent relative stability in palsa form and subsurface thermal characteristics over time may mask aggradational or degradational processes. Latent heat effects at depth may contribute to this apparent stability. The GPR showed promise in imaging the frozen - unfrozen interface at depth below the palsa margin, which if validated, could facilitate long-term monitoring of subsurface permafrost conditions.

The degree to which spatial dynamism in a palsa, characterized by complementary or interdependent aggradational and degradational processes operating on different parts of a single feature, is operative and contributes to apparent morphological stability warrants further consideration. Such investigation would likely depend largely on characterization of changes in subsurface thermal conditions and in plant communities on aggradational margins.

The data compiled in this study suggest that GPR may allow identification of stratigraphic signatures of pre-existing permafrost landforms which may not be detectable by coring. This may facilitate reconstruction of peatland history, particularly where collapsed permafrost features are not associated with persistent, identifiable surface features.

Taken independently, various of the morphological and thermal characteristics observed in the palsas could be indicative of either aggradation of permafrost in a growth phase of a palsa or degradation. However, given the observed consistent decline in palsa area at both sites over the period of study, the morphological and thermal characteristics are collectively inferred to reflect degradational, rather than aggradational, processes.

Although similarities in genesis and overall degradational trends are documented for the two sites, an explanation for contrasts in palsa form and rate of degradation remains elusive due to the lack of understanding of the synergy of geomorphic processes acting on the sites.

4.8 Literature Cited

- Allard, M., Seguin, M.K., and Lévesque, R. 1987. Palsas and mineral permafrost mounds in northern Québec. In V. Gardiner, editor, *International Geomorphology 1986 Part II*, 285-309.
- Fisher, E., McMechan, G.A., and Annan, A.P. 1992a. Acquisition and processing of wide-aperture ground-penetrating radar data. *Geophysics* 57, 495-504.
- Fisher, E., McMechan, G.A., Annan, A.P. and Cosway, S.W. 1992b. Examples of reverse-time migration of single-channel, ground penetrating radar profiles. *Geophysics* 57, 577-586.
- Harris, S.A. and Schmidt, I.H. 1994. Permafrost aggradation and peat accumulation since 1200 years B.P. in peat plateaus at Tuchitua, Yukon Territory (Canada). *Journal of Paleolimnology* 12, 3-17.
- Hayley, D.W. 1989. Maintenance of a railway grade over permafrost in Canada. *The Northern Engineer* 21(3), 4-10.
- Jowsey, P.C. 1966. An improved peat sampler. *New Phytologist*, 65:245-248.
- Kalantzis, F. 1994. Imaging of reflection seismic and radar wavefields: monitoring of steam heated oil reservoirs and characterization of nuclear waste repositories. Unpublished Ph.D. Thesis, Department of Physics, University of Alberta, Edmonton, Alberta. 297pp.
- Kershaw, G.P. 1983. *Long-term ecological consequences in tundra environments of the CANOL Crude Oil Pipeline Project, N.W.T., 1942-1945*. Ph.D. Thesis, Department of Geography, University of Alberta, Edmonton, Alberta.
- Kershaw, G.P. and Gill, D. 1979. Growth and decay of palsas and peat plateaus in the Macmillan Pass - Tsichu River area, Northwest Territories, Canada. *Canadian Journal of Earth Sciences* 16 (7), 1362-1374.
- Kershaw, G.P. and Skaret, K.D. 1993. Microclimatic characteristics of palsas along an altitudinal gradient, Mackenzie Mountains, NWT, Canada. In *Permafrost, Sixth International Conference, Proceedings*, South China University of Technology Press, 1, 338-343.
- Kettles, I.M. and Robinson, S.D. 1996. A ground-penetrating radar study of peat landforms in the discontinuous permafrost zone near Fort Simpson, Northwest Territories, Canada. In Trettin, C., M. Jurgenson, D. Grigal, M. Gale and J. Jeglum, editors, *Northern Forested Wetlands: Ecology and Management*, CRC, Lewis Publishers, Boca Raton, Florida, 147-160.

- Lachenbruch, A.H., Cladouhos, T.T., and Saltus, R.W. 1988. Permafrost temperature and the changing climate. In Senneset, K., editor, *Fifth International Conference on Permafrost*, Trondheim, Norway, Tapir, 3:9-17.
- Lerbekmo, J.F., Westgate, J.A., Smith, D.G.W., and Denton. 1975. New data on the character and history of the White River volcanic eruption, Alaska. In Suggate, R.P. and M.M. Cresswell, editors, *Quaternary Studies*. Royal Society of New Zealand. 203-209.
- Liang, L. and Kershaw, G.P. 1995. Climate change in the Mackenzie Mountains, N.W.T., Canada. *Climate Research* 5, 1-13.
- National Wetlands Working Group (Canada Committee on Ecological Land Classification). 1988. *Wetlands of Canada. Ecological Land Classification Series No. 24*. Sustainable Development Branch, Environment Canada, Ottawa and Polyscience Publications Inc., Montreal (452p.).
- Nelson, F.E., Hinkel, K.M. and Outcalt, S.I. 1992. Palsa-scale frost mounds. In Dixon, J.C. and Abrahams, A.D., editors, *Periglacial Geomorphology, Proceedings of the 22nd Annual Binghampton Symposium in Geomorphology*. John Wiley & Sons, Chichester, 305-325.
- Outcalt, S.I. and Nelson, F. 1984. Computer simulation of buoyancy and snow-cover effects in palsa dynamics. *Arctic and Alpine Research* 16(2), 259-263.
- Porsild, A.E. 1945. *The alpine flora of the east slope of Mackenzie Mountains, Northwest Territories*. Canada Department of Mines and Resources, Mines and Geology Branch. National Museum of Canada, Bulletin No. 101 (Biological Series No. 30) (35p.).
- Porsild, A.E. 1951. *Botany of southeastern Yukon adjacent to the Canol Road*. Canada Department of Resources and Development, National Parks Branch. National Museum of Canada, Bulletin No. 121 (Biological Series No. 41) (400p.).
- Seppälä, M. 1982. An experimental study of the formation of palsas. In H.M. French, editor, *Proceedings, 4th Canadian Permafrost Conference*. National Research Council of Canada, Ottawa, 36-42.
- Seppälä, M. 1988. Palsas and related forms. In M.J. Clark, editor, *Advances in Periglacial Geomorphology*. John Wiley & Sons, Chichester, 247-278.
- Skaret, K.D. 1995. Stratigraphic, microclimatic and thawing attributes associated with palsas located in the alpine tundra environment of the Macmillan Pass - Tsichu River region, N.W.T., Canada. M.Sc. Thesis, Department of Geography, University of Alberta, Edmonton, Alberta.

- Smith, M.W. 1993. Climatic change and permafrost. In H.M. French and O. Slaymaker, editors, *Canada's Cold Environments*, 291-312.
- Worsley, P., Gurney, S.D., and Collins, P.E.F. 1995. Late Holocene 'mineral palsas' and associated vegetation patterns: a case study from Lac Hendry, Northern Québec, Canada and significance for European Pleistocene thermokarst. *Quaternary Science Reviews* 14, 179-192.
- Zoltai, S.C. 1978. A portable sampler for perennially frozen stone-free soils. *Canadian Journal of Soil Science* 58:521-523.
- Zoltai, S.C. and Tarnocai, C. 1971. Properties of a wooded palsa in northern Manitoba. *Arctic and Alpine Research* 3(2), 115-129.

5.0 SUMMARY AND CONCLUSIONS

The objectives of this thesis were:

- Objective 1:** to evaluate the suitability of GPR for investigation of perennially frozen peatlands (including stratigraphy and identification of frozen - unfrozen and peat - mineral sediment interfaces) and evaluation of genetic processes;
- Objective 2:** to evaluate available techniques for processing GPR data containing noise, weak signals, and diffraction patterns which may obscure the stratigraphy and limit the usefulness of the raw data; and
- Objective 3:** to apply GPR, supplemented with conventional techniques, to characterize and compare trends in palsa evolution at two palsa fens in northern Canada.

To meet these objectives, an assessment of potential applications of GPR in perennially frozen peatlands was undertaken on the basis of a review of:

- available literature pertaining to GPR applications in peatlands;
- relevant theoretical geophysical principles; and
- analysis of data compiled from field trials.

In particular, this study tested a range of advanced data processing techniques developed for seismic data, to evaluate their effectiveness in enhancing image quality and improving ease of GPR data interpretation. Further, GPR and conventional data from two palsa fen sites were examined to identify contemporary, as well as spatial and temporal variations in, stratigraphic and morphologic characteristics of the palsas and peatlands which may reflect genetic and/or degradational processes.

Utility of GPR in Peatland Investigations

In this study, GPR successfully imaged sub-peat topography and internal fen stratigraphy, although only limited correlation between fen cores and radar profiles was possible. The presence of frozen conditions at depth was successfully mapped in both peat and mineral-cored palsas. Palsas typically generated chaotic radar returns distinct from generally laterally continuous returns from unfrozen fen. Unusual radar patterns were documented where the transition between frozen and unfrozen peat was known from coring to be non-vertical, and where the transect crossed the edge of a known palsa collapse scar.

The principal advantages of GPR in peatland investigations lie in rapid, accurate, and continuous imaging of sub-peat topography, evaluation of vertical and lateral homo/heterogeneity and stratigraphic continuity, and delineation of frozen-unfrozen interfaces at depth. In perennially frozen peatlands, GPR can provide continuous active layer profiling (with high frequency antennae), estimate depth of permafrost (with low frequency antennae), and can identify taliks and unfrozen areas within, adjacent to, and/or below permafrost. For these applications, the continuous imaging of GPR offers more comprehensive spatial data than could be collected by field studies based solely on manual point measurements. In

addition, continuous imaging minimizes the risk associated with data acquisition where anomalous subsurface conditions occur.

While GPR can rapidly image subsurface stratigraphy in peatlands and permafrost bodies in peatlands, the degree to which reliable inferences can be made regarding peat properties and permafrost characteristics depends on site-specific conditions and detailed point source verification. The relationship between radar events and causative peat properties remains poorly defined. Improved peat sample retrieval methods (*e.g.*, reduced water loss, compaction), in conjunction with more detailed coring and sample analyses, would facilitate reliable correlation of observed strata with radar reflections. However, the complex inhomogeneity of peatland characteristics and the numerous factors affecting the dielectric permittivity in peatlands suggest that GPR will remain of limited utility in detailed stratigraphic studies, with the exception of its ability to image vertical and lateral variability.

Given the current lack of understanding of radar response to variations in peat properties, it is recommended that future studies consider increased coring density, both at intervals along GPR transects and also as clusters at each coring location. The latter approach may allow information regarding peat properties derived from coring to better approximate the 'footprint' of the radar signal. Once the causal relationship between variations in peat properties and radar events is better understood, GPR may reduce the need for manual testing, depending on stratigraphic complexity and desired level of detail. (Notwithstanding this eventuality, coring will still be required to provide actual depth data for radar correlations.)

The ability of GPR to provide detailed stratigraphic and structural information in frozen peat is impaired by high signal propagation velocities, signal scatter due to ice, and signal attenuation in near-surface thawed or partially thawed layers. Nevertheless, data examined in this study were adequate to infer the presence of segregated ice, domed strata, permafrost depth in palsas, and location and orientation of frozen - unfrozen interfaces.

Most previous GPR-based studies present the radar data with depth scales to facilitate interpretation by the reader of the subsurface profiles. Topographic corrections are also typically added to the data to improve imaging of subsurface structure. However, depth scales for raw or processed radar data are frequently misleading and potentially erroneous due to vertical and lateral variability in signal velocity (Coffeen, 1984). Furthermore, variations in signal velocity may introduce erroneous time structures which are not representative of true stratigraphic structures at depth. In peatlands, strong signal velocity contrasts occur at the frozen - unfrozen interface, the frost table, and the acrotelm - catotelm interface. Artificial time structures may be generated by point reflectors and irregular transition zones (*e.g.*, palsa margin). For accuracy, reflector depth should only be calculated using the actual signal travel time measured on a given trace and formulae based on the specific survey configuration. Also, interpretation of time structures in transition zones is best undertaken with point source verification of subsurface conditions. It is common practice in the use of seismic data to not include depth scales for similar reasons; it is recommended that future published GPR studies omit depth scales (particularly in the absence of well defined velocity structures), provide the

reader instead with the tools necessary to infer depth information, and ensure the reader is cognizant of the limitations of this exercise.

Data Processing

Seismic data processing techniques, in particular deconvolution and coherency filtering, were successful in improving vertical resolution and lateral continuity of reflections in the fens, and to a lesser extent in the palsas. Various gain recovery options offer added flexibility in data manipulation to enhance either stratigraphic detail or relative amplitude information. Bandpass filtering and spectral shaping were useful in eliminating or reducing noise and enhancing data clarity. However, time-depth conversion and migration processing were generally not successful, as radar signal velocity variations across complex vertical and lateral transitions in ground thermal regime remain poorly defined. Better characterization of radar signal behaviour in transitional zones may enhance the utility of GPR for imaging the frozen - unfrozen transition at the palsa or peat plateau margin.

Unless the improved resolution offered by advanced data processing is accompanied by more detailed characterization of peat properties and radar signal behaviour, the time investment demanded by the use of seismic data processing techniques may not be warranted. Notwithstanding this, it is clear that advanced data processing can improve the quality of the data, particularly in unfrozen peat. Enhanced resolution offered by deconvolution and coherency filtering may be prerequisite to confirming subtle stratigraphic features, such as those generated by permafrost degradation.

Contribution of GPR to Investigation of Palsa Evolution

Conventional and GPR-derived data from both sites confirm palsa genesis by ice segregation. In this regard, the GPR substantiated evidence gathered using conventional techniques, but generally did not go beyond facilitating compilation of data regarding peat thickness, stratigraphy, and permafrost distribution.

GPR did not consistently image internal structure or detailed stratigraphy of peat-cored palsas, and further study on palsas and on frost mounds of different origins (*cf.* Nelson, *et al.*, 1992), using varying survey configurations (particularly antennae frequency) should be undertaken to test the ability of GPR to distinguish domed *vs.* flat-lying stratigraphy in frozen sediments.

The GPR showed promise in imaging the complex frozen - unfrozen interface at depth below the palsa margin, which if validated, could facilitate long-term monitoring of subsurface permafrost conditions and characterization of frost bulb development during aggradation or degradation. Advancement of this application requires improved characterization of radar signal velocity variation across transitional ground thermal conditions in the subsurface.

These applications of GPR complement conventional techniques, and facilitate data compilation, but otherwise do not make a substantive contribution to the advancement of our

understanding of palsa genesis. The key advantages of GPR in this regard include its ability to provide rapid, continuous imaging of subsurface conditions, and in some cases, to extend beyond the practical reach (*e.g.*, depth and ease of penetration, cost, time) of conventional techniques, such as coring. Perhaps the most significant contribution of GPR is its ability to image temporal and spatial transitions in subsurface conditions that would otherwise be undetectable by conventional techniques. It is recommended that future studies seek to compile radar data from more numerous transects intersecting features of interest at different angles, to allow improved, three-dimensional representation of subsurface conditions.

The data compiled in this study suggest that GPR may allow identification of stratigraphic signatures of pre-existing permafrost landforms, which would not otherwise be detectable by conventional coring techniques. This application may facilitate reconstruction of peatland history, particularly where collapsed permafrost features are not associated with persistent, identifiable surface features. However, further testing at sites of known palsa collapse scars and collapsing peat plateau margins is required to determine whether such features are consistently associated with stratigraphic signatures. Identification of subtle stratigraphic variations may rely on advanced data processing to enhance data clarity and resolution.

Notwithstanding the above described limitations of radar technology to advance our understanding of palsa evolution, GPR will continue to play an important role in peatland studies. The ice segregation model of palsa development is well documented, and its initiation demonstrated experimentally (Seppälä, 1982). However, the synergy of processes leading to the development of, or causing the transition between, the range of perennially frozen landforms of varying morphology (*i.e.*, mound, sinuous, complex, and plateau forms) and stages of development in peatlands (and in mineral soil, in the case of ‘minerogenic’ or mineral-cored features) remains poorly understood. Therefore, the theoretical basis is lacking from which the suite of conditions that may be expected to occur in association with a landform of a given origin or stage of development can be predicted.

To the extent that GPR can facilitate data compilation or contribute new data to peatland investigations, the technology warrants further application. Conversely, as our understanding of genetic processes advances, we may become able to make more effective use of available tools to test hypotheses concerning subsurface conditions that may be expected to result from geomorphic processes acting independently or synergistically.

5.1 Literature Cited

- Coffeen, J.A. 1984. *Interpreting Seismic Data*, Tulsa: PennWell Publishing Company (260p.).
- Nelson, F.E., Hinkel, K.M. and Outcalt, S.I. 1992. Palsa-scale frost mounds. In Dixon, J.C. and Abrahams, A.D., editors, *Periglacial Geomorphology, Proceedings of the 22nd Annual Binghampton Symposium in Geomorphology*: John Wiley & Sons, Chichester, 305-325.
- Seppälä, M. 1982. An experimental study of the formation of palsas. In H.M. French, editor, *Proceedings, 4th Canadian Permafrost Conference*. National Research Council of Canada, Ottawa, 36-42.

APPENDIX A

PRINCIPLES OF GROUND PENETRATING RADAR

APPENDIX A. PRINCIPLES OF GROUND PENETRATING RADAR

This appendix describes the operating principles of ground penetrating radar, and outlines the data collection, basic data processing steps, data presentation, and interpretation factors used in and relevant to this study. Advanced data processing techniques are described in Chapter 3 of this thesis.

A.1 Principles

Ground penetrating radar (GPR) enables the identification of subsurface boundaries by transmitting short, high frequency electromagnetic pulses into the ground and recording the travel time and amplitude of energy reflected back to the surface from interfaces with a contrast in electrical properties (Figure A-1); this contrast may be caused by one or more changes in the subsurface materials affecting the electrical properties, such as moisture content, temperature (*i.e.*, frozen *vs.* unfrozen), density, and composition (*i.e.*, peat *vs.* mineral sediment) (Annan, 1992). The electrical properties of materials in the subsurface (Table A-1) control the velocity of radar signal propagation, the attenuation of the radar signal, and the amplitude of energy reflected at interfaces with electric contrast (Davis and Annan, 1989).

Data are recorded as the two-way travel time, in nanoseconds, of the reflected energy *versus* position, in metres, at successive points along a survey transect, generating a profile of subsurface interfaces with electric contrast (Figure A-2). Inferences are then made regarding what each interface represents, based on the nature of the reflected energy, and on point verification by coring. The depth of each interface is estimated using the recorded two-way travel time and the signal propagation velocity through the subsurface, the latter derived from a velocity sounding (see Section A.3 below).

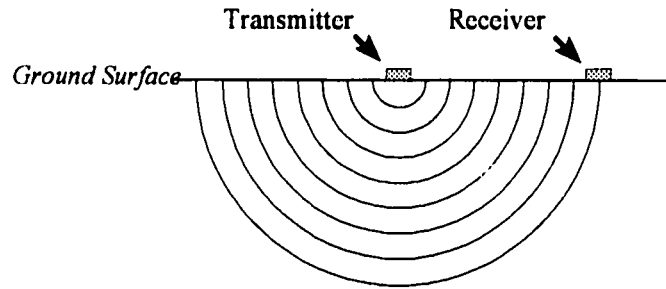
A.2 Radio wave behaviour and material electrical properties

The electromagnetic (EM) waves transmitted by the GPR system are typically in the range of 10 to 1000 MHz. Energy from the transmitted pulse travels directly through the air from the transmitter to the receiver, is refracted along the air-ground interface and in the shallow subsurface to the receiver, and propagates downward through the subsurface, where part of the signal energy is reflected upwards to the receiver from interfaces where there is a change in electrical properties (Figure A-3).

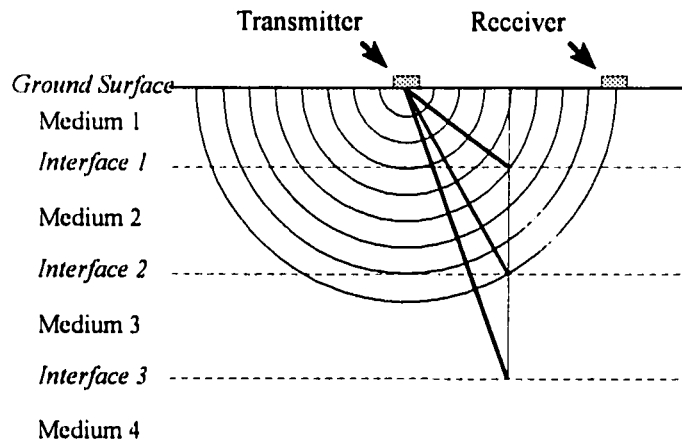
A.2.1 Dielectric constant

The velocity at which radar waves propagate is controlled by the dielectric constant, K (or relative permittivity, ϵ_r), of the material through which the signal passes. The dielectric constant is a measure of the capacitance of a material, and indicates the effect of the material on an electric field relative to free space (Daintith, 1981). When an EM field is applied to a medium with a relatively high dielectric constant (as when a voltage is applied to a capacitor), a secondary EM field is generated (Sprott, 1981), which interferes with, and effectively slows

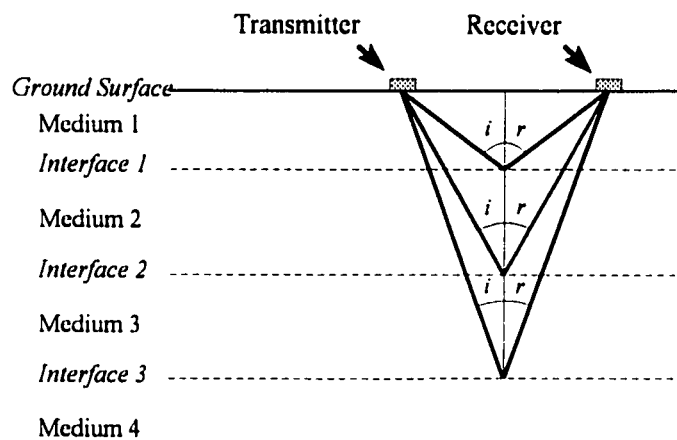
Figure A-1. Geometry of GPR signal path through simplified subsurface.



a) Radar energy travelling outwards from transmitter.



b) Straight ray paths show routes of individual points on the radar wave front.

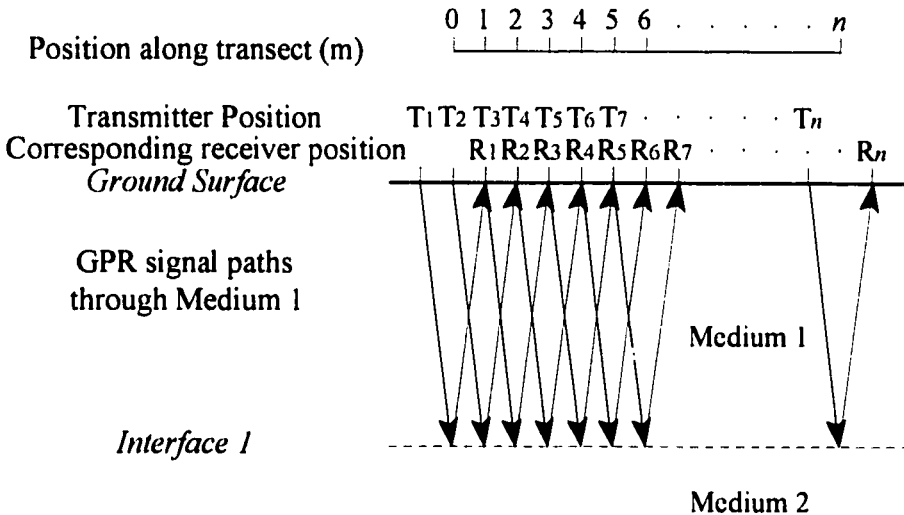


c) Radar energy is reflected (r) at an angle equal to the angle of incidence (i) from interfaces with a contrast in electrical properties.

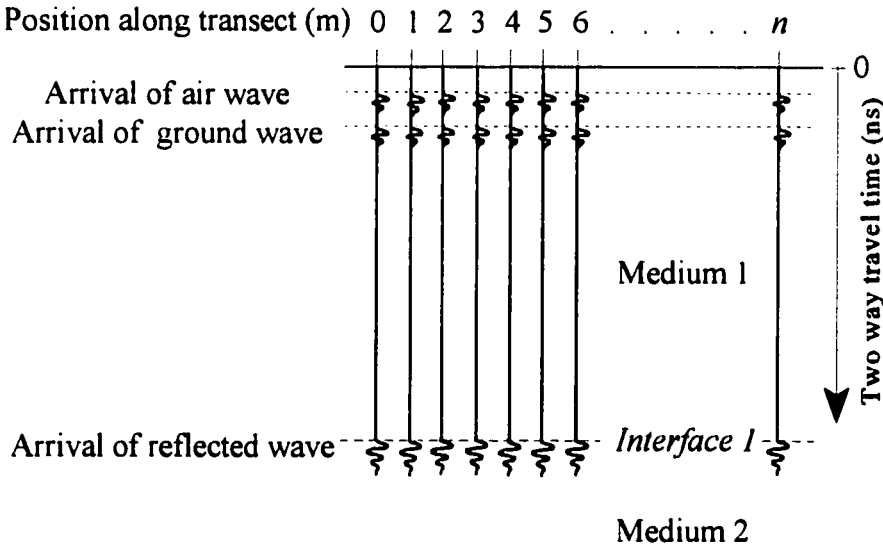
Table A-1. Typical electrical properties of common geological materials (conductivity, velocity, and attenuation measured for 100 MHz signal energy)¹				
Material	dielectric constant K_a	conductivity σ ($\text{mS}\cdot\text{m}^{-1}$)	velocity v ($\text{m}\cdot\text{ns}^{-1}$)	attenuation α ($\text{dB}\cdot\text{m}^{-1}$)
Air	1	0	0.30	0
Fresh water	80	0.5	0.033	0.1
Sea water	80	3×10^4	0.01	10^3
Dry sand	3-5	0.1	0.15	0.01
Saturated sand	20-30	0.1-1.0	0.06	0.03-0.3
Limestone	4-8	0.5-2	0.12	0.4-1
Shale	5-15	1-100	0.09	1-100
Silt	5-30	1-100	0.07	1-100
Clay	5-40	2-1000	0.06	1-300
Granite	4-6	0.01-1	0.13	0.01-1
Dry salt	5-6	0.01-1	0.13	0.01-1
Ice	3-4	0.01	0.16	0.01
Peat, icy frozen	n/a	n/a	0.08 - 0.12	n/a
Peat, saturated unfrozen	60-80*	n/a	0.03 - 0.04	n/a

¹ Davis and Annan (1989), except for * Hänninen (1992)

Figure A-2. Survey configuration to generate continuous subsurface radar reflection profile through simplified subsurface.



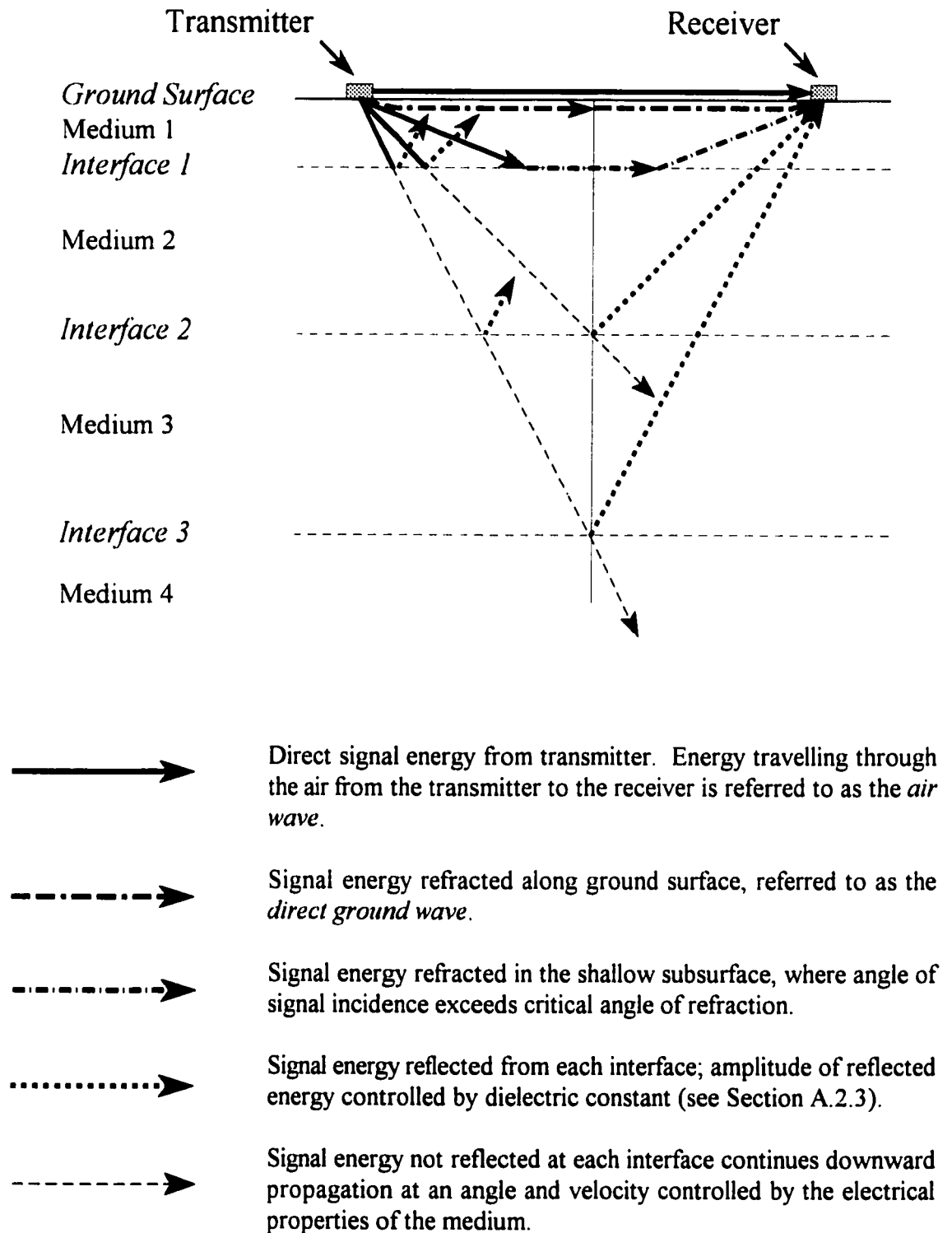
- a) Evenly spaced, successive transmitter (T_n) and receiver (R_n) positions in constant step-size survey configuration, to generate continuous profile of data from points on subsurface interface.



- b) Resulting GPR profile from configuration shown in (a). Each trace is plotted at mid-point between transmitter and receiver locations. Note signal from direct air wave, ground wave and reflected wave (see text).

Modified from Jol and Smith (1991).

Figure A-3. Possible paths of GPR signal energy propagation from the transmitter to the receiver.



the primary EM pulse. Conversely, a material with a low dielectric constant will display little or no interaction with the primary EM pulse, and wave velocities will remain high.

However, the complex dielectric constant includes both real and imaginary components, the latter associated with wave attenuation due to conductivity (see Section A.2.2 below); the velocity is a function of the real part of the dielectric constant (Davis and Annan, 1989; Fisher, *et al.*, 1992b; Robinson, 1993). Electric losses are low in most materials for which GPR is effective (A-Cubed, 1983), and the imaginary part of K is therefore assumed to be negligible; the real part of the dielectric constant is thus referred to as the apparent dielectric constant, K_a . Where electric losses are low, the velocity of EM wave propagation, v , in metres per nanosecond, is inversely proportional to the apparent dielectric constant, K_a , and may be expressed as:

$$v = \frac{c}{\sqrt{K_a}} \quad (1)$$

where c is the propagation velocity of EM waves through free space ($0.3 \text{ m}\cdot\text{ns}^{-1}$).

Where there is no interaction between the EM wave and the medium through which it travels, as in a vacuum, the EM wave travels at the propagation velocity of EM waves through free space, $0.3 \text{ m}\cdot\text{ns}^{-1}$. The dielectric constant of a vacuum is 1; as the propagation of EM waves through air approximates propagation through a vacuum, the dielectric constant of air is also given as 1. The dielectric constants of common geological materials are included in Table A-1.

A.2.2 Signal attenuation

Attenuation of the EM wave as it travels away from the transmitter is caused by geometrical spreading loss, scattering, and absorption in conductive materials. Geometrical or spherical spreading of the radar wave causes loss of signal amplitude at a rate inversely proportional to the square of the distance from the signal source (Davis and Annan, 1989; Robinson, 1993). The degree of scattering of the radar wave from small-scale heterogeneities such as irregular subsurface boundaries, point reflectors (*e.g.*, boulders; terminus, closure or pinch-out of faults or strata), or thin layers, is directly related to reflector geometry and roughness, contrast in electrical properties, and signal frequency and wavelength (Davis and Annan, 1989; Robinson, 1993; Coffeen, 1986). Attenuation causes the amplitude of reflected energy to be reduced and therefore difficult to distinguish from background noise recorded by the receiving antenna (Theimer, *et al.*, 1994).

Attenuation, α , of the radar signal due to conductive absorption, in $\text{dB}\cdot\text{m}^{-1}$, is directly proportional to the conductivity of the material, σ , in $\text{mS}\cdot\text{m}^{-1}$, and inversely related to the apparent dielectric constant, K_a , and may be expressed as (Davis and Annan, 1989):

$$\alpha = \frac{1.69 \times 10^3 \sigma}{\sqrt{K_a}} \quad (2)$$

The conductivity of geological materials is primarily controlled by moisture content, concentration of dissolved salts, and clay content (Doolittle, 1987). In materials with high conductivity, signal attenuation is high, and signal penetration, therefore, low. Thus, where conductivities exceed 10 to 15 mS·m⁻¹, the effectiveness of GPR is limited, although other factors such as system performance, frequency, depth to reflectors of interest, and other signal losses may influence the suitability of GPR for a particular application (Inkster, *et al.*, 1989).

A.2.3 Signal reflection

As the radar signal propagates downward through the subsurface, it encounters interfaces between materials with contrasting electrical properties; at each interface, part of the signal energy is reflected back towards the surface at an angle equal to the angle of incidence. The amount of energy reflected is a function of the dielectric contrast between the two materials, expressed as:

$$R = \frac{\sqrt{K_{a1}} - \sqrt{K_{a2}}}{\sqrt{K_{a1}} + \sqrt{K_{a2}}} \quad (3)$$

where R is the reflection coefficient, K_{a1} the apparent dielectric constant of the first medium, and K_{a2} the apparent dielectric constant of the second medium (Davis and Annan, 1989; Hänninen, 1992). Thus, where the dielectric contrast is high, R is higher, and the amplitude of energy reflected is greater; the magnitude of the electrical contrast at an interface may therefore be inferred from the amplitude of the reflected energy recorded by the receiver. The signal energy not reflected continues to propagate through the second medium, at a velocity determined by the electrical properties of that medium, and along a refracted path determined by the signal velocity. For signal energy to be reflected, the change in dielectric constant must be abrupt; Theimer, *et al.* (1994) suggest that to be detectable by GPR, the dielectric contrast must occur within a material distance of one-quarter of the signal wavelength.

A.2.4 Resolution

The resolution achieved by the GPR system is determined by the wavelength, λ , which is a function of the antennae frequency and the apparent dielectric constant of the medium, by the following relationship (Kalantzis, 1994; Hayt, 1981):

$$\lambda = \frac{c}{f \sqrt{K_a}} \quad (4)$$

where c is the propagation velocity of EM waves in free space ($0.3 \text{ m}\cdot\text{ns}^{-1}$), f is the centre frequency of the antennae, and K_a is the apparent dielectric constant of the medium, in which electric losses are assumed to be negligible. Subsurface horizons must be separated by a distance (along the signal path) greater than the wavelength for distinct reflections to be discernible on the data traces (Hänninen, 1992).

A.3 Velocity and Depth Calculations

In a typical radar reflection profile, data are plotted as two-way travel time *versus* position along the survey transect; thus, information regarding the shape and relative position of reflectors may be read directly from the profile. However, the actual depth of individual reflectors must be calculated, using known values for signal (two-way) travel time (measured directly from the profile) and signal propagation velocity through the subsurface. The latter may be derived from a Common Mid-Point (CMP) or Wide Angle Reflection and Refraction (WARR) survey (Annan, *et al.*, 1975; Annan and Davis, 1976; Arcone, 1984; also *cf.* Barry and Pollard, 1992; LaFleche, *et al.*, 1988).

In a CMP (or WARR) survey, signal propagation velocity is calculated by measuring the change in two-way travel time of energy reflected from an interface at depth, as antennae separation, and therefore signal path length, is increased at a known rate. The velocity sounding is carried out in an area of representative level terrain, where the subsurface strata are known or assumed to be relatively flat-lying (Barry and Pollard, 1992). The spacing between the transmitting and receiving antennae is incrementally increased, and successive traces collected for a single point midway between the antennae (Figure A-4).

In a velocity sounding typical of this study, the first radar event, A , is the direct air wave, which travels at the speed of light through the air from the transmitter to the receiver (Figure A-5). Its arrival time, t_A , in nanoseconds, is calculated as

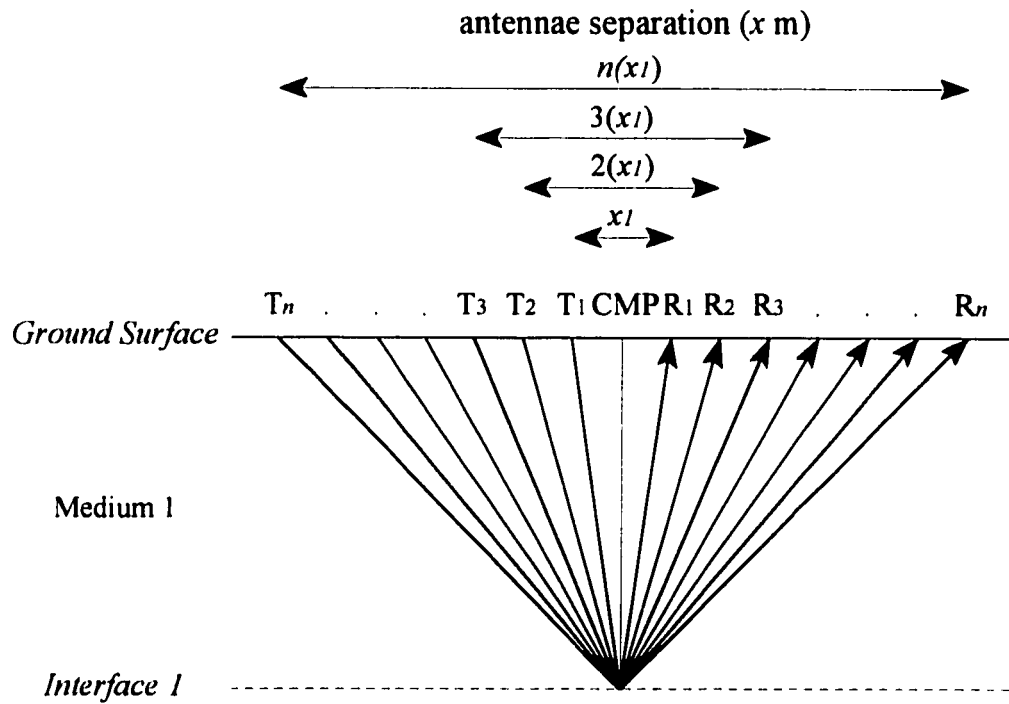
$$t_A = \frac{x}{c} \quad (5)$$

where x is the antenna separation in metres, and c is the velocity of electromagnetic waves in free space ($0.3 \text{ m}\cdot\text{ns}^{-1}$). The second radar event, G , is the direct ground wave, which travels along the air-ground interface from the transmitter to the receiver. Its arrival time, t_G , in nanoseconds, may be calculated by

$$t_G = \frac{x}{v_G} \quad (6)$$

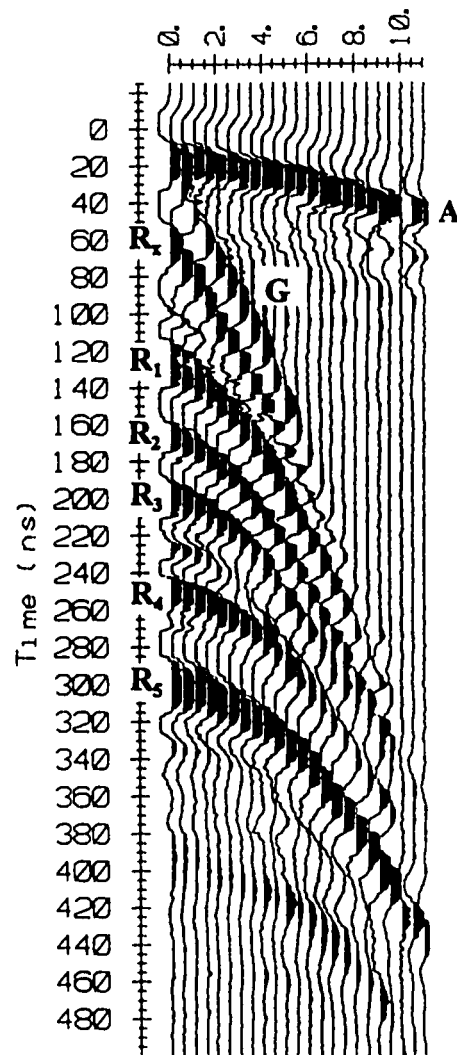
where x is the antenna separation in metres, and v_G is the signal propagation velocity through the ground in metres per nanosecond. These direct waves and any critically refracted waves

Figure A-4. Survey configuration for a Common Mid Point (CMP) velocity sounding.



Successive transmitter locations (T_x) are shown, with corresponding receiver locations (R_x).

Figure A-5. Sample Common Mid-Point (CMP) survey from unfrozen fen.



Typical Common Mid-Point (CMP) survey, with distinct direct air wave, *A*, and direct ground wave, *G*. Reflected energy from subsurface interfaces generates hyperbolic events on the velocity sounding, *R_n*. *R_x* appears as a near-linear event, and may represent signal energy refracted in the shallow subsurface.

Plot produced from pulseEKKO IV radar operating software.

generate straight-line events on the velocity sounding which demonstrate a linear relationship between travel time and antenna separation (Annan, *et al.*, 1975; Barry and Pollard, 1992). The slope of the straight-line event is inversely proportional to the signal propagation velocity (Barry and Pollard, 1992).

Reflected energy from subsurface interfaces generates hyperbolic events on the velocity sounding. The observed curvature is similar to the normal moveout (NMO) curvature seen in seismic Common Depth Point (CDP) surveys (*cf.* Coffeen, 1986), and decreases with increased depth of the reflector, as the variation in signal path length between successive increments of antennae separation is less for deeper reflectors than for shallow ones. To calculate signal propagation velocity, the arrival time squared of reflected energy, t_R^2 , is plotted *versus* the antenna separation squared, x^2 ; the slope of a least-squares line through the points is inversely proportional to the velocity squared, v^2 , through the subsurface to the depth of the reflector (Annan, *et al.*, 1975; Barry and Pollard, 1992). It is important to note that the signal propagation velocity calculated from any single reflector on a velocity sounding represents an integrated velocity over the entire signal path length to and from that reflector, which may encompass zones of greater and lesser velocity; calculation of velocities from successive reflectors may indicate variation in velocity with depth (*cf.* Barry and Pollard, 1992). (Note that the velocity may also be estimated directly from the CMP plot of two-way travel time *versus* antenna separation, as the slope of the near straight-line segment of the hyperbolic event.)

Depth to individual reflectors on the radar profile, D_R , measured vertically, in metres, can be estimated using a simple path calculation using the recorded two-way travel time and the calculated signal propagation velocities, by a formula based on Pythagoras' theorem (Figure A-6):

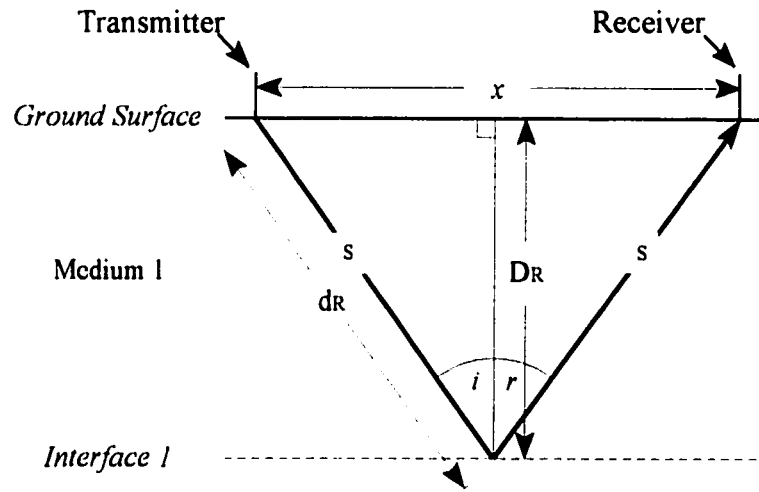
$$D_R = \sqrt{d_R^2 - \left(\frac{x}{2}\right)^2} \quad (7)$$

where x is the antenna separation in metres, and d_R is the distance from the transmitting antenna to the subsurface reflector measured along the signal path (equal to half the signal path length) in metres, calculated by

$$d_R = (v_R) \frac{t_R}{2} \quad (8)$$

where v_R is the calculated signal propagation velocity to the reflector in metres per nanosecond, and t_R is the travel time to and from the reflector in nanoseconds. Calculated depths may be correlated with actual depth to distinct horizons measured from cores at points on or close to the survey transect.

Figure A-6. Assumed configuration of system components and subsurface reflector for depth calculations.



$$D_R = \sqrt{d_R^2 - \left(\frac{x}{2}\right)^2} \quad (7)$$

where:

- D_R = depth to reflector (measured vertically)
- d_R = distance from transmitting antenna to subsurface reflector (*interface 1*), measured along signal path (*s*)
- x = antennae separation
- i = angle of incidence of signal energy
- r = angle of reflection of signal energy

The velocities of radar signal propagation through the ground calculated as above may also be used to estimate the bulk dielectric constant of the ground, by re-arranging the formula

$$v_g = \frac{c}{\sqrt{K_a}} \quad (9)$$

where v_g (in contrast to the direct ground wave, v_G) is the velocity of the radar signal through the ground in metres per nanosecond, c is the propagation velocity through air ($0.3 \text{ m}\cdot\text{ns}^{-1}$), and K_a is the apparent dielectric constant of the ground, as follows (Annan, *et al.*, 1975).

$$K_a = \left(\frac{c}{v_g} \right)^2 \quad (10)$$

A.4 Data Collection

The GPR data presented in this thesis were collected as a single-channel, constant-offset (or "bistatic"; Worsfold, *et al.*, 1986) radar reflection profile using a pulseEKKO IV GPR system developed and manufactured by Sensors & Software Inc., of Mississauga, Ontario, Canada. In a single-channel survey, data for each point or station along the survey transect are collected as a single trace using one transmitter and one receiver only. (In contrast, standard seismic data collection uses multi-channel survey configurations where multiple sources and/or multiple receivers are employed to provide greater survey resolution (*cf.* Coffeen, 1986); this technique has seen little application in GPR data collection due to higher costs and decreased equipment portability (Fisher, *et al.*, 1992a).)

A reflection profile is generated by collecting a trace from each equally-spaced station on the transect line; each trace corresponds with the midpoint between the transmitting and receiving antennae, the separation or "offset" of which remains constant throughout the survey. A constant antenna offset of 2 m (*cf.* Robinson, *et al.*, 1992; Robinson, *et al.*, 1993) and a constant 0.5 m station separation were used in this study.

Optimum antenna offset is a function of target depth and dielectric constant, while optimum station spacing is a function of wavelength and dielectric constant. The 2 m antenna separation and 0.5 m station separation used in this study were intermediate to the optimum parameters for unfrozen peat and frozen sediment, both of which were anticipated to be encountered along the transects.

The antenna offset contributes to the resolution of individual reflectors in the subsurface, by increasing the signal path length, and therefore the travel time and effective separation, between successive reflectors (see Section A.2.4 above). Increasing antenna separation also increases the reflectivity of flat-lying planar targets (Annan, 1992). However, the offset must

be limited to avoid excessive signal refraction in the shallow subsurface due to angles of signal incidence at or beyond the critical angle of refraction (*cf.* Coffeen, 1986, p.28), particularly where the signal will pass from material with slow signal propagation velocity to material with greater signal propagation velocity, as from the active layer to underlying permafrost.

The depth of penetration of the GPR signal is inversely proportional to the antenna frequency, and proportional to the output signal strength (Davis and Annan, 1989; Kalantzis, 1994). However, resolution is proportional to antenna frequency; thus, higher frequency antennae provide greater resolution in the shallow subsurface, while lower frequency antennae provide greater depth penetration but with decreased resolution (Annan and Davis, 1976, Davis and Annan, 1989). Robinson, *et al.* (1992) compared the resolution achieved by varying antenna frequency (and corresponding antenna separation): 100 MHz antennae provided resolution as low as 0.4 m with penetration depths on the order of 15 m; 50 MHz antennae gave 0.8 m resolution with penetration to 20 m; and, the maximum resolution and depth of penetration achieved with the 25 MHz antennae were 1.6 m and 30 m respectively. The 50 MHz antennae provided an acceptable balance between depth penetration and individual reflector resolution, allowing the identification of major contacts, which are of primary interest, without interference due to reflections from minor interfaces. This survey used antennae with a centre frequency of 50 MHz with the standard system output voltage of 400 V.

In this study, the data were collected using a transverse (or “perpendicular broadside”) configuration (Kalantzis, 1994; Annan, 1992), with the long axes of the transmitting and receiving antennae parallel to one another, and perpendicular to the line of the survey transect. This is the most commonly used GPR antenna configuration, in which the electric field is polarized parallel to the strike direction of the target, in this case, the frozen - unfrozen interface. (There is no optimal antenna configuration for an equi-dimensional target, such as flat-lying fen reflectors.).

To improve the signal-to-noise ratio, a stacked pulsed radar signal of 128 source excitations was transmitted for each trace (*cf.* Fisher, *et al.*, 1992a, 1992b; Kalantzis, 1994). (This field stacking is distinct from the stacking of individual traces that is a common processing step in seismic data processing (*cf.* Coffeen, 1986, p.134-138).) For each trace, the signal sine wave was sampled at 1000 points at a sampling interval of 800 ps, for a total time window (*i.e.*, duration of time in which reflected energy is recorded, and thus, the length of each trace) of 800 ns.

A.5 Basic Data Processing

As noted above, field stacking of the pulsed radar signal improved the signal-to-noise ratio of the data. The occurrence of dead or erroneous traces is noted during field surveying, and these traces are deleted from the data files during processing. Dead traces may result from breakage of the fibre optic cables connecting the antennae to the control unit, so that the radar pulse is not emitted or reflections are not recorded. Erroneous traces may result from duplication of traces or incorrect antenna placement, often due to poor surveying conditions (*e.g.*, difficult terrain which hampers movement of the antennae).

The raw GPR data are typically plotted with automatic gain control (AGC) to compensate for the decrease in amplitude of reflected energy with increased range from the signal source; AGC is a time variable gain amplifier which increases gain as travel time increases, thereby enhancing reflections from weak, deep reflectors (Annan and Davis, 1976). The data are also typically plotted with simple point averaging noise reduction filters, such as trace-to-trace averaging and down-trace averaging. Where dipping reflectors are known or suspected, trace-to-trace averaging may be omitted, as this function tends to flatten dipping reflectors.

Each trace begins at time zero, which, without topographic correction, is plotted as a flat surface. Thus, horizontal reflectors below a positive topographic feature would appear synclinal in form, as travel time to the reflectors would be increased due to the additional material above the zero elevation datum. Conversely, horizontal reflectors below a negative topographic feature would appear anticlinal in form, as travel time is decreased (Figure A-7) (Coffeen, 1986). To eliminate these false structures and plot the position of subsurface reflectors more accurately, topographic corrections are applied to the data. Elevation data were collected in the field using an Abney level, and a built-in software topographic correction function was applied to the data.

A.6 Display and Interpretation of Radar Data

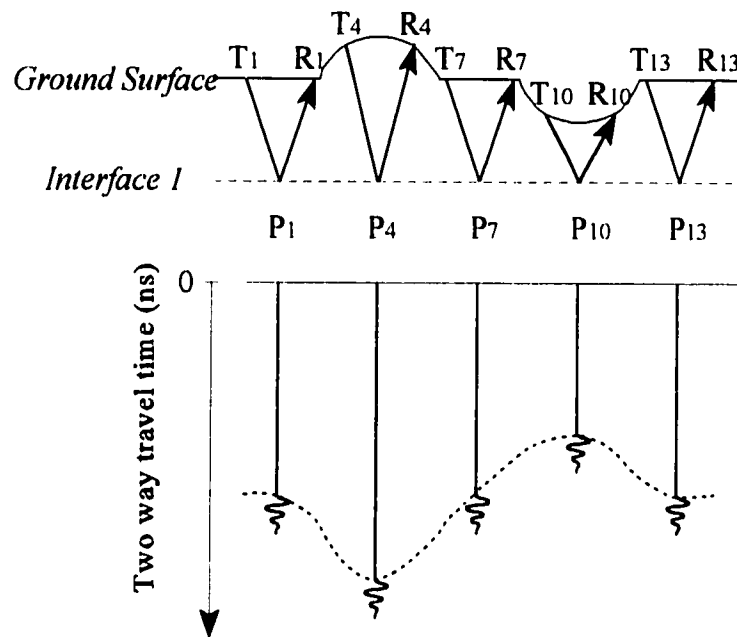
The GPR data are plotted as two-way travel time, in nanoseconds, of the reflected energy, *versus* position, in metres, along the survey transect, producing a two-dimensional radar reflection profile. Using seismic terminology, the traces are displayed as wiggle-variable area traces, with amplitude of the reflected energy wavelet represented by deviation of the wiggle trace from the vertical. Positive amplitude peaks to the right of the vertical are shaded for clarity and ease in identifying reflectors. Interfaces with high dielectric contrast generate high amplitude radar reflections. Information regarding the frequency of the reflected energy can also be derived from the traces, as high frequency signals will be of short duration, and will therefore plot shorter on the time axis than low frequency signals.

Time versus Depth Scales

The radar profiles presented in this thesis are plotted with time (in nanoseconds) on the vertical scale. The conversion of data from the time domain to depth is prone to error (Coffeen, 1984). Vertical and lateral velocity variations caused by subsurface anomalies, and the horizontal component of the signal path in the subsurface (particularly at shallow depths) compromise the accuracy of depth conversion. Furthermore, velocity determined from normal moveout curvature, as in a CMP survey, is not very accurate, and the accuracy of this technique decreases with depth (Coffeen, 1984).

The subsurface conditions encountered and survey configuration used in this study present several limitations to conversion of time data to depth: the presence of a surface layer of relatively low moisture content (upper thaw layer on palsas, acrotelm in fens) over deeper, saturated material presents a strong velocity contrast; the presence of frozen conditions, the boundary of which is known in places to be non-vertical (*i.e.*, wedge-like), presents a strong and irregular velocity contrast; peat characteristics display a large degree of vertical and

Figure A-7. Effect of topography on GPR signal travel time.



On the resulting radar profile, reflected energy is plotted at the mid-point (P_x) between the transmitter (T_x) and receiver (R_x). Assuming a hypothetical flat-lying subsurface reflector, and without topographic correction of the GPR data, positive relief is inverted in the imaged profile, because the signal energy takes longer to travel to and from the reflector. Conversely, negative relief appears shallower on the radar profile, due to the shorter signal travel time.

lateral variability, and thus, velocity; and antenna separation introduces a large horizontal component to the signal path, especially in the shallow subsurface. In addition, coring did not intercept major subsurface interfaces which could be unequivocally correlated to reflections on the radar profile; thus, depth values calculated from converted data could not be verified against real depth data.

Depth scales which account for the near-surface horizontal component of the signal path can be generated by the radar software (although not the seismic software), using velocity determined from CMP surveys. These depth scales are non-linear (*i.e.*, the vertical scale is more compressed at shallower depths where a larger proportion of the signal travel time is attributable to the horizontal component of the signal path). However, these depth scales would not account for the spatial velocity variations noted above.

Further, non-linear depth scales are of limited utility where topographic correction, which is itself a useful step to improve the illustration of subsurface structure, is applied to the data. Topographic correction introduces a non-uniform datum from which signal travel time is measured (and depth of reflections calculated); a non-linear depth scale would be applicable to only the one elevation with which the zero depth marker coincides.

In consideration of the above points, the radar profiles presented in this thesis are plotted with a time scale only. For the purposes of interpretation, depth of individual interfaces is estimated on the basis of the integrated velocity derived from the CMP survey and the actual two-way signal travel time of the reflection of interest. However, the reader will observe that the uppermost portion of each trace contains no signal information: this “dead” time is added to the trace to accommodate the illustration of relief. Thus, the actual two-way travel time of a reflection cannot be read directly from the vertical time scale, but must be determined by subtracting the “dead” time prior to the first radar event, the direct air wave. Because the travel time of the direct air wave is known, this radar event serves as a datum from which to measure two-way signal travel time. In all cases in this study, the direct air wave begins at 6.7 ns.

Notwithstanding the above, in text and figures, for the ease of the reader, reference to specific reflections in the radar profiles is given in nanoseconds, **read directly from the vertical time scale**. Approximate depth, estimated from the actual two-way signal travel time, is given in brackets, where relevant. Unless otherwise noted, depths noted in the text are calculated using signal propagation velocities of $0.038 \text{ m}\cdot\text{ns}^{-1}$ in unfrozen peat, and $0.095 \text{ m}\cdot\text{ns}^{-1}$ and $0.097 \text{ m}\cdot\text{ns}^{-1}$ in frozen peat at the Porsild’s Field and Dale Creek sites, respectively.

Certain processing functions (*i.e.*, NMO correction) cause extreme distortion in the shallow portion of the profile. On these profiles, the direct air and ground waves are muted, and cannot be used as a datum from which to determine two-way signal travel time. Therefore, depth values are not estimated for profiles to which this processing step has been applied. In cases where depth data are desired from these profiles, the depth of individual reflections may be estimated from other non-processed profiles on which the same reflections can be identified with confidence.

Topography

Topographic corrections have been applied to the data to provide a more realistic illustration of subsurface structure. The vertical exaggeration of each profile varies depending on plotting parameters and is indicated on each figure.

Factors in Interpretation

The earliest radar events on the radar profiles (the direct air and ground waves, and noise multiples) typically do not contain much, if any, information on subsurface conditions. Subsequent radar events represent interfaces within the peat and underlying mineral sediment, and are of greater interest to the interpreter. Key factors of which the reader should be aware when interpreting the radar profiles include the following.

- Radar signal velocity in frozen peat is approximately 2.5 times the velocity in unfrozen peat; thus, all subsurface reflections in frozen peat will appear considerably 'shallower' (*i.e.*, shorter two-way travel time) and vertically compressed on the radar profile relative to those in unfrozen peat. A single subsurface interface at a constant actual depth across the profile would therefore appear as distinct reflections plotted at different times on the vertical scale. This visual distortion must be considered when attempting to trace individual strata across transitional zones, and to relate stratigraphy in the fen with that observed in palsas.
- In transition areas or areas with anomalous subsurface conditions, artificial time structures may be evident on the radar profile in the time domain. For example, a zone of high velocity material will cause subsequent reflections to arrive sooner and appear shallower on the profile (velocity pullup; Coffeen, 1984). Thus, a flat-lying interface overlain in one area by a zone of high velocity (*e.g.*, frost) will appear as a flat reflection with a raised 'bump' below the zone of high velocity.
- Spatial aliasing may cause artificial structures to appear on the radar profile; this occurs when the eye sees an artificial pattern which is complementary or opposite to an actual pattern in the data.

A.7 Literature Cited

- A-Cubed Inc. 1983. *General state of the art review of ground probing radar*. Report to Energy, Mines and Resources Canada (89p.).
- Annan, A.P. 1992. *Ground penetrating radar workshop notes*. Sensors & Software Inc., Mississauga, Ontario.
- Annan, A.P. and Davis, J.L. 1976. Impulse radar sounding in permafrost. *Radio Science* 11(4), 383-394.
- Annan, A.P., Davis, J.L., and Scott, W.J. 1975. Impulse radar wide angle reflection and refraction sounding in permafrost. In *Report of Activities, Part C. Geological Survey of Canada Paper 75-1C*, 335-341.
- Arcone, S.A. 1984. *Pulse transmission through frozen silt*. U.S. Cold Regions Research and Engineering Laboratory, Report 84-17 (8p.).
- Barry, P.J. and Pollard, W.H. 1992. Ground penetrating radar investigations of ground ice on the Fosheim Peninsula, Ellesmere Island, Northwest Territories. In *Proceedings of the Third National Student Conference on Northern Studies*, Ottawa, Ontario: Musk-ox Special Publication 39, 59-66.
- Coffeen, J.A. 1986. *Seismic Exploration Fundamentals: seismic techniques for finding oil, second edition*, Tulsa: PennWell Publishing Company (347p.).
- Coffeen, J.A. 1984. *Interpreting Seismic Data*, Tulsa: PennWell Publishing Company (260p.).
- Daintith, J. (ed.) 1981. *The facts on file: dictionary of physics*. Facts on File Inc., New York (217p.).
- Davis, J.P. and Annan, A.P. 1989. Ground-penetrating radar for high-resolution mapping of soil and rock stratigraphy. *Geophysical Prospecting* 37, 531-551.
- Doolittle, J.A. 1987. Using ground-penetrating radar to increase the quality and efficiency of soil surveys. In Reynolds, W.U. and Petersen, G.W., editors, *Soil Survey Techniques*, Soil Science Society of America, Special Publication No. 20, 11-32.
- Fisher, E., McMechan, G.A., and Annan, A.P. 1992a. Acquisition and processing of wide-aperture ground-penetrating radar data. *Geophysics* 57, 495-504.
- Fisher, E., McMechan, G.A., Annan, A.P. and Cosway, S.W. 1992b. Examples of reverse-time migration of single-channel, ground penetrating radar profiles. *Geophysics* 57, 577-586.

- Hänninen, P. 1992. *Application of ground penetrating radar and radio wave moisture probe techniques to peatland investigations*. Geological Survey of Finland, Bulletin 361 (71p.).
- Hayt, W.H. 1981. *Engineering electromagnetics*. McGraw-Hill, New York (527p.).
- Inkster, D.R., Rossiter, J.R., Goodman, R., Galbraith, M., and Davis, J.L. 1989. Ground penetrating radar for subsurface environmental applications. In *Proceedings of the Thematic Conference on Remote Sensing for Exploration Geology (Seventh)*, 127-140.
- Kalantzis, F. 1994. *Imaging of reflection seismic and radar wavefields: monitoring of steam heated oil reservoirs and characterization of nuclear waste repositories*. Unpublished Ph.D. Thesis, Department of Physics, University of Alberta, Edmonton, Alberta (297p.).
- LaFleche, P.T., Judge, A.S., Moorman, B.J., Cassidy, B., and Bedard, R. 1988. Ground probing radar investigations of gravel roadbed failures, Rae Access road, N.W.T. In *Current Research, Part D. Geological Survey of Canada Paper 88-1D*, 129-135.
- Robinson, S.D., 1993. *Geophysical and geomorphological investigations of massive ground ice, Fosheim Peninsula, Ellesmere Island, Northwest Territories*. Unpublished M.Sc. Thesis, Department of Geography, Queen's University, Kingston, Ontario (171p.).
- Robinson, S.D., Moorman, B.J., Judge, A.S., and Dallimore, S.R. 1993. The characterization of massive ground ice at Yaya Lake, Northwest Territories using radar stratigraphy techniques. In *Current Research, Part B. Geological Survey of Canada Paper 93-1B*, 23-32.
- Robinson, S.D., Moorman, B.J., Judge, A.S., Dallimore, S.R., and Shimeld, J.W. 1992. The application of radar stratigraphic techniques to the investigation of massive ground ice at Yaya Lake, Northwest Territories. In *Proceedings of the Third National Student Conference on Northern Studies*, Ottawa, Ontario: Musk-Ox Special Publication 39, 39-49.
- Sprott, J.C. 1981. *Introduction to modern electronics*. John Wiley & Sons, New York (349p.).
- Theimer, B.D., Nobes, D.C. and Warner, B.G. 1994. A study of the geoelectrical properties of peatlands and their influence on ground-penetrating radar surveying. *Geophysical Prospecting* 42, 179-209.
- Worsfold, R.D., Parashar, S.K. and Perrott, T. 1986. Depth profiling of peat deposits with impulse radar. *Canadian Geotechnical Journal* 23, 142-154.

APPENDIX B

OBSERVATIONS OF PEAT CHARACTERISTICS FROM CORING

APPENDIX B. OBSERVATIONS OF PEAT CHARACTERISTICS FROM CORING

Coring was undertaken in the fens and on the palsas to identify stratigraphic horizons for correlation with radar profiles. Coring in fens was carried out using a Macaulay corer (Jowsey, 1966). Coring on palsas was carried out using a permafrost corer (Zoltai, 1978) with inside diameter of 250 mm. Interfaces of particular interest included the peat - mineral sediment interface, ice lenses in frozen peat, tephra layers, and major changes in moisture content (which may be manifested by a change in density and/or degree of decomposition).

GPR may detect changes in moisture content as low as one percent (Hänninen, 1992); detailed moisture content data of this accuracy were not compiled for this study. Sampling compression of the peat, due to the cutting resistance of fibrous matter, can affect the water content, particularly in less decomposed peat (Hobbs, 1986). Further, the Macaulay corer does not seal fully during sample recovery, and there was visible loss of water during core retrieval. In frozen peat, stratigraphic resolution is reduced due to high signal velocity and signal scattering by ice. The following tables summarize key features observed in the cores; depths are approximate.

B.1 Porsild's Field

Macaulay core # 1: July 21, 1994, 0 m on GPR Transect #1

Coring to intercept peat - mineral sediment interface; no core retained. Peat depth was greater than 5 m at this location. No mineral sediment was encountered.

Macaulay core # 2: July 21, 1994, 7 m on GPR Transect # 1

Table B-1. Porsild's Field: Macaulay core # 2	
Depth of Core (cm)	Observations
32 - 34	<ul style="list-style-type: none"> • tephra layer • poorly decomposed sedge peat to this depth
34 - 345	<ul style="list-style-type: none"> • generally uniform, moderately decomposed sedge peat • few (<i>ca.</i> 5 cm to 30 cm thick) denser peat layers occur at <i>ca.</i> 170 - 175 cm, 270 - 275 cm, 295 - 305 cm, 310 - 340 cm depth
345 - 410	<ul style="list-style-type: none"> • denser peat than above
410 - 455	<ul style="list-style-type: none"> • greater degree of decomposition
455 - 500	<ul style="list-style-type: none"> • gyttja
end-of-hole	

Macaulay core # 3: July 21, 1994, 7 m on GPR Transect # 1

Table B-2. Porsild's Field: Macaulay core # 3	
Depth of Core (cm)	Observations
29 - 32	<ul style="list-style-type: none"> • tephra layer • poorly decomposed sedge peat to this depth
32 - 290	<ul style="list-style-type: none"> • generally uniform, moderately decomposed sedge peat • few (<i>ca.</i> 3 cm to 15 cm thick) denser peat layers occur at <i>ca.</i> 185 - 188 cm, 250 - 260 cm, 265 - 280 cm depth
290 - 465	<ul style="list-style-type: none"> • generally uniform, moderately decomposed sedge peat, denser than above • less dense peat layer occurs at <i>ca.</i> 350 - 355 cm depth
465 - 500	<ul style="list-style-type: none"> • gyttja
end-of-hole	

Macaulay core # 4: July 21, 1994, near east edge of fen

Table B-3. Porsild's Field: Macaulay core # 4	
Depth of Core (cm)	Observations
50 - 53	<ul style="list-style-type: none"> • tephra layer
53 - 150	<ul style="list-style-type: none"> • generally uniform, moderately decomposed sedge peat
150 - 170	<ul style="list-style-type: none"> • less dense peat than above
170 - 280	<ul style="list-style-type: none"> • generally uniform, moderately decomposed sedge peat, as for 53 - 150 cm depth
280 - 290	<ul style="list-style-type: none"> • gyttja
290 - 300	<ul style="list-style-type: none"> • mineral sediment: clay and silt, with few small clasts
end-of-hole	

Macaulay core # 5: July 21, 1994, near east edge of fen

Table B-4. Porsild's Field: Macaulay core # 5	
Depth of Core (cm)	Observations
0 - 115	<ul style="list-style-type: none"> generally uniform, moderately decomposed sedge peat
115 - 130	<ul style="list-style-type: none"> denser peat than above
130 - 150	<ul style="list-style-type: none"> generally uniform, moderately decomposed sedge peat, as to 115 cm depth
150 - 280	<ul style="list-style-type: none"> generally uniform, moderately decomposed sedge peat, denser, as for 115 - 130 cm depth
280 - 295	<ul style="list-style-type: none"> gyttja
295 - 300	<ul style="list-style-type: none"> mineral sediment: silt and sand, with small clasts
end-of-hole	

Palsa core # 1: August 8, 1994, 17.3 m on GPR Transect #2

Core collected approximately 3.3 m from south edge of palsa # 1.

Table B-5. Porsild's Field: Palsa core # 1	
Depth of Core (cm)	Observations
0 - 30	<ul style="list-style-type: none"> unfrozen, poorly decomposed peat
30 - 40	<ul style="list-style-type: none"> diffuse tephra layer frozen below 30 cm
40 - 70	<ul style="list-style-type: none"> moderately decomposed peat with minor pore ice, ice crystals up to several mm diameter
70 - 80	<ul style="list-style-type: none"> increasing pore ice and horizontal ice lenses up to 1 cm thick
80 - 110	<ul style="list-style-type: none"> decreased pore ice, no ice lenses or veins
110 - 120	<ul style="list-style-type: none"> ice veins/lenses <i>ca.</i> 1 cm thick
120 - 130	<ul style="list-style-type: none"> 9 cm ice lens
130 - 190	<ul style="list-style-type: none"> pore ice, no lens ice

Table B-5. Porsild's Field: Palsa core # 1	
Depth of Core (cm)	Observations
190 - 220	<ul style="list-style-type: none"> • pore ice and lens ice up to 3 cm thick
220 - 420	<ul style="list-style-type: none"> • pore ice, virtually no lens ice (except few thin (1 mm) veins between 250 - 260 cm depth, one 1 cm ice diagonal ice lens at <i>ca.</i> 365 cm depth)
420 - 490	<ul style="list-style-type: none"> • pore ice and thin, variably oriented ice veins (< 5 mm thick)
490 - 500	<ul style="list-style-type: none"> • unfrozen peat
end-of-hole	

Palsa core # 2: August 8, 1994, 35 m on GPR Transect #3
Core collected approximately 5.3 m from east edge of palsa # 4.

Table B-6. Porsild's Field: Palsa core # 2	
Depth of Core (cm)	Observations
0 - 30	<ul style="list-style-type: none"> • unfrozen, poorly decomposed peat
30 - 65	<ul style="list-style-type: none"> • frozen below 30 cm depth • minor pore ice
65 - 190	<ul style="list-style-type: none"> • increasing pore ice, no lenses • mineral sediment lens, <i>ca.</i> 2 cm thick at <i>ca.</i> 95 cm depth
190 - 210	<ul style="list-style-type: none"> • pore ice and variably oriented ice veins 3 - 10 mm thick
210 - 230	<ul style="list-style-type: none"> • pore ice, no lens ice
230 - 250	<ul style="list-style-type: none"> • pore ice and variably oriented ice veins up to 10 mm thick
250 - 290	<ul style="list-style-type: none"> • pore ice, no lens ice
290 - 300	<ul style="list-style-type: none"> • increasing pore ice, vein <i>ca.</i> 8 mm thick, 30° to horizontal
300 - 320	<ul style="list-style-type: none"> • unfrozen peat
320	<ul style="list-style-type: none"> • mineral sediment
end-of-hole	

B.2 Dale Creek

Depth to mineral sediment was measured at 83 m along GPR Transect # 1; the peat - mineral sediment interface was encountered at 125 cm depth, between palsas # 2 and # 3.

Macaulay core # 1: August 21, 1994, 51 m on GPR Transect # 2

Core recovery was poor at this location. The permafrost corer was used to estimate depth to the peat - mineral sediment interface; mineral sediment was encountered at 230 cm depth at 51 m along GPR Transect # 2, approximately 4 m from the edge of palsa # 1.

Table B-7. Dale Creek: Macaulay core # 1	
Depth of Core (cm)	Observations
0 - 25	<ul style="list-style-type: none">poorly decomposed, sedge peat
25 - 150	<ul style="list-style-type: none">moderately decomposed, sedge peatlayers of more decomposed peat occur at <i>ca.</i> 50 - 65 cm and 70 - 85 cm depth
150 - 200	<ul style="list-style-type: none">no core recovered from unfrozen peat below 150 cm
end-of-hole	

Palsa core # 1: August 8, 1994, 34.5 m on GPR Transect #1

Core collected from palsa # 4.

Table B-8. Dale Creek: Palsa core # 1	
Depth of Core (cm)	Observations
0 - 45	<ul style="list-style-type: none">tephra layer near surfacepoorly decomposed peat to <i>ca.</i> 45 cm depth (frost table)
45 - 75	<ul style="list-style-type: none">pore ice, moderately decomposed peat
75 - 80	<ul style="list-style-type: none">no core recovered below 75 cm depth, refusal in mineral sediment at 80 cm depth
end-of-hole	

Palsa core # 2: August 8, 1994, 43.5 m on GPR Transect #1

Core collected from palsa # 4.

Table B-9. Dale Creek: Palsa core # 2	
Depth of Core (cm)	Observations
0 - 45	<ul style="list-style-type: none">poorly decomposed peat to <i>ca.</i> 45 cm depth (frost table)
45 - 105	<ul style="list-style-type: none">moderately decomposed peatpore ice and virtually no lens ice (except one sub-vertically oriented ice vein 8 mm thick at <i>ca.</i> 50 cm depth)minor sediment lens at <i>ca.</i> 85 cm depth
105 - 130	<ul style="list-style-type: none">mineral sediment, some peat, below 105 cm: clay with small clastspore ice, no lens ice
end-of-hole	

Palsa core # 3: August 21, 1994, 164 m on GPR Transect #1

Core collected from palsa # 1.

Table B-10. Dale Creek: Palsa core # 3	
Depth of Core (cm)	Observations
0 - 45	<ul style="list-style-type: none">poorly to moderately decomposed peat to <i>ca.</i> 45 cm depth (frost table)
45 - 55	<ul style="list-style-type: none">moderately decomposed peatlow ice content, pore ice, poorly cemented
55 - 70	<ul style="list-style-type: none">moderately to well decomposed peatlow ice content, pore ice, poorly cemented
70 - 95	<ul style="list-style-type: none">increasing pore ice, poorly cementedbelow 80 cm depth, variably oriented ice veins and lenses 2 -3 mm thick
95 - 110	<ul style="list-style-type: none">mineral sediment: silt with small clasts, few mm diameterincreasing iciness above sediment, lens 5 mm thick
end-of-hole	

Core # 4 (in meadow): August 21, 1994, 190 m on GPR Transect #1

Table B-11. Dale Creek: Core # 4 (in meadow)	
Depth of Core (cm)	Observations
0 - 30	<ul style="list-style-type: none">• poorly decomposed peat
30 - 60	<ul style="list-style-type: none">• poorly to moderately decomposed peat
60 - 70	<ul style="list-style-type: none">• denser peat than above, moderately decomposed
70 - 90	<ul style="list-style-type: none">• moderately decomposed peat, less dense than above
90 - 100	<ul style="list-style-type: none">• no core recovered
end-of-hole	

APPENDIX C

AREA CALCULATIONS OF PALSAS AT PORSILD'S FIELD AND DALE CREEK FOR 1949, 1972, AND 1981

APPENDIX C. AREA CALCULATIONS OF PALSAS AT PORSILD'S FIELD AND DALE CREEK FOR 1949, 1972, AND 1981

Detailed aerial photograph analysis was performed using the (August) 1949 (scale *ca.* 1:30,000) and (August) 1981 (scale *ca.* 1:10,500) datasets as endpoints, and the (August) 1972 (scale *ca.* 1:25,500) dataset as an intermediate point of the time series. Photographic enlargements of stereopairs from each of the two sites were made to facilitate mapping of the areal extent of the features. The enlarged images were scanned and enhancements (*i.e.*, contrast, brightening, sharpening) applied, to further assist image interpretation, using tools available in Photoshop software (version 2.5.1) for Windows. The use of digital, enhanced stereopairs compensated for the image quality of the 1949 photography, the resolution of which did not permit areal measurements to be taken directly from the original prints. Site-specific scale calculations were made for the original aerial photographs using the formula:

$$\text{scale} = \frac{\text{flying height (ft)} - \text{ground height (ft)}}{\text{lens length (inches)}} \times 12$$

Scale of the enlarged photographs was controlled using fixed points on the photos that remained unchanged over time. Using the scale of the photograph and a count of pixels over a measured distance, the area represented by each pixel was determined for each photograph. To calculate area of the palsas, each palsa was manually traced on the digital enhanced photograph, and the pixels within the enclosed trace counted using an automatic software function. Ten traces of each palsa were made for each stereopair, the highest and lowest area value discarded (shown in brackets in the following tables), and the average of the remaining eight values taken as the area of the palsa. Summary data are provided in Tables 4-1 and 4-2. The following tables include pixel areas, pixel counts, and area values for each stereopair for each year, for Porsild's Field and Dale Creek.

C.1 Porsild's Field

Table C-1. Porsild's Field: Pixel Area by Year	
Year of aerial photography	Pixel Area (m ²)
1949	0.320
1972	0.221
1981	0.217

Table C-2. Porsild's Field: Palsa #1, Area Calculations, 1949	
Pixel count	Palsa area (m²)
2987	955.8
2995	958.4
3003	961.0
2980	953.6
2991	957.1
2925	(936.0)
2925	936.0
2942	941.4
3025	(968.0)
3006	961.9
Average	953.1

Table C-3. Porsild's Field: Palsa #1a, Area Calculations, 1949	
Pixel count	Palsa area (m²)
476	(152.3)
488	156.2
506	161.9
511	163.5
528	(169.0)
528	169.0
504	161.3
496	158.7
479	153.3
488	156.2
Average	160.0

Table C-4. Porsild's Field: Palsa #2, Area Calculations, 1949	
Pixel count	Palsa area (m²)
2311	(739.5)
2395	766.4
2381	761.9
2375	760.0
2415	772.8
2473	(791.4)
2458	786.6
2496	798.7
2414	772.5
2367	757.4
Average	772.0

Table C-5. Porsild's Field: Palsa #4, Area Calculations, 1949	
Pixel count	Palsa area (m²)
726	232.3
724	231.7
756	241.9
791	(253.1)
734	234.9
695	(222.4)
755	241.6
770	246.4
735	235.2
701	224.3
Average	236.0

Table C-6. Porsild's Field: Palsa #5, Area Calculations, 1949	
Pixel count	Palsa area (m²)
1317	(421.4)
1363	436.2
1328	425.0
1371	438.7
1355	433.6
1392	(445.4)
1354	433.3
1381	441.9
1344	430.1
1339	428.5
Average	433.4

Table C-7. Porsild's Field: Palsa #6, Area Calculations, 1949	
Pixel count	Palsa area (m²)
807	(258.2)
712	227.8
674	(215.7)
726	232.3
714	228.5
716	229.1
716	229.1
682	218.2
722	231.0
715	228.8
Average	228.1

Table C-8. Porsild's Field: Palsa #7, Area Calculations, 1949	
Pixel count	Palsa area (m²)
487	155.8
490	156.8
491	157.1
487	155.8
476	152.3
455	(145.6)
473	151.4
495	(158.4)
495	158.4
473	151.4
Average	154.9

Table C-9. Porsild's Field: Palsa #8, Area Calculations, 1949	
Pixel count	Palsa area (m²)
585	187.2
561	179.5
558	178.6
545	(174.4)
581	185.9
554	177.3
557	178.2
566	181.1
558	178.6
596	(190.7)
Average	180.8

Table C-10. Porsild's Field: Palsa #9, Area Calculations, 1949	
Pixel count	Palsa area (m²)
645	206.4
581	(185.9)
653	209.0
697	(223.0)
677	216.6
641	205.1
665	212.8
651	208.3
659	210.9
662	211.8
Average	210.1

Table C-11. Porsild's Field: Palsa #1, Area Calculations, 1972	
Pixel count	Palsa area (m²)
4098	905.7
4226	(933.9)
4204	929.1
4207	929.7
4161	919.6
4131	912.9
4167	920.9
4129	912.5
4154	918.0
4087	(903.2)
Average	918.5

Table C-12. Porsild's Field: Palsa #1a, Area Calculations, 1972	
Pixel count	Palsa area (m²)
363	80.2
321	70.9
340	75.1
346	76.5
372	(82.2)
319	70.5
326	72.0
302	(66.7)
319	70.5
318	70.3
Average	73.2

Table C-13. Porsild's Field: Palsa #2, Area Calculations, 1972	
Pixel count	Palsa area (m²)
2639	583.2
2666	589.2
2638	583.0
2641	583.7
2769	611.9
2681	592.5
2813	621.7
2820	(623.2)
2594	(573.3)
2711	599.1
Average	595.5

Table C-14. Porsild's Field: Palsa #4, Area Calculations, 1972	
Pixel count	Palsa area (m²)
709	156.7
695	153.6
672	148.5
672	148.5
713	157.6
709	156.7
690	152.5
668	(147.6)
724	160.0
731	(161.5)
Average	154.3

Table C-15. Porsild's Field: Palsa #5, Area Calculations, 1972	
Pixel count	Palsa area (m²)
1296	286.4
1229	(271.6)
1274	281.5
1334	294.8
1331	294.1
1356	(299.7)
1313	290.2
1291	285.3
1265	279.6
1311	289.7
Average	287.7

Table C-16. Porsild's Field: Palsa #6, Area Calculations, 1972	
Pixel count	Palsa area (m²)
328	(72.5)
318	70.3
274	(60.5)
287	63.4
291	64.3
301	66.5
302	66.7
284	62.8
286	63.2
289	63.9
Average	65.1

Table C-17. Porsild's Field: Palsa #7, Area Calculations, 1972	
Pixel count	Palsa area (m²)
323	71.4
313	(69.2)
372	82.2
337	74.5
328	72.5
343	75.8
319	70.5
383	(84.6)
342	75.6
363	80.2
Average	75.3

Table C-18. Porsild's Field: Palsa #8, Area Calculations, 1972	
Pixel count	Palsa area (m²)
212	(46.8)
232	51.3
230	50.8
221	48.8
250	55.2
241	53.3
275	60.8
251	55.5
286	(63.2)
257	56.8
Average	54.1

Table C-19. Porsild's Field: Palsa #1, Area Calculations, 1981	
Pixel count	Palsa area (m²)
4245	(921.2)
4147	899.9
4123	894.7
4139	898.2
4138	897.9
4084	(886.2)
4117	893.4
4109	891.6
4139	898.2
4090	887.5
Average	895.2

Table C-20. Porsild's Field: Palsa #1a, Area Calculations, 1981	
Pixel count	Palsa area (m²)
455	98.7
445	96.6
449	97.4
404	(87.7)
428	92.9
443	96.1
427	92.7
418	90.7
472	(102.4)
441	95.7
Average	95.1

Table C-21. Porsild's Field: Palsa #2, Area Calculations, 1981	
Pixel count	Palsa area (m²)
2655	(576.1)
2599	564.0
2601	564.4
2569	557.5
2562	555.9
2540	(551.2)
2588	561.6
2567	557.0
2648	574.6
2650	575.0
Average	563.7

Table C-22. Porsild's Field: Palsa #4, Area Calculations, 1981	
Pixel count	Palsa area (m²)
652	(141.5)
668	145.0
690	149.7
662	143.6
683	148.2
678	147.1
675	146.5
685	148.6
683	148.2
710	(154.1)
Average	147.1

Table C-23. Porsild's Field: Palsa #5, Area Calculations, 1981	
Pixel count	Palsa area (m²)
1313	284.9
1305	(283.2)
1306	283.4
1324	287.3
1385	(300.5)
1375	298.4
1330	288.6
1361	295.3
1357	294.5
1347	292.3
Average	290.6

Table C-24. Porsild's Field: Palsa #6, Area Calculations, 1981	
Pixel count	Palsa area (m²)
328	71.2
314	68.1
334	72.5
320	69.4
345	74.9
300	(65.1)
352	76.4
328	71.2
357	(77.5)
317	68.8
Average	71.6

Table C-25. Porsild's Field: Palsa #7, Area Calculations, 1981	
Pixel count	Palsa area (m²)
249	54.0
237	(51.4)
243	52.7
259	56.2
252	54.7
255	55.3
260	56.4
257	55.8
272	(59.0)
252	54.7
Average	55.0

C.2 Dale Creek

Table C-26. Dale Creek: Pixel Area by Year	
Year of aerial photography	Pixel Area (m²)
1949	0.301
1972	0.183
1981	0.181

Table C-27. Dale Creek: Palsa #1, Area Calculations, 1949	
Pixel count	Palsa area (m²)
4483	1349.4
4629	1393.3
4454	(1340.6)
4546	1368.3
4626	1392.4
4603	1385.5
4724	1421.9
4745	(1428.2)
4692	1412.3
4733	1424.6
Average	1393.5

Table C-28. Dale Creek: Palsa #2, Area Calculations, 1949	
Pixel count	Palsa area (m²)
7108	(2139.5)
7512	(2261.1)
7353	2213.2
7424	2234.6
7182	2161.8
7233	2177.1
7232	2176.8
7348	2211.7
7269	2188.0
7343	2210.2
Average	2196.7

Table C-29. Dale Creek: Palsa #3, Area Calculations, 1949	
Pixel count	Palsa area (m²)
4912	1478.5
4898	1474.3
4829	1453.5
4840	1456.8
4785	1440.3
4769	(1435.5)
4774	1437.0
4851	1460.1
4885	1470.4
4994	(1503.2)
Average	1458.9

Table C-30. Dale Creek: Palsa #4, Area Calculations, 1949	
Pixel count	Palsa area (m²)
2728	821.1
2794	841.0
2798	(842.2)
2723	819.6
2670	803.7
2696	811.5
2745	826.2
2713	816.6
2669	(803.4)
2776	835.6
Average	821.9

Table C-31. Dale Creek: Palsa #5, Area Calculations, 1949	
Pixel count	Palsa area (m²)
1544	(464.7)
1580	475.6
1581	475.9
1580	475.6
1636	492.4
1628	490.0
1611	484.9
1566	471.4
1644	494.8
1651	(496.9)
Average	482.6

Table C-32. Dale Creek: Palsa #1, Area Calculations, 1972	
Pixel count	Palsa area (m²)
7178	(1313.6)
7027	1285.9
6929	1268.0
6999	1280.8
7013	1283.4
6916	(1265.6)
6980	1277.3
6968	1275.1
7043	1288.9
7133	1305.3
Average	1283.1

Table C-33. Dale Creek: Palsa #2, Area Calculations, 1972	
Pixel count	Palsa area (m²)
9954	1821.6
10007	1831.3
10126	1853.1
10038	1836.9
10174	(1861.8)
10097	1847.7
9930	(1817.2)
10031	1835.7
9971	1824.7
10016	1832.9
Average	1835.5

Table C-34. Dale Creek: Palsa #3, Area Calculations, 1972	
Pixel count	Palsa area (m²)
5793	1060.1
5708	1044.6
5757	1053.5
5725	1047.7
5768	1055.5
5621	(1028.6)
5751	1052.4
5821	1065.2
5759	1053.9
5823	(1065.6)
Average	1054.1

Table C-35. Dale Creek: Palsa #4, Area Calculations, 1972	
Pixel count	Palsa area (m²)
3958	(724.3)
4002	732.4
4015	734.7
4041	(739.5)
4009	733.6
3974	727.2
3998	731.6
4002	732.4
3975	727.4
3970	726.5
Average	730.7

Table C-36. Dale Creek: Palsa #5, Area Calculations, 1972	
Pixel count	Palsa area (m²)
2107	385.6
2064	(377.7)
2123	388.5
2105	385.2
2137	391.1
2144	392.3
2091	382.6
2200	(402.6)
2127	389.2
2147	392.9
Average	388.4

Table C-37. Dale Creek: Palsa #1, Area Calculations, 1981	
Pixel count	Palsa area (m²)
7122	1289.1
6918	(1252.2)
7099	1284.9
7000	1267.0
7129	1290.3
7226	1307.9
7108	1286.5
7276	(1317.0)
6993	1265.7
7126	1289.8
Average	1285.1

Table C-38. Dale Creek: Palsa #2, Area Calculations, 1981	
Pixel count	Palsa area (m²)
10091	1826.5
10155	1838.0
10035	(1816.3)
10082	1824.8
10164	1839.7
10304	1865.0
10375	(1877.9)
10302	1864.7
10145	1836.2
10085	1825.4
Average	1840.0

Table C-39. Dale Creek: Palsa #3, Area Calculations, 1981	
Pixel count	Palsa area (m²)
5580	1010.0
5573	1008.7
5519	(998.9)
5647	1022.1
5654	1023.4
5669	1026.1
5752	1041.1
5619	1017.0
5696	1031.0
5816	(1052.7)
Average	1022.4

Table C-40. Dale Creek: Palsa #4, Area Calculations, 1981	
Pixel count	Palsa area (m²)
3482	630.2
3416	(618.3)
3430	620.8
3519	636.9
3499	633.3
3425	619.9
3512	635.7
3497	633.0
3560	(644.4)
3420	619.0
Average	628.6

Table C-41. Dale Creek: Palsa #5, Area Calculations, 1981	
Pixel count	Palsa area (m²)
1837	332.5
1734	(313.8)
1793	324.5
1891	(342.3)
1797	325.3
1764	319.3
1793	324.5
1773	320.9
1823	330.0
1862	337.0
Average	326.7

APPENDIX D
THAW DEPTH MEASUREMENTS

APPENDIX D. THAW DEPTH MEASUREMENTS

Thaw depths at the time of the GPR surveys were measured using a YSI Tele-thermometer probe 90 cm in length, with a 0.5°C resolution. Thaw depth measurements were taken along the GPR transects, with alternate measurements taken close by when surface cracks were encountered.

Table D-1. Summary of Thaw Depths, 22 & 23 July, 1994 <i>Data summarized below exclude areas of slumping peat, palsa margins, and/or where thaw depths > 90 cm</i> <i>Palsa numbers at Porsild's Field as in Kershaw and Gill (1979).</i>		
Porsild's Field - GPR Transect 1 : crosses south to north over palsa # 1		
Palsa # 1		
Average thaw depth (cm) =	47.5	<i>(includes values from 39 m to 64 m)</i>
maximum thaw depth (cm) =	73.5	<i>(maximum measured at surface crack)</i>
minimum thaw depth (cm) =	29.5	
Porsild's Field - GPR Transect 2 : crosses east to west over palsas # 1 and # 2		
Palsa # 1		
Average thaw depth (cm) =	43.8	<i>(includes values from 16 m to 45 m)</i>
maximum thaw depth (cm) =	55	
minimum thaw depth (cm) =	29.5	
Palsa # 2		
Average thaw depth (cm) =	42.9	<i>(includes values from 63 m to 76 m)</i>
maximum thaw depth (cm) =	53.5	
minimum thaw depth (cm) =	32	
Porsild's Field - GPR Transect 3 : crosses east to west over palsas # 4 and # 5		
Palsa # 4		
Average thaw depth (cm) =	34.9	<i>(includes values from 31 m to 39 m)</i>
maximum thaw depth (cm) =	45	
minimum thaw depth (cm) =	24.5	
Palsa # 5		
Average thaw depth (cm) =	36.2	<i>(includes values from 93 m to 101 m)</i>
maximum thaw depth (cm) =	52.5	
minimum thaw depth (cm) =	27	

Table D-1. Summary of Thaw Depths, 22 & 23 July, 1994

Data summarized below exclude areas of slumping peat, palsa margins, and/or where thaw depths > 90 cm. Palsa numbers at Porsild's Field as in Kershaw and Gill (1979).

Dale Creek - GPR Transect 1 : crosses east to west, from palsa # 5 to palsa # 1, onto "meadow"**Palsa # 5 from west**

Average thaw depth (cm) =	45.7	<i>(includes values from 3 m to 16 m)</i>
maximum thaw depth (cm) =	64	
minimum thaw depth (cm) =	34.5	

Palsa # 4 from west

Average thaw depth (cm) =	45.3	<i>(includes values from 25 m to 42 m)</i>
maximum thaw depth (cm) =	69	
minimum thaw depth (cm) =	34	

Palsa # 3 from west

Average thaw depth (cm) =	39.9	<i>(includes values from 52 m to 81 m)</i>
maximum thaw depth (cm) =	49	
minimum thaw depth (cm) =	33	

Palsa # 2 from west

Average thaw depth (cm) =	40.4	<i>(includes values from 101 m to 139 m)</i>
maximum thaw depth (cm) =	70	
minimum thaw depth (cm) =	28	

Palsa # 1 from west

Average thaw depth (cm) =	39.7	<i>(includes values from 154 m to 171 m)</i>
maximum thaw depth (cm) =	47	
minimum thaw depth (cm) =	31	

Dale Creek - GPR Transect 2 : crosses north to south over palsa # 1 from west**Palsa # 1 from west**

Average thaw depth (cm) =	43.1	<i>(includes values from 14 m to 43)</i>
maximum thaw depth (cm) =	67	
minimum thaw depth (cm) =	28	

Table D-2. Thaw Depths: Porsild's Field, GPR Transect # 1, July 23, 1994		
Transect position (m)	Thaw depth (cm)	Comments
37	n/a ¹	fen
38	n/m ²	palsa margin
39	29.5	
40	31	
41	58	
42	50.5	
43	54.5	
44	66	crack: thaw depth adjacent to crack = 50 cm
45	73.5	crack: thaw depth adjacent to crack = 50 cm
46	51.5	
47	42.5	
48	42	
49	33	
50	33.5	
51	46.5	
52	54.5	
53	58	
54	48.5	
55	47.5	
56	43	
57	41	
58	39.5	
59	49.5	
60	49	
61	42	
62	54.5	
63	52	
64	44	
65	n/m	slumping, palsa margin
66	n/m	slumping, palsa margin
67	n/m	slumping, palsa margin

¹

n/a = not applicable

²

n/m = not measured

Table D-2. Thaw Depths: Porsild's Field, GPR Transect # 1, July 23, 1994		
Transect position (m)	Thaw depth (cm)	Comments
68	n/m	slumping, palsa margin
69	n/m	palsa margin
70	n/a	fen
72.5	n/a	fen

Table D-3. Thaw Depths: Porsild's Field, GPR Transect # 2, July 23, 1994		
Transect position (m)	Thaw depth (cm)	Comments
13	n/a	fen (5 cm deep standing water)
14	n/m	palsa margin, slumping
15	n/m	palsa margin, slumping
16	31.5	
17	29.5	
18	54.5	crack: thaw depth adjacent to crack = 42 cm
19	46	
20	53.5	
21	53	
22	51.5	
23	53.5	
24	55	
25	42.5	
26	46.5	
27	38	
28	33	
29	43	
30	33.5	
31	34.5	
32	35	
33	42	
34	49.5	crack: thaw depth adjacent to crack = 35 cm
35	54	crack: thaw depth adjacent to crack = 43 cm
36	44.5	
37	43	
38	48.5	
39	50.5	crack: thaw depth adjacent to crack = 44.5 cm

Table D-3. Thaw Depths: Porsild's Field, GPR Transect # 2, July 23, 1994		
Transect position (m)	Thaw depth (cm)	Comments
40	44.5	
41	45	
42	35	
43	38	
44	41	
45	45	
46	n/m	palsa margin
47	n/m	palsa margin
48	n/m	palsa margin
46.5 m - 59 m standing water		
58	n/a	fen (5 cm water)
59	n/m	palsa margin
60	n/m	palsa margin
61	n/m	palsa margin
62	n/m	palsa margin
63	49.5	
64	45.5	
65	43	
66	39	
67	39	
68	46.5	
69	32	
70	41	
71	47.5	
72	42	
73	38	
74	40	
75	53.5	
76	43.5	
77	n/m	palsa margin, slumping
78	n/m	palsa margin
79	n/m	palsa margin
78.5 m - 84.5 m standing water, level fen		

Table D-4. Thaw Depths: Porsild's Field, GPR Transect # 3, July 23, 1994		
Transect position (m)	Thaw depth (cm)	Comments
29	n/a	fen, saturated moss at surface
30	n/m	palsa margin
31	36.5	
32	24.5	
33	31	
34	32	
35	37	
36	37	
37	39	
38	32.5	
39	45	
40	n/m	palsa margin
41	n/m	palsa margin
40 m - 92.5 m, fen		
92	n/a	fen
93	30	only slightly raised above fen, <10 cm
94	27	
95	35.5	
96	43	
97	36	
98	52.5	
99	36	
100	32	
101	33.5	
102	n/a	fen
103	n/a	15 - 20 cm deep standing water

Table D-5. Thaw Depths: Dale Creek, GPR Transect # 1, July 22, 1994		
Transect position (m)	Thaw depth (cm)	Comments
0	n/m	palsa margin, slump blocks
1	n/m	palsa margin, slump blocks
2	n/m	palsa margin, slump blocks
3	64	
4	41	

Table D-5. Thaw Depths: Dale Creek, GPR Transect # 1, July 22, 1994		
Transect position (m)	Thaw depth (cm)	Comments
5	50.5	
6	46.5	
7	44	at 20 cm deep crack
8	40	
9	47	
10	44	
11	42.5	
12	44	
13	42	
14	41	
15	34.5	
16	59	
17	n/a	fen
18	n/a	fen
19	n/m	palsa margin
20	n/m	palsa margin
21	n/m	palsa margin, slump blocks
22	n/m	palsa margin, slump blocks
23	n/m	palsa margin, slump blocks
24	n/m	palsa margin, slump blocks
25	69	
26	65	
27	57	
28	36	
29	42	
30	46	
31	39	
32	48	
33	46.5	
34	35	
35	46.5	
36	45	
37	34	
38	35	
39	38.5	

Table D-5. Thaw Depths: Dale Creek, GPR Transect # 1, July 22, 1994		
Transect position (m)	Thaw depth (cm)	Comments
40	42	
41	46	
42	45	
43	n/m	palsa margin
44	n/m	palsa margin
45	n/m	palsa margin
46	n/a	fen
47	n/a	fen
48	n/a	fen
49	n/m	palsa margin
50	n/m	palsa margin
51	n/m	palsa margin
52	47.5	
53	48	
54	49	
55	41	
56	37	
57	46	
58	37	
59	42	
60	39	
61	38.5	
62	39	
63	44	
64	36	
65	40	
66	40	
67	42	
68	38	
69	33	
70	33.5	
71	40.5	
72	37.5	
73	34	
74	40	

Table D-5. Thaw Depths: Dale Creek, GPR Transect # 1, July 22, 1994		
Transect position (m)	Thaw depth (cm)	Comments
75	39	
76	41	
77	30	
78	40	
79	38	
80	45	
81	43	
82	n/m	palsa margin
83	n/m	palsa margin
84 m - 92.5 m water		
93	n/m	palsa margin, stone at <i>ca.</i> 73 cm
94	n/m	palsa margin, stone at <i>ca.</i> 78 cm
95	n/m	palsa margin, slumping
96	n/m	palsa margin, slumping, bare peat
97	n/m	palsa margin, slumping
98	n/m	palsa margin, slumping
99	n/m	palsa margin, slumping
100	n/m	palsa margin, slumping
101	47	
102	42.5	
103	52	
104	49	
105	42.5	
106	43	
107	43	
108	37	
109	44	
110	42.5	
111	41	
112	39.5	
113	35	
114	35	
115	36.5	
116	41.5	
117	40	

Table D-5. Thaw Depths: Dale Creek, GPR Transect # 1, July 22, 1994		
Transect position (m)	Thaw depth (cm)	Comments
118	39.5	
119	43	
120	38	
121	38	
122	32.5	
123	38.5	
124	28	
125	36.5	
126	40	
127	42.5	
128	40	
129	33	
130	41.5	
131	40	
132	37	
133	36	
134	35	
135	42.5	
136	33	
137	70	
138	51	
139	31	
140	n/m	palsa margin, slumping
141	n/m	palsa margin
142	n/m	palsa margin
143	n/a	fen
144	n/a	fen
145	n/a	fen
146	n/m	palsa margin, bare peat, slumping
147	n/m	palsa margin, bare peat, slumping
148	n/m	palsa margin, bare peat, slumping
149	n/m	palsa margin, bare peat, slumping
150	n/m	palsa margin, bare peat, slumping
151	n/m	palsa margin, bare peat, slumping
152	n/m	palsa margin, slumping

Table D-5. Thaw Depths: Dale Creek, GPR Transect # 1, July 22, 1994		
Transect position (m)	Thaw depth (cm)	Comments
153	n/m	palsa margin, slumping
154	38	
155	47	
156	41.5	
157	37	
158	34	
159	35.5	
160	35	
161	33	
162	42	
163	31	
164	39.5	
165	42.5	
166	43	
167	42.5	
168	41	
169	43	
170	44	
171	45.5	
172	n/m	palsa margin
173	n/m	palsa margin
174	n/m	deep crack, 75 cm
175	n/m	palsa margin, slumping
176	n/m	palsa margin, slumping
177	n/m	palsa margin, slumping
178	n/m	palsa margin, slumping
179	n/m	palsa margin, slumping
180	n/m	palsa margin, slumping

Table D-6. Thaw Depths: Dale Creek, GPR Transect # 2, July 22, 1994		
Transect position (m)	Thaw depth (cm)	Comments
0	n/a	meadow
2.5	n/a	meadow
5	n/a	meadow

Table D-6. Thaw Depths: Dale Creek, GPR Transect # 2, July 22, 1994		
Transect position (m)	Thaw depth (cm)	Comments
7.5	n/a	meadow
10	n/a	meadow
11	n/a	meadow
12	n/m	palsa margin
13	n/m	palsa margin
14	30	
15	28	
16	35.5	
17	42.5	
18	37.5	
19	36.5	
20	37.5	
21	35	
22	39.5	
23	41.5	
24	37	
25	33.5	
26	54	
27	41.5	
28	40	
29	48.5	
30	28	
31	45.5	
32	48.5	
33	52	
34	47.5	
35	38	
36	48	
37	51	
38	52	
39	45.5	
40	44.5	
41	52.5	
42	54.5	
43	67	

Table D-6. Thaw Depths: Dale Creek, GPR Transect # 2, July 22, 1994		
Transect position (m)	Thaw depth (cm)	Comments
44	n/m	palsa margin, slumping
45	n/m	palsa margin, slumping
46	n/m	palsa margin, slumping
47	n/m	palsa margin, slumping
48	n/m	palsa margin, slumping

APPENDIX E
LETTERS OF COPYRIGHT PERMISSION

26 AUG 1996

Post-it® Fax Note	7671	Date	Aug 16	Page	1
To	John HORN	From			
Co./Dept.		Co.			
Phone #		Phone #	(403) 781-5493		
Fax #	(416) 236-4446	Fax #	(403) 263-7116		

Cecilia Horvath
10938 63rd Ave.
Edmonton, Alberta
T6H 1R2 Canada

August 15, 1996

Mr. John Horn
Copyright Permissions
John Wiley & Sons
via FACSIMILE: (416) 236-4446

Dear Mr. Horn:

Re: Copyright Permission

I am seeking permission to use the material described below as supporting information in my Masters of Science thesis. The material would be used to support discussion of a related field of study, and would be used in conjunction only with a very limited amount of other copyrighted material (two other figures anticipated).

Author: Seppälä, Matti
Title of Paper: Pulsas and related forms.
Volume Title: Advances in Periglacial Geomorphology.
Editor: M. J. Clark.
Copyright Date: 1988.
ISBN: 0 471 90981 5
Material Requested: Figure 11.14 and caption, pages 272-273, in Chapter 11.
Copies to be Used: No more than 3 (for introductory and analyses chapters of thesis).
University: University of Alberta, Edmonton, Alberta, Canada.
Course Name: Thesis.
Semester, Year: Fall 1996.
Supervisor: Prof. G. Peter Kershaw.

I trust the above information is sufficient for you to process this request. Should you have any questions or require any additional information, please do not hesitate to contact me at (403) 781-5493 or at the above noted address. Thank you for your assistance in this matter.

Sincerely,



Permission granted,
Cecilia Horvath
Linda Sampford 5/9/96

is Department
Wiley & Sons Ltd.
your work with credit to another
from that source is required.

Credit should include the following components: Title, author(s) and/or editor(s), Copyright () (date and owner). Reprinted by permission of John Wiley & Sons, Ltd.

Post-It Fax Note	7671	Date	Aug 16	# of pages	1
To	Eileen Fink	From	Celesa		
Co./Dept.	NRC Research Press	Co.	Press		
Phone #	(403) 781-5493	Phone #	(403) 781-5493		
Fax #	(613) 952-7656	Fax #	(403) 263-7116		

Celesa Horvath
10938 63rd Ave.
Edmonton, Alberta
T6H 1R2 Canada

August 16, 1996

Ms. Eileen Fink
National Research Council
Research Press
Building M-55
Ottawa, ON
K1A 0R6
via FACSIMILE: (613) 952-7656

Dear Ms. Fink:

Re: Copyright Permission

I am seeking permission to use the material described below as supporting information in my Masters of Science thesis. The material would be used to support discussion of a related field of study, and would be used in conjunction only with a very limited amount of other copyrighted material (one other figure anticipated).

Authors: Steve C. Zoltai and Charles Tarnocai.
Title of Paper: Perennially Frozen Peatlands in the Western Arctic and Subarctic of Canada.
Journal Title: Canadian Journal of Earth Sciences.
Reference: Vol. 12, pages 28-43.
Copyright Date: 1975.
ISSN: 0008-4077.
Material Requested: Figures 3 and 5 with captions, and caption from Figure 2, pages 33-35.
Copies to be Used: No more than 3 (for introductory and analyses chapters of thesis).
University: University of Alberta, Edmonton, Alberta, Canada.
Course Name: Thesis.
Semester, Year: Fall 1996.
Supervisor: Prof. G. Peter Kershaw.

I trust the above information is sufficient for you to process this request. Should you have any questions or require any additional information, please do not hesitate to contact me at (403) 781-5493 or at the above noted address. Thank you for your assistance in this matter.

Sincerely,

Celesa Horvath

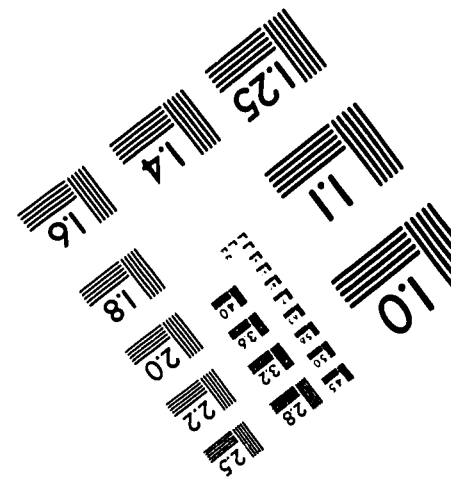
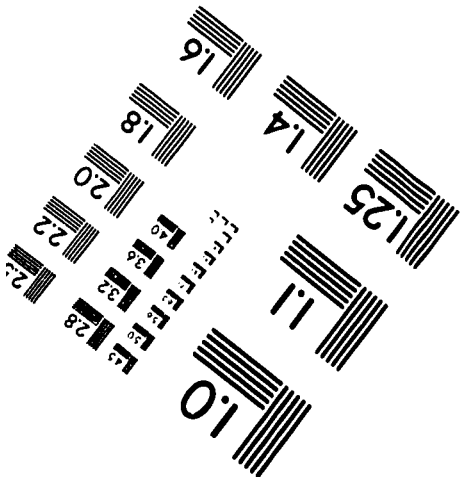
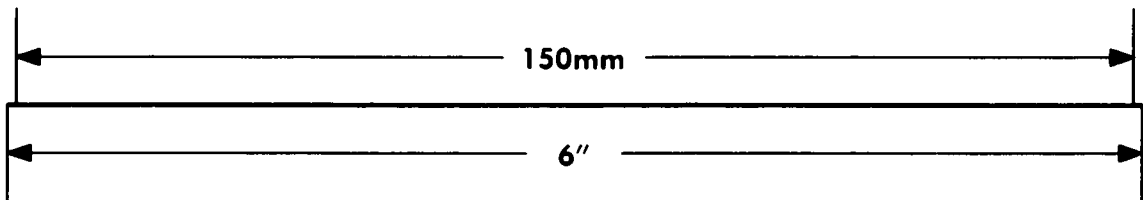
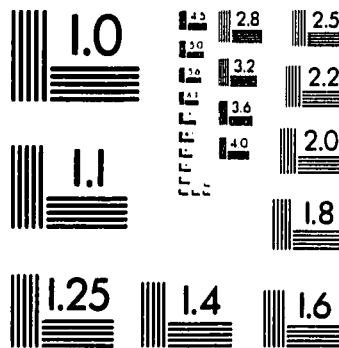
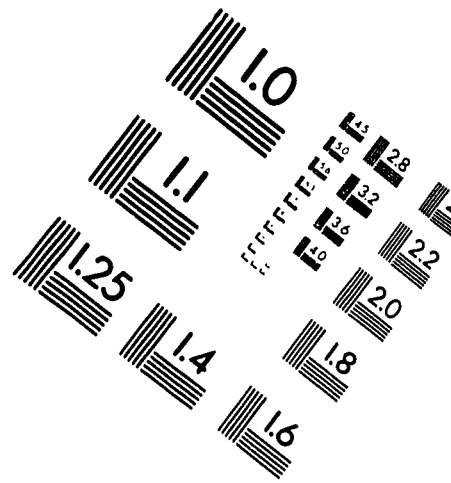
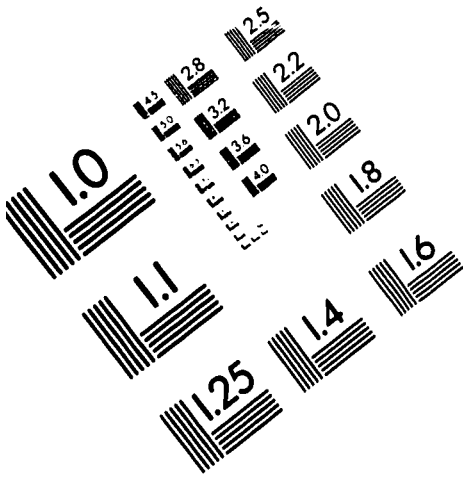
Celesa Horvath

Permission is granted for the use of the material described above, provided acknowledgement is given to the source.

Date: Aug 16/96

Paul McClymont
Paul McClymont
Business Manager

IMAGE EVALUATION TEST TARGET (QA-3)



APPLIED IMAGE, Inc.
1653 East Main Street
Rochester, NY 14609 USA
Phone: 716/482-0300
Fax: 716/288-5989

© 1993, Applied Image, Inc., All Rights Reserved